Applications of human microdosing with accelerator mass spectrometry: assessment of ability to predict drug-drug interactions and determine the pharmacokinetics of enantiomers

Marie Louise Croft BSc (Hons)

PhD

University of York

Chemistry

October 2012

Abstract

In this thesis, new applications of microdosing were explored in two clinical trials. Methods were developed for the separation and quantification of ^{14}C-labelled analytes in human plasma using two-dimensional HPLC and accelerator mass spectrometry (AMS). Caffeine, midazolam, tolbutamide and fexofenadine were quantified in plasma after administration of a ^{14}C-labelled cassette microdose to human volunteers via a HPLC-AMS recovery constant method. Mean accuracy for all analytes was within 13% of the measured plasma concentration with precision of <20% CV, meeting recommended acceptance criteria for HPLC-AMS assays. Complete resolution of each analyte was demonstrated by two-dimensional HPLC. Pharmacokinetic data obtained after cassette microdose administration were in close agreement with those previously obtained after administration of therapeutic doses. Co-administration of the cassette microdose with known inhibitors of metabolism enzymes and transporters resulted in a significant ($p<0.01$) increase in the area under the concentration-time curve from time zero to infinity ($AUC_{0-\infty}$) for caffeine (x8.2), midazolam (x11.7), fexofenadine (x3.2) and tolbutamide (x1.8, $p<0.05$).

Administration of a combined ^{11}C and ^{14}C-labelled verapamil microdose allowed distribution in the brain to be monitored by PET imaging, while simultaneously obtaining plasma pharmacokinetics by AMS. The separation of ^{14}C-verapamil by two-dimensional HPLC and AMS analysis resulted in the individual pharmacokinetics of *R*- and *S*-verapamil being consistent with those reported after therapeutic doses. In addition, a significant difference in pharmacokinetic data obtained for the two enantiomers clearly showed the preferential clearance of *S*-verapamil. Data were accurate within 12% of the true value with precision of <18% CV. Pharmacokinetic data obtained after PET analysis were consistent with those obtained during AMS analysis, proving the concept of combining the two techniques in clinical studies and enabling maximum information to be achieved from one single study.

Contents

Abstract ..... **i**
Contents ..... **ii**
Tables ..... **xi**
Figures ..... **xv**
Work published in this thesis ..... **xx**
Acknowledgements ..... **xxi**
Declaration ..... **xxii**
CHAPTER 1 Introduction **1**
1.1 Introduction 2
1.2 Drug development 4
1.2.1 Pre-clinical development 5
1.2.2 Phase 0 5
1.2.3 Phase 1 5
1.2.4 Phase 2 6
1.2.5 Phase 3 6
1.2.6 Phase 4 6
1.3 Drug metabolism 7
1.3.1 Phase I reactions 8
1.3.2 Phase II reactions 9
1.3.3 Phase III reactions 10
1.3.4 Elimination 11
1.4 Pharmacokinetics 11
1.5 Cytochrome P450 (CYP) 12
1.5.1 CYP Inducers 14
1.5.2 CYP Inhibition 15
1.5.2.1 Competitive CYP inhibition 15
1.5.2.2 Non-competitive CYP inhibition 15
1.5.2.3 Mechanism-based CYP inhibition 16
1.5.3 CYP polymorphisms 16
1.5.4 CYP1A2 16
1.5.5 CYP2C9 17
1.5.6 CYP3A4 18
1.6 P-glycoprotein 18
1.6.1 P-glycoprotein (P-gp) and absorption of orally administered drugs 19
1.7 Drug-drug interactions (DDIs) 19

1.7.1 Evaluation of DDIs 21
1.8 Microdosing 22
1.8.1 Microdosing studies – pharmacokinetic linearity tests 25
1.8.1.1 Human microdosing studies 25
1.8.1.2 Animal studies 28
1.8.2 Microdosing studies – Further applications 32
1.8.2.1 Early pharmacokinetics and candidate selection 32
1.8.2.2 Metabolite identification 33
1.8.2.3 Detection of polymorphic effects 34
1.8.2.4 Microdosing in DDI studies 36
1.8.2.5 Cassette microdosing and DDI studies 37
1.9 Accelerator mass spectrometry 38
1.9.1 AMS vs. MS 40
1.9.2 AMS sample processing procedure 40
1.9.3 Terminology used in AMS analysis 44
1.9.3.1 Isotope ratio (percent modern carbon) 44
1.9.3.2 Units of radioactivity 44
1.9.3.3 Specific radioactivity 45
1.9.3.4 HPLC fractionation and the kinetic isotope effect (KIE) 45
1.9.3.5 Carbon carrier and isotopic dilutor 45
1.9.4 Processing of plasma prior to analysis by HPLC 46
1.9.5 Chromatographic resolution 46
1.9.6 Current methods for quantification of analyte concentrations 47
1.9.7 Limitations of the recovery curve method 51
1.9.7.1 Analyte purity 51
1.9.7.2 Linear analyte response 51
1.9.7.3 Uniform analysis 51
1.10 Aims of this thesis 52
1.10.1 Ability to detected DDIs after cassette microdose administration 52
1.10.2 Combination of positron emission tomography and AMS in obtaining pharmacokinetic and imaging data after microdose administration 53
CHAPTER 2 Development of HPLC and AMS methods for quantification of caffeine, midazolam, tolbutamide and fexofenadine in plasma 55
2.1 Introduction 56
2.1.1 Development of an HPLC-AMS assay 56
2.1.2 Compounds chosen for cassette dose administration 56
2.1.2.1 Caffeine 56

2.1.2.2 Midazolam 57
2.1.2.3 Tolbutamide 58
2.1.2.4 Fexofenadine 59
2.1.2.5 Absorption and distribution of caffeine, midazolam, tolbutamide and fexofenadine 60
2.2 Aims 63
2.3 Results and discussion 65
2.3.1 Development of methods for pre-treatment of plasma 65
2.3.1.1 Development of protein precipitation extraction Method 1 65
2.3.1.2 Development of extraction Methods 2a and 2b 67
2.3.2 Development of a HPLC method for separation of caffeine, midazolam, tolbutamide and fexofenadine in human plasma 68
2.3.2.1 Determination of detector wavelength 68
2.3.2.2 HPLC Method A1 method transfer 69
2.3.2.3 Development of HPLC Method A2 70
2.3.2.4 Analysis of plasma filtrate by HPLC using Method A2 74
2.3.2.5 Development of protein precipitation extraction Method 3 75
2.3.2.6 Development of HPLC method A3 76
2.3.2.7 Assessment of method repeatability and carryover 79
2.3.3 Development of a HPLC method to separate caffeine, midazolam, tolbutamide and fexofenadine in human plasma 80
2.3.3.1 Caffeine HPLC method B1 81
2.3.3.2 Midazolam HPLC method B2 81
2.3.3.3 Tolbutamide HPLC method B3 82
2.3.3.4 Fexofenadine HPLC method B4 82
2.3.3.5 Assessment of method repeatability 83
2.3.4 Determination of the internal standard level 84
2.3.4.1 Assessment of detector response linearity 84
2.3.4.2 Determination of non-labelled caffeine, midazolam, tolbutamide and fexofenadine present in clinical plasma 86
2.3.4.3 Calculation of amount of internal standard 87
2.3.5 Verification of the chromatographic separation of caffeine, midazolam, tolbutamide and fexofenadine by HPLC 88
2.3.6 Quantification of ^{14}C-caffeine, fexofenadine, tolbutamide and midazolam in plasma by HPLC-AMS 94
2.3.6.1 Confirmation of analyte purity 94
2.3.6.2 Preparation of recovery curve 95

2.3.6.3 Limitations of the developed method 102
2.4 Conclusions 107
CHAPTER 3 Determination of drug-drug interactions using a radiolabelled cassette microdose 109
3.1 Introduction 110
3.2 Aims 111
3.3 Results and discussion 112
3.3.1 Clinical study design and implementation 112
3.3.1.1 Selection of microdose compounds 112
3.3.1.2 Selection of inhibitors 113
3.3.1.3 Dose administration design 113
3.3.1.4 Implementation of clinical study 114
3.3.2 Dose solution preparation and determination of specific activity 115
3.3.2.1 Cassette dose administration and sample collection 115
3.3.2.2 Determination of ^{14}C-caffeine, midazolam, tolbutamide and fexofenadine concentrations in post-dose plasma 115
3.3.2.3 Limit of quantification 116
3.3.3 Determination of total ^{14}C-concentrations in pre-dose plasma 117
3.3.4 Subject genotyping 118
3.3.5 Caffeine microdosing data 118
3.3.5.1 Caffeine microdosing data vs. literature data 119
3.3.5.2 Effect of inhibitor administration on the pharmacokinetics of caffeine .. 120
3.3.6 Midazolam microdosing data 123
3.3.6.1 Midazolam microdosing data vs. literature data 124
3.3.6.2 Effect of inhibitor administration on the pharmacokinetics of midazolam ... 125
3.3.6.3 CYP3A4 polymorphisms affecting the metabolism of midazolam 126
3.3.7 Tolbutamide microdosing data 126
3.3.7.1 CYP2C9 polymorphisms affecting the metabolism of tolbutamide 127
3.3.7.2 Tolbutamide microdosing data vs. literature data 131
3.3.8 Fexofenadine microdosing data 133
3.3.8.1 Fexofenadine microdosing data vs. literature data 135
3.3.8.2 Effect of inhibitor administration on the pharmacokinetics of fexofenadine 136
3.4 Conclusions 138

CHAPTER 4 Development of HPLC and AMS methods for quantification of R- and S-verapamil in plasma 144
4.1 Introduction 145
4.1.1 Verapamil 145
4.1.1.1 Chiral discrimination in HPLC chromatography 148
4.2 Aims 149
4.3 Results and discussion 151
4.3.1 Development of methods for pre-treatment of plasma 151
4.3.2 Development of a chiral HPLC method for separation of R- and S-verapamil (Method C1) 152
4.3.2.1 Assessment of method repeatability and carryover 154
4.3.3 Compatibility of the protein precipitation extraction and HPLC method C1 155
4.3.3.1 Assessment of detector interference from plasma filtrate 155
4.3.3.2 Assessment of fraction alignment and isotopic fractionation 155
4.3.4 Development of a HPLC method for demonstration of separation of R- and S-verapamil (Method D1) 157
4.3.4.1 Assessment of method repeatability 157
4.3.5 Verification of the chromatographic separation of R- and S-verapamil . 158
4.3.6 Determination of the internal standard concentration 161
4.3.6.1 Assessment of detector response linearity 161
4.3.6.2 Determination of non-labelled verapamil in clinical plasma 162
4.3.6.3 Calculation of internal standard amount 163
4.3.7 Development of a method for quantification of ^{14}C-R- and S-verapamil in plasma by HPLC-AMS 163
4.3.7.1 Confirmation of analyte purity 164
4.3.7.2 Preparation of the recovery curve 165
4.3.7.3 Processing of AMS data to generate recovery curve 168
4.3.7.4 Recovery curves and assessment of precision 170
4.3.8 Suitability of the developed methods 173
4.3.8.1 Selectivity 173
4.3.8.2 Carryover 174
4.3.8.3 Recovery 174
4.3.8.4 Accuracy and precision of the assay 175
4.3.9 Development of an alternative quantification method using a recovery constant 177
4.3.10 Dose solution preparation and analysis 179

4.3.10.1 Dosing solution analysis and determination of specific activity 179
4.3.10.2 Determination of ^{14}C-verapamil concentration in dosing solution by LSC 179
4.3.10.3 Determination of amount of R- and S-verapamil present as a result of non-labelled and ^{14}C-verapamil addition 180
4.3.10.4 Measurement of R- and S-verapamil ratio in dosing solution by HPLC-UV 181
4.4 Conclusions 184
CHAPTER 5 Combination of accelerator mass spectrometry and positron emission tomography in the determination of R- and S-verapamil pharmacokinetics after administration of a microdose 185
5.1 Introduction 186
5.2 Aims 188
5.3 Results and discussion 189
5.3.1 Clinical study 189
5.3.1.1 Choice of test compound 189
5.3.1.2 Clinical study design and implementation 191
5.3.1.3 Dose administration and sample collection 191
5.3.2 Determination of ^{14}C-R- and S-verapamil concentrations in plasma 192
5.3.3 R- and S-verapamil data obtained after administration of a microdose of verapamil 193
5.3.3.1 Period 1 batch suitability 193
5.3.3.2 Period 1 R- and S-verapamil plasma concentration data 194
5.3.4 R- and S-verapamil data obtained after administration of a microdose of verapamil concomitantly with a therapeutic dose 196
5.3.4.1 Period 2 batch suitability 196
5.3.4.2 Period 2 R- and S-verapamil plasma concentration data 198
5.3.5 Comparison of period 1 and 2 data and assessment of dose linearity 201
5.3.6 Comparison of R- and S-verapamil pharmacokinetics with previous studies 203
5.3.7 Comparison of R- and S-verapamil AMS data with PET data 205
5.4 Conclusions 207
CHAPTER 6 Overall conclusions and further work 210
6.1 Overall summary and conclusions 211
6.2 Future work and applications 213
CHAPTER 7 Materials and methods 216
7.1 Chemicals 217

7.1.1 Reagents used in preparation of reference material, protein precipitation and HPLC analysis 217
7.1.2 Reagents used in LSC analysis 217
7.1.3 Reagents used in the graphitisation process 217
7.2 Reference material 217
7.2.1 Control plasma 217
7.2.2 Non-labelled reference material 217
7.2.3 ^{14}C-labelled reference material 218
7.2.4 Preparation of reference standard solutions 218
7.3 Preparation of internal standard solutions 219
7.3.1 Preparation of caffeine, midazolam, tolbutamide and fexofenadine internal standard solution 219
7.3.2 Preparation of verapamil internal standard solution 219
7.4 Preparation of recovery standard and QC plasma 219
7.4.1 Preparation of caffeine, midazolam, tolbutamide and fexofenadine recovery standard and QC plasma 219
7.4.2 Preparation of verapamil recovery standard and QC plasma 220
7.5 Methods for determination of extraction efficiency 221
7.5.1 Protein precipitation extraction method development for caffeine, midazolam, tolbutamide and fexofenadine from plasma (Method 1, 2a, 2b and 3) 221
7.5.2 Protein precipitation extraction method development for verapamil 222
7.6 Preparation and analysis of plasma filtrates for assessment of HPLC method compatibility 223
7.6.1 Preparation and analysis of plasma filtrate containing caffeine, midazolam, tolbutamide and fexofenadine for HPLC Method A3 assessment 223
7.6.2 Preparation and analysis of plasma filtrate for HPLC Method A3 assessment 224
7.6.3 Preparation and analysis of plasma filtrate for verification of caffeine, midazolam, tolbutamide and fexofenadine separation in clinical plasma 224
7.6.4 Assessment of compatibility of protein precipitation extraction method with HPLC method C1 225
7.6.5 Preparation and analysis of samples for assessment of verapamil fraction alignment and isotopic fractionation 225
7.6.6 Preparation and analysis of plasma filtrates for verification of the chromatographic separation of R- and S-verapamil 226

7.7 Preparation of plasma filtrates from clinical, recovery standard and QC plasma.. 226
7.7.1 Preparation of plasma filtrates from clinical, recovery standard and QC plasma containing caffeine, midazolam, tolbutamide and fexofenadine..... 226
7.7.2 Preparation of plasma filtrates from clinical, recovery standard and QC plasma containing verapamil..... 227
7.8 HPLC methods..... 227
7.8.1 HPLC methods for separation of caffeine, midazolam, tolbutamide and fexofenadine..... 227
7.8.2 HPLC methods for separation of R- and S-verapamil 231
7.9 LSC analysis 231
7.10 Spectrophotometric analysis of caffeine, midazolam and tolbutamide 232
7.11 AMS analysis..... 232
7.11.1 Preparation of samples for AMS analysis 232
7.11.2 AMS analysis of graphite samples 233
7.11.3 AMS sample acceptance criteria 234
7.11.4 Limit of quantification 234
7.11.4.1 Limit of quantification for method development 234
7.11.4.2 Limit of quantification for caffeine, midazolam, tolbutamide and fexofenadine in clinical plasma 235
7.11.4.3 Limit of quantification for verapamil in clinical plasma..... 235
7.12 Clinical study design and sample collection..... 235
7.12.1 Preparation of cassette dosing solutions..... 235
7.12.2 Cassette dose administration and sample collection 236
7.12.3 Preparation of verapamil dosing solution..... 236
7.12.4 Verapamil dose administration and sample collection..... 237
7.13 Pharmacokinetic data analysis..... 238
7.13.1 Determination of pharmacokinetics of caffeine, midazolam, tolbutamide and fexofenadine 238
7.13.2 Determination of pharmacokinetics of R- and S-verapamil..... 238
7.14 Statistical data analysis..... 238
7.14.1 Statistical analysis of caffeine, midazolam, tolbutamide and fexofenadine data 238
7.14.2 Statistical analysis of R- and S-verapamil data 238
Appendices..... 239
Appendix 1. PET analysis 240
A1.1 PET and MRI analysis..... 240

A1.2 Blood and metabolite analysis 240
A1.3 Pharmacokinetic modelling 241
A1.4 Statistical analysis 241
A1.5 PET imaging data 241
Appendix 2. Caffeine plasma concentration data 243
Appendix 3. Midazolam plasma concentration data 244
Appendix 4. Tolbutamide plasma concentration data 245
Appendix 5. Fexofenadine plasma concentration data 246
Appendix 6. R-verapamil plasma concentration data 247
Appendix 7. S-verapamil plasma concentration data 248
Appendix 8. Caffeine pharmacokinetic data 249
Appendix 9. Midazolam pharmacokinetic data 250
Appendix 10. Tolbutamide pharmacokinetic data 251
Appendix 11. Fexofenadine pharmacokinetic data 252
Appendix 12. R-verapamil pharmacokinetic data 253
Appendix 13. S-verapamil pharmacokinetic data 254
Glossary 255
References 257

Tables

Table 1: Examples of CYP enzyme substrates, inhibitors and inducers. 14
Table 2: Substrates and inhibitors of P-glycoprotein. 19
Table 3: Summary of human microdosing data. 23
Table 4: Summary of animal microdosing data exploring dose linear PK. 24
Table 5: Biopharmaceutical Classification System for drug absorption. 30
Table 6: Summary of non-linear pharmacokinetic data. 31
Table 7: pK_a and logP of caffeine, midazolam, tolbutamide and fexofenadine. 61
Table 8: $logD_{(pH7.4)}$ of caffeine, midazolam, tolbutamide and fexofenadine. 62
Table 9: Caffeine, midazolam, tolbutamide and fexofenadine extraction efficiency data (Method 1). 67
Table 10: Caffeine, midazolam, tolbutamide and fexofenadine extraction efficiency data (Method 2). 67
Table 11: Typical proportions of analyte available for HPLC analysis on extraction using Methods 2a and 2b. 68
Table 12: Typical retention times of caffeine, midazolam, tolbutamide and fexofenadine plus selected metabolites (HPLC Method A3). 76
Table 13: pK_a, logP and logD of caffeine, midazolam, tolbutamide and fexofenadine. . 77
Table 14: Intra-day repeatability data for caffeine, tolbutamide, fexofenadine and midazolam (Day 1, HPLC Method A3). 79
Table 15: Inter-day repeatability data for caffeine, tolbutamide, fexofenadine and midazolam (HPLC Method A3). 80
Table 16: Intra-day repeatability data for caffeine, midazolam, tolbutamide and fexofenadine (HPLC methods B1-B4). 83
Table 17: C_{max} data for caffeine, midazolam, tolbutamide and fexofenadine as reported in the literature. 86
Table 18: Calculation of estimated caffeine, midazolam, tolbutamide and fexofenadine C_{max} data after microdose administration. 87
Table 19: AMS data obtained on analysis of non-labelled caffeine, fexofenadine, tolbutamide and midazolam reference standards. 95
Table 20: AMS data obtained on analysis of ^{14}C-solutions and the determination of recovery standard and QC plasma concentrations. 97
Table 21: Caffeine, midazolam, tolbutamide and fexofenadine QC accuracy and precision data (n=5). 101
Table 22: Recommended samples for verification of analyte resolution by 2D chromatography. 103

Table 23: Analysis of pre-dose plasma samples for determination of background ^{14}C levels. 117
Table 24: Genotyping summary CYP3A4, CYP1A2 and CYP2C9. 118
Table 25: Plasma pharmacokinetic data obtained after administration of a caffeine microdose (25 µg) vs. literature data obtained after therapeutic doses. 120
Table 26: Plasma pharmacokinetic data obtained after administration of a caffeine microdose (25 µg) and after administration of a caffeine microdose (25 µg) concomitantly with an inhibitor dose (*n*=6, mean, SD in parentheses). 120
Table 27: Plasma pharmacokinetic data obtained after administration of a caffeine microdose plus inhibitors vs. literature data obtained after administration of a therapeutic dose. 121
Table 28: CYP1A2 genotyping of subjects 1-6. 122
Table 29: Plasma pharmacokinetic data obtained after administration of a microdose (25 µg) of caffeine – all subjects. 122
Table 30: Plasma pharmacokinetic data obtained after administration of a midazolam microdose (25 µg) vs. literature data obtained after a microdose and therapeutic doses. 124
Table 31: Plasma pharmacokinetic data obtained after administration of a midazolam microdose (25 µg) and after administration of a midazolam microdose (25 µg) concomitantly with an inhibitor dose (*n*=6, mean, SD in parentheses). 125
Table 32: Plasma pharmacokinetic data obtained after administration of a midazolam microdose plus inhibitor vs. literature data obtained after administration of a therapeutic dose. 125
Table 33: CYP2C9 genotyping of subjects 1-6. 128
Table 34: Plasma pharmacokinetic data obtained after administration of a tolbutamide microdose (25 µg) vs. literature data obtained after therapeutic doses. 131
Table 35: Plasma pharmacokinetic data obtained after administration of a tolbutamide microdose (25 µg) and after administration of a tolbutamide microdose (25 µg) concomitantly with an inhibitor dose (*n*=6, mean, SD in parentheses). 132
Table 36: Plasma pharmacokinetic data obtained after administration of a tolbutamide microdose (25 µg) and after administration of a tolbutamide microdose (25 µg) concomitantly with an inhibitor dose (*n*=6, subjects 3 and 4 excluded). 132
Table 37: Plasma pharmacokinetic data obtained after administration of a tolbutamide microdose plus inhibitors vs. literature data obtained after administration of a therapeutic dose. 133
Table 38: Plasma pharmacokinetic data obtained after administration of a fexofenadine microdose (25 µg) vs. literature data obtained after therapeutic doses. 135

Table 39: Plasma pharmacokinetic data obtained after administration of a fexofenadine microdose (25 µg) and after administration of a fexofenadine microdose (25 µg) concomitantly with an inhibitor dose (*n*=6, mean, SD in parentheses). 136
Table 40: Plasma samples analysed by HPLC-AMS with concentrations below the LOQ. 140
Table 41: Verapamil extraction efficiency data for Methods 1 – 4. 152
Table 42: Day 1 repeatability data for *R*-and *S*-verapamil (HPLC Method C1). 154
Table 43: Day 2 repeatability data for *R*-and *S*-verapamil (HPLC Method C1). 155
Table 44: Verification of *R*-and *S*-verapamil peak purity. 156
Table 45: Intra-day and inter-day repeatability data for verapamil (HPLC Method D1). 158
Table 46: Non-labelled verapamil analysis by AMS for determination of background ^{14}C. 164
Table 47: Spiking solution AMS data and calculation of ^{14}C-verapamil concentrations. 166
Table 48: QC resolution data for *R*- and *S*-verapamil. 167
Table 49: QC accuracy and precision data for *R*- and *S*-verapamil (*n*=8). 172
Table 50: *R*-verapamil QC data calculated using m values determined from recovery constants (RC) and recovery curve (RS). 177
Table 51: *S*-verapamil QC data calculated using m values determined from recovery constants (RC) and recovery curve (RS). 178
Table 52: Determination of ^{14}C-verapamil concentration in dosing solution. 180
Table 53: Determination of non-labelled verapamil present in ^{14}C-verapamil. 181
Table 54: Determination of *R*- and *S*-verapamil ratio in dosing solution. 182
Table 55: Confirmation of *R*-and *S*-verapamil ratio in selected samples of dosing solutions. 182
Table 56: Determination of total mass of *R*- and *S*-verapamil present in dosing solution. 183
Table 57: Determination of specific radioactivity of *R*- and *S*-verapamil in dosing solution. 184
Table 58: Period 1 QC resolution data for *R*- and *S*-verapamil. 193
Table 59: Period 1 QC plasma concentration data for *R*- and *S*-verapamil. 194
Table 60: Period 1 *R*- and *S*-verapamil microdosing pharmacokinetic summary data (*n*=6, mean, SD in parentheses). 196
Table 61: Period 2 QC resolution data for *R*- and *S*-verapamil. 197
Table 62: Comparison of period 1 and period 2 mean pharmacokinetic data for *R*- and *S*-verapamil. 197

Table 63: Period 2 QC plasma concentration data for *R*- and *S*-verapamil. 198
Table 64: Period 2 *R*- and *S*-verapamil microdosing pharmacokinetic summary data (*n*=6, mean, SD in parentheses) 200
Table 65: Comparison of period 1 and period 2 mean pharmacokinetic data for *R*- and *S*-verapamil. 202
Table 66: Comparison of *R*-verapamil pharmacokinetic data obtained after administration of a microdose and a microdose concomitantly with an oral therapeutic dose of *R/S*-verapamil, with literature data obtained after a 5 mg intravenous dose. 204
Table 67: Comparison of *S*-verapamil pharmacokinetic data obtained after administration of a microdose and a microdose concomitantly with an oral therapeutic dose of *R/S*-verapamil, with literature data obtained after a 5 mg intravenous dose. 205
Table 68: Preparation of recovery standard and QC spiking solutions. 220
Table 69: Preparation of recovery standard and QC spiking solutions. 221
Table 70: Preparation of spiked plasma 222
Table 71: Sample volumes for protein precipitation extraction Method 1, Method 2a, Method 2b and Method 3. 222
Table 72: Sample volumes for verapamil protein precipitation. 223
Table 73: HPLC Conditions for separation of caffeine, midazolam, tolbutamide and fexofenadine (Method A1). 228
Table 74: HPLC Conditions for separation of caffeine, midazolam, tolbutamide and fexofenadine (Method A2). 228
Table 75: HPLC Conditions for separation of caffeine, midazolam, tolbutamide and fexofenadine (Method A3). 229
Table 76: HPLC Conditions for resolution of caffeine (Method B1). 229
Table 77: HPLC Conditions for resolution of midazolam (Method B2). 230
Table 78: HPLC Conditions for resolution of tolbutamide (Method B3). 230
Table 79: HPLC Conditions for resolution of fexofenadine (Method B4). 230
Table 80: HPLC Conditions for separation of *R*- and *S*-verapamil (Method C1). 231
Table 81: HPLC Conditions for isolation of verapamil (Method D1). 231
Table 82: Sample volumes taken for analysis by AMS 232
Table 83: Caffeine, tolbutamide, midazolam and fexofenadine dose solution analysis and determination of specific radioactivity. 236

Figures

Figure 1: Schematic showing the main routes of drug elimination (reproduced with the permission of the author [19]). 7
Figure 2: Oxidation reaction [19]. 8
Figure 3: Reduction reaction [19]. 8
Figure 4: Hydrolysis reaction [19]. 8
Figure 5: Rearrangement reaction [19]. 9
Figure 6: Conjugation of a drug or a product with glutathione [19]. 10
Figure 7: Schematic of the glutathione pathway [19]. 10
Figure 8: Cytochrome P450 nomenclature. 13
Figure 9: Schematic of a tandem pelletron accelerator mass spectrometer [121]. 39
Figure 10: Sample processing prior to analysis by AMS. 41
Figure 11: HPLC and AMS analysis of plasma. 43
Figure 12: Caffeine and the major routes of metabolism via CYP1A2 [134]. 57
Figure 13: Midazolam and the major routes of metabolism via CYP3A. 58
Figure 14: Tolbutamide and the major routes of metabolism [37]. 59
Figure 15: Fexofenadine. 59
Figure 16: Schematic of method development and verification of methods for the quantification of caffeine, midazolam, tolbutamide and fexofenadine. 64
Figure 17: Outline of the method for plasma extraction and liquid scintillation counting (LSC) of samples. 66
Figure 18: HPLC chromatogram of a mixture of midazolam, 1'-hydroxymidazolam and 4-hydroxymidazolam (Method A1) at 240 nm. 69
Figure 19: HPLC chromatogram of a mixture of caffeine, midazolam, tolbutamide and fexofenadine (Method A1) at 240 nm. 70
Figure 20: HPLC chromatogram of a mixture of midazolam and tolbutamide at 240 nm (a), caffeine at 270 nm (b) and fexofenadine at λ_{ex} 220 nm and λ_{em} 290 nm (c) (Method A2). 71
Figure 21: HPLC chromatogram of a mixture of midazolam, 1'-hydroxymidazolam and 4-hydroxymidazolam at 240 nm (Method A2). 72
Figure 22: HPLC chromatogram of a mixture of tolbutamide, 4-hydroxytolbutamide and carboxytolbutamide at 240 nm (Method A2). 73
Figure 23: HPLC chromatogram of a mixture of caffeine, theobromine, theophylline and paraxanthine at 270 nm (Method A2). 73
Figure 24: HPLC chromatogram of pre-dose clinical plasma spiked with caffeine and extracted with acetonitrile. 74

Figure 25: HPLC chromatogram of caffeine extracted from plasma with methanol. 75
Figure 26: HPLC chromatogram of a mixture of caffeine (270 nm), midazolam (240 nm), tolbutamide (240 nm) and fexofenadine at λ_{ex} 220 nm and λ_{em} 290 nm (Method A3). 77
Figure 27: logD (pH 7) plot for caffeine, midazolam, tolbutamide and fexofenadine separated on a C18 reverse phase column eluted with acetonitrile: 0.1 M ammonium acetate 78
Figure 28: HPLC chromatogram of caffeine at 270 nm (Method B1). 81
Figure 29: HPLC chromatogram of midazolam at 240 nm (Method B2). 82
Figure 30: HPLC chromatogram of tolbutamide at 240 nm (Method B3) 82
Figure 31: HPLC chromatogram of fexofenadine at λ_{ex} 220 nm and λ_{em} 290 nm (Method B4). 83
Figure 32: UV detector response for caffeine. 84
Figure 33: UV detector response for midazolam. 85
Figure 34: UV detector response for tolbutamide. 85
Figure 35: Fluorescence detector response for fexofenadine. 86
Figure 36: Schematic representation of the two-dimensional HPLC separation and isolation method. 89
Figure 37: Reconstructed caffeine radio-chromatogram, period 1, legend: blue = 1 h, red = 5 h, green = 12 h, purple = 24 h. 90
Figure 38: Reconstructed caffeine radio-chromatogram, period 2, legend: blue = 1 h, red = 5 h, green = 12 h, purple = 24 h. 90
Figure 39: Reconstructed midazolam radio-chromatogram, period 1, legend: blue = 1 h, purple = 5 h, 12 h and 24 h. 91
Figure 40: Reconstructed midazolam radio-chromatogram, period 2: legend: blue = 1 h, red = 5 h, green = 12 h, purple = 24 h. 91
Figure 41: Reconstructed tolbutamide radio-chromatogram data, period 1, legend: blue = 1 h, red = 5 h, green = 12 h, purple = 24 h. 92
Figure 42: Reconstructed tolbutamide radio-chromatogram data, period 2, legend: blue = 1 h, red = 5 h, green = 12 h, purple = 24 h. 92
Figure 43: Reconstructed fexofenadine radio-chromatogram, period 1, legend: blue = 1 h, red = 5 h, green = 12 h, purple = 24 h. 93
Figure 44: Reconstructed fexofenadine radio-chromatogram, period 2, legend: blue = 1 h, red = 5 h, green = 12 h, purple = 24 h. 93
Figure 45: Schematic of sample preparation and analysis for preparation of caffeine, midazolam, tolbutamide and fexofenadine recovery curve and QC samples 96
Figure 46: Caffeine recovery curve (y = 0.00756x) 99

Figure 47: Midazolam recovery curve (y = 0.00508x). 99
Figure 48: Tolbutamide recovery curve (y = 0.0140x). 100
Figure 49: Fexofenadine recovery curve (y = 0.0281x). 100
Figure 50: Schematic of cassette microdosing, sample collection and analysis of plasma samples by HPLC and AMS. 112
Figure 51: Dosing schedule of cassette microdose and inhibitors. 115
Figure 52: HPLC chromatogram of a plasma filtrate containing caffeine (270 nm), midazolam (240 nm), tolbutamide (240 nm) and fexofenadine at λ_{ex} 220 nm and λ_{em} 290 nm (Method A3). 116
Figure 53: Semilog plot of mean caffeine plasma concentration data, before (closed squares, *n*=6 to 12 h, *n*=4 to 18 h and *n*=2 to 24 h) and after (open squares, *n*=6 to 72 h) daily repeat dosing of fluvoxamine and ketoconazole. Error bars represent one standard deviation. 119
Figure 54: Semilog plot of midazolam mean plasma concentration, before (closed squares, *n*=6 to 4 h, *n*=2 to 8 h and *n*=1 to 12 h) and after (open squares, *n*=6 to 36 h, *n*=5 to 48 h and *n*=3 to 72 h) daily repeat dosing of fluvoxamine and ketoconazole. Error bars represent one standard deviation. 123
Figure 55: Semilog plot of tolbutamide mean plasma concentration, before (closed squares, *n*=6 to 36 h, *n*=5 to 48 h and *n*=2 to 72 h) and after (open squares, *n*=6 to 72 h) daily repeat dosing of fluvoxamine and ketoconazole. Error bars represent one standard deviation. 127
Figure 56: Concentration-time curves of ^{14}C-tolbutamide in venous plasma after administration of a microdose, CYP2C9 (*1/*1) genotyped subjects, *n*=4 (squares), CYP2C9 (*1/*2) genotyped subject 4, *n*=1 (triangles) and CYP2C9 (*1/*3) genotyped subject 3, *n*=1 (circles). 129
Figure 57: Concentration-time curves of ^{14}C-tolbutamide in venous plasma after microdose plus daily repeat dosing of fluvoxamine and ketoconazole, CYP2C9 (*1/*1) genotyped subjects, *n*=4 (squares), CYP2C9 (*1/*2) genotyped subject 4, *n*=1 (triangles) and CYP2C9 (*1/*3) genotyped subject 3, *n*=1 (circles). 130
Figure 58: Semilog plot of fexofenadine mean plasma concentration, before (closed squares, *n*=6 to 4 h, *n*=5 to 8 h and *n*=2 to 12 h) and after (open squares, *n*=6 to 12 h, *n*=4 to 18 h, *n*=3 to 24 h and *n*=1 to 48 h) daily repeat dosing of fluvoxamine and ketoconazole. Error bars represent one standard deviation. 134
Figure 59: Semilog plot of fexofenadine plasma concentration before and after daily repeat dosing of fluvoxamine and ketoconazole with α-$t_{1/2}$ and β-$t_{1/2}$. 136
Figure 60: P-glycoprotein and OATP at hepatocytes and enterocytes [165]. 138
Figure 61: Main routes of verapamil metabolism. 146

Figure 62: Structures of *S*- and *R*-verapamil showing assignment of groups attached to the chiral centre according to Cahn Ingold Prelog priority rules. 147
Figure 63: Schematic of method development and verification of methods for quantification of *R*- and *S*-verapamil..... 150
Figure 64: Lux Cellulose-1 stationary phase [172]..... 153
Figure 65: HPLC chromatogram of verapamil at λ_{ex} 276 nm and λ_{em} 290 nm (Method C1)..... 154
Figure 66: HPLC chromatogram of verapamil at λ_{ex} 276 nm and λ_{em} 290 nm (Method D1)..... 157
Figure 67: Reconstructed *R*-verapamil radio-chromatogram, legend: blue line = 1 h, red line = 5 h..... 159
Figure 68: Reconstructed *S*-verapamil radiochromatogram legend: blue line = 1 h, red line = 5 h..... 160
Figure 69: Assessment of detector response for *R*-verapamil (R^2=0.999)..... 161
Figure 70: Assessment of detector response for *S*-verapamil (R^2=0.999). 162
Figure 71: Schematic of sample preparation and analysis for preparation of a recovery curve and QC samples..... 165
Figure 72: *R*-verapamil recovery curve. 171
Figure 73: *S*-verapamil recovery curve..... 171
Figure 74: ^{11}C emission and collision with an electron. 186
Figure 75: Production of gamma rays and detection by PET camera..... 187
Figure 76: Schematic of verapamil dosing, sample collection and analysis of plasma samples by HPLC and AMS. 189
Figure 77: Example chromatogram, analysis of plasma filtrate containing verapamil at λ_{ex} 276 nm and λ_{em} 290 nm (Method D1)..... 192
Figure 78: Example chromatogram, analysis of reconstituted HPLC fraction containing verapamil at λ_{ex} 276 nm and λ_{em} 290 nm (Method C1)..... 193
Figure 79: Semilog plot of mean *R*-verapamil (triangles, *n*=6 to 12 h, *n*=5 to 24 h) and *S*-verapamil (squares, *n*=6 to 12 h, *n*=6 to 24 h) plasma concentration data after administration of an intravenous microdose (nominally 50 µg) of ^{14}C-verapamil (*n*=6). Error bars represent one standard deviation. 195
Figure 80: Semilog plot of mean *R*-verapamil (triangles, *n*=6) and *S*-verapamil (squares, *n*=6 to 12 h, *n*=5 to 24 h) plasma concentration data, after administration of an oral therapeutic dose (80 mg) of verapamil, followed by an intravenous microdose (nominally 50 µg) of ^{14}C-verapamil (*n*=6). Error bars represent one standard deviation..... 199

Figure 81: Semilog plot of mean *R*-verapamil plasma concentration data, after administration of an intravenous microdose (nominally 50µg) of ^{14}C-verapamil (filled triangles, *n*=6) and after administration of an oral therapeutic dose (80 mg) of verapamil followed by an intravenous microdose (nominally 50µg) of ^{14}C-verapamil (open triangles, *n*=7). Error bars represent one standard deviation.... 201
Figure 82: Semilog plot of mean *S*-verapamil plasma concentration data, after administration of an intravenous microdose (nominally 50µg) of ^{14}C-verapamil (filled triangles, *n*=6) and after administration of an oral therapeutic dose (80 mg) of verapamil followed by an intravenous microdose (nominally 50µg) of ^{14}C-verapamil (open triangles, *n*=7*)*. Error bars represent one standard deviation.... 202
Figure 83: Semilog plot of mean total ^{11}C-radioactivity (squares) and ^{11}C-*R*-verapamil (circles) in arterial plasma. Period 1 = open symbols, period 2 = filled symbols. 206
Figure 84: Semilog plot of total ^{11}C-radioactivity in whole brain grey matter. Period 1 = open symbols, period 2 = filled symbols..... 206

Work published in this thesis

Lappin, G., M Simpson, Y. Shishikura and C. Garner, *High-performance liquid chromatography accelerator mass spectrometry: Correcting for losses during analysis by internal standardization.* Analytical Biochemistry, 2008. **378**: p. 93-95 (Chapter 2 and Chapter 4)

Simpson, M., G. Lappin, and B.J. Keely, *Development of 2D chiral chromatography with accelerator mass spectrometry for quantification of (14)C-labeled R- and S-verapamil in plasma.* Bioanalysis, 2010. **2**(3): p. 397-405. (Chapter 4)

Wagner, C.C., M. Simpson, M. Zeitlinger, M. Bauer, R. Karch, A. Abrahim, T. Feurstein, M. Schutz, K. Kletter, G. Lappin and O. Langer *A Combined Accelerator Mass Spectrometry-Positron Emission Tomography Human Microdose Study with ^{14}C- and ^{11}C-Labelled Verapamil.* Clinical Pharmacokinetics, 2010. **50** (2): p111-20 (Chapter 5)

Croft, M., B. Keely, I. Morris, L.Tann and G. Lappin, *Predicting drug candidates of drug-drug interactions, using microdosing.* Clinical Pharmacokinetics, 2012. **51** (4): p237-46 (Chapter 3)

Note: publications have been submitted using the author's current name and previous name (Marie Simpson). Any literature references that appear within this thesis that are not listed above, but were authored by Marie Simpson or Marie Croft, are based on commercial studies in which the author contributed. These studies were outside of the scope of this thesis.

Acknowledgements

I would like to thank Xceleron for presenting this generous opportunity and the financial support to complete this thesis. Thank-you to all of my colleagues past and present for your support and encouragement along the way. Special thanks go to Graham Lappin for providing continuous guidance, support and encouragement.

Thank-you to the University of York for providing this opportunity and to Brendan Keely and Ian Morris for their guidance and support.

Finally thank-you to my family and friends who have supported me throughout my PhD. Thank-you to my Mum and Dad for always believing in me, and to Clint for your endless patience and understanding.

Declaration

I hereby declare that the work presented in this thesis is my own work, except where otherwise acknowledged. This work has not been submitted for a degree at the University of York or any other university.

CHAPTER 1

Introduction

1.1 Introduction

The cost of developing of a new drug, from its discovery through to registration and marketing is estimated to be between $800 million to $1.7 billion, with the process taking approximately ten years [1-3]. At the early stages of development, the drug is known as a new chemical entity (NCE). An ideal NCE is one that may be dosed in amounts that maintain efficacy at the site of action without causing toxic side effects. The balance between these two parameters is dependent upon the systemic concentrations and the site of action, which in turn is dependent upon the dose administered. In some therapeutic areas, for example the development of life saving cancer therapies, the tolerance for side effects may be greater than in other therapeutic areas where even mild side effects may be deemed unacceptable. A key parameter in the relationship between the dose and the efficacy of an NCE are its pharmacokinetics (PK, Section 1.4). Although PK data may be obtained from laboratory animal species relatively early in the drug development process, human PKs are only obtained once the NCE reaches clinical trials. Clinical trials are the most costly phase of drug development. In addition, it is estimated that of any NCE which reaches the first phase of clinical trials, only 8% will eventually become a marketed drug [1]. Recognition and elimination of NCEs that possess poor PK profiles prior to human clinical trials not only considerably reduces cost, but also reduces unnecessary exposure of human volunteers to a potentially unsuitable drug. Allometric scaling using animal *in vivo* data and use of *in vitro-in vivo* modelling are two commonly used methods in predicting human PK [4]. Although these methods have their value, they are often unreliable. In fact, typically only 60-80% of NCEs have been found to have human PK within two-fold of predictive methods [4, 5]. Human microdosing was first suggested as an alternative method for the prediction of PK in 2003 [6]. The US food and drug administration (FDA) released a 'Guidance for Industry' document in 2006, recognising the use of microdosing within phase 0 (Section 1.8) prior to phase 1 trials. Microdosing has been consistently recommended in recent years to predict human PK at the earliest possible stage of drug development in human volunteers [5, 7, 8].

Microdosing (Section 1.8) is defined as the administration of a test compound to human volunteers at less than 1/100th of the calculated pharmacological dose (based on animal data) with a maximum dose of 100 µg [9]. PK data obtained after microdose administration are then scaled to enable prediction of PK at the therapeutic dose. Due to the low dose administered in a microdosing study, the regulatory authorities allow studies to be implemented with reduced safety and toxicology data, thus allowing them to take place earlier in the drug development process than more conventional phase 1 studies (Section 1.2.3). It is the relatively early administration that provides microdosing with its major advantage, its potential to identify problematic compounds at an early stage of drug development.

A concern with microdosing from the outset was its ability to predict the PK after administration of a therapeutic dose, from the very small doses administered [8, 10]. A number of human microdosing studies have been carried out in recent years [11, 12] with the primary aim of examining how predictive microdosing is of therapeutically relevant doses (Section 1.8.1.1). In addition, microdosing studies have been carried out to investigate development drugs (Section 1.8.2.1) and these data have been used in decision making processes resulting in compounds being rejected or chosen for further development [13, 14]. More recently, microdosing has been utilised in more specific study designs, such as the detection of polymorphic effects (Section 1.8.2.3) and the detection of drug-drug interactions (DDI; Section 1.8.2.4 and Section 1.8.2.5).

This thesis details the design and implementation of two microdosing clinical studies and the subsequent determination of analyte concentrations and PK data. Both studies were designed around novel applications of microdosing. The first was designed to determine whether DDI effects could be detected using cassette microdosing in human volunteers. HPLC and AMS methods for the determination of analyte concentrations in clinical plasma samples were required and these are presented in Chapter 2. The clinical study design, implementation and analyte plasma concentration and PK data are presented in Chapter 3. The second clinical study was an investigation of the feasibility of combining an imaging study (using positron emission tomography) and a conventional

microdosing study. The imaging study is not of concern in this thesis, rather the PKs obtained. The primary objective for the work presented here was to determine a method for the quantification of enantiomers after administration of a chiral compound dosed as a racemic mixture. Methods for chiral HPLC and AMS analysis were required and these methods are detailed in Chapter 4. Subsequent analysis of clinical plasma samples and determination of PK parameters of enantiomers is detailed in Chapter 5.

1.2 Drug development

The drug development process is traditionally divided into a number of discrete phases, including discovery and pre-clinical analysis, through to the several phases of clinical trials, and a brief overview of each phase is given in Sections 1.2.1 – 1.2.6. In practice, these phases can overlap and although there is no specific pathway that a drug will follow in development, these phases are useful in describing the development process [2].

Before a drug can be registered, mandatory data are required by the various regulatory authorities throughout the world and these data are collated throughout the stages of drug development. Once an NCE has been identified for development it will undergo pre-clinical testing (Section 1.2.1) followed by several phases of clinical drug development (typically phase 1 to phase 3, and sometimes phase 0, Section 1.2.2 – 1.2.5), followed by post-marketing surveillance studies (phase 4, Section 1.2.6). Animal models are used in pre-clinical testing; however, humans are only permitted to participate in phase 0 through to phase 4 studies, once sufficient pre-clinical data is available to ensure the compound can be safely administered to volunteers at specific doses. Participants may be patients or healthy human volunteers, and although females may be enrolled in clinical studies, the majority are carried out using male volunteers [2].

1.2.1 Pre-clinical development

Pre-clinical development primarily concerns the assessment of the safety, pharmacology, toxicity and genotoxicity of an NCE prior to its first administration to humans. These tests are normally performed using *in vitro* or in animal models. There are a number of pre-clinical tests which must be completed prior to the administration of the drug to humans [2].

1.2.2 Phase 0

Phase 0 studies (or microdose studies) can be performed with only limited pre-clinical safety data, due to the administration of doses much lower than those intended for therapeutic use [15]. Due to the exposure of the volunteer in a microdosing study to relatively small amounts of test compound, a complete toxicology package is not required prior to its implementation [9]. For example, it is often possible to minimize pre-human *in vivo* testing to a single dose, two week toxicity study in the rat [9, 16]. This is in contrast to a regular phase 1 study that requires a more lengthy study, including at least two species. The inclusion of microdosing studies allows identification of PK data at a much earlier stage of the drug development process than was previously possible with reduced costs [17]. Microdosing can be more costly and time consuming than traditional scaling models and is often only applied when there are concerns around the reliability of these models or where PK properties are key to the continued development of an NCE.

1.2.3 Phase 1

Phase 1 studies are undertaken to determine the maximum tolerated dose (MTD), PK, pharmacodynamic (PD) and food effects. These studies are typically carried out in small numbers of healthy human volunteers (approximately 6-12) [2]. Prior to the commencement of a phase 1 study in Europe, a clinical trials application (CTA) must be submitted to the relevant regulatory authority. The CTA includes a summary of pre-clinical data (and information obtained in phase 0 where available) and highlights potential risks to study volunteers [2]. In the US, the equivalent document is an Investigational New Drug (IND) application

[2]. Approval of these documents by the relevant regulatory body is required prior to commencement of a phase 1 study.

1.2.4 Phase 2

Phase 2 studies are performed on limited numbers of patients (typically 100-300) and are the first trials which assess the efficacy of the NCE in treating the target disease [2]. Polymorphisms, food-drug and drug-drug effects are all examined during phase 2 [2].

1.2.5 Phase 3

Phase 3 trials are performed using large numbers of patients (typically 100s to 1000s) and often take place in more than one country. During phase 3 trials, the NCE may be compared to a placebo, or if available a currently marketed drug, and these are normally double-blind studies. Double blind studies are those where neither the physician nor the patient is aware of whether it is the placebo or the drug that is being administered [2]. Efficacy in treating the target disease is a major focus in phase 3 studies.

1.2.6 Phase 4

Although the drug has undergone rigorous testing in phase 3, the numbers of subjects are much smaller than those who will be exposed to the drug post-approval. If adverse effects are observed after its release in a wider and more diverse population of patients, the drug may have to be withdrawn [2]. A recent example of a withdrawal of this type is sitaxentan, which was prescribed for pulmonary arterial hypertension. This drug was found to cause unpredictable serious hepatic toxicity, including one fatal case on the UK in 2009 and two cases from clinical trials in India and the Ukraine in 2010. In December 2010 the drug was withdrawn for worldwide usage by the license holder [18].

1.3 Drug metabolism

Drug metabolism is the study of the processes (mostly enzymic) which result in the formation of drug metabolites and which become the main elimination pathway for most drugs. The processes are usually described as being divided into four phases: absorption, distribution, metabolism and elimination (ADME). This process may also apply to a range of chemical substances entering the body, known generically as xenobiotics. In this case, it is assumed that the xenobiotic is a prescribed drug.

Following the oral administration of a drug, absorption occurs into the gastrointestinal (GI) tract, the surrounding capillaries and the hepatic portal vein. Intravenous administration results in the drug entering the systemic circulation directly (Figure 1).

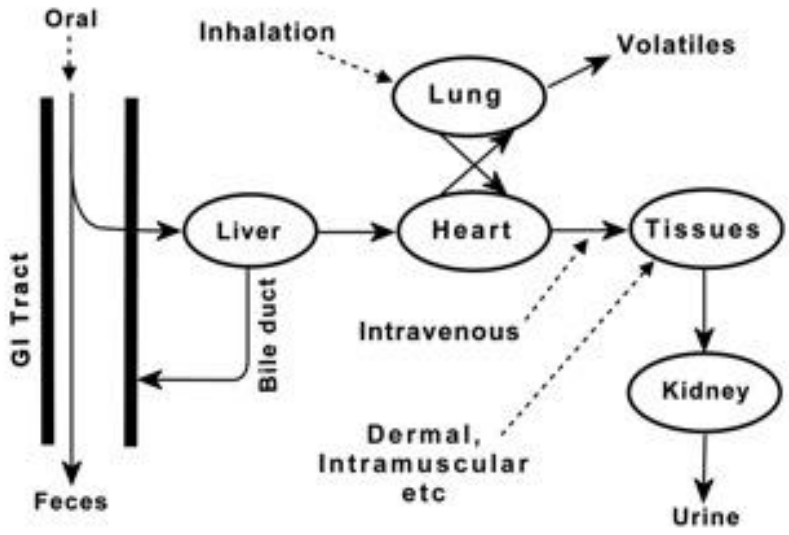

Figure 1: Schematic showing the main routes of drug elimination (reproduced with the permission of the author [19]).

The hepatic portal vein transports the drug to the liver where it either enters the systemic circulation or the bile [19], largely dependent upon its molecular weight. Absorption is followed by the reversible distribution of the drug into tissue where metabolism of the drug may occur. Enzymatic metabolism or biotransformation is responsible for converting the drug into a hydrophilic

metabolite which is more readily excreted into bile or urine than the drug [20]. The majority of metabolic mechanisms fall into one of three categories, phase I, phase II and phase III reactions [21].

1.3.1 Phase I reactions

Phase I reactions include oxidation, reduction, hydrolysis and rearrangement reactions (Figure 2 – Figure 5).

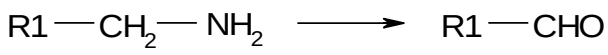

Figure 2: Oxidation reaction [19].

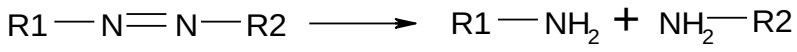

Figure 3: Reduction reaction [19].

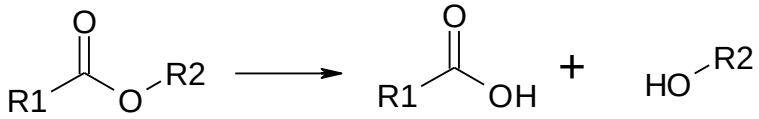

Figure 4: Hydrolysis reaction [19].

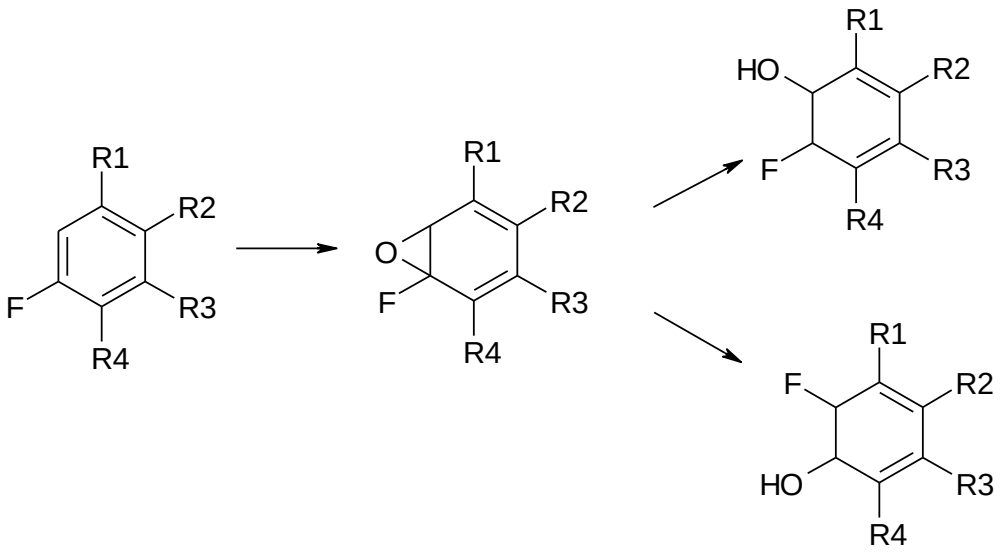

Figure 5: Rearrangement reaction [19].

Phase I reactions are mediated by a wide range of enzymes including the Cytochrome P450 enzymes (Section 1.5), which are largely responsible for the metabolic clearance of drugs. Following oral absorption, a drug enters the liver via the hepatic portal vein where it can be metabolised, resulting in the drug and metabolites reaching the systemic circulation. This effect is known as first-pass metabolism. An example of a drug that undergoes extensive first pass metabolism is the benzodiazepine midazolam. Following oral administration, midazolam is hydroxylated by the enzyme CYP3A4 (Section 1.5.6) in the GI tract and the liver, resulting in a significantly lower amount of midazolam reaching the circulation than was initially administered [19].

1.3.2 Phase II reactions

Phase II reactions are generally conjugative processes. They occur when active groups either inherent to a drug or formed as a result of a phase I reaction, react with large water soluble compounds prior to excretion [19]. Conjugation with sugars, amino acids and glutathione are examples of phase II biotransformations [19] (Figure 6).

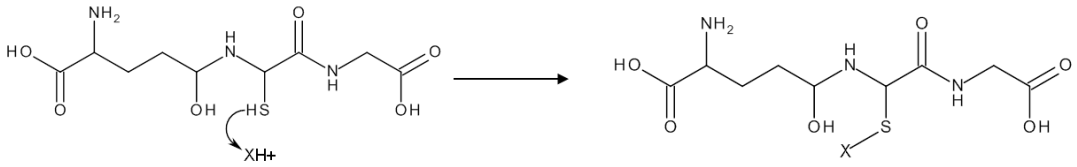

Figure 6: Conjugation of a drug or a product with glutathione [19].

1.3.3 Phase III reactions

Phase III reactions involve further metabolism of products of phase II reactions. An example is the metabolism of glutathione conjugates to N-acetylcysteine, commonly known as mercapturic acid (Figure 7).

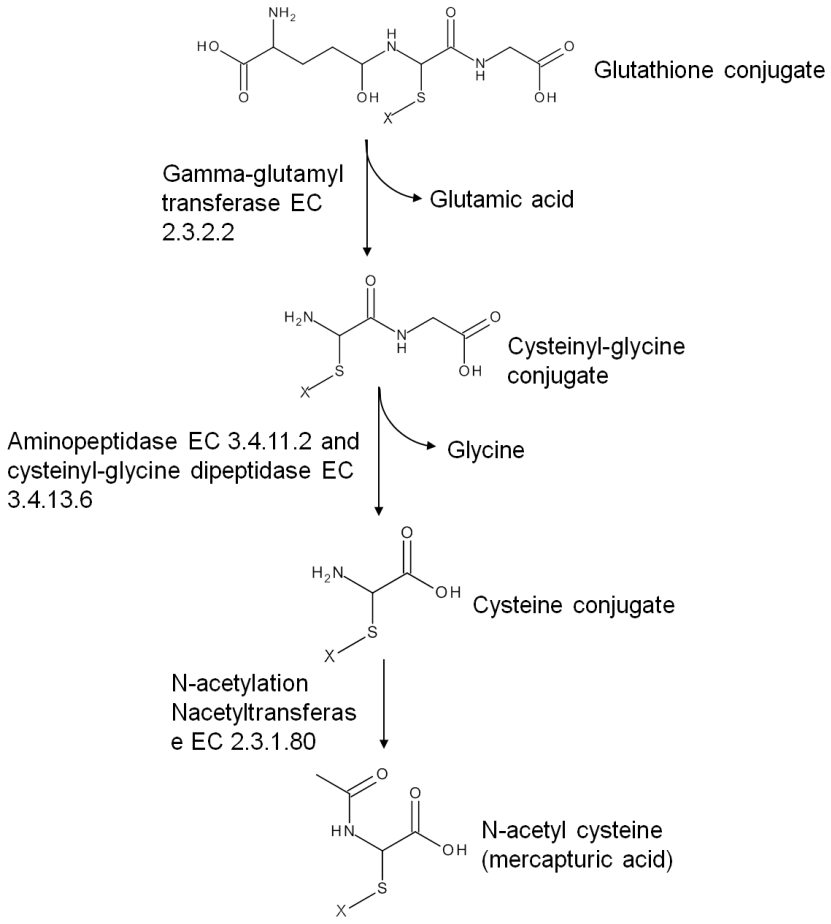

Figure 7: Schematic of the glutathione pathway [19].

1.3.4 Elimination

Another important mechanism removing drugs from the body involves transporters such as P-glycoprotein (P-gp). P-gp is an efflux pump that prevents water-soluble products of metabolism and un-metabolised drugs from entering cells, resulting in their removal from the body (Section 1.6). Fexofenadine is an example of a drug that is excreted via a transporter mechanism [22]. Fexofenadine undergoes very minimal metabolism, with unchanged fexofenadine being the major circulating component [23].

1.4 Pharmacokinetics

Pharmacokinetic (PK) parameters are mathematical descriptions of the systemic fate of a drug from its administration to the point of elimination [19]. Typically, post-dose drug concentrations are determined in plasma samples collected at various time points post-dose. The data are plotted to construct a concentration-time curve, which is used to determine PK parameters. PK parameters that are pertinent to this thesis are summarised below:

C_{max} is the maximum drug concentration reached after administration. The units for C_{max} are typically mass concentration per volume, for example pg of drug per mL of plasma [19].

t_{max} is the time at which C_{max} is reached and is expressed in units of time, commonly h [19].

The elimination half-life, $t_{1/2,}$ is described as the time taken for the drug concentration to fall by one half and is determined from the slope of the drug concentration – time curve during the elimination phase [19].

$AUC_{0\text{-}t}$ is the area under the drug concentration – time curve from time zero to time t, where t is a given time-point, often the last measurable sample. Typical units are h.ng/mL [19].

$AUC_{0-\infty}$ is the area under the drug concentration – time curve from time zero extrapolated to infinity. Typical units are h.ng/mL. The higher the percentage extrapolation from the AUC_{0-t} to the $AUC_{0-\infty}$, the less robust the value for $AUC_{0-\infty}$ becomes. As a general guide, extrapolation which is much greater than 20% is a sign that that extended sample collection times may have been appropriate [19].

F represents the fraction of the drug absorbed or its absolute bioavailability and is calculated using Equation 1 [19].

$$F = \left(\frac{AUC_{EV}}{AUC_{IV}}\right)\left(\frac{Dose_{IV}}{Dose_{EV}}\right) \qquad \textbf{Equation 1}$$

Where: EV = extra-vascular and IV = intravenous

F is a ratio from zero to 1, where zero represents a drug that is not bioavailable and 1 is a drug that is 100% bioavailable. F may also be expressed as a percentage (F%).

CL describes the clearance of the drug. The clearance is the volume of plasma from which the drug is irreversibly removed per unit time, and is expressed in units of volume per unit time, typically L/h [19]. CL is calculated following an intravenous dose.

V is the volume of distribution, and describes the apparent volume of plasma accounting for a given concentration of the drug at equilibrium. This parameter is calculated following an intravenous dose, and typically has units of L or L/kg body weight [19].

1.5 Cytochrome P450 (CYP)

Cytochrome P450 (CYP) is responsible for the metabolism of over 85% of currently marketed drugs [20]. When discovered, the P450 or CYP enzymes were named as they were observed to absorb UV light at 450 nm when undergoing reduction and binding to carbon monoxide [24]. Although the name P450 has remained, their classification is now based on the DNA sequence of the

relevant gene. CYPs are categorized by a family and a subfamily notation (Figure 8). Following the family number is a letter denoting the subfamily and finally a number, which defines the gene number. For example, an individual enzyme numbered 2 and belonging to subfamily A within the family CYP1 is named CYP1A2 [25].

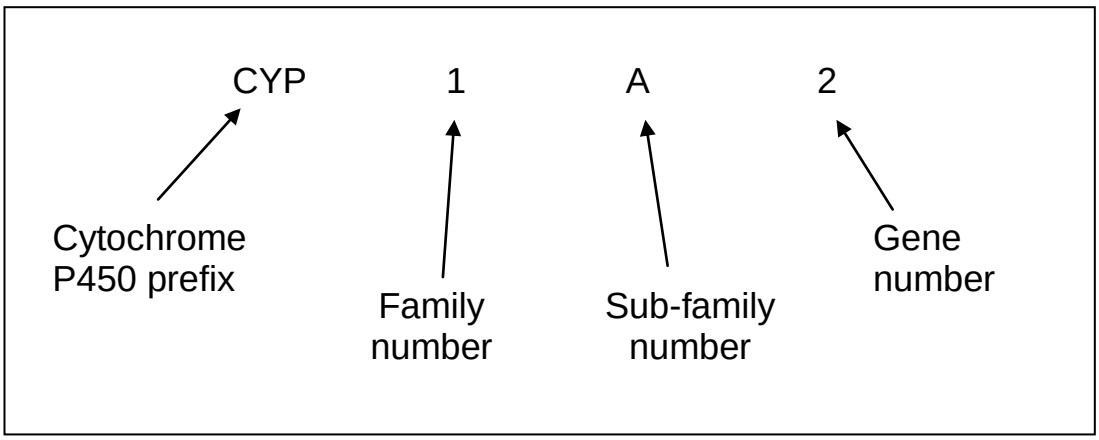

Figure 8: Cytochrome P450 nomenclature.

Enzymes which show greater than 40% amino acid sequence homology are designated the same family number. Where two or more subfamilies exist, enzymes that show greater than 60% homology are allocated the same subfamily number. The gene number is assigned on an incremental basis [26]. CYP enzymes are membrane bound and are located mainly in the endoplasmic reticulum with fewer in the mitochondria. They are prevalent in the major organs, particularly the liver and the intestinal epithelia [26]. The most commonly recognized CYP mechanism in the metabolism of a drug is the oxidation of a substrate in the presence of oxygen leading to the formation of a molecule of water and a metabolite of the drug [20]. Human CYP enzymes may be inhibited or induced by drugs, dietary supplements, food and environmental effects. The major CYPs and some substrates, inducers and inhibitors are summarised in Table 1. CYP3A4 and CYP2D6 are responsible for the metabolism of the largest proportion of currently marketed drugs, with approximately 40% being metabolised by CYP3A4 and 25% by CYP2D6 [20].

Table 1: Examples of CYP enzyme substrates, inhibitors and inducers.

Enzyme	Inducers	Inhibitors	Substrates
CYP3A4	rifampin [26], phenytoin [20], phenobarbital [27], St Johns wort [28]	fentanyl [29], St Johns wort [30, 31], testosterone [32], ketoconazole, grapefruit juice [26, 33]	midazolam, triazolam, erythromycin, nifedipine [26], cyclosporine [28]
CYP2D6	rifampin [34]	quinidine, ritonavir [26], hyperforin, omeprazole [35]	debrisoquine, dextromethophan, metoprolol [26]
CYP2C9	rifampin [36]	fluconazole, phenylbutazone, [36], sulphaphenazole [26], fluvoxamine [37], ketoconazole [38]	fluoxetine, losartan, tolbutamide, *S*-warfarin [36], phenytoin [26]
CYP2C19	St John's wort [39], ginkgo biloba [33]	fluvoxamine [40, 41], fluoxetine [26, 40]	[1]mephenytoin[32], proguanil, omeprazole [42], diazepam, imipramine [26]
CYP2E1	St John's wort [43], ethanol [44]	disulfiram [45], 4-methylpyrazole [20]	chlorzoxazone [46], paracetamol [47]
CYP1A2	[2]omeprazole, cigarette smoke [26]	fluvoxamine [48], α-naphtholone [20], furafylline [26]	propranolol, caffeine, theophylline, tacrine [26]

[1] not suitable for poor metabolisers, [2] dose dependent inducer

1.5.1 CYP Inducers

The induction of a CYP enzyme results the increased metabolism of the inducer (also known as auto-induction) or of a co-administered substrate. This effect results in increased clearance rates and hence an altered PK profile. The induction of CYP has been found to be largely due to a process involving RNA and transcription factors [30], where ligand activation leads to over expression of CYP3A4. An example is the induction of CYP3A4 by binding to the pregnane X receptor (PXR). Many xenobiotics bind to PXR which is ligand activated, inducing synthesis of CYP3A4 [30].

The induction of an enzyme responsible for clearance of xenobiotics may be beneficial or potentially undesirable, depending on the circumstances. For example, St John's wort is a non-prescription herbal remedy often administered for depression and induces CYP3A4. Cyclosporine is an immune suppressant used to prevent transplant rejection after surgery. Co-administration with St John's wort leads to enhanced cyclosporine metabolism resulting from CYP3A4

induction via St John's wort. Insufficient plasma cyclosporine levels result, which can have serious implications including rejection of the transplanted organ [28].

1.5.2 CYP Inhibition

CYP inhibition leads to a decrease in the activity of an enzyme and is generally a more rapid reaction than induction. If the metabolism of a drug is inhibited, the plasma concentrations of the drug can reach dangerously high levels, particularly after repeat dosing. Examples of the different types of inhibition are summarised in Sections 1.5.2.1 – 1.5.2.3.

1.5.2.1 Competitive CYP inhibition

Competitive inhibition occurs when the drug and the inhibitor have similar reversible affinities for CYP active sites. Substrates are normally metabolised to a molecule with reduced affinity for the active site. Owing to its stronger binding action, an inhibitor blocks substrate from the active site, reducing metabolism of the substrate. Binding to the active site is also concentration dependent, hence if the inhibitor concentration is low, substrate concentration may be increased to counteract the inhibitory effect [26]. Azoles are P450 inhibitors; ketoconazole is a very potent competitive inhibitor of CYP3A4 [49, 50].

1.5.2.2 Non-competitive CYP inhibition

Non-competitive inhibition involves the active site and the binding of an inhibitor to an allosteric site. Binding of the inhibitor causes the active site to be altered and substrate-active site binding decreases [26]. Examples of non-competitive inhibitors are hyperforin (potent *in vitro* inhibitor of CYP2D6) and omeprazole (potent *in vivo* inhibitor of CYP3A4) [35].

1.5.2.3 Mechanism-based CYP inhibition

Mechanism-based inhibition generally follows the same principles as competitive inhibition, but involves the covalent binding of a metabolite to the active site [26]. In addition, mechanism-based inhibitors may also occupy an allosteric site in CYP and therefore may also be classed as non-competitive inhibitors [35]. Mechanism-based inhibitors such as constituents of grapefruit can damage an enzyme to such an extent that it no longer functions (also known as suicide inhibition). The damage can take several days to repair, as the enzyme must be re-synthesised before returning to its normal function [35].

1.5.3 CYP polymorphisms

A polymorphism occurs when more than one genotype is present in a population for a particular enzyme and is one of the major causes of inter-individual variation in drug metabolism. Genetic polymorphisms of CYP enzymes result in groups within the population that differ in their ability to carry out biotransformation reactions and are generally caused by gene mutations [51]. The first CYP polymorphism was discovered in the 1980s during a study of the metabolism of mephenytoin. This anticonvulsant drug is enantiomeric and the *S*-isomer is more rapidly metabolised than the *R*-isomer. The pathway for *S*-warfarin was confirmed to be polymorphic [52] and has since been determined to be due to a CYP2C19 polymorphism. CYP2C19 and CYP2C9 are especially prone to such polymorphisms [52]. The specificity of CYP enzymes varies from species to species. Human CYP are of specific interest in the work on DDIs presented here and CYPs that are particularly relevant to this thesis are examined in Section 1.5.4 – Section 1.5.6.

1.5.4 CYP1A2

CYP1A2 is highly expressed in the liver with the level of expression varying from species to species. In humans, CYP1A2 accounts for approximately 13% of active CYP enzymes in the liver and is responsible for the metabolism of approximately 4% of drugs currently on the market, including propranolol, caffeine and theophylline [53, 54]. The structure of CYP1A2 is considered to be

such that only planar structures may occupy the binding site [20, 26]. It does not have an obvious preference for acidic or basic molecules, as is the case with some other CYPs [26]. CYP1A2 may be induced by the diet, in particular on ingestion of cruciferous vegetables and char-grilled red meat [55, 56], environmental factors such as cigarette smoke, and several marketed drugs. Induction of CYP1A2 can result in reduced plasma concentrations of drugs that are metabolised by it, such as the antipsychotic drugs olanzipine and clozapine [57]. An example of the mechanism-based inhibition of CYP1A2 is by furafylline, a structural analogue of theophylline, which results in the decreased metabolism of caffeine [26, 58]. Fluvoxamine is another well documented potent inhibitor of CYP1A2 and causes increased caffeine concentrations on co-administration, even at low doses (10-20 mg), due to reversible inhibition of CYP1A2 [41, 59].

1.5.5 CYP2C9

CYP2C9 is responsible for the metabolism of approximately 15% of currently marketed drugs including fluoxetine, tolbutamide and *S*-warfarin [36]. Approximately 20% of hepatic CYP content is represented by CYP2C9 [60]. Substrates are generally weak acids with pK_a values ranging from 3.8 – 8.1 [26]. Their interaction with CYP2C9 is due to electrostatic interactions between the electronegative substrate and the electropositive enzyme [26]. CYP2C9 is induced by several drugs, the mechanisms being complex and involving at least three known nuclear receptors: glucocorticoid (GR), PXR and constitutive androstone receptor (CAR). The induction of CYP2C9 by rifampin, hyperforin (an active ingredient of St John's wort) and phenobarbital has been confirmed to be due to PXR [61]. CYP2C9 has several isoforms, each of which demonstrate different clearance rates for particular compounds, tolbutamide being one example [62]. A total of 33 human CYP2C9 polymorphic variants are known [60]. These polymorphisms have raised particular concern in treatment involving administration of non-steroidal anti-inflammatory agents, sulfonylurea anti-diabetic drugs and oral anticoagulants belonging to the class of vitamin K epoxide reductase inhibitors [60].

1.5.6 CYP3A4

CYP3A4 is the most abundant CYP isoform in the human liver [63] and is responsible for the metabolism of the largest number of drugs currently on the market (approximately 60%) [64]. These include chemotherapeutic drugs, antipsychotics, and benzodiazepines. Substrates for CYP3A4 are generally lipophilic, the majority being neutral or basic [20]. Oxidation reactions are the major route of metabolism, particularly N-dealkylation reactions [20]. The CYP3A4 substrate midazolam has been studied extensively *in vitro* and *in vivo* in investigations of the enzyme activity [65-67]. CYP3A4 is induced by a large number of drugs including carbamazepine [27], phenobarbital [27] and rifampin [20]. There are species differences in the induction of CYP3A4 for example rifampin induces CYP3A4 in humans and the rabbit, but not in the rat [20]. CYP3A4 has been found to be induced by the binding of PXR to xenobiotics (Section 1.5.1) and is susceptible to reversible and irreversible inhibition. Reversible inhibition is often caused by enzyme activation as CYP3A4 converts the drug into a reactive metabolite. An example of a CYP3A4 inhibition with serious consequences to patient health is given in Section 1.7, with ketoconazole being a recognised competitive inhibitor of CYP3A4 *in vivo* [68].

1.6 P-glycoprotein

The membrane-associated efflux pump P-gp was first discovered in cytotoxin-resistant Chinese hamster ovary (CHO) cells in 1976 [69]. P-gp is encoded by the multidrug resistance (MDR) gene, which is also known as ABCB1. The ABC or adenosine triophosphate (ATP) binding cassette proteins transport molecules across extra- and intra-cellular membranes. P-gp is present in almost all barrier tissues [70] and is highly expressed in tumour cells [71] leading to resistance to anti-cancer drugs [72]. Inhibitors of P-gp (Table 2) dramatically decrease the plasma clearance of anti-cancer agents and, consequently, the dose of the anti-cancer agent must often be reduced. P-gp also acts as an efflux transporter at the blood-brain barrier (BBB) [73]. Substrates (Table 2) cover a wide range of chemical classes, and the presence of P-gp in epithelial and endothelial barrier tissues modulates the transport of these compounds. Inhibitors of P-gp fall within the same chemical class as substrates,

and many share the following properties: presence of nitrogen group, aromatic group, planar domains, molecular mass of > 300 Da and positively charged at physiological pH [69].

Table 2: Substrates and inhibitors of P-glycoprotein.

Inhibitors & Modulators	Substrates
verapamil, quinidine, cyclosporine-A [70], ketoconazole [74]	digoxin [70], doxorubicin [69], pravastatin [69], loperamide [69]

1.6.1 P-glycoprotein (P-gp) and absorption of orally administered drugs

For orally administered drugs to be absorbed directly from the GI tract they must first pass through a barrier of enterocytes in the intestine [69]. The poor absolute bioavailability of drugs is often attributed to either first pass metabolism in the liver, limited absorption, or a combination of the two. P-gp controls the rate at which a substrate permeates across intestinal enterocytes into the blood. P-gp can potentially reduce the rate of absorption, and therefore decrease the C_{max} and AUC of an administered drug [70]. The reduction in permeation may also have a secondary effect of increasing intestinal metabolism. P-gp is also expressed in hepatocytes and has the potential to enhance biliary excretion. Inhibition of P-gp may, therefore, increase the amount of substrate which enters systemic circulation [69].

1.7 Drug-drug interactions (DDIs)

The dose of drug must be high enough to be efficacious without causing adverse effects to the patient, effects which in some cases may even be dangerous and potentially life threatening. The appropriate concentration-time profile is determined during the drug development process and is known as the therapeutic window [75, 76]. Circulating drug concentrations remain within the therapeutic window as long as the dose is administered correctly and the circulating levels are not altered by the physiology of the patient. Co-administration of therapeutic agents may induce or inhibit the enzymes responsible for the elimination of the

drug, which can alter the PK and in some cases result in a life threatening effect, known as a drug-drug interaction (DDI). It is not unusual for patients to receive a number of drugs concomitantly, which increases the potential incidence of a DDI. Recent research involving a cohort of over 3000 patients aged 75 and over, found that almost one third were prescribed three or more drugs which were taken along with three or more dietary supplements each day [77]. With the administration of multiple therapies comes increasing risk of undesirable interactions, hence, DDIs are of major concern to the health industry, patients and the medical profession [78].

An example of a serious interaction is that between ketoconazole and terfenadine. Ketoconazole competitively inhibits CYP3A4, which is responsible for the metabolism of terfenadine [68]. A study published in 1993 examined the effect of the co-administered drugs on the QT interval (the time between the start of the Q wave and the end of the T wave in the electrical cycle) of the heart. Of the six subjects participating in the study, only two were able to complete the course. The remaining four received a shortened course due to 'significant electrocardiographic re-polarization abnormalities' [79]. A further study found that terfenadine caused decreased hepatic extraction of terfenadine coupled with significant increase in first pass extraction when dosed with ketoconazole at steady state [50]. Terfenadine was removed from the US market in 1997 [80] due to the toxic effects encountered when co-administered with ketoconazole. Fexofenadine, which is a primary active derivative of terfenadine, is now used as an alternative.

Drug interactions may not always have such serious consequences and can even prove advantageous in drug therapy, and so can be used to the benefit of the patient. For example, the antiretroviral drug saquinavir is administered as a human immunodeficiency virus (HIV) protease inhibitor (PI). PIs generally exhibit poor systemic bioavailability and large numbers of capsules or tablets are often required to be ingested in order to obtain the required therapeutic dose. This can be costly as well as inconvenient for the patient taking the medication. PIs are susceptible to DDIs, which can be used favourably in the treatment of HIV. The simultaneous administration of saquinavir and ritonavir, another PI,

results in up to a 30-fold increase in saquinavir concentrations, allowing reduced doses to be administered [81]. Both of the DDIs described here are due to some extent to the effect of the co-administered drug on the CYP enzyme CYP3A4 (1.4.6), which is responsible for their metabolism. Over the last 15-20 years, the role of the CYP enzymes has been a major focus in DDI studies.

1.7.1 Evaluation of DDIs

Understanding the interaction of an NCE with CYP and transporter systems is an important step in its development. NCEs that are primarily metabolised by one enzyme are vulnerable to the effects of a co-administered drug that is metabolised by the same enzyme. In addition, NCEs that significantly inhibit or induce specific enzymes or transporters may lead to interactions with already marketed drugs. Potential interactions of NCEs with CYP enzymes may be evaluated *in vitro* using hepatocytes, microsomes and expressed human drug metabolizing enzymes [82]. A common approach is to administer the NCE with a substrate whose selection is based on its metabolism being driven primarily by a particular enzyme [83]. Substrates with such specificity are known as probe substrates. DDI studies are normally first performed *in vitro* using cocktails, typically comprising between three and six probe substrates, together with a candidate drug suspected of affecting a particular drug metabolizing or clearance mechanism. During *in vivo* studies designed in the same way, urine and plasma samples may be collected and analysed to determine probe substrate concentrations over time. If the test drug affects the activity of a drug metabolizing enzyme or transporter, this will be reflected by changes in the PK of the probe substrate. It is vital that probe substrates dosed within a cocktail do not interact with each other and the combined use of the probes must be assessed prior to use in DDI studies. Several cocktails have been validated in this way, which include well-established probes that are known to be metabolised by a particular enzyme [65, 84, 85].

1.8 Microdosing

A microdose is defined as the administration of a test compound at less than 1/100th of the calculated pharmacological dose and at a maximum dose of 100 µg to human volunteers [9]. Due to the very small doses administered through microdosing, sensitive analytical techniques are required for the quantification of analyte. Accelerator mass spectrometry (AMS, Section 1.10) and positron emission tomography (PET, Section 5.1) are two highly sensitive techniques utilised in microdosing studies [6]. AMS quantifies drug-related material in biological samples such as plasma, blood and urine and allows PK information to be obtained. PK data obtained after microdose administration are then scaled to predict PK at the therapeutic dose. At the time of the first publication of microdosing data, AMS was the preferred analytical method for obtaining PK data due to the analytical sensitivity of the instrument [6], however in recent years data have been obtained using LC-MS/MS [86, 87]. AMS determines an isotope ratio; hence, the drug must be radiolabelled prior to administration. This is not necessary for studies where LC-MS/MS can quantify drug concentrations with sufficient precision. Although valuable PK data may be obtained in microdosing studies, it is not possible to assess the safety or the efficacy of an NCE via this technique as doses are typically administered at less than 1/100th of the dose required to yield a pharmacological effect [9]. This presents perhaps the biggest uncertainty around microdosing, which is its ability to predict the PK of a pharmacological dose [17]. A growing number of studies examining the predictability of a microdose have appeared in the literature over the last few years (Table 3 and Table 4).

Table 3: Summary of human microdosing data.

Year of publication	Drug	Primary purpose of study	Source
2003	α_{1A}-adrenoreceptor	Proof of concept/PK linearity assessment	[6]
2006	Warfarin	PK linearity assessment	[12]
2006	Midazolam	PK linearity assessment	[12]
2006	Diazepam	PK linearity assessment	[12]
2006	Erythromycin	PK linearity assessment	[12]
2006	ZK-253	PK linearity assessment	[12]
2007/2010	Fexofenadine	Determination of absolute bioavailability & assessment of PK linearity	[23, 87, 88]
2007	Zidovudine	PK linearity assessment	[89]
2009	Diphenhydramine, NB-1 NB-2, NB-3, NB-4	Compound selection & determination of PK	[14]
2009	Nicardipine	Metabolite identification	[86]
2009	IDX899 & IDX989	Determination of PK	[90]
2009	Atenolol, enalapril, losartan	PK linearity assessment	[91]
2010/2011	Acetaminophen (paracetamol)	Determination of PK & metabolite identification/PK linearity assessment	[11, 92]
2011	Clarithromycin	PK linearity assessment	[11]
2011	Sumatriptan	PK linearity assessment	[11]
2011	Propafenone	PK linearity assessment	[11]
2011	Phenobarbital	PK linearity assessment	[11]
2011	Verapamil	PK linearity assessment	[93]
2011	Quinidine	PK linearity assessment	[93]
2011	Atorvastin	DDI study	[94]
2011	Celiprolol / Fexofenadine & Atenolol	Detection of PK differences due to polymorphisms	[95]
2011	Telmisartan	Detection of PK differences due to polymorphisms	[96]
2011	Metformin	DDI study	[97]
2012	PF-4776548	Determination of PK	[13]

Table 4: Summary of animal microdosing data exploring dose linear PK.

Year of publication	Species	Drug	Source
2004	Beagle dog	7-deaza-2'-C-methyl adenosine	[98]
2006	Rat	Tolbutamide	[99]
2006	Rat	Fluconazole	[99]
2006	Rat	MLNX	[99]
2007	Monkey	PHA-XXX	[100]
2008	Rat	Antipyrine	[101]
2008	Rat	Atenolol	[101]
2008	Rat	Carbemazepine	[101]
2008	Rat	Digoxin	[101]
2008	Rat	Metoprolol	[101]

The first AMS microdosing study was reported in 2003 and investigated the PK of an orally active α-adrenoreceptor antagonist, which was administered to six healthy male volunteers at doses of 5, 50 and 500 μg (1.11×10^5 disintegrations per minute, dpm). Drug concentrations were obtained and a linear relationship was observed over the dose range [6]. Due to speculation over the ability of microdosing to predict PK at the therapeutic dose, further studies were performed (Section 1.8.1). The generally accepted criterion for dose linearity in allometric scaling and extrapolation from *in vitro* to *in vivo* data is where data lie within a two-fold range [5, 102]. Although this is a general guide, it should be treated with caution, particularly where the therapeutic window is narrow. In such cases, a two-fold difference may not be appropriate. If a two-fold difference results in the drug no longer being within the therapeutic window, toxic effects or loss of efficacy may result. As discussed by Lappin et al. [11], although allometric scaling uses the comparison of CL, V or F, the peak shape, overall AUC and the C_{max} are also important factors.

1.8.1 Microdosing studies – pharmacokinetic linearity tests

1.8.1.1 Human microdosing studies

Two collaborative studies reported in 2006 and 2011 were designed with the primary objective of assessing dose linear PK after administration of a microdose. The studies were carried out by the consortium for resourcing and evaluating AMS microdosing (CREAM), and the European microdosing accelerator mass spectrometry (AMS) partnership programme (EUMAPP). Data were reported for four compounds administered during the CREAM study: warfarin, midazolam, diazepam and the development drug ZK-253 (donated by Schering-Plough). The EUMAPP project successfully investigated six compounds, fexofenadine (published in 2010 [23]) and a further five marketed drugs, clarithromycin, sumatriptan, paracetamol, phenobarbital and propafenone. Drug concentrations after microdose administration were quantified via HPLC and AMS.

Warfarin was chosen to represent a low clearance acidic drug, whose clearance could not be accurately predicted in humans (*in vivo*) from *in vitro* data. Microdose warfarin data (100 µg) did not show linearity with data obtained after the therapeutic dose (5 mg), consistent with previous observations in rats [12]. When microdose (100 µg) and therapeutic dose (5 mg) data were dose normalised to 1 mg, there was no concordance in the concentration time curves (120 h) [12]. The microdose t_{max} was reached earlier followed by a sharp drop in plasma concentration and a prolonged terminal phase, when compared with the therapeutic dose data. This non-linearity is thought to be due to the low volume of distribution of the drug, its uptake by high affinity, low capacity binding sites and target mediated disposition [12]. The individual enantiomers of *S*- and *R*-warfarin were not quantified in this study, which would have enabled the presence of enantiomeric differences in PK parameters to be determined after microdose administration. Midazolam, diazepam and ZK-253 showed linear PK within a factor of 2 [12] over a 75-fold, 100-fold and 500-fold dose range respectively.

During the EUMAPP study, paracetamol and phenobarbital were administered as a microdose only, due to the large amount of PK data already available. The remaining four compounds were administered as an oral and an IV microdose and as an IV microdose, concomitant with the oral therapeutic dose, to assess disposition kinetics and absolute bioavailability. Determination of absolute bioavailability data has been reported several times using this approach [23, 103, 104] and has become a widely accepted use of the technology [105, 106]. The combination of the two doses precludes classification as a phase 0 microdose study due to the co-administered therapeutic dose. Such studies, classified as microtracer studies, have a different design and regulatory requirements and are typically performed in phase 1. The mass of the intravenous dose in a microtracer study is equivalent to a microdose (maximum of 100 µg) and is administered after administration of an oral therapeutic dose. Systemic concentrations are, therefore, dependent on the mass of intravenous dose and the circulating oral dose. Microtracer studies allow PK data to be obtained using the IV tracer, but under therapeutically relevant conditions. For example, should a particular PK parameter be dose dependent, a difference will be observed between an IV microdose alone vs. that obtained after co-administration of an IV tracer and a therapeutic dose.

Comparison of values for CL, V, V_{ss} and $t_{1/2}$ obtained after IV administration with those obtained after administration of a concomitant IV and oral therapeutic dose (clarithromycin, sumatriptan and propafenone) showed good agreement [11]. C_{max} and AUC data obtained after administration of an oral microdose (100 µg) and an oral therapeutic dose (250 mg, clarithromycin; 50 mg, sumatriptan; 150 mg, propafenone) did not agree as closely, resulting in a difference in derived values for bioavailability [11]. Clarithromycin showed an approximate two-fold increase in bioavailability between the microdose and therapeutic dose, which was attributed to saturation of the CYP3A enzyme or P-gp efflux. This dose-dependent increase in bioavailability had been observed previously, with a higher value being calculated after administration of a 500 mg dose [11] compared with the 250 mg dose. The bioavailability of sumatriptan decreased almost three-fold and whilst it was hypothesised that this may also be due to saturation of a transporter responsible for the uptake of the drug, there was no

evidence to support this. Finally, propafenone saw an approximate two-fold increase in F between the microdose and therapeutic oral dose. Propafenone is known to demonstrate dose dependent PK over the therapeutic dose range due to saturation of first pass CYP2D6, which is observed in the current data [11]. Paracetamol IV and oral microdose PK data and phenobarbital oral microdose PK data were both linear on comparison with literature data over a 14000 and 2400-fold dose range [11]. This was further supported for paracetamol in a second microdosing study published in 2010 [92] where linearity was seen over a comparison range of 5000-fold (Section 1.8.2.2). Data obtained after IV and oral administration of fexofenadine were comparable with data obtained after a therapeutic dose of 120 mg [23]. Fexofenadine was previously administered as a microdose in a similar study and the analytical methodology using LC/ESI-MS/MS was reported. Although linearity between microdosing and clinical profiles were observed, the data were not presented [88]. A follow up study confirmed the findings of Lappin et al. [23], where data were confirmed to be linear over a 600-fold dose range from 100 µg to 60 mg [87].

Subsequent to the two reported collaborative studies, two further microdose studies were performed to investigate dose linear PK. The first confirmed microdose PK data for atenolol, losartan and enalapril (100 µg, 4.44 x 10^6) to be dose linear with therapeutic doses [91]. A second study was performed to investigate the dose dependent non-linear kinetics of verapamil and quinidine. Quinidine and verapamil were orally administered to human volunteers at four doses followed by quantification of verapamil and quinidine plasma concentrations by LC-MS/MS. Quinidine was dosed at 100 µg (microdose) and 1.29, 1.82 and 2.56-fold increases and 1.34, 1.97 and 2.99-fold increases in dose normalized AUCs and C_{max} were observed after administration of 1 mg, 10 mg and 100 mg doses. Verapamil was dosed at 100 µg (microdose), 3 mg, 16 mg and 80 mg, and 1.02, 1.92 and 2.34-fold increases in dose-normalised C_{max} and 1.19, 1.83 and 2.30-fold increases in AUCs were observed after the respective doses [93]. Although some of these parameters only become non-linear when applying the convention of a > 2-fold difference in PK (i.e. at the highest administered dose), there is a clear trend observed between increasing dose and increase in PK parameter. A proposed theory for this was MDR1-mediated

efflux saturation and/or saturation of CYP3A4 in the small intestine. When measuring metabolite concentrations and determining K_m values for production of major metabolites, the authors were able to attribute a dose dependent effect to each of the above [93].

The most recent study reported the microdose administration of zidovudine, a drug approved for the treatment of HIV, to one human volunteer [89]. After administration, zidovudine is rapidly absorbed and passively diffuses into peripheral mononuclear cells (PBMCs) where it undergoes phosphorylation and results in the termination of viral replication. The uptake and phosphorylation of zidovudine is highly variable between patients and has not been found to correlate with either plasma concentrations or extracellular concentrations of zidovudine [89]. After oral microdose administration (520 ng, 2.22 x 10^5 dpm), zidovudine and metabolite concentrations were quantified by UPLC and AMS and were dose linear with previously obtained data over a 1 million-fold range. In addition, the assay was of adequate sensitivity to determine PBMC concentrations of all ZDV related material and therefore able to determine the cell uptake of zidovudine [89].

1.8.1.2 Animal studies

Microdosing has the potential to reduce the use of animals in early clinical development [107]. Animal studies have been useful in corroborating the linearity observed between a microdose and a therapeutic dose. The first, in 2004, examined 7-deaza-2'-C-methyl adenosine in beagle dogs. Total ^{14}C and 7-deaza-2'-C-methyl adenosine plasma concentrations were determined by AMS and LC-MS/MS after administration of 1 mg/kg (37.7 dpm/mg) and 0.02 mg/kg (1212 dpm/mg) oral doses and a 0.02 mg/kg (950 dpm/mg) IV dose. Total ^{14}C measurements obtained during AMS analysis incorporate all drug-related material, including drug and metabolites, hence direct comparison with data for the drug can result in misleading conclusions, as discussed by Lappin et al. [10]. Total ^{14}C concentration data in this study, however, were very close to ^{14}C parent drug concentrations, indicating that the majority of drug-related material circulating in plasma was in fact 7-deaza-2'-C-methyl adenosine [98]. On this

assumption, 7-deaza-2'-C-methyl adenosine and total radioactivity plasma concentration data were compared and linearity in PK data was observed over a 50-fold range [98].

Two further studies involved the administration of a range of compounds to rats with the quantification of plasma drug concentrations by LC-MS/MS. In the first study, tolbutamide, fluconazole and the development drug MLNX were orally administered at 1, 0.1, 0.01, 0.002 and 0.001 mg/kg (tolbutamide), 5, 0.05, 0.005 and 0.001 mg/kg (fluconazole), and 10, 1, 0.1 and 0.01 mg/kg (MLNX) [99]. Tolbutamide and fluconazole concentrations were linear over a 1000 and 5000-fold dose range respectively, which was in agreement with previous studies of dose linear PKs in humans. $AUC_{0-\infty}$ comparisons for MLNX were non-linear in the 1 to 10 mg/kg range, where an approximate 4.2-fold increase was observed [99]. Although the conclusion drawn by the authors was that this information is useful in determining the compounds for which microdosing may be suitable, limited information was provided regarding the properties of the compound. Accordingly, further conclusions regarding the cause of the non-linearity cannot be drawn.

In the second study, atenolol, antipyrine, carbemazepine, digoxin and metoprolol were orally administered at doses of 0.167, 1.67, 16.7, 167 and 1670 µg/kg. The compounds were selected from different classes (I-III) of the Biopharmaceutical Classifications System (BCS), which classifies compounds based on their permeability and solubility (Table 5).

Table 5: Biopharmaceutical Classification System for drug absorption [108].

Class	Solubility	Permeability
I	High	High
II	Low	High
III	High	Low
IV	Low	Low

Four of the five compounds (across BCS classes I-III) demonstrated linearity between AUC and C_{max} data obtained over the 10000-fold dose range. The fifth compound, metoprolol, a BCS class I compound, showed a linear C_{max} response, however the AUC was non-linear. The AUC exposure of metoprolol is known to be low due to its metabolic stability and high liver extraction ratio. This resulted in only a partial PK profile being obtained for the 16.7 µg/kg dose and may account for the non-proportional increases in AUC. The study concluded that although LC-MS/MS was a feasible alternative to AMS for use in microdosing studies it did not have adequate sensitivity to quantify metoprolol levels after administration of lower doses. A final compound, an NCE named PHA-XXX was administered intra-gastrically (IG) at 10 mg/kg as well as a separate microdose at 0.5 µg/kg (20000 times lower). Plasma drug concentrations were obtained by LC-MS/MS analysis and PK found to be dose linear across the two dose ranges [100].

Efforts have been made to determine the cause of non-linearity to ascertain the value of microdosing in early drug development (Table 6).

Table 6: Summary of non-linear pharmacokinetic data.

Drug	Linear within a factor of two	Dose range where non-linearity observed	Dose route	Species	Hypothesis for non-linearity	Source
Warfarin	No	100 µg to 5 mg	Oral	Human	Saturation of tissue binding	[12]
Clarithromycin	No[1]	100 µg to 250 mg	Oral	Human	Saturation of CYP3A4 metabolism or P-gp efflux	[11]
Sumatriptan	No	100 µg to 50 mg	Oral	Human	Saturation of an uptake	[11]
Propafenone	No	100 µg to150 mg	Oral	Human	Saturation of CYP2D6 enzyme	[11]
Verapamil	No	100 µg to 100 mg	Oral	Human	Saturation of MDR1-mediated efflux or CYP3A4 enzyme	[93]
Quinidine	No	100 µg to 100 mg	Oral	Human		[93]
MLNX	No	1 to 10 mg/kg	Oral	Rat	No hypothesis made	[99]

[1]PK data for oral dose are linear within a factor of 1.8, whereas IV data show much closer agreement

In the case of clarithromycin, sumatriptan and propafenone, linear PK data were observed after administration of intravenous doses, whereas oral microdose data for the same compounds showed some degree of non-linearity suggesting that the disposition kinetics are linear [11, 23]. Non-linearity was in all cases hypothesised to be due to saturation of CYP enzymes or transporters (efflux and uptake). This hypothesis was supported by previous data for two compounds (propafenone and clarithromycin) but could not be supported for the third compound, sumatriptan [11]. All of the compounds listed in Table 6 are BCS class I or II compounds [93, 109, 110] with the exception of clarithromycin [110]. The relevance of the classification was explored by Balani et al. [99] in the previously described five compound rat study, where compounds producing linear data crossed the I-III classification. Class I and II compounds are primarily eliminated via metabolism, whereas classification III and IV compounds are primarily excreted unchanged into the urine and bile [109]. Although the data presented here are limited, the majority of compounds that tended towards dose linear PK were class I or Class II compounds. This may suggest that data obtained after administration of a microdose of a class III or IV

compound may be more representative of those obtained after administration of a therapeutic dose, than class I and II compounds, due to the lack of metabolism of the compound. Further studies are required to investigate this further.

The investigations described above have led to researchers further understanding the limitations of microdosing and the technique has seen an increase in use in recent years [15, 16, 105]. Section 1.8.2 focuses on specific applications demonstrating the value of microdosing in drug development, particularly in the selection of drug candidates in phase 0. In addition, the use of microdosing in the detection of polymorphic effects, determination of metabolites and identification of DDIs is also discussed.

1.8.2 Microdosing studies – Further applications

1.8.2.1 Early pharmacokinetics and candidate selection

A 2008 study demonstrated for the first time, the use of microdosing in obtaining early PK data for several NCEs by a pharmaceutical company using microdosing for candidate selection. Diphenhydramine, a marketed antihistamine, was administered to human volunteers. NBI-1 a comparator drug, previously administered in a phase 1 trial, and three candidates for further development, NBI-2, NBI-3 and NBI-4, each under development for the treatment of insomnia were also administered. A microdose of each ^{14}C-labelled compound (100 µg, 4.44 x 10^5 dpm) was administered orally and then IV to four healthy human volunteers in a randomized two period study design. Plasma concentration-time curves were obtained after HPLC and AMS analysis and PK data obtained after microdose administration were linear with respect to previously published C_{max} and AUC data for diphenhydramine (50 mg dose) and NBI-1 (10 mg). Examination of PK data and mechanistic information led to NBI-2 being selected as the most suitable drug candidate, due to its high bioavailability and low clearance, essential parameters for an insomnia drug [14].

The microdose studies of NCEs IDX-899 and IDX989 [90] and PF4776548 [13] were published in 2009 and 2012 respectively. Data obtained after oral and IV IDX-899 and IDX-989 microdose administration (100 µg, 2.22 x 10^5 dpm),

followed by HPLC-AMS analysis of plasma and urine, showed rapid and extensive drug absorption, extensive metabolism and absolute bioavailability of >60%. IDX-899 plasma AUC data were compared with those obtained after administration of doses of up to 1200 mg, and were found to be linear, as were urine excretion data. IDX899 was taken forward for clinical development, although reasons for the choice of this specific compound are not given in the publication [90].

A second study determined plasma PF4776548 concentrations by HPLC-AMS to be very low after oral administration, with a >100-fold increase observed in the C_{max} obtained after an IV dose. The data were used in order to make a rapid decision regarding PF4776548 resulting in the termination of further development shortly after completion of the microdosing study. This decision was due to an inappropriate PK profile, particularly the low systemic bioavailability of the compound after oral administration [13].

1.8.2.2 Metabolite identification

In recent years there has been growing interest in the safety of drug metabolites resulting in the issue of the FDA Guidance for Safety Testing of Drug Metabolites (MIST) and International Conference on Harmonisation M3 (ICHM3) [111, 112]. The former makes the recommendation that prior to phase 3 trials, a report must be made of any metabolites which have a systemic exposure of > 10% of the parent drug, with the latter recommending that metabolite exposure must not be greater than 10% of the entire exposure [92]. A study was reported in 2010, which was the first to present metabolite data after microdose administration. The PK of the established drug acetaminophen (paracetamol) and its metabolites were examined [92]. Although acetaminophen is a widely available drug, this was the first reported clinical study to investigate the PK of its metabolites. After oral microdose administration (100 µg, 4.262 x 10^5 dpm) of ^{14}C-acetominophen to healthy human volunteers, three metabolites were identified in plasma, and seven in urine. Recovery in the urine was approximately 96% with the remaining 4% being present in faeces after 24 h. The two major metabolites identified in urine, acetaminophen-glucuronide and

acetaminophen 4-*O*-sulfate both accounted for less than 10% of the total radioactivity and satisfy the requirements of MIST and ICHM3 [92].

Nicardipine was the second drug for which metabolite data were obtained after microdose administration. A 2008 publication reported the development of an LC/MS-MS assay for quantification of nicardipine in plasma and also metabolite determination by linear ion trap fourier transform ion cyclotron resonance mass spectrometry (LIT-FTICRMS) [86]. These methods were applied to samples obtained after administration of nicardipine (100 µg) and six metabolites were detected in human plasma by LC/MS-MS and reported in 2011. Using the LIT-FTICRMS assay, metabolite structures were elucidated and concentration-time profiles determined up to 8 h [113]. As well as supporting the identification of metabolites after microdose administration, this report highlights the sensitivity capabilities of an analytical method other than HPLC and AMS. The analytical techniques presented have an advantage over AMS, the capability to identify metabolites based on their structure and mass, which is not possible with AMS.

1.8.2.3 Detection of polymorphic effects

Two papers published by Ieiri et al. in 2011 [95, 114] examined the use of microdosing in the detection of polymorphic differences between individuals using celiprolol, atenolol, fexofenadine and telmisartan as test compounds. The absorption of celiprolol has been found to decrease on concomitant ingestion of grapefruit juice [95]. Inhibition of organic anion transporting polypeptide (OATP) uptake by grapefruit juice is suggested to be the cause, in particular the inhibition of the OATP2B1 isoform, encoded by the SLCO2B1 gene. A similar response is observed on co-administration with fexofenadine [95]. Similarly, orange juice reduces the AUC of atenolol, which was also hypothesised to be an OATP2B1 substrate. Thirty male volunteers were selected, and each volunteer was administered a single microdose (period one) containing celiprolol (37.5 µg), fexofenadine (30 µg) and atenolol (30 µg). In period two, the microdose was concomitantly administered with a therapeutic dose of celiprolol (100 mg). In period three, grapefruit juice (200 mL) was administered twice daily for two

days, followed by administration of the microdose. A further 400 mL of grapefruit juice was ingested at 0.5 and 1.5 h after the microdose administration. Each drug was quantified by LC-MS/MS in plasma samples collected post-dose.

The results showed that the contribution of the SLCO2B1 polymorphism in celiprolol PKs was associated with differences in PK profiles between individuals after administration of the therapeutic dose. These differences were not observed after microdose administration. The celiprolol PKs obtained after microdose administration were not comparable to therapeutic dose PKs. It was hypothesised that this difference was due to saturation of transporters responsible for the efflux of celiprolol after therapeutic dose administration. In addition, data obtained from the fexofenadine and atenolol microdose gave further information regarding the involvement of specific transporters. Although the data obtained were useful in the study of celiprolol and the impact of polymorphic differences in individuals, these effects could not have been predicted from the microdose data alone in this case. Further work was recommended to be carried out to determine the ability of a microdose to determine polymorphic effects [95].

In a separate study, the inter-individual variability in telmisartan plasma concentrations and dose dependent PK differences after oral administration were examined. The role of the OATP1B3 in hepatic uptake was investigated, specifically the involvement of SLC01B3 and UGT1A polymorphisms, by administration of a microdose (100 μg) alone and concomitantly with a therapeutic dose (80 mg) of telmisartan in the same subjects. Telmisartan and telmisartan glucuronide concentrations were determined by LC-MS/MS and dose normalised plasma concentration-time curves were found to differ between the two doses, particularly in the absorption phase. No inter-individual differences were observed for either dose for individuals with SLC01B3 polymorphisms. Significant variability was observed between individuals with UGT1A3 polymorphisms, and this was observed after microdose administration as well as the therapeutic dose. While the specific involvement of SLCO1B3 polymorphisms requires further investigation, the study showed the ability of a microdose to probe polymorphic effects [115].

1.8.2.4 Microdosing in DDI studies

The first DDI microdosing study was reported in 2011 with the primary objective of investigating the ability of a microdose to detect a DDI in human volunteers [116]. Metformin, used in the treatment of type 2 diabetes mellitus, was administered to eight healthy human volunteers as a microdose (100 µg) and following a 7 day washout period, a therapeutic dose (250 mg) was administered followed by metformin quantification in urine and plasma samples. Following a further washout period the same subjects were administered identical doses, with concomitant oral administration of pyrimethamine (50 mg). Pyrimethamine is a potent multidrug and toxin extrusion inhibitor and slightly delayed the elimination of metformin. The amount of metformin excreted in urine was reduced, with significant difference in renal clearance observed for both the microdose and therapeutic dose. The C_{max} and $AUC_{0\text{-}12h}$ for metformin were significantly greater on co-administration of pyrimethamine than for the metformin dose alone. No significant increase was observed in the microdose data (alone and with pyrimethamine). This was attributed to the more marked decrease in renal clearance observed in the therapeutic dose. It should be noted that although an overall trend was observed, the inter-subject variability was quite large, with some subjects showing no marked increase in AUC and C_{max} (in some cases, a slight decrease was observed). Nevertheless, clear overall differences were determined, which supports the concept of the ability of a microdose to detect changes in PK on co-administration of a known inhibitor [97].

1.8.2.5 Cassette microdosing and DDI studies

2011 saw the publication of the first cassette microdosing study designed to determine DDIs, specifically the role of CYP3A4 and OATP in the hepatic clearance of atorvastatin [117]. A cassette microdose consisting of atorvastatin, pravastatin (a substrate of OATP) and midazolam (a substrate of CYP3A4) was administered to eight healthy human volunteers (33 µg dosed per compound, total dose 99 µg). The cassette microdose was administered alone (phase one) to determine the PK of each compound and co-administered (phase two) with the OATP inhibitor rifampicin (600 mg, oral dose). In a third phase (phase three), the cassette microdose was co-administered with the CYP3A4 inhibitor itraconazole (200 mg IV dosed one hour prior to cassette microdose administration).

Atorvastin, 2-hydroxyatorvastatin (metabolite), pravastin and midazolam concentrations in plasma were determined by LC-MS/MS. PK parameters obtained from these measurements showed that atorvastatin and 2-hydroxyatorvastatin plasma concentrations obtained in phase two were higher than phase one, therefore increasing on co-administration of rifampicin. Metabolite concentrations were decreased on co-administration of itraconazole however no significant change in atorvastin concentrations were observed (phase three). The atorvastatin $AUC_{0\text{-}10h}$ only saw a significant increase during the phase two rifampicin treatment and was unchanged during phase three. The findings were identical for pravastatin. Conversely, midazolam concentrations were only altered by itraconazole and not rifampicin. These data were used to determine that hepatic uptake via OATP is dominant in the hepatic elimination of atorvastatin, after microdose administration and opens up the possibility of identifying rate determining processes for other compounds after microdose administration.

The publication did not compare microdose data with those available in the literature, which would have supported the reliability of the control data; however, the findings do support the use of a cassette microdose. There is no clear evidence to suggest interactions took place between the drugs themselves,

and the low levels administered should prevent such an event from occurring [83]. One further observation is the failure to administer the cassette microdose after repeat dosing of rifampicin and itraconazole, and therefore at steady state conditions. This is briefly discussed by the author in the case of itraconazole, which was administered IV instead of orally to avoid exposure of intestinal CYP3A4 to itraconazole. It is also noted that midazolam undergoes greater increases in plasma concentrations on repeat administration of itraconazole, due to accumulation, which leads to mechanism-based inhibition. In addition, previous studies had reported an increase in the AUC of pravastatin on co-administration of itraconazole, which was not observed in this study. The previous studies both included a repeat daily dose of itraconazole, for 4 days prior to administration of pravastatin [118, 119]. The half-life of itraconazole is reasonably long at approximately 24 h, however to make a direct comparison repeat dosing would be more appropriate.

The microdosing literature discussed here focus heavily on the ability of a microdose to predict the PK of a compound when administered at a therapeutic dose [11, 12]. More recent studies have focused on particularly problematic compounds, where dose linearity is suspected to be an issue, particularly around enzyme and transporter saturation [93]. In addition, the use of microdosing in metabolite identification has been reported and initial investigations into the ability to detect polymorphisms and DDIs using a microdose have been carried out. Microdosing studies have also allowed key decisions to be made in the further development of NCEs [13, 14, 90].

1.9 Accelerator mass spectrometry

Accelerator mass spectrometry (AMS) is a highly sensitive technique, which was developed in the 1970s for radiocarbon dating [120, 121]. AMS determines the isotope ratio of a sample and has been used in human microdosing studies [11, 12, 23, 89], IV tracer and mass balance studies [103, 122], where the concentration of an analyte is determined after the administration of a ^{14}C-labelled drug (Section 1.8). A schematic of a tandem pelletron accelerator mass spectrometer is shown in Figure 9 [121]. Prior to analysis by AMS, the sample

must be converted to graphite and pressed into an aluminium cathode (Section 1.9.2). The cathode is placed into a sample wheel (a) containing up to 127 samples, which is subjected to the MC-SNICS ion source (b). The ion source consists of a caesium oven, a heated ionizing surface and an extractor, all of which are under high vacuum conditions (10^{-6} to 10^{-9} Torr, where 1 Torr is 13.595 kg/m^2).

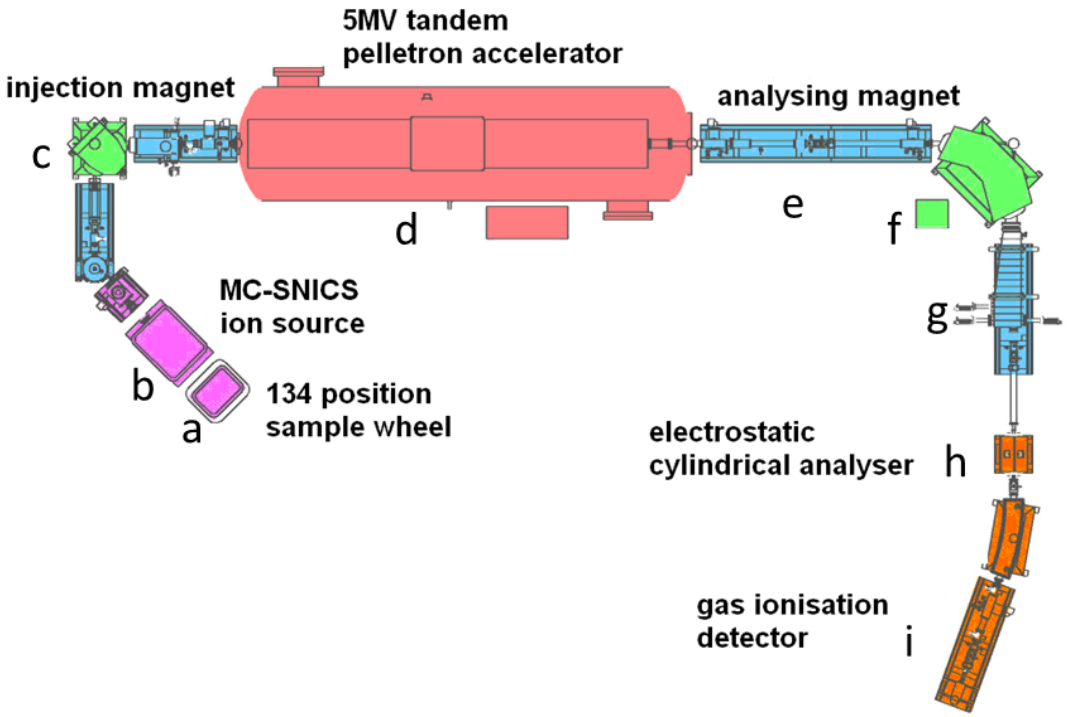

Figure 9: Schematic of a tandem pelletron accelerator mass spectrometer [121].

Caesium vapour from the oven is ionised, which results in Cs^+ ions being accelerated towards the cathode where carbon atoms sputter negative ions. The negative ions are extracted by plates that are held at a voltage several thousand times more positive than the ion source, and enter the injection magnet (c). The injection magnet separates ^{12}C, ^{13}C and ^{14}C according to their mass/charge ratio and they are pulsed out of the injection magnet into the 5MV particle accelerator (d). The negative ions are subjected to a potential difference towards a high voltage positive terminal, which causes their energy to increase. This high-energy ion beam is focused to collide with argon gas molecules within the positive terminal, stripping the outer valence electrons. The negative ions

become positively charged and are therefore accelerated away from the positive terminal towards the analysing magnet (e). The analysing magnet separates ^{12}C, ^{13}C and ^{14}C by their mass-momentum-charge state ratio. ^{12}C and ^{13}C are measured by Faraday cups (f). ^{14}C is focused by a quadruple (g) and analysed by an electrostatic cylindrical analyser (h), which selects ions according to their energy-charge state ratio. The final stage is the analysis of the ^{14}C ions by a gas ionisation detector (i) [123].

1.9.1 AMS vs. MS

There are several fundamental differences between AMS and conventional mass spectrometry (MS). Analysis by AMS differs from conventional MS, in that structural information is not obtained. While MS determines *m/z* ratios of ions, the identities of which may be used to differentiate between analytes, AMS only measures the isotope ratio of the analyte [124]. In addition, the process of conversion of ^{14}C-analyte to graphite (Section 1.10.2) results in the loss of structural information making it impossible to distinguish the analyte by molecular mass or to obtain information on chemical structure [124]. Matrix effects in MS can be caused by interferences from constituents at the retention time of the analyte with *m/z* ratios that can interfere with the analysis, or cause ion suppression [124]. The nature of the graphitisation (Section 1.10.2) and AMS process means that matrix effects are not observed, as it is only ^{14}C-analyte which is measured, and non-labelled constituents cannot cause interference with the measurement [124]. Finally, AMS is a lengthy process with the time from dispensing the sample for AMS to obtaining data taking at least three days compared to a few hours for MS.

1.9.2 AMS sample processing procedure

A large proportion of the analysis time in AMS lies in the processing of the sample prior to AMS measurement. This processing involves a complex off-line procedure (Figure 10).

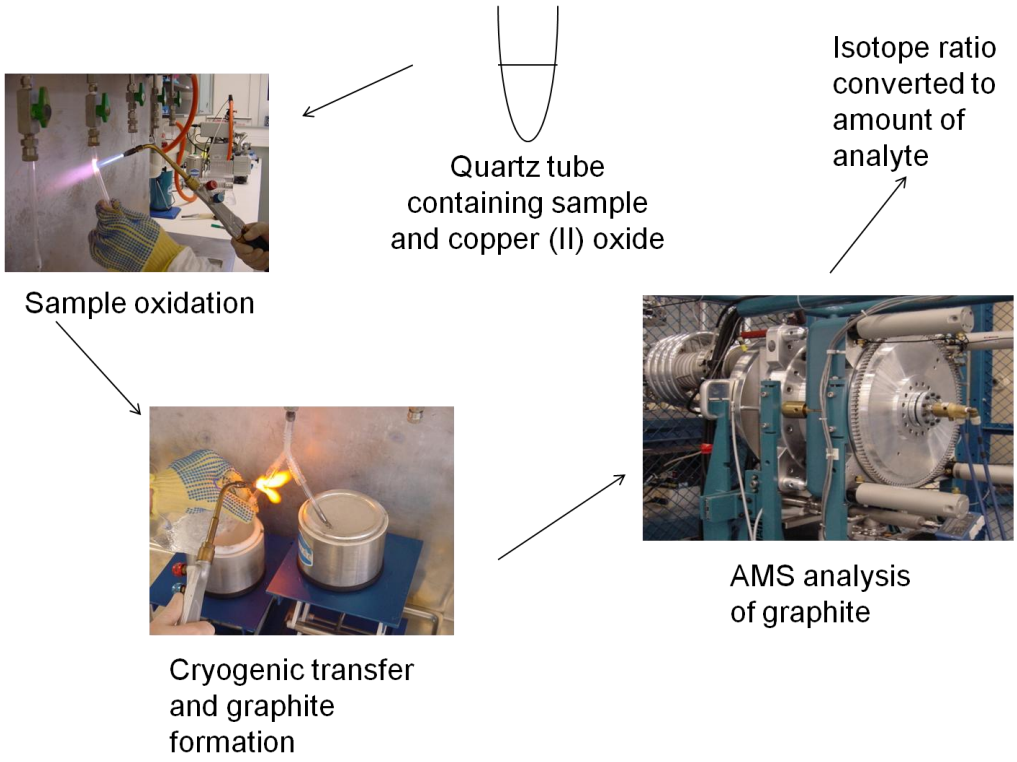

Figure 10: Sample processing prior to analysis by AMS.

Sample preparation is conducted under conditions of a continuous background of naturally occurring ^{14}C. Precautions must be taken during sample processing to exclude this background, which otherwise could introduce contamination. For example, all glassware used in the process described below is pre-treated at a high temperature prior to use. In addition, all laboratory areas and equipment must be closely monitored to ensure that background levels of ^{14}C do not increase to a level that may compromise the integrity of the sample.

The sample is dispensed into a quartz tube containing copper (II) oxide. If the sample does not contain sufficient background carbon (Section 1.9.3.5), carbon carrier is also added to the quartz tube. Analysis of additional carbon carrier controls is important as a monitor of potential background contamination. Solvent is removed from the sample in a rotary evaporator. The quartz tube is inserted into a larger tube with a break-seal point at one end. The tubes are evacuated and sealed, using a glass-blowing torch. The sealed tube is placed in a furnace for 2 h at 900°C, resulting in the production of CO_2 (Equation 2).

$$2C_xH_{x+2} + 6CuO \rightarrow 6Cu + 2CO_2 + 2H_2O$$ **Equation 2**

The CO_2 is transferred across a temperature gradient into a second tube containing cobalt and zinc (II) titanium hydride. The first tube is immersed in a mixture of dry ice and isopropanol and the second tube is immersed in liquid nitrogen. The end of each tube is placed into y-shaped tubing and a vacuum applied. The tip of the sealed tube is snapped at the break point allowing the cryogenic transfer of CO_2 into the second tube, which is sealed using a glass-blowing torch. The sealed tube is placed in a furnace at 600°C for 10 h. This process results in the catalytic conversion of CO_2 to graphite, which is formed in the tube containing cobalt (Equation 3a and Equation 3b).

$$ZnTiH_2 \leftrightarrow ZnTi + H_2$$ **Equation 3a**

$$CO_2 + H_2 \rightarrow C + H_2O$$ **Equation 3b**

The cobalt/graphite mixture is then pressed into an aluminium cathode and the cathode inserted into the AMS prior to analysis [125]. Assuming the sample graphitised was an untreated biological sample this measurement would provide the total radioactivity of the sample, which would include both drug and any metabolites produced *in vivo.* Due to the nature of the sample processing, samples are occasionally lost, or the graphite may be of poor quality. It is essential that sufficient sample remains to carry out repeat analysis if necessary. HPLC separation of the analytes prior to AMS analysis allows quantification of individual analytes. At the commencement of the work presented in this thesis, there was no available interface between HPLC and AMS, however, a prototype has recently been developed [126]. The offline process is described in Figure 11.

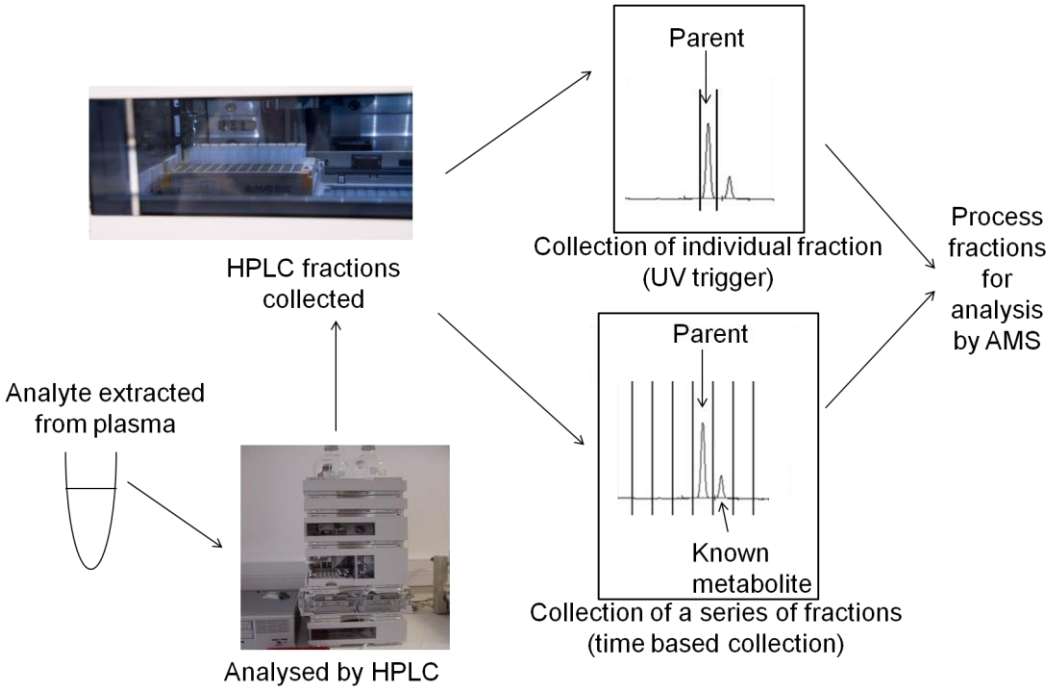

Figure 11: HPLC and AMS analysis of plasma.

A chromatographic marker, typically non-labelled analyte, is added to the plasma and the non-labelled and ^{14}C-labelled analyte is co-extracted from the plasma. The resulting plasma filtrate is injected onto the HPLC and the eluate collected as a single fraction or as a series of fractions. These HPLC fractions may be collected by time or by UV detection. The UV detection mode uses the UV signal of the chromatographic marker to trigger the start and stop of the fraction collector. As the retention time of the non-labelled and the ^{14}C-labelled analyte are assumed the same (see Section 1.10.3.4), the fraction collected based on the response for the non-labelled analyte should also contain the ^{14}C-labelled analyte. Time-based collection may be programmed to collect one fraction or a series of fractions (Figure 11). The collection of fractions across an entire HPLC run is a common approach for the qualitative analysis of the administered drug and its metabolites, whereas single collections normally focus on a particular analyte.

At the outset of this research (2006) there were no specific guidelines for the development and validation of HPLC-AMS assays. Guidelines for bioanalytical method validation were published by the FDA in 2001, however these did not

specifically refer to HPLC-AMS assays, only to procedures such as LC-MS, LC-MS-MS and GC-MS-MS [127]. Quantification of an analyte by HPLC and AMS is a complex process, which has been developed over the last 10 years. Much of the approach was established during the development of the methods applied in this thesis and the entire assay is described in Section 1.10.6.

1.9.3 Terminology used in AMS analysis

1.9.3.1 Isotope ratio (percent modern carbon)

The isotope ratio (^{14}C:^{12}C) obtained after AMS analysis is expressed in units of percent modern carbon (pMC). Units of pMC were introduced for radiocarbon dating, since AMS was first developed for this purpose. The pMC values obtained from AMS analysis can be converted to radioactive concentrations (Section 1.10.6). 100 pMC is equal to 98 attomoles (10^{-18} mole) of ^{14}C per mg of carbon [128]. 100 pMC was originally quoted as the level of background ^{14}C in the atmosphere. Background ^{14}C was elevated after the atomic bomb tests in the 1950s, which introduced additional ^{14}C into the atmosphere. The pMC in a biological sample taken from a human post 1950s is approximately 110 pMC [123]. Carbon carriers used in AMS analysis (Section 1.9.3.5) are taken from petrochemical sources and contain no ^{14}C. The isotope ratio of a carbon carrier from a petrochemical source is typically less than 8 pMC (Section 7.11.1).

1.9.3.2 Units of radioactivity

Radioactivity is expressed as the number of decay events per unit of time [128] i.e. disintegrations per minute (dpm) or disintegrations per second (dps). The SI unit for radioactivity is the Becquerel (Bq), where 1 Bq is 1 dps (1 MBq = 6 x 10^7 dpm). Typically units of dpm are more commonly used in drug development and studies of metabolism. Many of the equations used in conversion of pMC values obtained from AMS analysis also use dpm. Radioactive concentrations are presented in this thesis either in pMC for raw AMS data, or dpm where ^{14}C concentrations are required.

1.9.3.3 Specific radioactivity

The value for a specific radioactivity is based on an average [128]. For example, ^{14}C-labelled analyte can be synthesised such that the ^{12}C at a specific position is replaced with ^{14}C. Radiolabelled material may be diluted with non-labelled material to obtain the required dose. A solution which is a mixture of ^{14}C-material and non-labelled material will have a mass and a radioactivity associated with it. The required specific radioactivity dictates the composition of this mixture. Units of specific radioactivity are expressed as units of radioactivity per mole or per weight of analyte, e.g. Bq/mmole, Bq/mg or dpm/mg [128].

1.9.3.4 HPLC fractionation and the kinetic isotope effect (KIE)

In experiments where a radiotracer is used, it is assumed that the radioisotope and stable isotopic forms of the compound under study have identical chemical properties [128]. There is, however, a difference in the vibrational frequencies of the chemical bonds of isotopes, which is dependent upon the mass of the bonded isotopes [128]. The mass difference between ^{12}C and ^{14}C is 14%, compared to 300% between ^{3}H and ^{1}H [128]. The KIE can be described mathematically using the rate constant for each isotope, and is equal to k^L/k^H, where K^L represents the rate constant for the light isotope and K^H represents the heavy isotope. Typical values for KIE are 2.52 for ^{1}H/^{3}H and 1.07 for ^{12}C/^{14}C (calculations not shown [128]) revealing a small magnitude for the effect. Consequently, its influence on factors such as retention time can be expected to be minimal and it is assumed that the chromatographic detector response for the non-labelled species adequately reflects the retention time of the equivalent ^{14}C-analyte [128].

1.9.3.5 Carbon carrier and isotopic dilutor

The amount of graphite required for AMS analysis is approximately 2 mg [124]. Samples such as plasma, faeces and blood contain sufficient background carbon to be taken directly for AMS analysis, without additional carbon being required. Samples such as HPLC fractions do not contain sufficient carbon and require addition of a carbon carrier, such as liquid paraffin [12]. Carbon carrier is also

termed an isotopic dilutor, as it disturbs the natural ^{14}C:^{12}C ratio of the sample [129].

1.9.4 Processing of plasma prior to analysis by HPLC

^{14}C-labelled analytes must be extracted from plasma samples prior to HPLC analysis. The extraction method must provide a sample that is free from chromatographic interferences (such as plasma proteins) without compromising the recovery of the analyte, either from lack of recovery or due to degradation. While the recovery of the analyte need not be 100%, it should be consistent and reproducible [127]. In addition, the sample should be compatible with the HPLC method and must not cause the performance of the column to be compromised [130]. The extraction step is just one part of a multi-step offline process and liquid-liquid extraction methods are often chosen for their simplicity. Ranges of 96-well extraction plates containing removable vials are commercially available which are specifically designed to carry out large numbers of extractions. An advantage of using 96-well plates is the collection of plasma filtrate directly into the collection vial, reducing the number of manual steps.

1.9.5 Chromatographic resolution

Plasma extracts from liquid-liquid extractions typically contain the ^{14}C-drug and ^{14}C-metabolites. Complete resolution of the target analyte is essential prior to AMS analysis. HPLC methods are typically developed with non-labelled reference standards and metabolites where available. With established drugs, where the PK profile is well known, resolution of the analyte may be relatively straightforward. During analysis of NCEs where limited metabolism data are available, or following administration of a cassette dose, the HPLC resolution of the analyte(s) and metabolites must be demonstrated. Two-dimensional chromatographic methods, where the analyte is separated using two different modalities, can provide the best separation and resolution (Section 2.3.5 and 4.3.5).

1.9.6 Current methods for quantification of analyte concentrations

The first publication to report microdose data with specific analytical details was published in 2006 [12]. Human plasma was subjected to liquid-liquid extraction followed by HPLC analysis, with isolation of the analyte by the collection of eluate fractions. HPLC fractions corresponding to the analyte (typically 2-3 fractions), were combined and analysed by AMS. The isotope ratio was converted to a concentration, reported as dpm per fraction. Concentrations were calculated as follows (Equation 4 – Equation 6), using one of the administered drugs, midazolam, as an example.

$$dpm\,midazolam\,per\,extract = \frac{dpm\,per\,fraction}{HPLC\,injection\,volume(mL)}\ x\ extract\,volume(mL)$$

Equation 4

$$dpm\ midazolam\ \ per\ mL\ \ plasma = \frac{dpm\ midazolam\ \ per\ extract}{volume\ extracted\ \ (mL)}$$

Equation 5

$$ng\ midazolam\,per\,mL\ \ plasma = \frac{dpm\,midazolam\,per\,mL\ \ plasma}{Specific\,radioactivity\,(dpm/ng)}$$

Equation 6

There are several areas in the procedure where experimental errors are unaccounted for in the reported plasma concentrations. The calculations assume 100% analyte recovery; however, ^{14}C-midazolam recovery from plasma was stated to be 92%, introducing an error of 8% in plasma midazolam concentrations. In practice, this error may vary from sample to sample. The method assumes a chromatographic column recovery of 100%. If left unaccounted, loss of ^{14}C-midazolam prior to AMS analysis may lead to errors in the final midazolam concentration.

In recognition of the above, the quantification process was developed further and reported in 2008 [129]. These developments occurred in parallel with the development of the HPLC-AMS assay for the research detailed in Chapters 2 and 4. The method describes the quantification of ^{14}C-labelled analyte via a recovery constant generated from a recovery curve. It should be noted that a recovery curve differs from a conventional LC-MS calibration curve in that the latter

calibrates the MS signal output with an analyte concentration. In LC-AMS, however, the AMS is calibrated as a single entity. A recovery curve corrects for loss of analyte from every single sample during the processing steps prior to AMS analysis. The procedure is summarised below, with a summary of the basic equations and further derivations given for clarity.

Vogel and Love published the equation for determination of total ^{14}C concentrations (i.e. analyte plus metabolites) in a biological sample [131] and was simplified by Salehpour et al. (Equation 7).

$$K = (R_m - R_n)\Psi (W/L)$$ **Equation 7**

[129]

Where K = analyte concentration (mass equivalents per volume)
R_m = ^{14}C:^{12}C isotope ratio of analyte (pMC)
R_n = natural background ^{14}C:^{12}C isotope ratio of the sample (pMC)
Ψ = carbon mass fraction in the sample (percent of carbon in the sample)
W = molecular mass of the analyte
L = specific molar radioactivity (pMC per unit mass)

R_m and R_n are expressed in units of pMC, where 100% modern carbon is defined as 98 attomole of ^{14}C per mg of carbon. To calculate the drug concentration from an isotope ratio the fraction of the sample consisting of carbon must be known. For samples such as plasma, the carbon fraction (% carbon) is determined by a carbon analyser. Where HPLC fractions are analysed, only the carbon content of the isotope dilutor needs to be accounted for, as inherent carbon is very small. The pMC value is converted to units of Modern prior to further manipulation as follows (Equation 8):

$$Modern = \frac{pMC}{100}$$ **Equation 8**

Equation 7 is simplified by expressing the specific radioactivity of the drug administered (dpm/mg) and by expressing $R_m - R_n$ as R_{net} (Equation 9).

$$K = \frac{R_{net}\Psi}{L_{mass}}$$ **Equation 9**

Equation 9 is used in the determination of the total ^{14}C concentration of a sample in plasma (or other biological matrices), where it is taken directly for AMS analysis. Analyses of HPLC fractions require the addition of an isotopic dilutor (Section 1.10.3.5). Equation 9 does not account for procedural losses encountered during sample processing and assumes 100% sample recovery. Equation 9 was modified to account for the addition of isotopic dilutor and for procedural losses (Equation 10).

$$K = \frac{R_D \Phi}{L_{mass} \theta}$$ **Equation 10**

Where
K = analyte concentration
Φ = the amount of carbon added as isotopic dilutor
R_D = the ^{14}C:^{12}C ratio after isotopic dilution
θ = analytical recovery
L_{mass} = specific radioactivity of the analyte

Equation 10 assumes that the recovery is the same for all samples analysed. As θ varies between samples due to differences in analyte recovery, this value should be determined for each sample analysed. Introduction of a recovery constant accounts for procedural losses during the quantification of ^{14}C-analyte via use of an internal standard. The internal standard employed in HPLC and AMS analysis is normally the non-labelled analyte, which acts as a chromatographic marker and is typically measured by UV absorption. The amount of carbon present in the internal standard is negligible compared to the carbon carrier and is ignored in calculations. The internal standard method accounts for sample-to-sample variation by differences in the UV response of an analyte during HPLC analysis. The internal standard method is discussed in detail by Lappin et al. [129].

A recovery curve is typically constructed as follows:

- plasma samples are prepared at several different ^{14}C-analyte concentrations (at least 4 concentrations, plus a blank) and the concentration of each plasma sample is determined;

- replicate aliquots of plasma (typically *n*=5) are dispensed, internal standard (i.e. non-labelled analyte) is added and each sample is extracted and analysed by HPLC;

- the internal standard response (peak area) is recorded for each HPLC analysis and the eluate corresponding to the internal standard is collected as a HPLC fraction;

- HPLC fractions are analysed by AMS and the isotope ratio of the fraction is determined.

Plasma concentrations are plotted on the *x*-axis and HPLC fraction concentration / UV response is plotted on the *y*-axis. A curve is fitted to the data by linear regression and substitution of the equation y = mx + c into Equation 10 results in Equation 11.

$$K = \frac{\left(\frac{R_A - c}{mU}\right)}{L_{mass}} \Phi \qquad \textbf{Equation 11}$$

Where:

R_A = isotope ratio of sample – isotope ratio of isotopic dilutor
m = recovery constant (slope of recovery curve)
c= intercept of recovery curve
U = HPLC detector response
Φ = amount of carbon added as isotopic dilutor
L_{mass} = specific radioactivity of analyte (pMC per unit mass)

The slope of the line (m) is the recovery constant. The recovery curve is used in the quantification of analyte concentrations in clinical plasma as follows:

- internal standard is added to plasma and analyte is extracted;

- plasma extract is analysed by HPLC with fraction collection and the UV response of the analyte recorded;

- the HPLC fraction is analysed by AMS and the isotope ratio determined;

- analyte concentration in plasma is determined using Equation 11.

1.9.7 Limitations of the recovery curve method

The recovery curve quantification method described in Section 1.10.6 is a basic overview of the process. There are several further considerations to be made in developing such an assay for HPLC-AMS analysis (Section 1.10.7.1 – 1.10.7.2).

1.9.7.1 Analyte purity

As ^{14}C-analyte is spiked into plasma in the generation of the recovery curves, its purity is essential to the accuracy of the data obtained and significant impurities must be accounted for in the calculation of analyte concentrations. In the example in Section 1.10.6, test substances were between 98% and 99.8% radiochemical purity, which results in a maximum error of 2% in the plasma concentration determined. In addition, non-labelled analyte must be demonstrated to be free of residual ^{14}C.

1.9.7.2 Linear analyte response

AMS analysis is linear up to the point of saturation of the detector. In practice, reaching this saturation level must be avoided as it is damaging to the instrument. Assays are designed so that the maximum amount of ^{14}C placed in the AMS is below the saturation limit. In addition, the AMS detector is programmed to stop when it reaches a specific number of counts, after which point the statistical accuracy of the analysis is reduced. Samples that are counted for less than the required number of cycles, owing to this programmed stop, are deemed statistically inaccurate and are not used. The HPLC detector response for the sample must also be ascertained prior to development of an assay and must be accounted for in the quantity of internal standard added to each sample.

1.9.7.3 Uniform analysis

Determination of plasma analyte concentrations using Equation 11 allows direct conversion of the isotopic ratio of the sample obtained on AMS analysis to a mass concentration per mL. The method requires that particular analytical

processes remain constant throughout sample analyses. Specifically, the plasma volume taken for extraction, the proportion of plasma extract taken for HPLC analysis, the HPLC fraction volume and proportion taken for AMS must be considered. In addition, the amount of isotopic dilutor and the specific radioactivity applied must remain constant. In practice, some of the above may vary which impacts on the processing of the samples.

1.10 Aims of this thesis

The literature reviewed in Section 1.8 illustrates progression in the use of microdosing, from proof of concept studies using established drugs, to more recent studies where NCEs have been investigated and in some cases, go/no-go decisions have been taken on progressing with the development of a compound. More recent studies have explored the use of microdosing in detecting DDIs and also introduced the cassette microdosing approach. At the outset of the work presented in this thesis limited published examples of novel applications of microdosing were available as the wider use of the technique was still being accepted by the industry. This thesis presents two applications of microdosing, which were not previously detailed in the literature. The first is the detection of DDIs after cassette microdose administration, a concept that has recently been supported (Section 1.8.2.4 and 1.8.2.5). The second is the use of microdosing to determine PK data along with drug distribution data via the combined use of microdosing and an imaging technique (Section 1.9.1 and 1.9.2). AMS (Section 9) was chosen for quantification of the analyte in each study due to the low doses administered.

1.10.1 Ability to detected DDIs after cassette microdose administration

There are several examples in the literature of an NCE being administered for the first time in a microdosing study (Section 1.8.1.1). Adding a second arm to each of these studies, where the NCE was co-administered with known inhibitors of major P450 enzymes or transporters would have the added benefit of identifying DDIs at the earliest stage of development. The administration of a cassette microdose allows multiple compounds to be administered to the same subjects in one single dose. Cassette dosing has been widely used in the investigation of

DDIs (Section 1.7) as a common time-saving approach, particularly in screening and candidate selection [83]. This approach remains controversial due to the potential for interactions to occur between compounds within the cassette [83]. Due to the very low levels of drug administered in a microdose there is a very low risk of interactions occurring [83], with the recent work published by Maeda et al. [117], further supporting this theory (Section 1.8.2.5). The clinical study described in this thesis (Chapter 2 and Chapter 3) was designed to prove the concept of detecting DDIs after administration of a cassette microdose. Chapter 2 describes the analytical methods developed to allow the AMS quantification of four ^{14}C-labelled analytes in human plasma after administration of a cassette microdose. The development of a preparation method for plasma filtrate and a HPLC method for isolation of ^{14}C-labelled analyte are detailed in Chapter 2. The verification of analyte resolution by two-dimensional chromatography is also presented in Chapter 2. Finally, Chapter 2 details the construction of a recovery curve for ^{14}C-analyte quantification after AMS analysis of HPLC fractions containing ^{14}C-analyte. Chapter 3 details the design and implementation of the clinical study and the analysis of plasma samples using the methods developed in Chapter 2. Mass concentration data are determined and PK data are presented, discussed and compared with literature data to assess linearity with therapeutic doses. PK data obtained after administration of a cassette microdose alone and with CYP and P-gp inhibitors are compared to determine the ability of the cassette microdose to determine DDIs.

1.10.2 Combination of positron emission tomography and AMS in obtaining pharmacokinetic and imaging data after microdose administration

Microdosing studies allow drug concentrations to be quantified in samples such as blood, plasma, urine and faeces, providing PK data that may be used to determine the systemic fate of the drug. These types of study do not provide information regarding the distribution of a drug within the rest of the body.

Positron emission tomography (PET) is routinely used to study the distribution and PK of a drug labelled with a positron emitting isotope such as ^{11}C or ^{18}F [6]. It is a non-invasive nuclear imaging technique with applications in drug disposition studies. There are two commonly used approaches in the design of

PET imaging studies. Ligand displacement studies involve the administration of a positron emitting radiolabelled ligand followed by administration of a pharmacologically active dose of NCE. Displacement of the ligand designed to bind specifically to a particular receptor is determined by measurement of the positron emitter. This approach is particularly useful in the development of central nervous system (CNS) drugs, in establishing whether an NCE reaches the brain and also if it binds to the target site [87]. Alternatively an NCE itself may be radiolabelled and traced in target tissues [87] to measure uptake. Under these circumstances, the radiolabelled drug is administered as a microdose. The microdosing study reported in this thesis (Chapter 4 and Chapter 5) is a proof of concept study to investigate the feasibility of obtaining plasma PK data along with drug distribution data in the same subjects after a single dose administration. In addition, the ability to quantify enantiomers in plasma after administration of a ^{14}C-labelled racemic mixture was explored. Chapter 4 describes the analytical methods developed to prepare plasma filtrate and isolate ^{14}C-labelled enantiomers by HPLC. Verification of analyte resolution using a two-dimensional C18-chiral HPLC method and the construction of a recovery curve for quantification of ^{14}C-enantiomers is described in Chapter 4. Chapter 5 details the design and implementation of a clinical study and the analysis of venous plasma samples for ^{14}C-enantiomer concentrations. PK data obtained after microdose only and concomitant microdose and therapeutic dose administrations are compared, to determine dose linearity. PK data obtained for each enantiomer are described, discussed and compared with imaging data obtained by PET analysis to determine the applicability of combining the two techniques.

CHAPTER 2

Development of HPLC and AMS methods for quantification of caffeine, midazolam, tolbutamide and fexofenadine in plasma

2.1 Introduction

This chapter reports the development of methods used to analyse clinical samples derived from a study whereby a cassette microdose consisting of ^{14}C-caffeine, ^{14}C-midazolam, ^{14}C-tolbutamide and ^{14}C-fexofenadine was administered to healthy human volunteers. The main objectives for the clinical study were to quantify caffeine, midazolam, tolbutamide and fexofenadine concentrations by AMS analysis. The cassette microdose consisted of a combined mass of 100 µg and radioactive dose of 4.44 x 10^5 dpm (i.e. 25 µg, 1.11 x 10^5 dpm of each compound). Due to the very low doses administered, AMS detection was chosen for quantification of each drug in the plasma samples collected during the study, with prior separation of each analyte by HPLC. This chapter describes how the HPLC-AMS technologies were developed for use with the clinical samples.

2.1.1 Development of an HPLC-AMS assay

The two main considerations for the practical development of an HPLC AMS assay are the isolation and the quantification of the analyte. It is necessary to consider the development of a suitable method for sample pre-treatment as well as the development of an HPLC method with sufficient chromatographic resolution. A typical HPLC-AMS assay is outlined in Section 1.10.6. The properties and metabolism of each analyte for which quantification is required are detailed below (Section 2.1.2).

2.1.2 Compounds chosen for cassette dose administration

2.1.2.1 Caffeine

Caffeine is a psychoactive substance found in coffee, tea and chocolate. Low to moderate doses of caffeine (50-300 mg) result in increased alertness and energy. Higher doses can result in anxiety, restlessness and tachycardia [132]. Caffeine is metabolised in the liver to form dimethyl and monomethylxanthines [133], a process mediated by CYP1A2 (Figure 12).

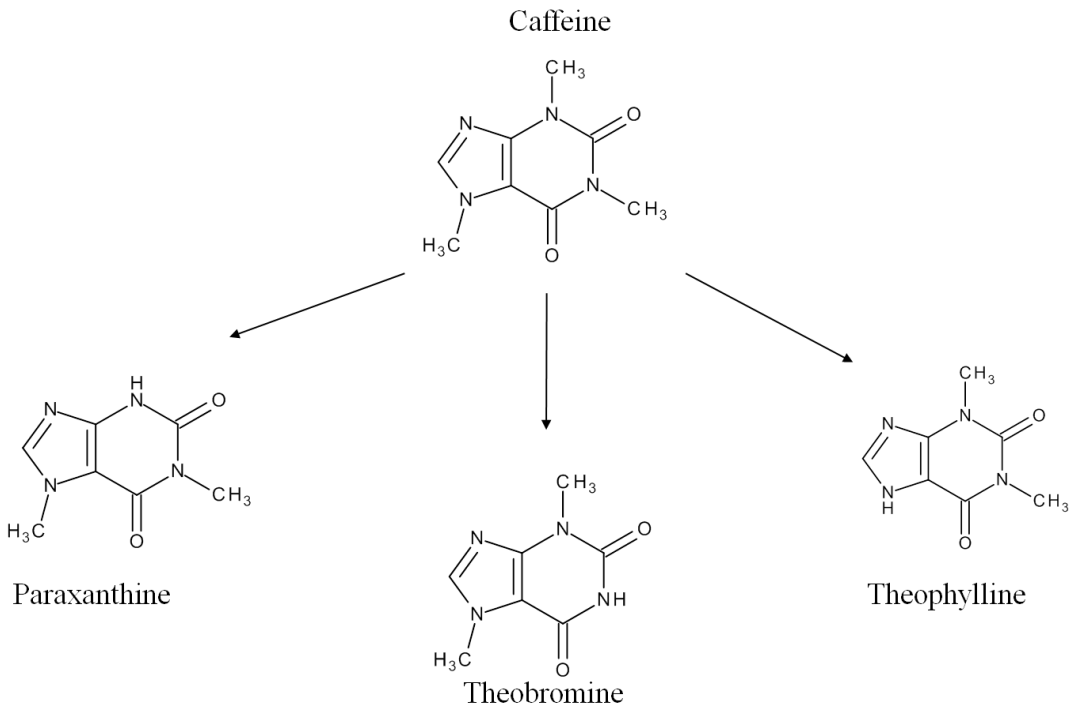

Figure 12: Caffeine and the major routes of metabolism via CYP1A2 [134].

2.1.2.2 Midazolam

Midazolam is widely used as an intravenous anaesthetic [29]. It is rapidly metabolised by CYP3A in the liver to the major hydroxylated metabolite, 1'-hydroxymidazolam and two minor metabolites, 4-hydroxymidazolam and 1'4-hydroxymidazolam [135] (Figure 13).

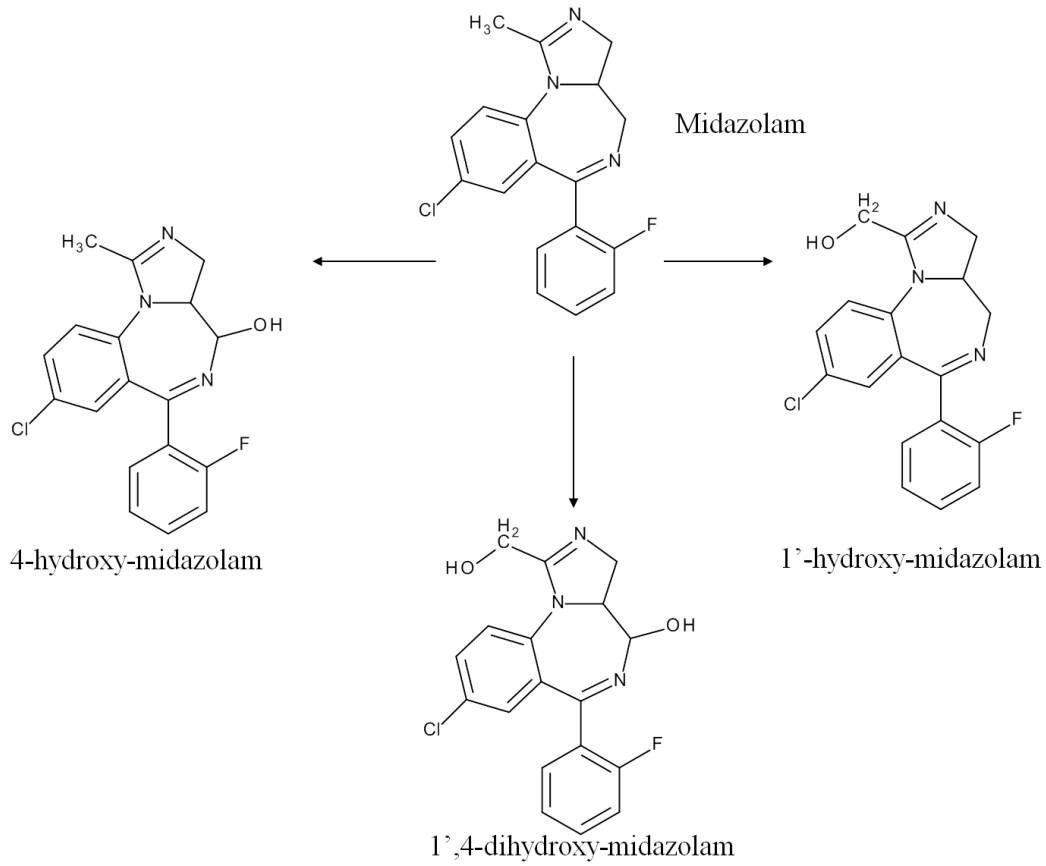

Figure 13: Midazolam and the major routes of metabolism via CYP3A.

2.1.2.3 Tolbutamide

Tolbutamide is a sulphonylurea, used in the treatment of diabetes [136]. It is metabolised by CYP2C9 to hydroxytolbutamide. Hydroxytolbutamide undergoes further metabolism by hydrogenases to carboxytolbutamide [37] (Figure 14).

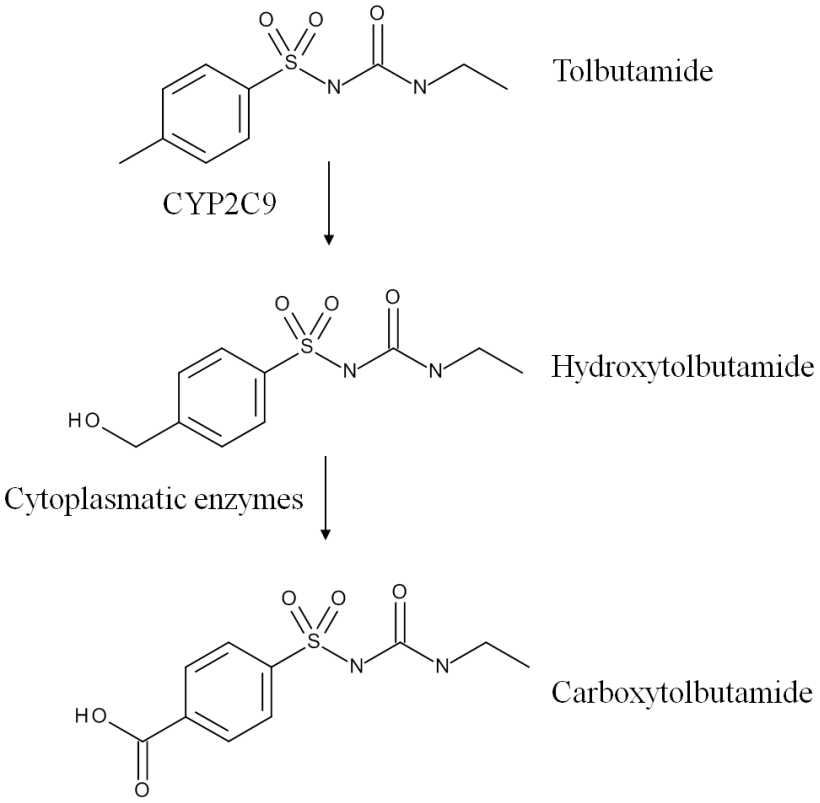

Figure 14: Tolbutamide and the major routes of metabolism [37].

2.1.2.4 Fexofenadine

Fexofenadine (Figure 15) is a drug used for the treatment of allergic rhinitis and chronic uticaria [137]. Approximately 95% of fexofenadine is excreted in the urine and faeces unchanged. It is not significantly metabolised by CYP and is a substrate of P-glycoprotein [137].

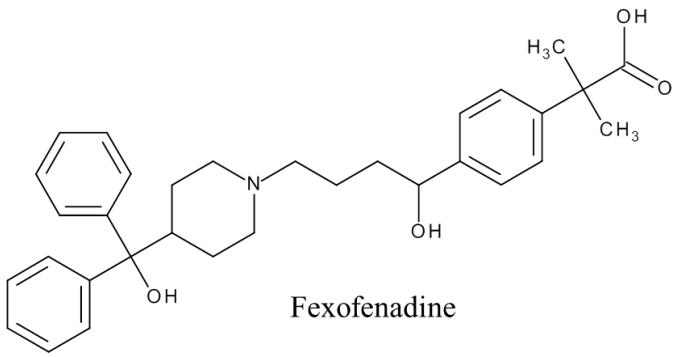

Figure 15: Fexofenadine.

2.1.2.5 Absorption and distribution of caffeine, midazolam, tolbutamide and fexofenadine

After oral administration, most drugs are absorbed by diffusion across biological membranes. Absorption of a drug by passive diffusion through the GI tract is dependent upon its partitioning between aqueous fluids in the GI tract and the lipid membrane [138]. The un-ionised form of a compound will more freely partition into lipophilic membranes than the ionised form, whereas the ionised form favours the aqueous phase. This absorption process is described by pH-partition theory [138, 139].

Dissociation of weak acids and weak bases is quantified by the dissociation constant K_a, often expressed as pK_a (the negative logarithm of the acid dissociation constant). The extent of ionisation is dependent upon the pH of the solution [139]. The pH range of the human stomach is approximately pH 1 – pH 3, and the lumen of the duodenum to the colon ranges from pH 5 to pH 8 [139]. The pH of the blood is 7.4, hence blood perfused tissues are at a similar pH [138]. The relationship between the pH and the pK_a is described by the Henderson-Hasselbalch equation for acidic and basic compounds (Equations 12a and 12b).

$$pK_a = pH + log\left(\frac{[HA]}{[A^-]}\right)$$ **Equation 12a [139]**

Where:
$[A^-]$ = concentration of ionised compound
[HA] = concentration of the un-ionised compound (acid)

$$pK_a = pH + log\left(\frac{[BH^+]}{[B]}\right)$$ **Equation 12b [139]**

Where:
[B] = concentration of the un-ionised compound (base)
$[BH^+]$ = concentration of ionised compound

The pK_a of a compound is the pH at which the un-ionised and ionised forms are present in equal concentrations [138]. The pK_as for caffeine, midazolam, tolbutamide and fexofenadine are given in Table 7.

Table 7: pK_a and logP of caffeine, midazolam, tolbutamide and fexofenadine.

Analyte	pK_a	logP	References
Caffeine	14[1]/0.8[2]	-0.55	[138, 140, 141]
Midazolam	6.57	3.33	
Tolbutamide	4.33	2.30	
Fexofenadine	4.04[1]/9.01[2]	2.94	

[1]acidic [2] basic

Midazolam is a basic compound, tolbutamide is acidic, caffeine is neutral and fexofenadine is zwitterionic. The Henderson-Hasselbalch equation allows the ratio of ionised: un-ionised compound in aqueous solution at a given pH to be determined. For example, at pH<2, which is typical of the stomach environment, tolbutamide with a pK_a of 4.33 exists predominantly in the un-ionised form. The un-ionised form dominates until the drug reaches an environment of approximately pH 4.3 and above, hence the pH of the stomach favours the absorption of tolbutamide. Midazolam is predominantly in the un-ionised form at approximately pH 8.5 and fexofenadine at approximately pH<2 and pH>11. Based upon the physicochemical properties of midazolam, the pH of the large intestine would favour its absorption. Fexofenadine will be highly ionised in the stomach and absorption would be favoured in the small intestine, where it is zwitterionic.

Absorption dependent on pH is expected for bases with pK_a values between 5 and 11, and acids with pK_as of less than 7.5 [138]. The two pK_a values for caffeine both fall outside of these ranges, hence caffeine shows no pH dependent absorption. Caffeine is rapidly absorbed from the gastrointestinal tract and reaches the C_{max} at around 45 min in humans [133].

The partition coefficient (logP) is the ratio of the concentrations of an un-ionised compound in each of the two phases of a biphasic mixture of solvents, typically

an octanol and water mixture at equilibrium [139]. Octanol and water most closely represent the polarities of the epithelial membrane. Compounds which favour the aqueous phase have low logP values (<1), whereas those with higher logP values (>3.5) favour the octanol phase [142].

Caffeine has a logP value of -0.55 (Table 7). Compounds with logP values in this range tend to be polar and have good aqueous solubility. Midazolam, tolbutamide and fexofenadine all have logP values between 2 and 4.5 (Table 7). Compounds that fall within this range tend to be of intermediate polarity, with a good balance between aqueous and lipid solubility [142]. Based on its logP caffeine should less readily cross the epithelial membrane than the other three compounds.

The distribution coefficient (logD) represents the distribution between octanol and water at a defined pH. Unlike logP, logD includes the amount of ionised compound in the aqueous phase. Definitions of logD for an acid and a base are given in Equations 13a and 13b, respectively:

$$\log D = \log P - \log[1 + 10^{(pH - pKa)}] \qquad \textbf{Equation 13a}$$

$$\log D = \log P - \log[1 + 10^{(pKa - pH)}] \qquad \textbf{Equation 13b}$$

Following absorption into the blood a compound experiences a pH environment of 7.4. The calculated logD values for caffeine, midazolam, tolbutamide and fexofenadine at pH 7.4 are given in Table 8.

Table 8: $logD_{(pH7.4)}$ of caffeine, midazolam, tolbutamide and fexofenadine.

Analyte	**$logD_{(pH7.4)}$**
Caffeine	0.00[1]/-0.55[2]
Midazolam	3.27
Tolbutamide	-0.57
Fexofenadine	-0.21[1]/0.81[2]

[1]acidic [2]basic

Based on their $logD_{(pH7.4)}$ values, caffeine, tolbutamide and fexofenadine would be expected to favour the aqueous phase and should exhibit good systemic distribution. Midazolam has $logD_{(pH7.4)}$ of 3.27 and as the most lipophilic of the four compounds may favour the lipid phase to the greatest extent. This is supported by the higher volume of distribution of midazolam (V=1.1 L/kg) compared with caffeine (0.5 L/kg) and tolbutamide (0.12 L/kg) [143].

Fexofenadine is an efflux transporter substrate. The P-gp mediated efflux of fexofenadine across the membrane and back into the lumen of the GI tract limits its bioavailability [23]. Thus, the absorption and distribution of fexofenadine cannot be predicted by its physicochemical properties alone.

2.2 Aims

The primary aims of the work presented in this chapter were (Figure 16):

- to develop a method for the extraction of caffeine, midazolam, tolbutamide and fexofenadine from plasma, prior to separation by HPLC;

- to develop an HPLC method for the separation of caffeine, fexofenadine, midazolam and tolbutamide and their commercially available metabolites in human plasma;

- to assess the compatibility of the plasma extraction and HPLC methods;

- to develop methods to verify the chromatographic separation of caffeine, midazolam, tolbutamide and fexofenadine from ^{14}C-drug related material and to demonstrate their applicability to samples of human plasma;

- to develop a quantification method for caffeine, fexofenadine, midazolam and tolbutamide in samples of human plasma;

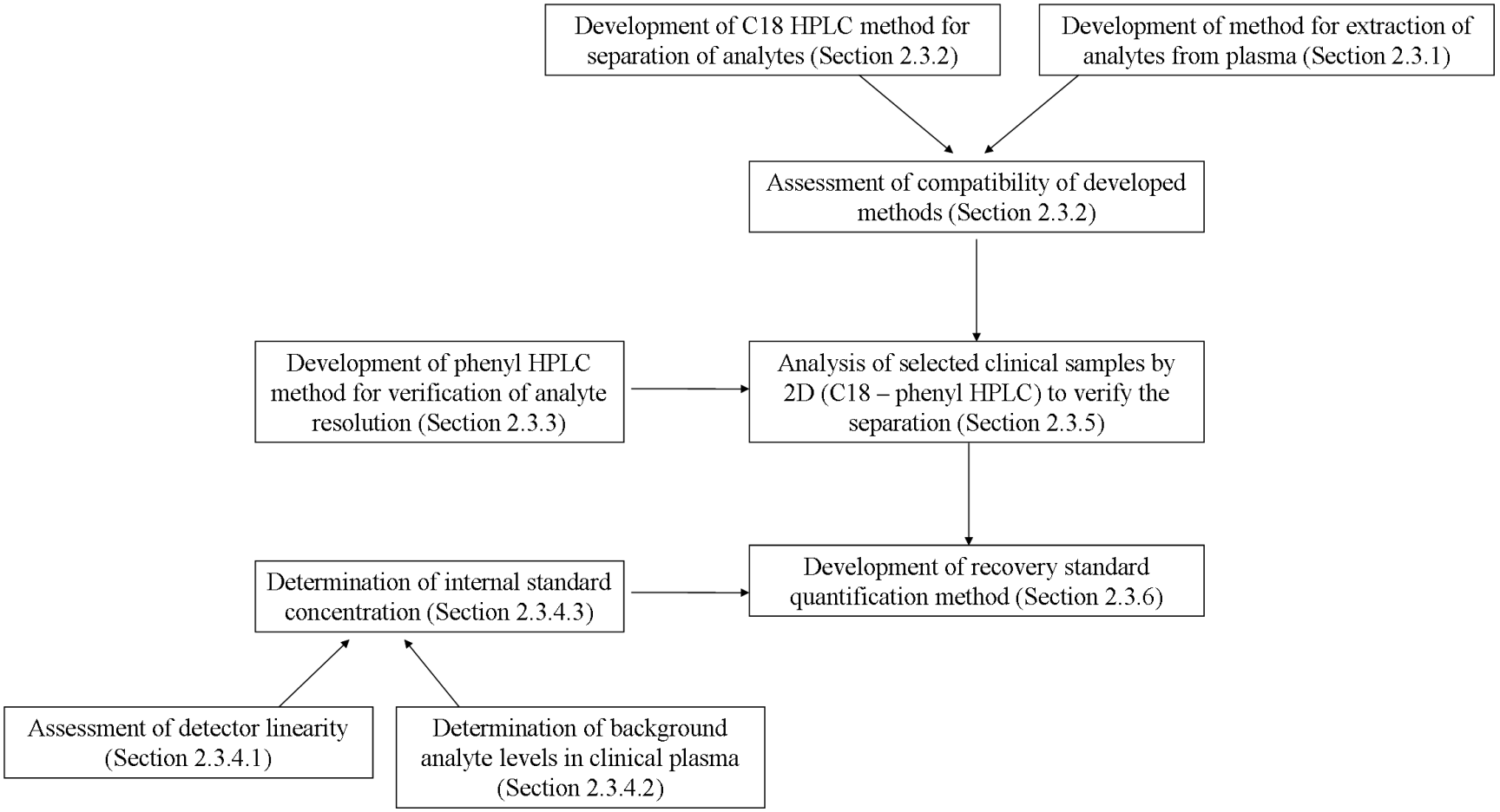

Figure 16: Schematic of method development and verification of methods for the quantification of caffeine, midazolam, tolbutamide and fexofenadine.

2.3 Results and discussion

2.3.1 Development of methods for pre-treatment of plasma

A protein precipitation extraction method was selected for development. The advantages of using a protein precipitation plate are detailed in Section 1.9.4 and this method was selected due to its ability to extract large numbers of samples consistently. The method involves the use of a 96-well plate (Sirocco, Waters [144]) capable of accommodating 600 µL of solvent and 200 µL of plasma (3:1 v/v) to yield approximately 700 µL of plasma filtrate. The maximum injection volume for HPLC analysis is 100 µL (Agilent 1200 series; Section 7.8). Altering plasma: solvent ratios and/or introducing a sample volume reduction step (typically under N_2) could increase the concentration of the analyte for HPLC injection. For example sample reduction followed by reconstitution in 200 µL would result in all of the analyte extracted being present in the plasma filtrate, with half of this potentially available for analysis by HPLC.

Several published methods employ acetonitrile in the protein precipitation extraction of caffeine, midazolam and tolbutamide [12, 65, 145] and it was chosen for use in the initial development of the extraction method. The purpose of method development was to evaluate:

- the overall recovery from plasma vs. recovery from plasma with the addition of a volume reduction step;

- the volume of plasma required for extraction.

2.3.1.1 Development of protein precipitation extraction Method 1

Spiked plasma samples were prepared and subjected to protein precipitation extraction (Figure 17; Section 7.5.1). Spiked plasma and filtrate samples were analysed by LSC (Figure 17; Section 7.9).

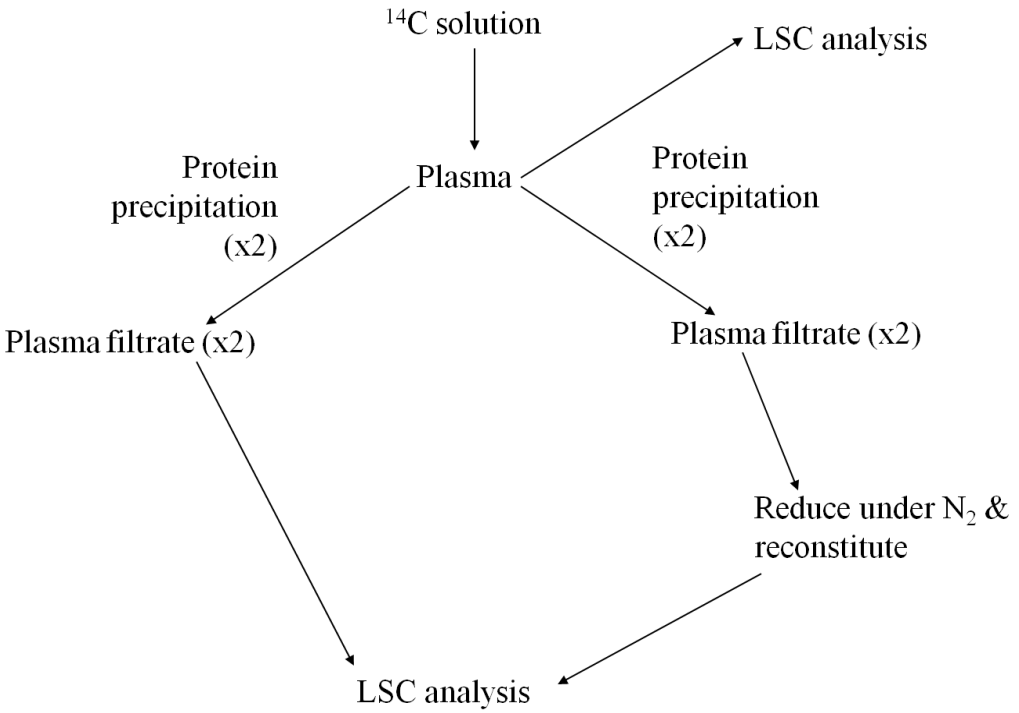

Figure 17: Outline of the method for plasma extraction and liquid scintillation counting (LSC) of samples.

Mean extraction efficiencies were calculated for each analyte (Equation 14).

$$Extraction efficiency = \frac{dpm recovered in\ plasma\ filtrate}{dpm in\ plasma taken for\ protein precipitation} \times 100$$

Equation 14

The mean recovery of all analytes from plasma was >79% (Table 9). The introduction of a volume reduction step followed by reconstitution of the dried filtrate in acetonitrile (200 μL) resulted in less efficient recovery. The loss was most marked in the case of fexofenadine and tolbutamide where less than 20% of the radioactivity was recovered (Table 8). Data for fexofenadine showed high variability between the two replicates (% difference from the mean = 37.61%).

Table 9: Caffeine, midazolam, tolbutamide and fexofenadine extraction efficiency data (Method 1).

Analyte	Neat plasma filtrate- mean extraction efficiency (%)[1]	Reduced and reconstituted plasma filtrate – mean extraction efficiency (%)[1]
Caffeine	90.7 (0.89)	69.8 (1.90)
Midazolam	79.4 (16.64)	60.6 (15.64)
Tolbutamide	86.5 (0.95)	18.4 (9.90)
Fexofenadine	91.2 (0.73)	12.0 (37.61)

[1]Mean of duplicate analyses (% difference from the mean stated in parentheses)

2.3.1.2 Development of extraction Methods 2a and 2b

Method 1 was modified to include a smaller extraction solvent to plasma ratio to achieve maximum concentrations without a volume reduction step. Spiked plasma samples were prepared and subjected to protein precipitation in duplicate (Section 7.5.1) with the following plasma and solvent volumes:

- Method 2a – plasma 100 µL / acetonitrile 200 µL;
- Method 2b – plasma 100 µL / acetonitrile 300 µL.

Mean extraction efficiencies were calculated for each analyte using Equation 14 (Section 2.3.2.1; Table 10). Analyte recovery was >76% (*n*=2) for Method 2a. Better recoveries were observed for Method 2b (>81%).

Table 10: Caffeine, midazolam, tolbutamide and fexofenadine extraction efficiency data (Method 2).

Analyte	Extraction efficiency (%) Method 2a	Extraction efficiency (%) Method 2b
Caffeine	86.6 (2.4)	83.4 (5.5)
Midazolam	86.5 (2.6)	91.0 (2.6)
Tolbutamide	76.1 (5.1)	81.9 (0.7)
Fexofenadine	82.6 (0.2)	87.7 (2.7)
Mean recovery (%)	83.0	86.0

Mean from duplicate analyses (% difference from the mean stated in parentheses)

Although there is not a large difference in the recoveries for the two methods, the greater final volume for Method 2b means that the analyte and hence the

radioactivity is more dilute. When accounting for the filtrate volumes, Method 2a (Table 11) results in a larger proportion of analyte being analysed by HPLC, based on an injection volume of 100 µL. This method was chosen for use in further development of the HPLC-AMS assay.

Table 11: Typical proportions of analyte available for HPLC analysis on extraction using Methods 2a and 2b.

Method	Approximate filtrate volume (µL)	Approximate amount of analyte per 100 µL of plasma filtrate assuming 100% analyte recovery (%)	Approximate amount of analyte per 100 µL of plasma filtrate accounting for mean analyte recovery (%)
2a	240	42	35
2b	340	29	25

2.3.2 Development of a HPLC method for separation of caffeine, midazolam, tolbutamide and fexofenadine in human plasma

A HPLC method for midazolam using an Xterrra MS C18 column was previously reported [12]. The method employed isocratic elution, which gave the flexibility to introduce a gradient in order to achieve separation of the four analytes. Waters Xterra columns consist of a silica stationary phase, in which the hydroxyl of every third silanol is replaced with a methyl group [146]. This feature enables the column to operate at elevated temperatures (up to 60°C) over a wide pH range (pH 1 – pH 12). The reported method [12] was developed to separate midazolam from its metabolites and was used as a starting point for the further development of a HPLC method to separate caffeine, midazolam, fexofenadine and tolbutamide.

2.3.2.1 Determination of detector wavelength

The λ_{max} of each analyte was determined by UV spectrophotometry (Section 7.10). Optimum wavelengths were determined as 270 nm for caffeine and 240 nm for midazolam and tolbutamide. Fexofenadine does not have a strong UV absorbance. Instead fluorescence detection (λ_{ex} 220 nm and λ_{em} 290 nm) was used as reported by Uno et al [147].

2.3.2.2 HPLC Method A1 method transfer

A mixed reference standard comprising caffeine, midazolam, tolbutamide and fexofenadine (0.25 mg analyte/mL; Section 7.2.4) was injected onto a HPLC column, using the reported method for midazolam [12] (Method A1; Section 7.8.1). UV peaks were observed at 2 and 7.3 min (Figure 18).

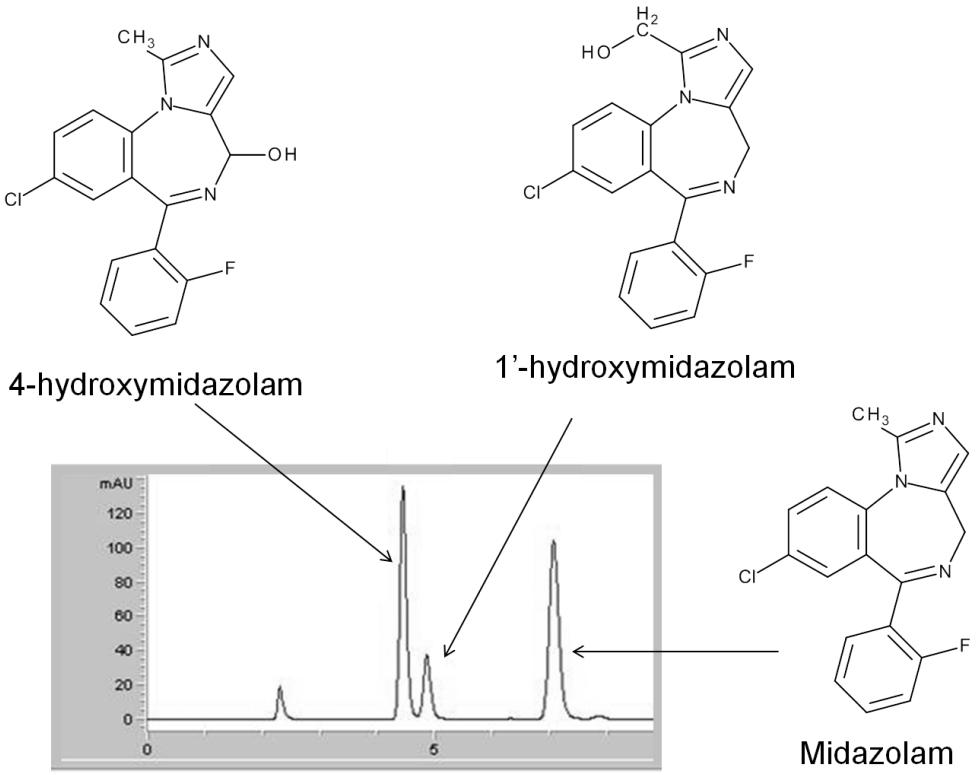

Figure 18: HPLC chromatogram of a mixture of midazolam, 1'-hydroxymidazolam and 4-hydroxymidazolam (Method A1) at 240 nm.

Injection of individual caffeine, midazolam, tolbutamide and fexofenadine reference standards (1 mg/mL; Section 7.2.4) showed midazolam to elute at 7.3 min, and the poor retention and co-elution of the three remaining analytes at approximately 2 min (Figure 19).

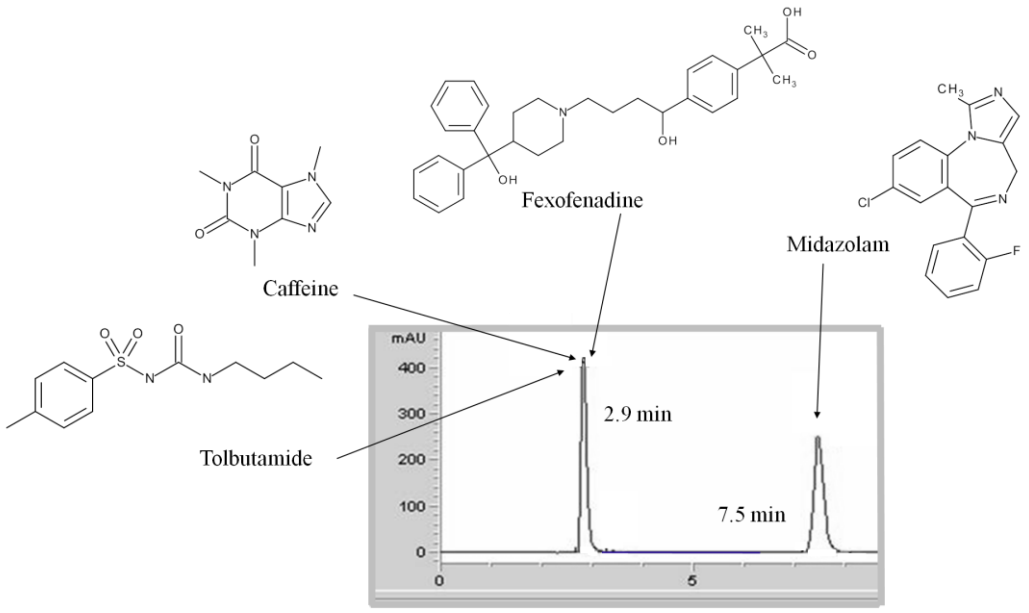

Figure 19: HPLC chromatogram of a mixture of caffeine, midazolam, tolbutamide and fexofenadine (Method A1) at 240 nm.

2.3.2.3 Development of HPLC Method A2

Method A1 was modified to introduce a gradient with the acetonitrile: ammonium acetate ratio increasing from 10:90 (v/v) to 50:50 (v/v) over 15 min, followed by a column flush (90% acetonitrile) and re-equilibration (Method A2; Section 7.8.1).

Individual reference standards (1 mg analyte/mL) were analysed by HPLC as well as the following mixed reference standards (Section 7.2.4):

- caffeine, midazolam, tolbutamide and fexofenadine (0.25 mg analyte/mL);
- caffeine and metabolites theobromine, theophylline and paraxanthine (0.25 mg analyte/mL);
- tolbutamide and metabolites 4-hydroxytolbutamide and carboxytolbutamide (0.33 mg analyte/mL);

- midazolam and metabolites 1'-hydroxymidazolam and 4-hydroxymidazolam (0.33 mg analyte/mL).

Metabolites of fexofenadine are not reported to be present in significant concentrations in plasma [22, 137] and so were not included. Reducing the ratio of acetonitrile in the initial mobile phase composition from 50% to 10% in Method A2 reduced the initial solvent strength and resulted in the increased retention of each analyte. Caffeine, fexofenadine, midazolam and tolbutamide were baseline resolved (Figure 20).

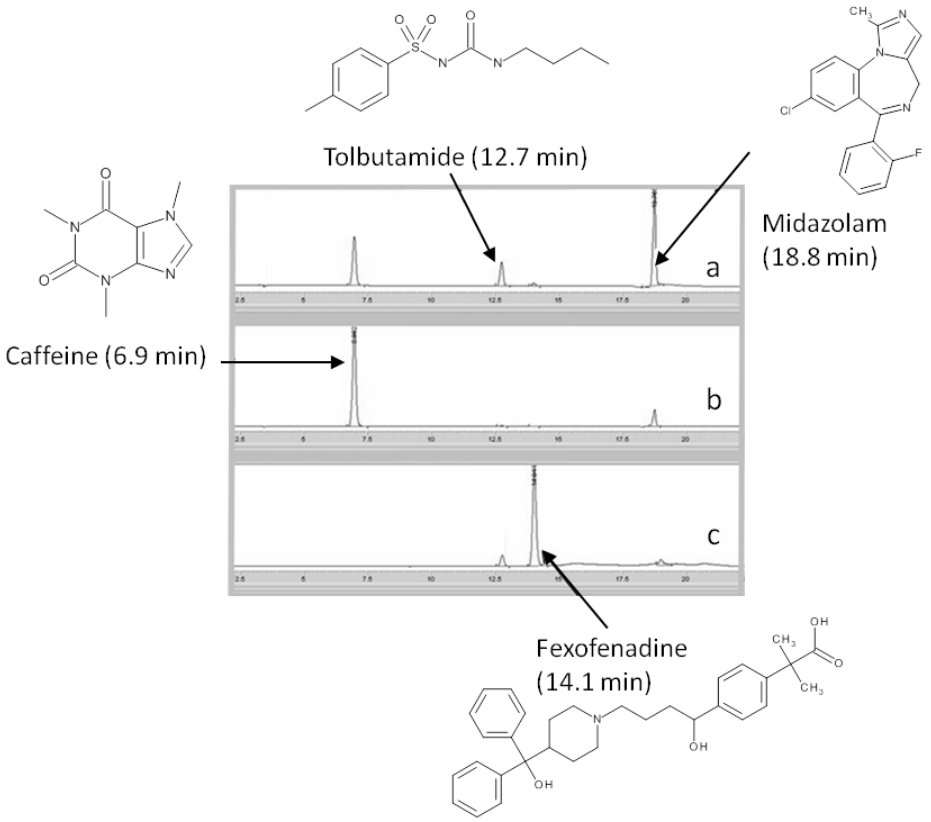

Figure 20: HPLC chromatogram of a mixture of midazolam and tolbutamide at 240 nm (a), caffeine at 270 nm (b) and fexofenadine at λ_{ex} 220 nm and λ_{em} 290 nm (c) (Method A2).

In addition, baseline separation was also observed between each analyte and its metabolites (Figure 21 – Figure 23).

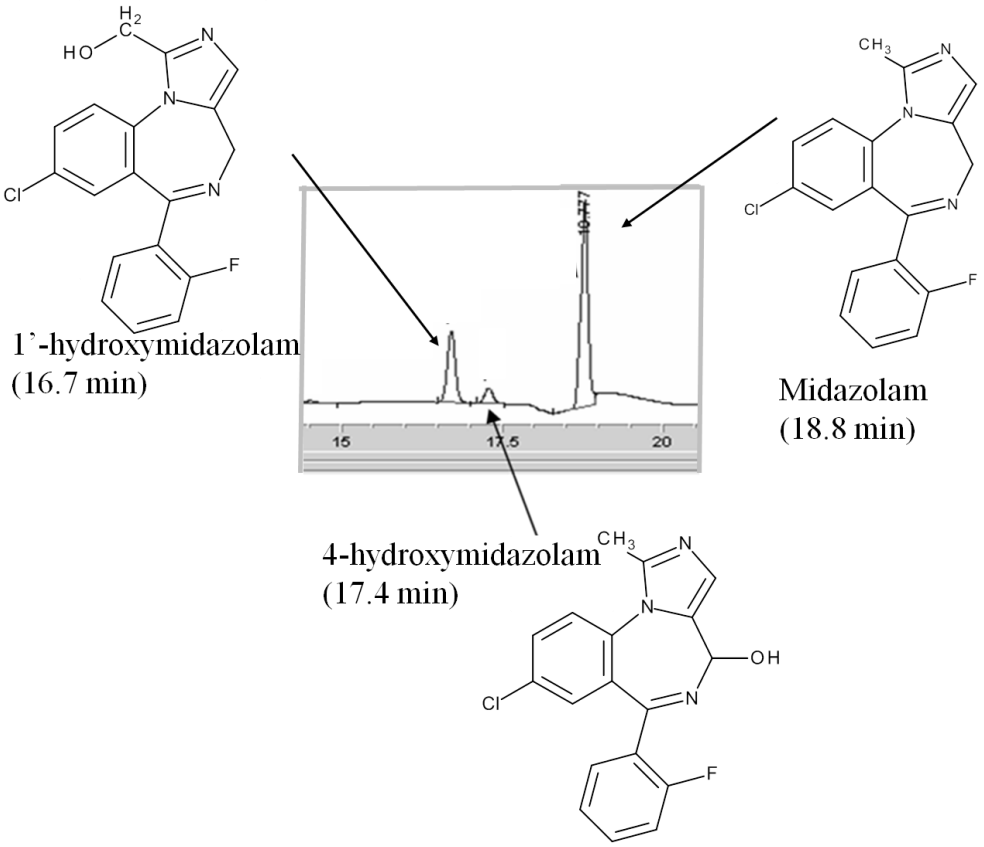

Figure 21: HPLC chromatogram of a mixture of midazolam, 1'-hydroxymidazolam and 4-hydroxymidazolam at 240 nm (Method A2).

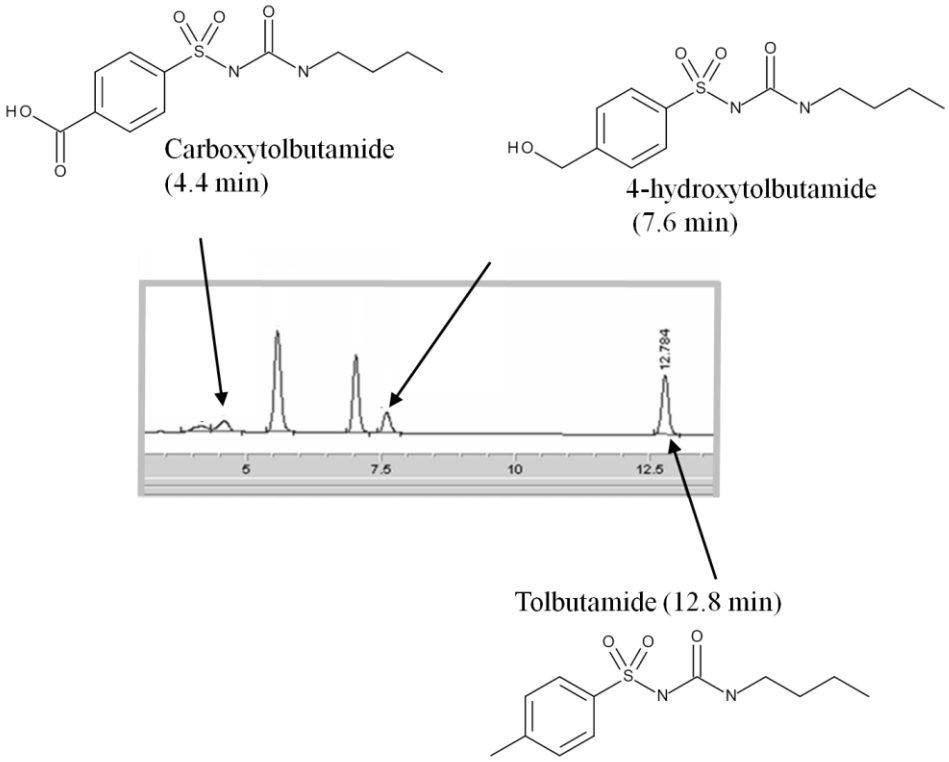

Figure 22: HPLC chromatogram of a mixture of tolbutamide, 4-hydroxytolbutamide and carboxytolbutamide at 240 nm (Method A2).

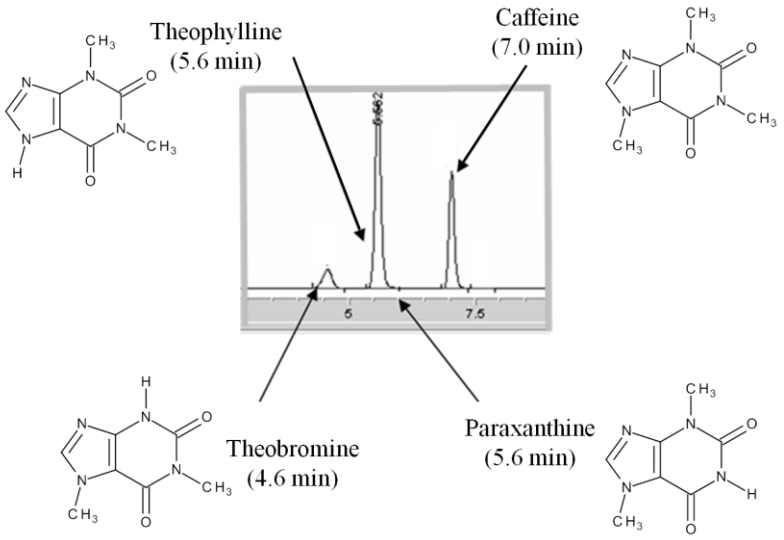

Figure 23: HPLC chromatogram of a mixture of caffeine, theobromine, theophylline and paraxanthine at 270 nm (Method A2).

Method A2 was satisfactory in terms of separation of the four analytes, caffeine, midazolam, tolbutamide and fexofenadine, and commercially available metabolites. Slight modifications were required to further separate caffeine and 4-hydroxytolbutamide, and tolbutamide and fexofenadine. Prior to further development of HPLC Method A2 the chromatography was assessed for compatibility with protein precipitation Method 2a.

2.3.2.4 Analysis of plasma filtrate by HPLC using Method A2

Spiked predose plasma samples were prepared and subjected to protein precipitation extraction. Aliquots of each filtrate were analysed by HPLC under Method A2 conditions (Section 7.6.1). The chromatogram obtained for plasma filtrate containing caffeine contains a broad peak eluting up to the retention time of caffeine, resulting in poor resolution of the analyte (Figure 24).

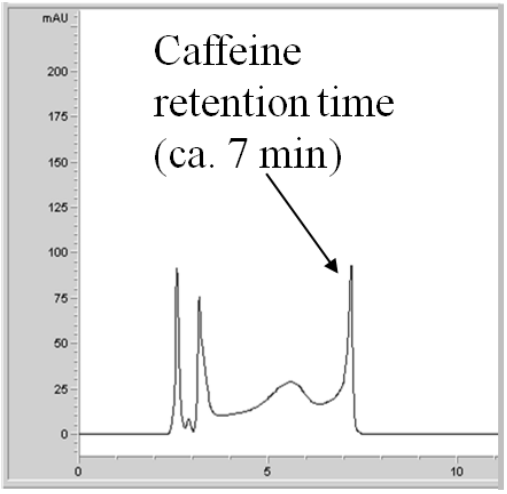

Figure 24: HPLC chromatogram of pre-dose clinical plasma spiked with caffeine and extracted with acetonitrile.

This poor resolution was not observed during analysis of the caffeine reference standard. Where possible, the analyte should be dissolved in the mobile phase prior to analysis by HPLC. All reference material used to generate chromatograms shown in Figure 20 – 23 was prepared in ethanol. Although the ethanol solution was at a higher solvent strength than the mobile phase (acetonitrile: ammonium acetate 10:90 v/v) at initial conditions, the relatively low injection volume of 5 – 10 µL resulted in no significant loss of resolution of

the reference material. The plasma filtrate shown in Figure 24 consists of a large proportion of acetonitrile (approximately 75-80%) and the injection volume was much higher (100 µL). The combination of the increased solvent strength and the large injection volume of a solvent incompatible with the initial mobile phase conditions resulted in the poor resolution of caffeine in plasma filtrate. The extraction method was further developed with the lower strength solvent, methanol (Section 2.3.2.5).

2.3.2.5 Development of protein precipitation extraction Method 3

Pre-dose plasma filtrate was prepared with methanol in place of acetonitrile and analysed by HPLC Method A2 (Section 7.6.2). No interfering peaks were present in the chromatogram (Figure 25) and caffeine was baseline resolved. Protein precipitation extraction with methanol was deemed suitable for use and was employed in all further method development.

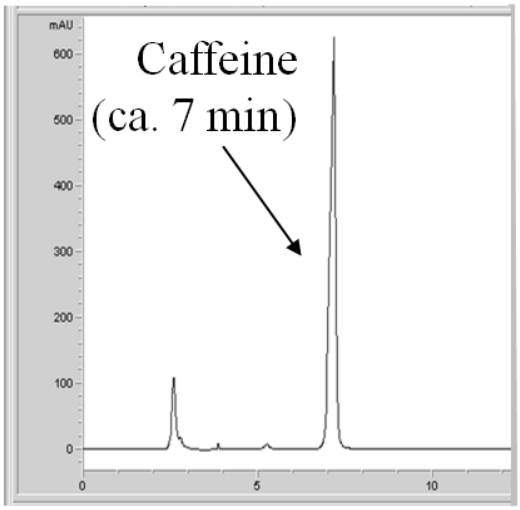

Figure 25: HPLC chromatogram of caffeine extracted from plasma with methanol.

The effect on the recovery of each analyte when using methanol to precipitate plasma proteins was assessed. Spiked plasma samples were prepared and extracted (Section 7.5.1) and the extraction efficiencies calculated using Equation 14 (Section 2.3.2.1). Plasma extraction efficiencies were > 74% for all analytes, with recoveries of 76.3%, 77.2%, 74.1% and 74.4% for caffeine, midazolam, tolbutamide and fexofenadine in turn with good precision (CV<5%).

2.3.2.6 Development of HPLC method A3

The gradient used in method A2 was modified between 0 and 22 min (Section 7.8.1) to allow separation of the four most closely eluting analytes. The method achieved greater separation, due to the slower introduction of acetonitrile and therefore increased retention of each analyte. Caffeine and 4-hydroxytolbutamide, and tolbutamide and fexofenadine were each separated by a further 0.5 min. Separation between all other analytes was maintained (Table 12). Separation of caffeine, midazolam, tolbutamide and fexofenadine using Method A3 is shown in Figure 26.

Table 12: Typical retention times of caffeine, midazolam, tolbutamide and fexofenadine plus selected metabolites (HPLC Method A3).

Analyte	Retention time (min)
Carboxytolbutamide	4.1
Theobromine	4.5
Theophylline / paraxanthine	5.5
Caffeine	7.6
4-hydroxytolbutamide	8.7
Tolbutamide	16.5
Fexofenadine	18.4
1'-hydroxymidazolam	21.7
4-hydroxymidazolam	22.3
Midazolam	24.3

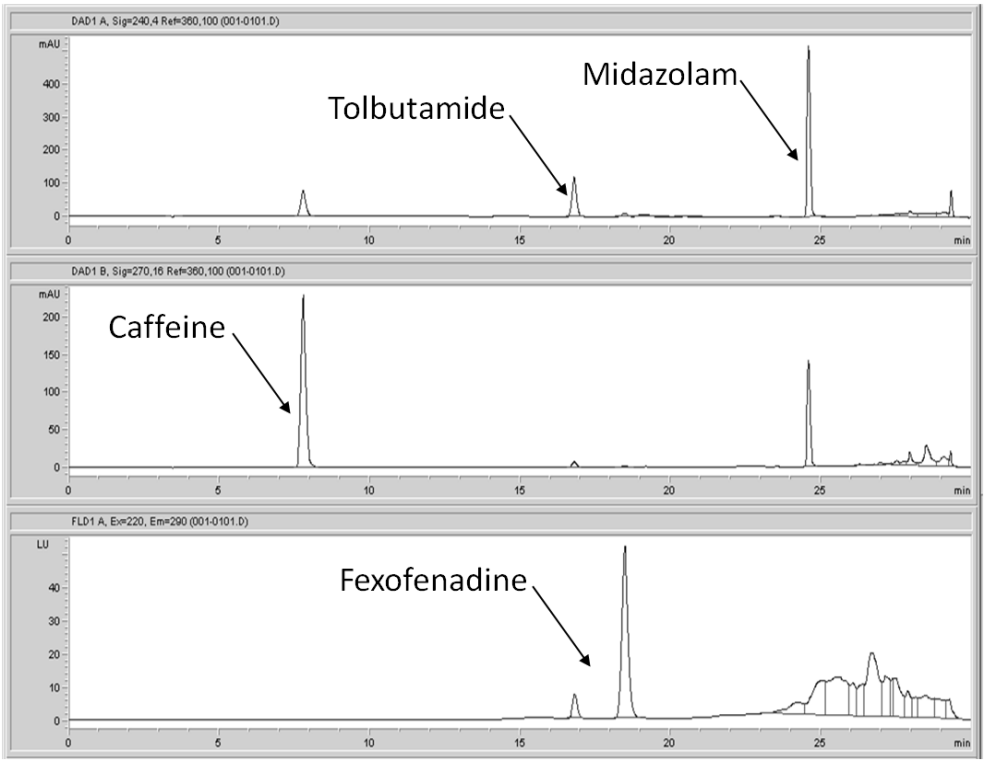

Figure 26: HPLC chromatogram of a mixture of caffeine (270 nm), midazolam (240 nm), tolbutamide (240 nm) and fexofenadine at λ_{ex} 220 nm and λ_{em} 290 nm (Method A3).

Of the four major analytes, caffeine is the most polar compound and eluted first at 7.6 min under Method A3 conditions. Separation of the analytes was mediated by their partition between the C18 stationary phase and the mobile phase. The introduction of acetonitrile to the mobile phase over time decreased the polarity of the mobile phase. The pH of the mobile phase was not measured but is assumed to be pH 7. The logD for each analyte at pH 7 is shown in Table 13.

Table 13: pK_a, logP and logD of caffeine, midazolam, tolbutamide and fexofenadine.

Analyte	pK_a	logD (pH 7)	References
Caffeine	14[1]/0.8[2]	0.07	[138, 140, 141]
Midazolam	6.57	3.98	
Tolbutamide	4.33	2.36	
Fexofenadine	4.04[1]/9.01[2]	2.94	

[1]acidic [2] basic

The linear relationship between the partition coefficients (logD) versus the retention time of the analyte is described in Figure 27. The elution time is mediated by the polarity of the mobile phase at a given time.

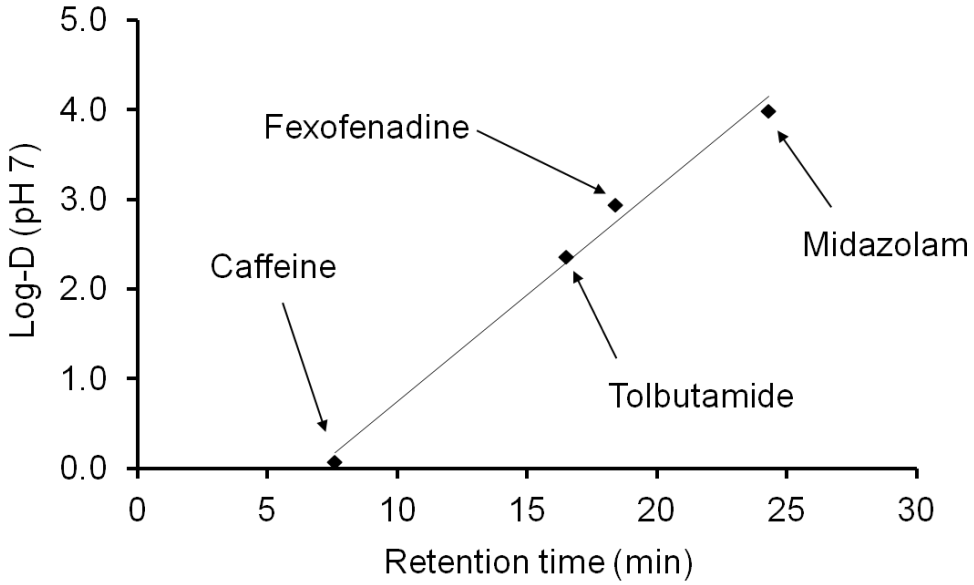

Figure 27: logD (pH 7) plot for caffeine, midazolam, tolbutamide and fexofenadine separated on a C18 reverse phase column eluted with acetonitrile: 0.1 M ammonium acetate.

Where the logD of two analytes are close together, separation may be increased by a slower change in the polarity of the mobile phase. This was deemed unnecessary as all analytes were fully resolved. As an alternative to gradient modifications, separation could have been achieved using a buffered mobile phase and a pH gradient. The effect of pH on the partition coefficient (logP) of an analyte could have been used to predict the retention time under these modified conditions. It is well established that altering the pH within 1 pH unit at either side of the pK_a of an analyte results in the most marked changes in retention time [148].

2.3.2.7 Assessment of method repeatability and carryover

Caffeine, midazolam, tolbutamide and fexofenadine reference standards (0.25 mg analyte/mL; Section 7.2.4) were analysed by HPLC Method A3 (Section 7.8.1). Repeatability was evaluated by multiple injections of each reference standard (n=3) and a blank injection was made after injection 3 for evaluation of carryover. Further analyses were performed on four consecutive days to assess the inter-day repeatability of the HPLC method.

Replicate injections (n=3) on day 1 resulted in mean retention times of 7.7 min, 24.6 min, 16.9 min and 18.5 min for caffeine, midazolam, tolbutamide and fexofenadine in turn (Table 14). The precision at each retention time was good (CV<0.5%). The blank injections gave no detector response at the retention times corresponding to caffeine, midazolam, tolbutamide and fexofenadine, indicating that there was no detectable carryover.

Table 14: Intra-day repeatability data for caffeine, tolbutamide, fexofenadine and midazolam (Day 1, HPLC Method A3).

	Caffeine retention time (min)	Tolbutamide retention time (min)	Fexofenadine retention time (min)	Midazolam retention time (min)
Injection 1	7.77	16.81	18.51	24.60
Injection 2	7.73	16.89	18.51	24.60
Injection 3	7.73	16.89	18.51	24.60
Mean	7.74	16.87	18.51	24.60
% CV	0.30	0.27	0.00	0.00

The mean retention times over 5 days were identical to those obtained on day 1 (Table 15).

Table 15: Inter-day repeatability data for caffeine, tolbutamide, fexofenadine and midazolam (HPLC Method A3).

	Caffeine retention time (min)	Tolbutamide retention time (min)	Fexofenadine retention time (min)	Midazolam retention time (min)
Day 1 (mean)	7.74	16.87	18.51	24.60
Day 2	7.73	16.89	18.51	24.60
Day 3	7.71	16.87	18.46	24.57
Day 4	7.70	16.85	18.47	24.58
Day 5	7.80	16.90	18.51	24.57
Mean	7.74	16.88	18.49	24.58
% CV	0.51	0.12	0.13	0.06

2.3.3 Development of a HPLC method to separate caffeine, midazolam, tolbutamide and fexofenadine in human plasma

The purity of caffeine, tolbutamide, midazolam and fexofenadine fractions obtained using HPLC Method A3 (Section 7.8.1) was assessed prior to its use in the analysis of clinical plasma samples using two-dimensional chromatography. All commercially available metabolites were separated from each of the four analyte peaks in the UV chromatogram (Section 2.3.1.4) using the C18 Method A3. The presence of further ^{14}C-containing components in clinical plasma samples was investigated via a second method using a different (phenyl) stationary phase contrasting with the C18 stationary phase used in the initial separation. Two columns were selected, a Phenomenex Synergi Polar RP and a Phenomenex Gemini C6-phenyl (Method B1 – B4; Section 7.8.1). Both columns feature phenyl groups bound to the silica stationary phase, via an ether linkage in the case of the Synergi column and via a 6-carbon chain in the case of the Gemini column (Phenomenex Column Literature). The interaction of the analyte with the phenyl stationary phase differs from the hydrophobic interactions observed in C18 HPLC analysis (HPLC Method A3). The π electrons in the phenyl ring of the stationary phase interact with the π electrons of the analyte, which are not present in a C18 stationary phase. This difference in selectivity was exploited in the development of a two-dimensional HPLC separation method. A phenyl HPLC method was developed and assessed (Section 2.3.3.1 – Section 2.3.3.4) for caffeine, midazolam, tolbutamide and fexofenadine standards

(5 µL; 1 mg/mL; Section 7.2.4). The aim of phenyl method development was to obtain a chromatogram free of baseline interferences, to enable the analyte to be isolated by HPLC fractionation. Significant development of the methods was not required. The mobile phase conditions (Section 2.3.3.1 – Section 2.3.3.4) were the initial conditions chosen for each system. These conditions gave satisfactory peak shapes and peak widths to enable each analyte to be isolated by HPLC fractionation. Optimisation of the HPLC methods was not considered, however had further development been necessary the principles considered in Section 2.3.2.3 would also be applicable here.

2.3.3.1 Caffeine HPLC method B1

The Synergi Polar RP column (40°C) was eluted with a water: methanol gradient decreasing from 90:10 v/v to 50:50 v/v over 3 min, then to 10:90 v/v over 5 min. The gradient was held at 10:90 v/v for 3 min and re-cycled to 90:10 v/v (Section 7.8.1). Elution of caffeine at 9.3 min (Figure 28) was determined by UV detection (270 nm).

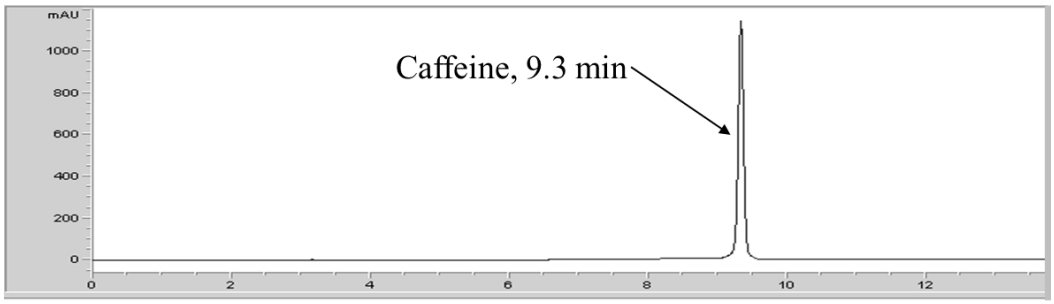

Figure 28: HPLC chromatogram of caffeine at 270 nm (Method B1).

2.3.3.2 Midazolam HPLC method B2

The Synergi Polar RP column (40°C) was eluted with a 10 mM aq. KH_2PO_4: acetonitrile gradient decreasing from 90:10 v/v to 50:50 over 3 min, then to 0:100 v/v over 7 min. The gradient was held at 0:100 v/v for 1 min, and re-cycled to 90:10 v/v (Section 7.8.1). Elution of midazolam at 10.2 min (Figure 29) was determined by UV detection (220 nm).

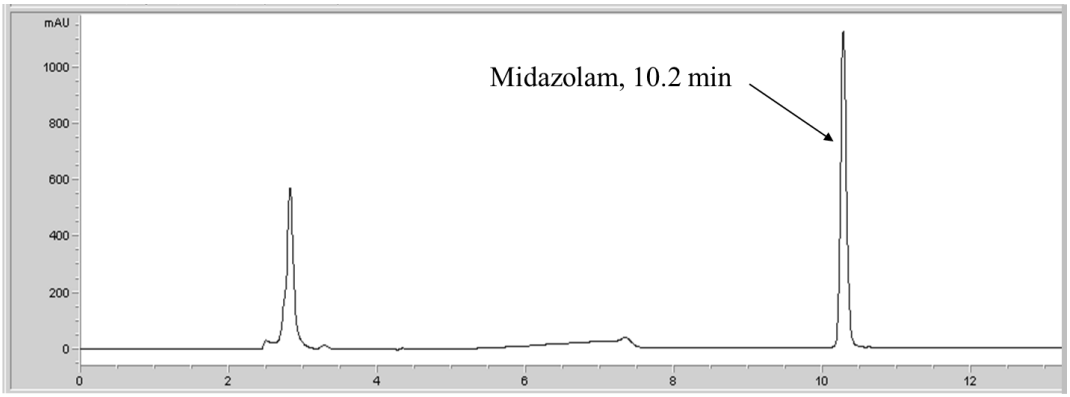

Figure 29: HPLC chromatogram of midazolam at 240 nm (Method B2).

2.3.3.3 Tolbutamide HPLC method B3

The Gemini C6-phenyl column (40°C) was eluted with a 0.1% aq. formic acid: methanol gradient decreasing from 70:30 v/v to 10:90 v/v over 25 min. The gradient was held at 10:90 v/v for 1 min, and re-cycled to 70:30 v/v (Section 7.8.1). Elution of tolbutamide at 12.9 min (Figure 30) was determined by UV detection (240 nm).

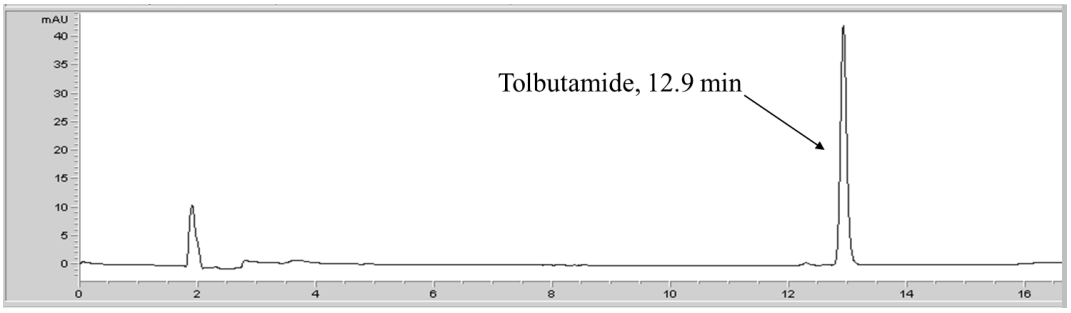

Figure 30: HPLC chromatogram of tolbutamide at 240 nm (Method B3).

2.3.3.4 Fexofenadine HPLC method B4

The Gemini C6-phenyl column (40°C) was eluted with a water: acetonitrile gradient decreasing from 90:10 v/v to 10:90 v/v over 10 min The gradient was held at 10:90 v/v/ for 2 min followed by 0:100 v/v for 2 min and re-cycled to 90:10 v/v (Section 7.8.1). Elution of fexofenadine at 9.8 min (Figure 31) was determined by fluorescence detection (λ_{ex} 220 nm and λ_{em} 290 nm).

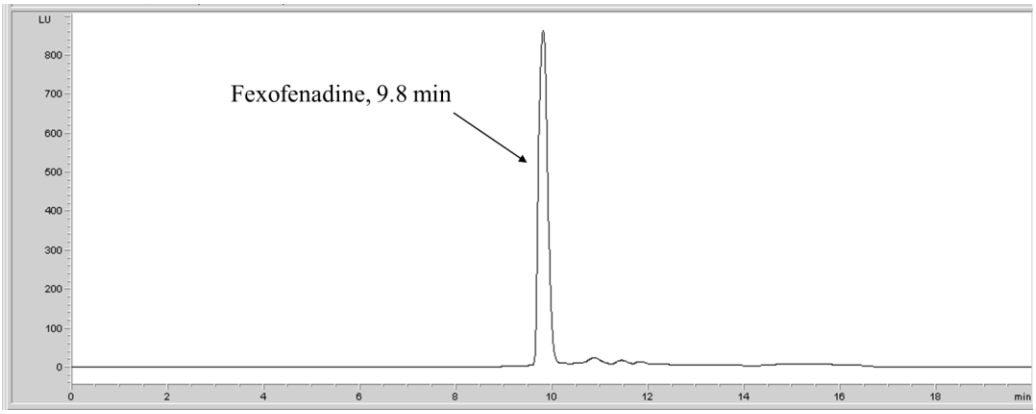

Figure 31: HPLC chromatogram of fexofenadine at λ_{ex} 220 nm and λ_{em} 290 nm (Method B4).

2.3.3.5 Assessment of method repeatability

Repeatability of the HPLC methods (B1 – B4) was evaluated by analysis of replicate injections (3 x 5 µL) of each reference standard (1 mg/mL; Section 7.2.4), with a blank injection after injection 3 for evaluation of carryover. Mean retention times were 9.3 min for caffeine, 10.2 min for midazolam, 12.9 min for tolbutamide and 9.8 min for fexofenadine. The precision at each retention time was good (CV<0.3%). Blank injections gave no detector response at the retention times corresponding to caffeine, midazolam, tolbutamide and fexofenadine, indicating that there was no carryover (Table 16).

Table 16: Intra-day repeatability data for caffeine, midazolam, tolbutamide and fexofenadine (HPLC methods B1-B4).

	Caffeine retention time (min) Method B1	**Midazolam retention time (min) Method B2**	**Tolbutamide retention time (min) Method B3**	**Fexofenadine retention time (min) Method B4**
Injection 1	9.33	10.24	13.00	9.85
Injection 2	9.33	10.23	12.92	9.79
Injection 3	9.33	10.23	12.93	9.81
Mean	9.33	10.23	12.95	9.82
% CV	0.00	0.06	0.34	0.31

2.3.4 Determination of the internal standard level

In HPLC-AMS analysis, the internal standard used in analysis is the non-labelled analyte of interest [106]. The amount of internal standard for HPLC analysis must be above the LOQ of the detector without exceeding the linear range. In addition, endogenous levels of non-labelled analyte in plasma must be negligible with respect to the amount of internal standard added. In the present study, levels of non-labelled analyte after microdose administration are expected to be relatively small, but should still be taken into consideration.

2.3.4.1 Assessment of detector response linearity

Reference standard solutions were prepared over the range 1 – 5 µg for caffeine and tolbutamide and 2 – 10 µg for midazolam and fexofenadine (Section 7.2.4) and the detector response assessed for HPLC Method A3 (5 µL; Section 7.8.1). The amount of analyte vs. detector response gave correlation coefficients (r^2) of > 0.999 for all analytes over the given concentration ranges (Figure 32 – Figure 35).

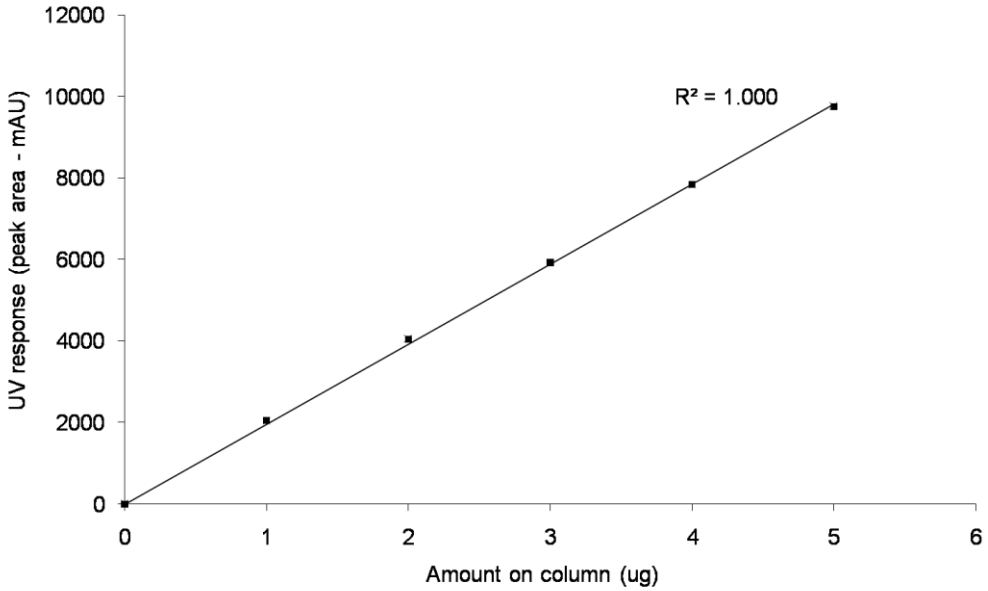

Figure 32: UV detector response for caffeine.

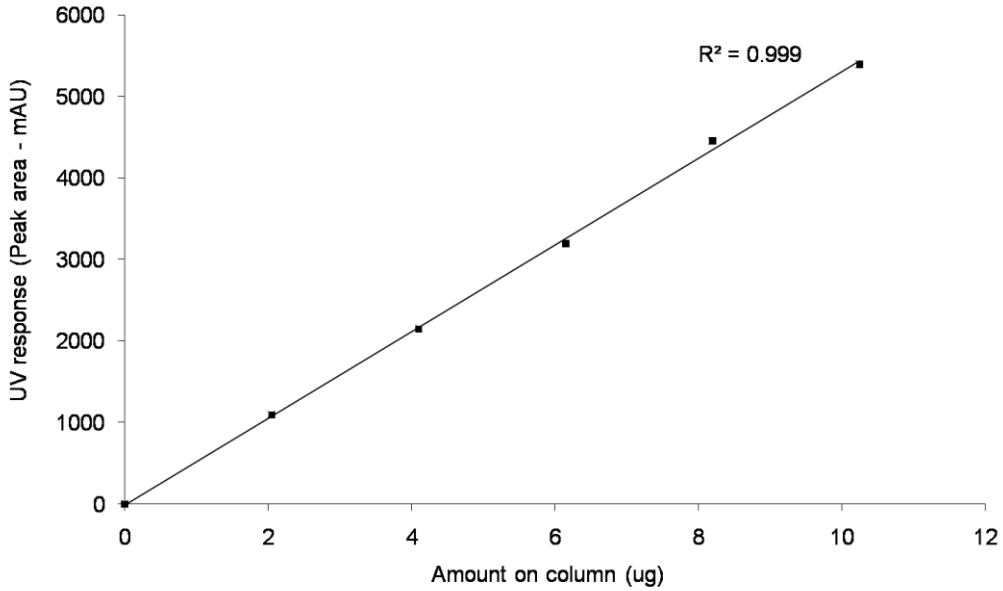

Figure 33: UV detector response for midazolam.

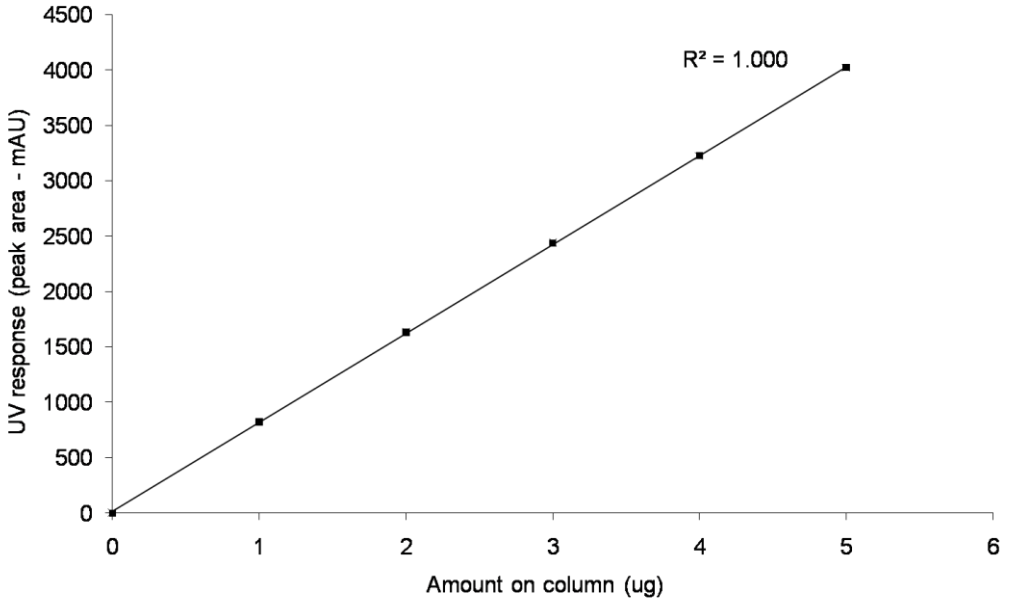

Figure 34: UV detector response for tolbutamide.

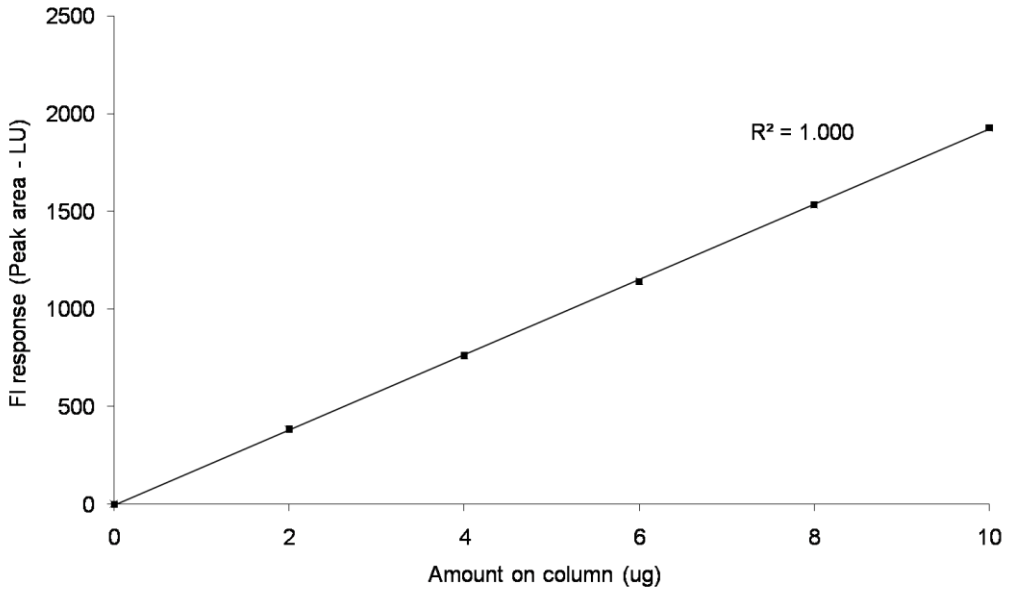

Figure 35: Fluorescence detector response for fexofenadine.

2.3.4.2 Determination of non-labelled caffeine, midazolam, tolbutamide and fexofenadine present in clinical plasma

The expected C_{max} of caffeine, midazolam, tolbutamide and fexofenadine after oral administration have been previously reported and these data were used to estimate the C_{max} after administration of a 25 µg oral microdose (Table 17).

Table 17: C_{max} data for caffeine, midazolam, tolbutamide and fexofenadine as reported in the literature.

Analyte	Dose (mg)	C_{max} (ng/mL)	Calculated C_{max} after 25 µg dose (ng/mL)	Source
Caffeine	100	2390	0.60	[42]
Midazolam	0.1 (microdose)	0.37	0.092	[12]
	7.5	34	0.11	[12]
Tolbutamide	125	16300	3.3	[149]
Fexofenadine	0.1 (microdose)[1]	0.31	0.078	[23]
	60	286	0.072	[150]

[1]data not available at time of present work, used only for retrospective comparison

Assuming dose linearity between C_{max} obtained after microdose administration and those obtained after higher doses, values for the estimated C_{max} of 0.6 ng/mL, approximately 0.1 ng/mL (mean value), 3.3 ng/mL and approximately 0.075

ng/mL (mean value), were determined for caffeine, midazolam, tolbutamide and fexofenadine respectively. Where data were available for a microdose and a higher therapeutic dose, a mean of the two values was assumed.

The protein precipitation method (Section 7.6.1) and HPLC method A3 (Section 7.8.1) developed (Section 2.3.2.2. and Section 2.3.1.4) uses the following volumes:

- plasma volume taken for extraction – 100 µL;
- resulting plasma filtrate volume – approximately 240 µL;
- plasma filtrate volume analysed by HPLC – 100 µL.

Application of the above volumes results in the equivalent of 42% of the analyte that is present in 1 mL of plasma being available for HPLC analysis. Hence, the minimum amount of internal standard was calculated (Table 18).

Table 18: Calculation of estimated caffeine, midazolam, tolbutamide and fexofenadine C_{max} data after microdose administration.

Analyte	Calculated C_{max} after 25 µg dose (ng/mL)	Mass present in 240 µL aliquot taken for extraction (ng)	Mass present in 100 µL of plasma filtrate taken for HPLC analysis (ng)	Minimum amount to be added as internal standard (ng)[1]
Caffeine	0.60	0.060	0.025	2.5
Midazolam	0.10	0.010	0.0040	0.42
Tolbutamide	3.3	0.33	0.14	13.8
Fexofenadine	0.075	0.0075	0.0031	0.031

[1]x100 carbon mass present in 100 µL of plasma filtrate taken for HPLC analysis

2.3.4.3 Calculation of amount of internal standard

The amount of internal standard was determined to be a maximum of 5 µg for caffeine and tolbutamide, and 10 µg for fexofenadine and midazolam, as determined from the HPLC detector response (Figure 32 – Figure 35). An internal standard mass of 3 µg was chosen for eventual HPLC analysis, which

gives a UV response within the range assessed for detector linearity. This is also at least 9000 times the tolbutamide C_{max} after microdose administration.

2.3.5 Verification of the chromatographic separation of caffeine, midazolam, tolbutamide and fexofenadine by HPLC

Prior to its application in the clinical study, the complete isolation of caffeine, midazolam, tolbutamide and fexofenadine from other ^{14}C containing components using HPLC Method A3 (Section 7.8.1) was tested. This was performed using clinical plasma samples that contained all four analytes plus *in vivo* metabolites. This check was carried out at several time-points, should metabolites be time-point specific. Clinical plasma samples were pooled in equal volumes across all six subjects. As there were two separate dosing regimens, samples for each dosing period were analysed separately resulting in eight pooled plasma samples as follows:

- 1, 6, 12 and 24 h post administration, dosing period 1;
- 1,6,12 and 24 h post administration, dosing period 2.

Pooled plasma samples were prepared and subjected to protein precipitation extraction. Plasma filtrates were analysed by HPLC with C18 stationary phase (Method A3). Fractions were collected over the retention times for caffeine, midazolam, tolbutamide and fexofenadine and analysed by HPLC with phenyl stationary phase using Method B1 to Method B4 (Figure 36; Section 7.6.3).

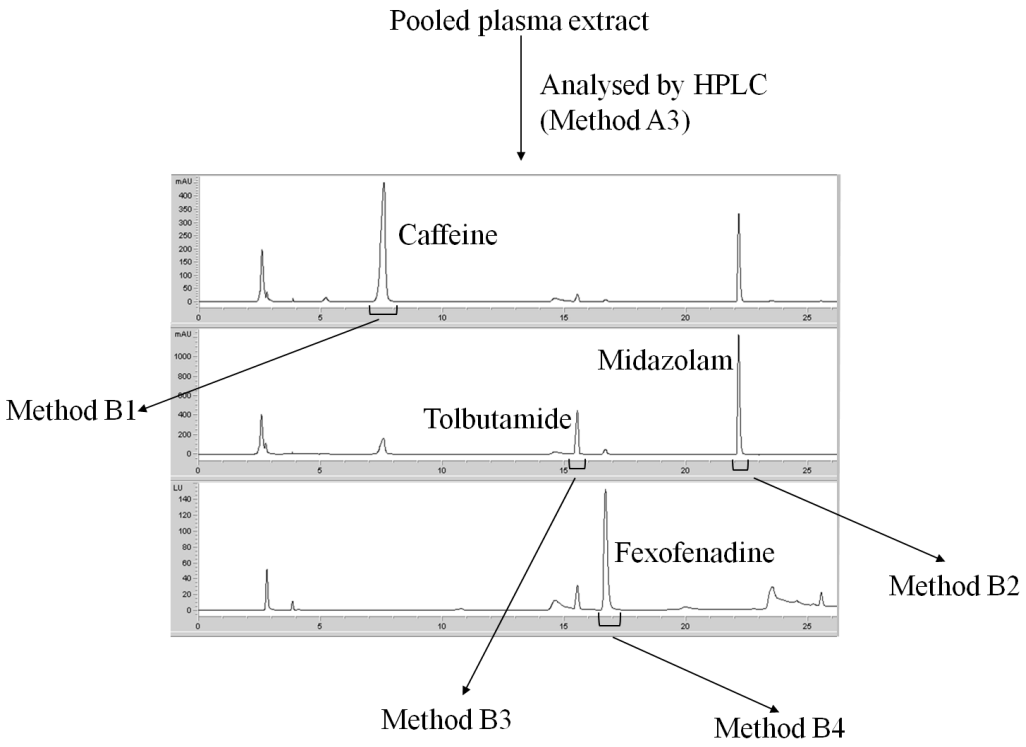

Figure 36: Schematic representation of the two-dimensional HPLC separation and isolation method.

Fractions of 15 second duration were collected over each of the second dimension separations and were analysed by AMS. The concentration of each fraction was plotted vs. the fraction collection time (Figure 37 – Figure 44; Section 7.6.3).

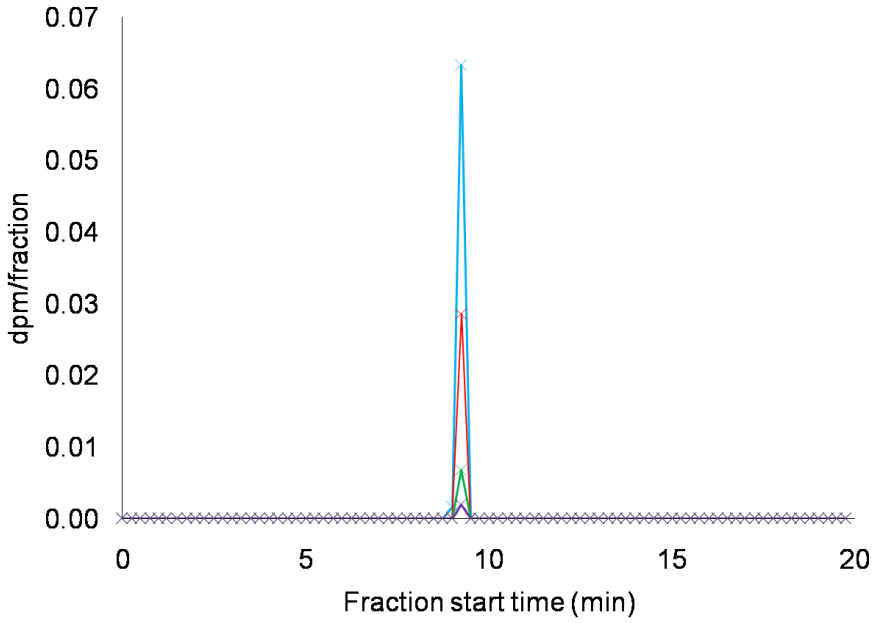

Figure 37: Reconstructed caffeine radio-chromatogram, period 1, legend: blue = 1 h, red = 5 h, green = 12 h, purple = 24 h.

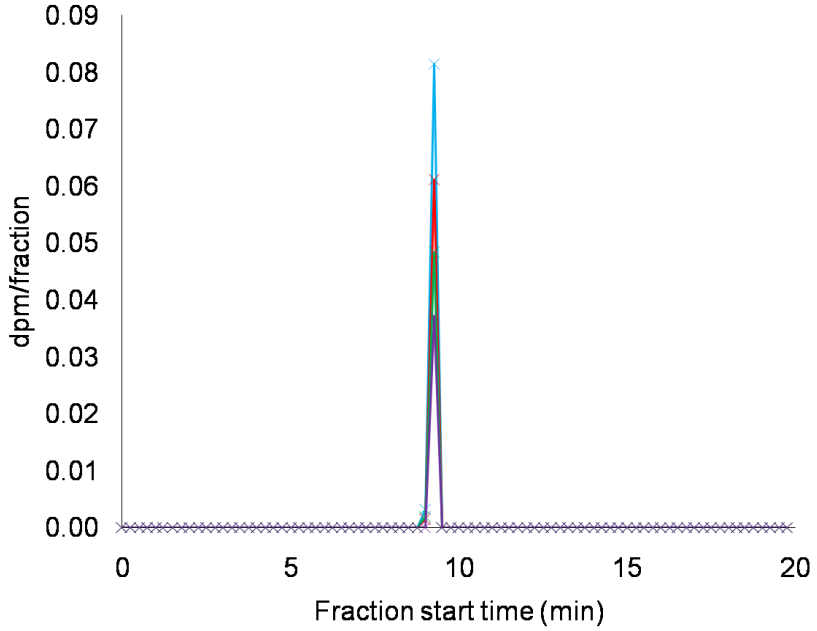

Figure 38: Reconstructed caffeine radio-chromatogram, period 2, legend: blue = 1 h, red = 5 h, green = 12 h, purple = 24 h.

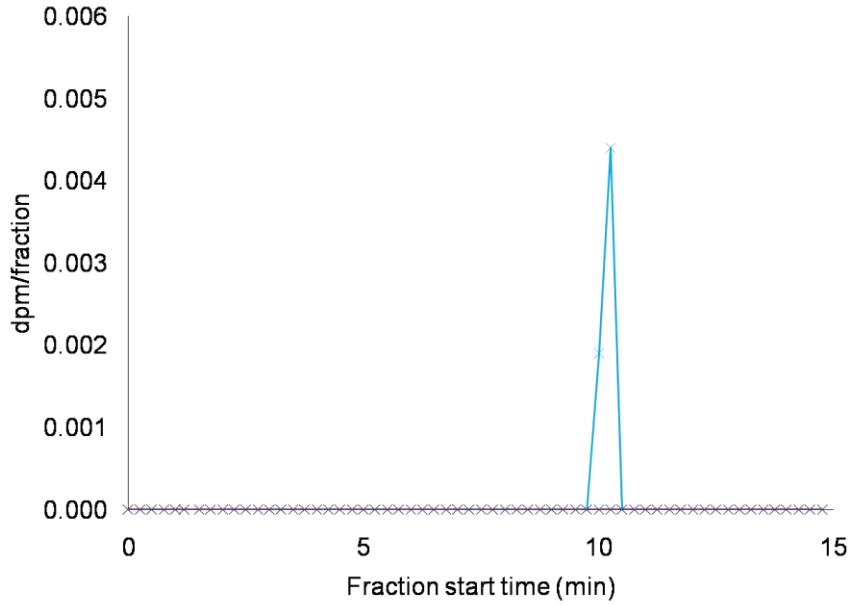

Figure 39: Reconstructed midazolam radio-chromatogram, period 1, legend: blue = 1 h, purple = 5 h, 12 h and 24 h.

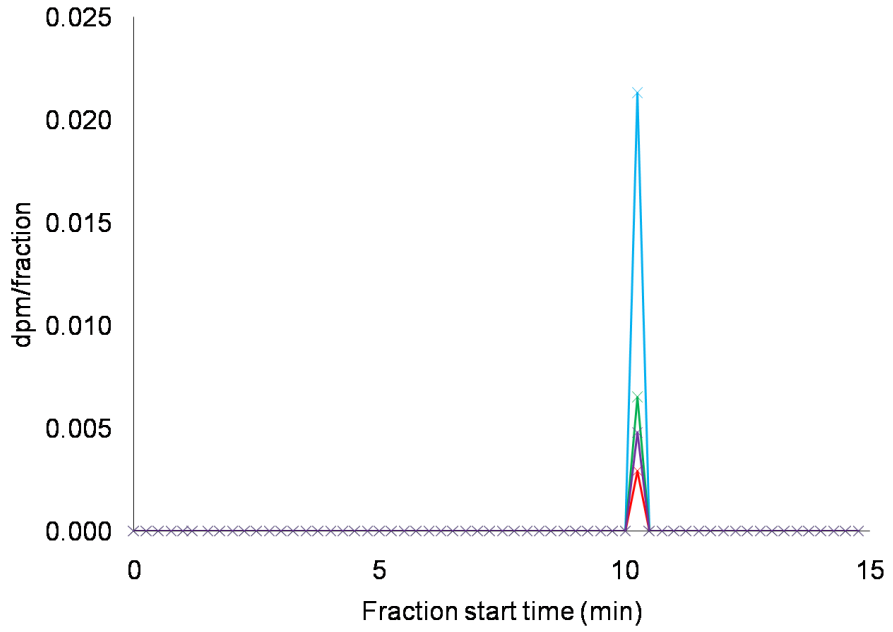

Figure 40: Reconstructed midazolam radio-chromatogram, period 2: legend: blue = 1 h, red = 5 h, green = 12 h, purple = 24 h.

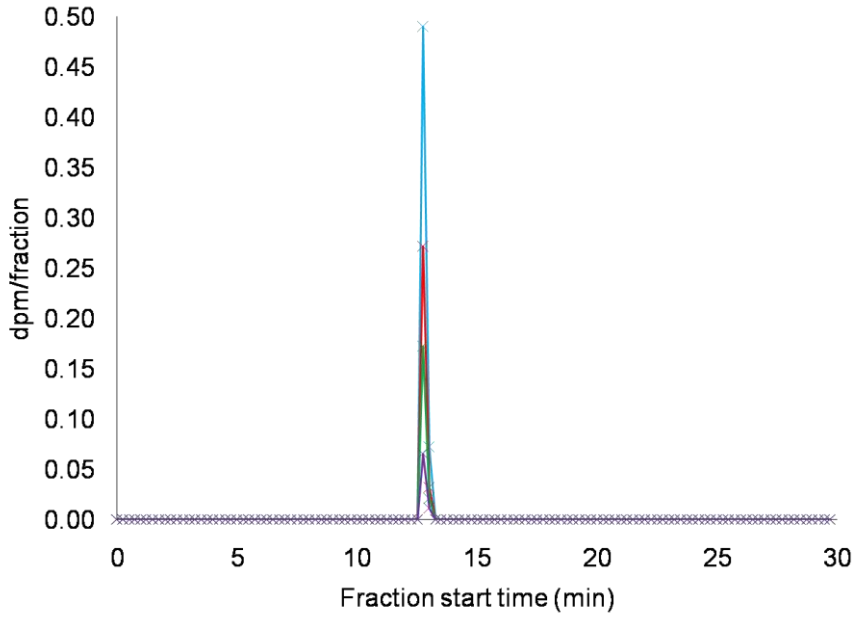

Figure 41: Reconstructed tolbutamide radio-chromatogram data, period 1, legend: blue = 1 h, red = 5 h, green = 12 h, purple = 24 h.

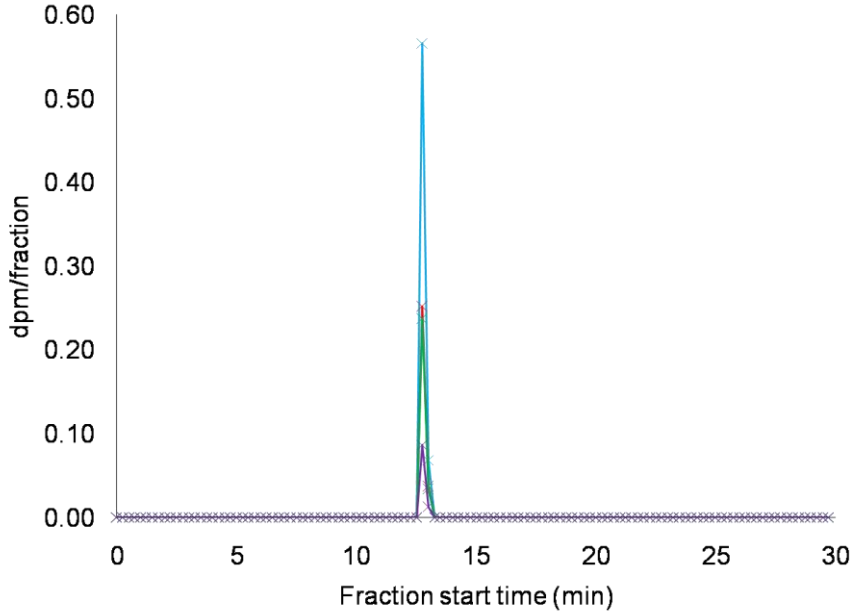

Figure 42: Reconstructed tolbutamide radio-chromatogram data, period 2, legend: blue = 1 h, red = 5 h, green = 12 h, purple = 24 h.

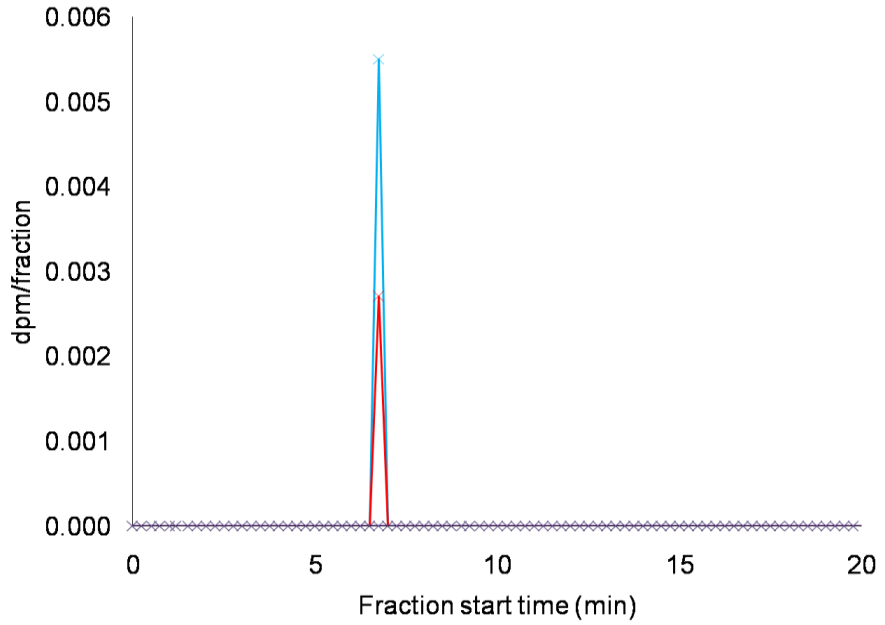

Figure 43: Reconstructed fexofenadine radio-chromatogram, period 1, legend: blue = 1 h, red = 5 h, green = 12 h, purple = 24 h.

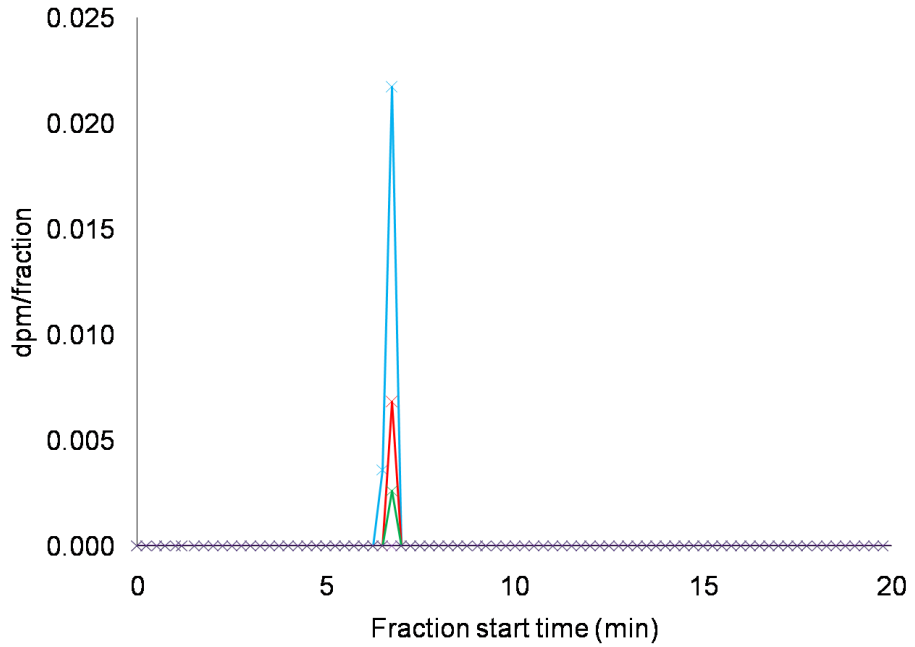

Figure 44: Reconstructed fexofenadine radio-chromatogram, period 2, legend: blue = 1 h, red = 5 h, green = 12 h, purple = 24 h.

^{14}C-midazolam concentrations of the 6, 12 and 24 h plasma samples for period 1 were below the AMS limit of quantification (LOQ; Section 7.11.4.1). Similarly, ^{14}C data were only obtained for the 1 and 6 h plasma sample for fexofenadine, the remainder being below the AMS LOQ (Section 7.11.4.1).

All of the radioactivity recovered from the fractions collected using the Method A3 (C18 analysis) for caffeine, midazolam, tolbutamide and fexofenadine was contained exclusively in the fractions corresponding to the analyte, as identified by the internal standard during phenyl HPLC analysis (Methods B1 – B4). The absence of ^{14}C in the eluate collected over the remainder of the chromatogram verifies that the peak obtained from HPLC Method A3 contained only the analyte.

2.3.6 Quantification of ^{14}C-caffeine, fexofenadine, tolbutamide and midazolam in plasma by HPLC-AMS

A quantification method to complement the extraction and separation methods was developed by modifying the recovery curve quantification method (Section 1.10). Recovery curve sample preparation is detailed below (Section 2.3.6.2), followed by a discussion of the modifications made to the original method (Section1.10.6).

2.3.6.1 Confirmation of analyte purity

Radiochemical purity values for caffeine, midazolam, tolbutamide and fexofenadine provided by the suppliers were >96% (96%, 99%, 99% and 98% for caffeine, midazolam, tolbutamide and fexofenadine (Section 7.2.3). Non-labelled caffeine, midazolam, tolbutamide and fexofenadine were purchased at >98% chemical purity (Section 7.2.2) and were assessed for ^{14}C contamination by AMS analysis prior to development of the assay. Non-labelled caffeine, midazolam, tolbutamide and fexofenadine were analysed by AMS (Table 19; Section 7.11). All samples returned pMC values below the LOQ of the AMS instrument (Section 7.11.4.1).

Table 19: AMS data obtained on analysis of non-labelled caffeine, fexofenadine, tolbutamide and midazolam reference standards.

Analyte	pMC
Caffeine	1.99
Fexofenadine	1.39
Tolbutamide	0.80
Midazolam	2.13

2.3.6.2 Preparation of recovery curve

A recovery curve was prepared and QC plasma samples were analysed to determine the accuracy and precision of the method.

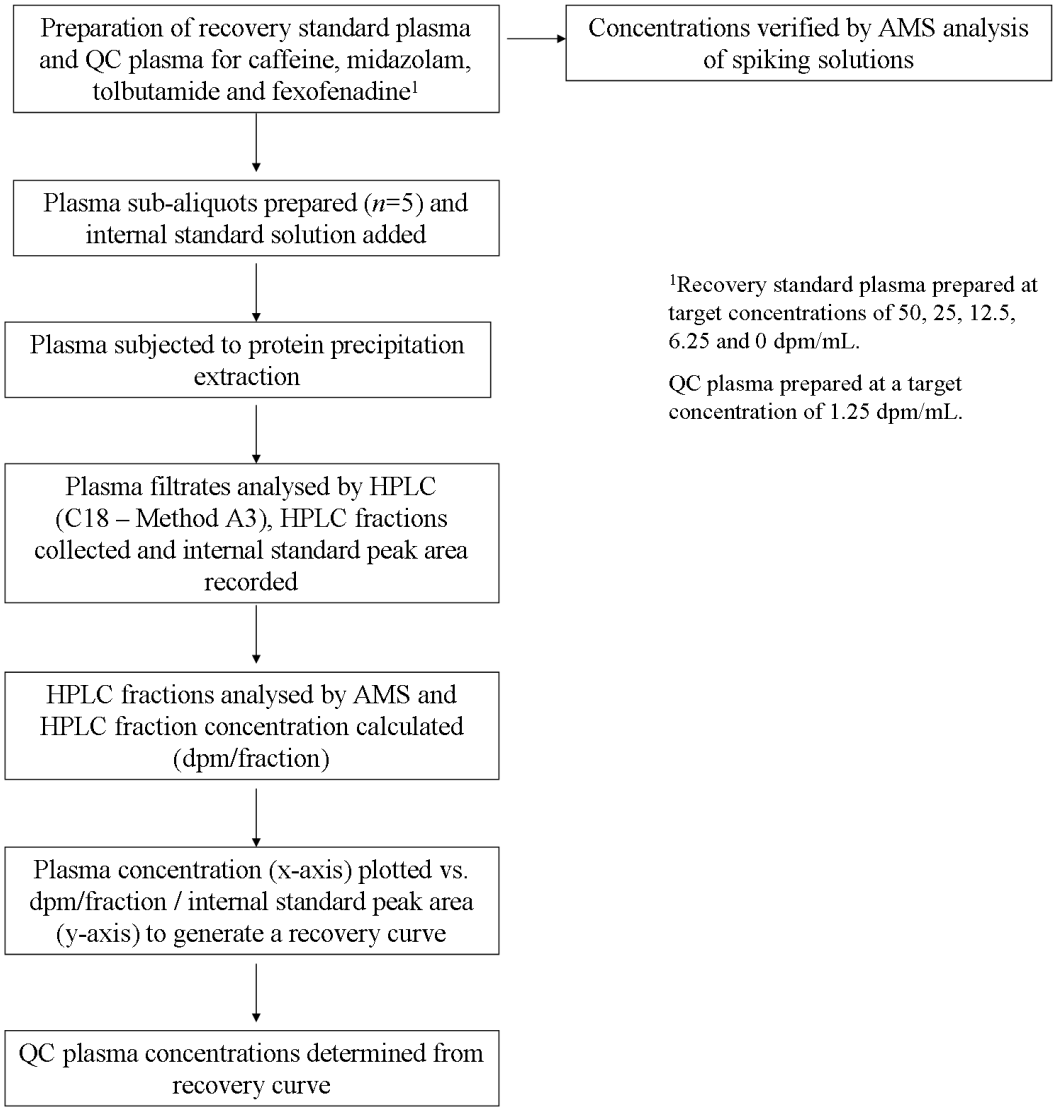

Figure 45: Schematic of sample preparation and analysis for preparation of caffeine, midazolam, tolbutamide and fexofenadine recovery curve and QC samples.

Recovery standards and QC plasma samples were prepared (Section 7.4.1). Accurate recovery standard and QC plasma concentrations were determined by AMS analysis of spiking solutions used in their preparation (Section 7.1.1; *n*=2). The concentration data were used along with plasma and solvent volumes (V_p and V_s) to calculate the concentration of each recovery standard and QC plasma sample (Equation 15; Table 20).

$$K_p = \frac{K_s \, x \, V_s}{V_p}$$ **Equation 15**

Where K_s = spiking solution concentration (dpm/mL)
K_p = plasma concentration (dpm/mL)

Table 20: AMS data obtained on analysis of ^{14}C-solutions and the determination of recovery standard and QC plasma concentrations.

Analyte	Sample ID	Spiking solution concentration (dpm/mL)[1]	Target plasma concentration (dpm/mL)	Calculated plasma concentration (dpm/mL)
Caffeine	Recovery standard 1	1128 (10.8)	50	56.4
	Recovery standard 2	688.2 (0.5)	25	34.4
	Recovery standard 3	305.0 (2.2)	12.5	15.3
	Recovery standard 4	125.8 (8.8)	6.25	6.29
	QC	23.66 (5.4)	1	1.18
	Recovery standard 5	0.00 (N/A)	0	0
Midazolam	Recovery standard 1	1266 (3.8)	50	63.3
	Recovery standard 2	629.8 (8.9)	25	31.5
	Recovery standard 3	349.7 (3.8)	12.5	17.5
	Recovery standard 4	185.3 (3.8)	6.25	9.27
	QC	25.06 (2.4)	1	1.25
	Recovery standard 5	0.00 (N/A)	0	0
Tolbutamide	Recovery standard 1	1628 (2.9)	50	81.4
	Recovery standard 2	647.3 (1.6)	25	32.4
	Recovery standard 3	346.6 (0.5)	12.5	17.3
	Recovery standard 4	169.7 (2.9)	6.25	8.49
	QC	25.52 (4.2)	1	1.28
	Recovery standard 5	0.00 (N/A)	0	0
Fexofenadine	Recovery standard 1	1435 (3.9)	50	71.8
	Recovery standard 2	618.6 (4.3)	25	30.9
	Recovery standard 3	354.9 (7.9)	12.5	17.7
	Recovery standard 4	183.4 (10.7)	6.25	9.17
	QC	24.24 (1.1)	1	1.21
	Recovery standard 5	0.00 (N/A)	0	0

[1] % difference from mean value in parentheses

Recovery standards and QC plasma were subjected to protein precipitation extraction (*n*=5; Section 7.7.1), C18 HPLC analysis (Method A3; Section 7.8.1) and AMS analysis (Section 7.11) of caffeine, midazolam, tolbutamide and fexofenadine fractions. The concentration of ^{14}C caffeine, midazolam, tolbutamide and fexofenadine in each HPLC fraction was determined (Equation 16, modified from Equation 11).

$$K = \frac{R_D \Phi}{A_v} x\, F_v \qquad \textbf{Equation 16}$$

Where
K = concentration of HPLC fraction (dpm/fraction)
R_D = isotope ratio of sample – isotope ratio of isotopic dilutor (in Modern)
Φ = amount of isotopic dilutor
A_v = volume of sample taken for AMS analysis (mL)
F_v = total fraction volume (mL)

Equation 16 assumes that the specific radioactivity and process recovery are both equal to 1. The specific radioactivity is not used at this stage. Plasma concentrations (dpm/mL) were plotted on the *x*-axis against fraction concentrations (dpm/fraction, determined via Equation 16) / internal standard (IS) detector response (peak area mAU) on the *y*-axis. With the exception of one datum point for fexofenadine (9 dpm/mL; replicate a), which failed to meet the acceptance criteria, all recovery standards successfully analysed by HPLC were included in the recovery curves (Figure 46 – Figure 49).

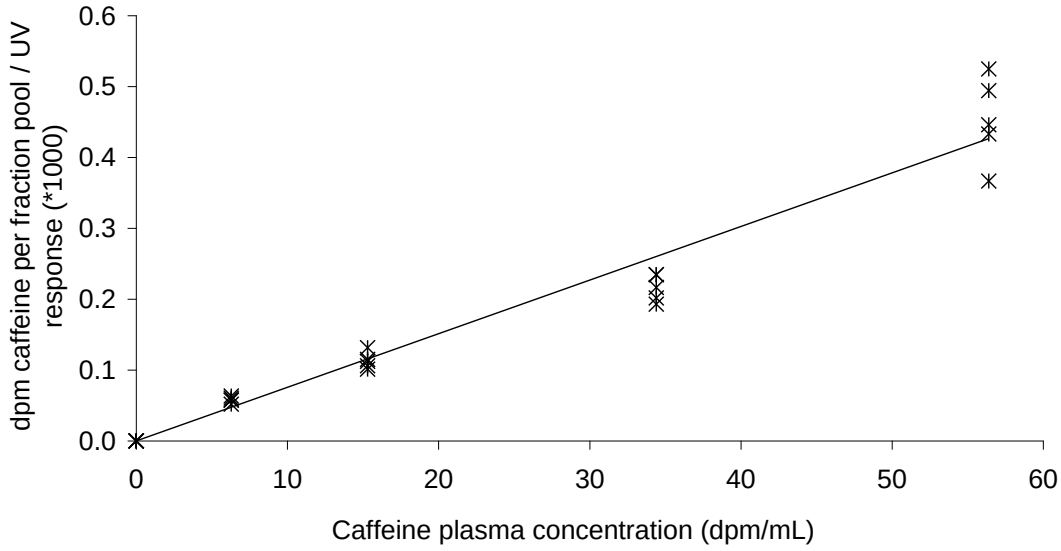

Figure 46: Caffeine recovery curve (y = 0.00756x).

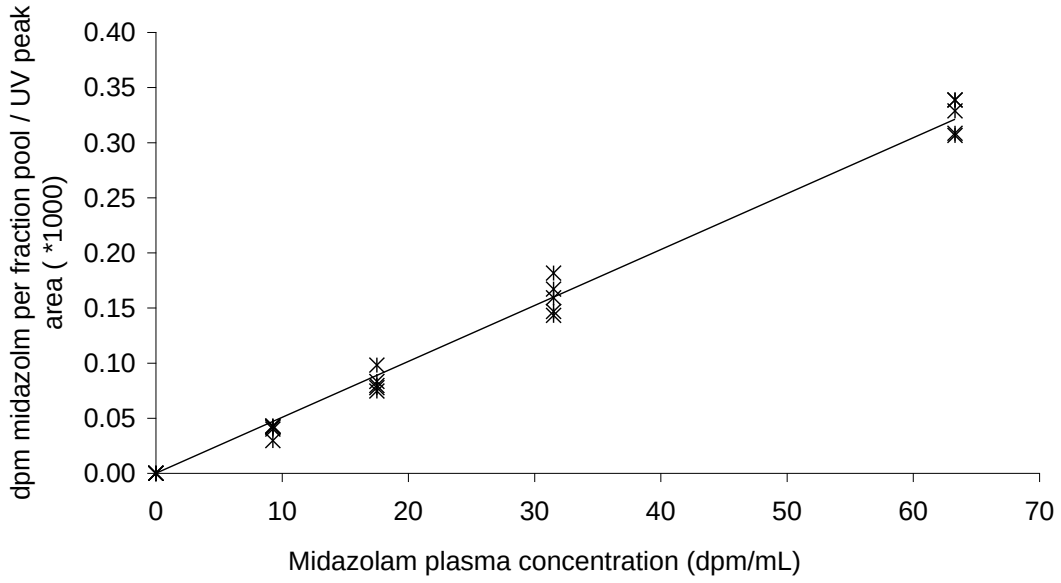

Figure 47: Midazolam recovery curve (y = 0.00508x).

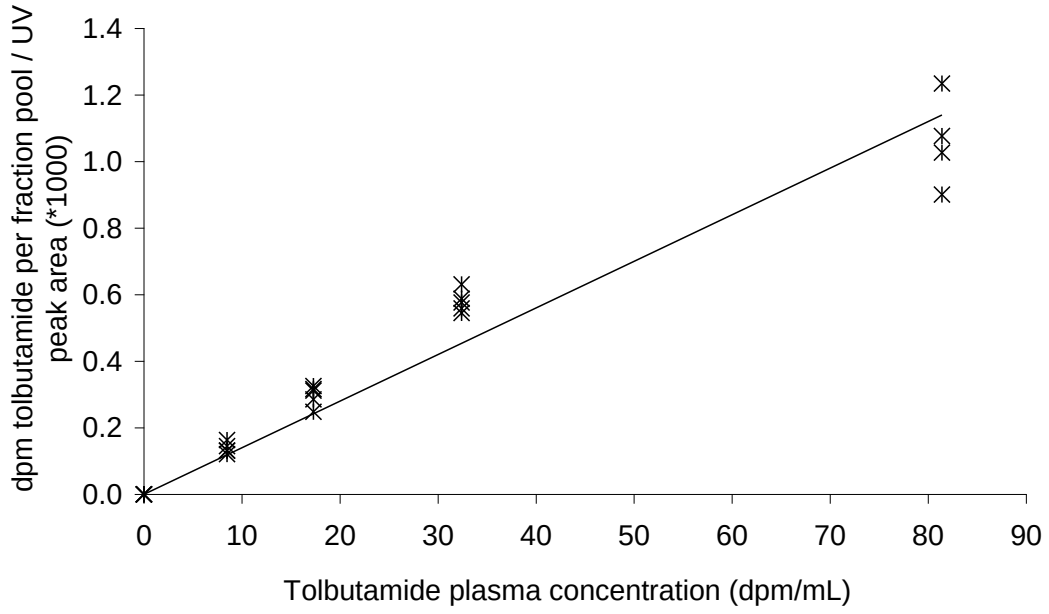

Figure 48: Tolbutamide recovery curve (y = 0.0140x).

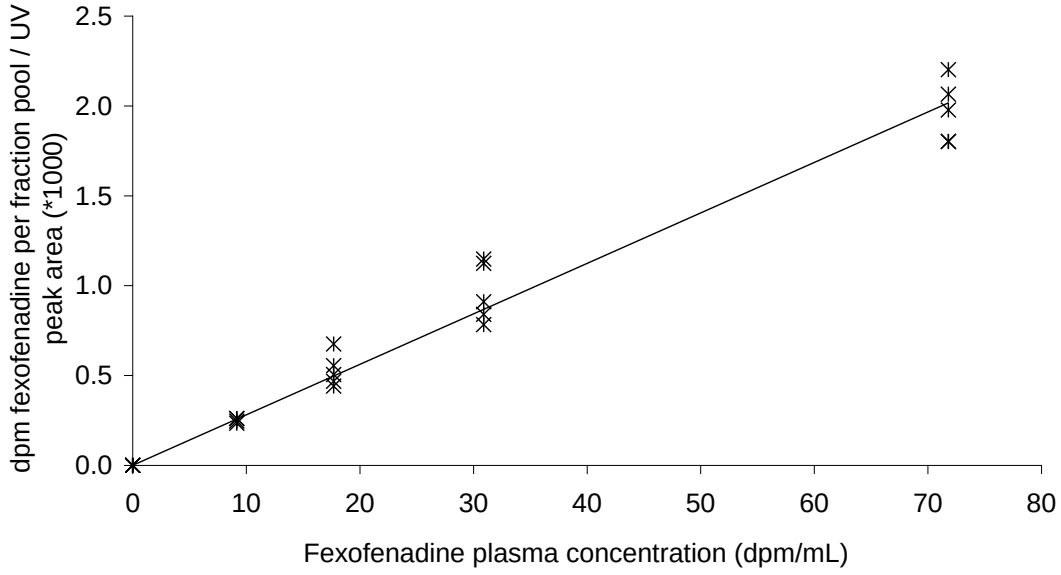

Figure 49: Fexofenadine recovery curve (y = 0.0281x).

The slope of the curve (m) and intercept on the *y*-axis (c) were used to determine the concentration of the QC plasma. The precision of the method was assessed by evaluation of QC concentrations (*n*=5) via the recovery curve (Table 21). Mean accuracy for all analytes was within 13% of the measured plasma concentration with good precision (CV<20%).

Table 21: Caffeine, midazolam, tolbutamide and fexofenadine QC accuracy and precision data (*n*=5).

Replicate	Caffeine plasma concentration (dpm/mL)	Midazolam plasma concentration (dpm/mL)	Tolbutamide plasma concentration (dpm/mL)	Fexofenadine plasma concentration (dpm/mL)
1	1.11	1.13	1.40	1.28
2	1.19	1.17	1.07	0.877
3	0.931	1.05	1.56	1.19
4	1.00	1.15	1.73	1.42
5	1.52	1.09	1.44	1.17
Mean plasma concentration (dpm/mL)	1.15	1.12	1.44	1.19
Actual plasma concentration (dpm/mL)	1.18	1.25	1.28	1.21
Mean accuracy (%)	97.5	89.4	112.5	98.1
Mean precision (% CV)	19.9	4.64	16.9	16.8

As discussed in Section 1.10.7.3, key variables must remain constant throughout the analysis of samples for construction of a recovery curve. In practice, this was not always possible. In particular, the proportion of the HPLC fraction taken for AMS varied in cases where one of the replicates failed to meet the AMS acceptance criteria (Section 7.11.3). Initial AMS analysis was carried out using a constant proportion (50%) of each HPLC fraction. Samples that failed to meet the AMS acceptance criteria were re-graphitised. This is standard procedure in AMS analysis due to the nature of the graphitisation process (Section 1.10.2). In order to allow sufficient sample to be available in the event that the repeat AMS analysis also failed to meet the acceptance criteria (Section 7.11.3), only 25% of the fraction volume was taken for repeat analysis. Consequently, the method was modified to account for the variation in HPLC fraction volumes.

Conversion of pMC values to concentrations in units of dpm corrects for differences in volume and allows the plasma concentration of the QC sample and during clinical sample analysis to be determined in dpm/mL. This concentration is then converted to a mass concentration per mL plasma using the specific radioactivity (Equation 17).

$$Concentraion(pg\ \ per\,mL) = \frac{Concentraion(dpm/mL)}{Specificactivity(dpm/mg)} \qquad \textbf{Equation 17}$$

The specific radioactivity was excluded from the calculations, and is discussed in more detail in Section 2.3.6.3.

2.3.6.3 Limitations of the developed method

At the outset of this research, no guidelines for carrying out a HPLC-AMS assay had been published. Since the completion of the experimental work for this thesis recommended guidelines have been published [124]. The method developed in the current study is compared with these recommendations, specifically in four key areas; 1) the selectivity and chromatographic resolution of the analyte 2) carryover, 3) recovery and 4) accuracy and precision.

Selectivity is an important consideration, particularly for LC-MS, where matrix may contain a constituent that co-elutes with the target analyte [124]. It is also a concern for HPLC-AMS assays. Due to the graphitisation step prior to analysis, co-elution must be eliminated during HPLC isolation as it is not possible to identify and correct for it at the AMS stage. Two factors that may compromise selectivity are the presence of background ^{14}C due to volunteers taking part in a clinical trial where ^{14}C was administered, and the presence of unknown ^{14}C-metabolites that co-elute with the target analyte during HPLC analysis. Subjects chosen for the study summarised in Chapter 3 had not participated in a ^{14}C study in the year prior to commencing the present study. In addition, all pre-dose plasma samples were analysed for ^{14}C content. All results were below the LOQ of the AMS and are reported in Chapter 3.

Pooled clinical plasma samples for 1, 6, 12 and 24 h were evaluated for the presence of unknown ^{14}C-metabolites. The HPLC fraction corresponding to each analyte after isolation by C18 HPLC was subjected to further separation by phenyl HPLC. ^{14}C was only detected in the phenyl HPLC fractions corresponding to each analyte. No ^{14}C was detected throughout the remainder of the chromatogram, verifying that the C18 method produces a pure analyte peak and therefore confirming the method valid for use in analysis of human plasma samples. Only selected samples (1, 6, 12 and 24 h) were chosen for the determination of peak purity. The recommended guidelines suggest taking samples from the elimination phase ideally at 1 – 2 times the half-life [124]. Approximate half-lives of 4, 3.5, 8 and 14 h have been reported for caffeine [42, 59], midazolam [12, 151] tolbutamide [149] and fexofenadine [23, 150], respectively (Table 22).

Table 22: Recommended samples for verification of analyte resolution by 2D chromatography.

Analyte	Reported $t_{1/2}$ (h)	Recommended sampling time at 1-2 x $t_{1/2}$ (h)	Source
Caffeine	4	4-8	[42, 59]
Midazolam	3.5	3.5-7	[42, 59]
Tolbutamide	8	8-16	[149]
Fexofenadine	14	14-28	[23, 150]

The sampling times are within 1 – 2 times the $t_{1/2}$ (Table 22) and therefore comply with recommended guidelines. In addition, samples were taken across both dosing periods, which were expected to reflect marked differences in metabolism due to the co-administration of inhibitors. The resolution of each analyte using the developed C18 method demonstrates the suitability of the method for analysis of samples obtained during both dosing periods.

A consideration for future analysis would be to quantify analyte after subjecting every plasma sample to the 2D-HPLC method. Only a selection were analysed in the present study due to the large number of samples (768) and the lengthy HPLC-AMS procedure.

Assessment of carryover should be accounted for and minimised in method development [150]. Carryover of non-labelled material was assessed by HPLC analysis of blank injections made following replicate injections of analyte reference standards. The absence of an appreciable detector response at the retention time of each analyte confirmed negligible carryover. Carryover should also be determined for blank plasma analysed immediately after plasma samples containing relatively high concentrations of ^{14}C, i.e. in QC or recovery standards. In retrospect, this check should have been included in the method development, however samples were randomised (Chapter 3) and there was no evidence of carryover observed in pre-dose plasma samples analysed following samples containing relatively high levels of ^{14}C (Section 3.3.3). Although the evidence suggests that carryover is not present, a blank plasma sample following a QC or recovery standard at a relatively high ^{14}C concentration should ideally have been analysed to demonstrate this.

The recovery in a HPLC-AMS assay applies both to the mass and the radioactivity concentration of the sample [124]. It is only the radioactive concentration that is measured during AMS analysis with the majority of ^{12}C measured being isotopic diluent, not ^{12}C inherent to the sample. It is recommended within the guidelines for HPLC-AMS analysis that the material used in the preparation of the recovery standards and QCs contains the same ^{14}C and mass ratio, i.e. has the same specific radioactivity, as the material administered to volunteers in the clinical study. This approach eliminates mass-concentration-dependent effects during sample processing, particularly during addition of ^{14}C-material to plasma, and subsequent extraction of the analyte [124]. In the present work, recovery curves and QC samples were prepared from neat radiolabelled material, which was at a much higher specific radioactivity than that dosed in the clinical study (Chapter 3). For example, ^{14}C-caffeine used as a recovery standard and for QC purposes, was at a specific radioactivity of approximately 5.95×10^8 dpm/mg. The nominal specific radioactivity of the dose administered in the clinical study was 4.44×10^6 dpm/mg, an approximate 135-fold difference in mass concentration. Unfortunately, it is not possible to ascertain the impact of this effect retrospectively. The addition of internal standard prior to extraction has the advantage of introducing a significantly

larger amount of non-labelled analyte to the sample in addition to the ^{12}C inherent to the radiolabelled material. For example, the QC for caffeine has a mass concentration of 1.98 pg/mL due to the ^{14}C-analyte, of which 0.2 pg is taken for analysis by AMS. The amount of internal standard present (typically 3 µg), is significantly higher than the carbon inherent to the sample and mass concentration dependent effects on extraction are potentially reduced. This does not negate the potential for poor distribution of the ^{14}C-material in the spiked plasma due to non-specific binding of very small amounts (mass) of material. QC data obtained do not show evidence of this occurring. All data are accurate within 13% of the measured plasma concentration, with good precision (CV<20%). If non-specific binding had occurred, the data would be expected to show much more variation, due to non-homogeneity of the sample.

Recommended guidelines for accuracy and precision of a HPLC AMS method state that measured QC values should be within 20% of the true concentration and that CV should not exceed 20%. Several individual QC values do not meet the criteria for accuracy. Three samples (one QC for caffeine, fexofenadine and tolbutamide) are within ±25%, one caffeine QC is within ±30% and one fexofenadine QC is within ±40%. Nevertheless, the mean accuracy and precision data meet the acceptance criteria stated in the guidelines. Mean accuracy and precision data were determined from analysis of QC samples at just one concentration. The recommended guidelines state that QC samples are typically prepared at 3 concentrations and encompass the range of plasma concentrations anticipated in the clinical study (in mass/mL) [124]. Although the QC standards prepared were in the range of anticipated radioactive plasma concentrations (approximately 1 dpm/mL) this equates to 2 fg/mL compared with 0.2 ng/mL for clinical plasma samples of the same radioactive concentration.

The guidelines also recommend that true plasma concentrations are determined by direct AMS analysis of the plasma sample. In the present study, the concentrations were determined from AMS determination of ^{14}C-spiking solution concentrations and the volumes used in preparing spiked plasma. The solutions were diluted where radioactive concentrations exceeded the AMS upper limit of detection. The dilution step does introduce a potential source of error. While the

recommendation is that direct AMS analysis is used, that is only possible for samples with concentrations sufficiently above the AMS background. The concentrations in HPLC fractions can be at significantly lower levels than those in plasma, due to the lower level of background carbon (Section 1.10). Plasma concentrations below the LOD must be estimated based on dilution steps or by direct analysis of spiking solutions.

A potential improvement to this method, which also introduces an independent measurement of plasma concentrations, is to determine plasma concentrations by LSC analysis. Determination of stock solution concentrations to achieve a statistically accurate count time (typically at least 2%2σ) together with a dilution scheme to calculate plasma concentrations eliminates additional sample manipulation. To obtain a more robust method for future work the following procedure is recommended:

- prepare a recovery curve using recovery standards at a minimum of five concentrations including a blank sample;
- analyse five replicates at each concentration;
- prepare recovery standards by serial dilution of a stock spiking solution prepared at the specific radioactivity of the dose administered in the clinical study;
- determine the concentration of stock solution by LSC and hence determine recovery standard concentrations;
- prepare QC samples at three concentrations representative of the expected plasma concentration range in the clinical study;
- determine the concentrations in the same way as for recovery standards;

- intersperse QC samples between analyses of recovery standards and analyse blank plasma filtrate (plasma containing only internal standard) after QC samples at the highest concentrations to determine carryover.

Taking duplicate aliquots for HPLC analysis would allow a back-up sample to be generated that is identical to the original sample. The entire fraction from the first injection may be taken for AMS, with the second being retained should reanalysis be required. This method would eliminate the need for the conversion of pMC values to dpm/fraction concentrations, as the entire aliquot injected onto HPLC each time is taken forward for AMS, therefore keeping this potential variable constant. A recovery curve prepared in this way will be representative of clinical plasma samples in terms of mass concentration as well as radioactive concentrations.

2.4 Conclusions

This chapter details the development of sample treatment and separation methods and their use in the development of a quantification method for ^{14}C-caffeine, ^{14}C-midazolam, ^{14}C-tolbutamide and ^{14}C-fexofenadine.

The plasma extraction method developed has good repeatability and yielded recoveries of >74% for all analytes. A C18 HPLC method, which gives complete resolution of all four target analytes and their metabolites, was demonstrated by analysis of non-labelled reference standards. A second HPLC method using a phenyl stationary phase was developed. Pooled clinical plasma samples were analysed using both HPLC methods in series and peaks corresponding to each of the four analytes were confirmed to be free of interfering ^{14}C-material. Peak purity was demonstrated, verifying the C18 separation method to be suitable for the isolation of caffeine, midazolam, tolbutamide and fexofenadine from clinical plasma.

A quantification method was developed, by adapting the recovery curve method reported previously [129]. The accuracy and precision of the method was assessed by analysis of QC plasma at a ^{14}C-concentration of approximately 1

dpm/mL. Mean concentration data for QCs derived using the recovery curve for all analytes were within 13% of the target plasma concentrations. In addition, the error associated with the quantification method for each analyte was less than 20%. Recommendations for improvement of the method are given above. Based on the acceptability of the QC data available, the method is deemed suitable for determination of plasma concentration in the clinical study outlined in Chapter 3.

CHAPTER 3

Determination of drug-drug interactions using a radiolabelled cassette microdose

3.1 Introduction

Where employed, microdosing studies have often been utilised at the very early stages of drug development in phase 0 (Section 1.8). Microdosing studies can permit the early identification of undesirable PKs, which can lead to withdrawal of the NCE from further development, allowing conservation of valuable resources. During a typical drug development programme, DDI studies are not performed until phase 2. These trials can take place up to 5 years after the implementation of a phase 0 study, depending on the type of drug under investigation. Given that a major DDI effect can lead to the abandonment of the drug development programme, detection of a potential DDI during early phase 0 studies would be of benefit.

This chapter focuses on the implementation of an exploratory study to evaluate the ability of microdosing to detect DDIs. The study was designed to test the hypothesis that the PK of an NCE administered at a microdose, represented here by caffeine, midazolam, tolbutamide and fexofenadine, would be significantly altered by co-administration of enzyme and transporter inhibitors administered at a pharmacologic dose. Administration of the cassette microdose alone and concomitantly with CYP and P-gp inhibitors was intended to highlight the potential to identify a DDI. At the time of this study design, neither a cassette microdose study nor a microdose DDI investigation had been carried out, however the studies published in 2011 (Sections 1.8.2.4 and 1.8.2.5) [95, 117] now support the use of microdosing in this way. It is important to note that while known compounds and their inhibitors are used here, the cassette microdose is intended to be made up of NCEs, with inhibitors of the major CYP and P-gp being co-administered to determine DDI effects. Cassette microdosing of multiple NCEs in this way may allow candidate selection to take place after just one clinical study. Administration of the cassette microdose alone allows baseline PK data to be obtained, which can then be compared with PK data obtained after concomitant administration of the cassette microdose with the inhibitors. Differences in PK parameters may then be attributed to an inhibitory effect. In addition to comparison between doses, the PK data obtained after administration of the cassette microdose alone may be compared to therapeutic

dose data to determine PK linearity. Should microdose data be available, these data may be examined to determine the effects of the administration of each drug alone vs. part of a cassette microdose.

3.2 Aims

The overall aim for this chapter was to design and implement a microdose-based clinical trial in healthy human volunteers to predict changes in PK in NCEs that result from the co-administration of marketed drugs (Figure 50). Specific objectives were:

- to quantify caffeine, midazolam, tolbutamide and fexofenadine in plasma samples collected from healthy human male volunteers after administration of the following:
    - cassette microdose containing caffeine, tolbutamide, midazolam and fexofenadine;
    - cassette microdose (as above) co-administered with enzyme and transporter inhibitors, ketoconazole and fluvoxamine;
- to assess the feasibility of administering multiple compounds within a cassette microdose;
- to compare the PK of caffeine, midazolam, tolbutamide and fexofenadine when administered as a microdose, with literature data obtained after administration at a pharmacologic dose;
- to evaluate differences observed in PKs of the compounds of the cassette microdose after concomitant administration with fluvoxamine and ketoconazole and compare these data with literature data, where available.

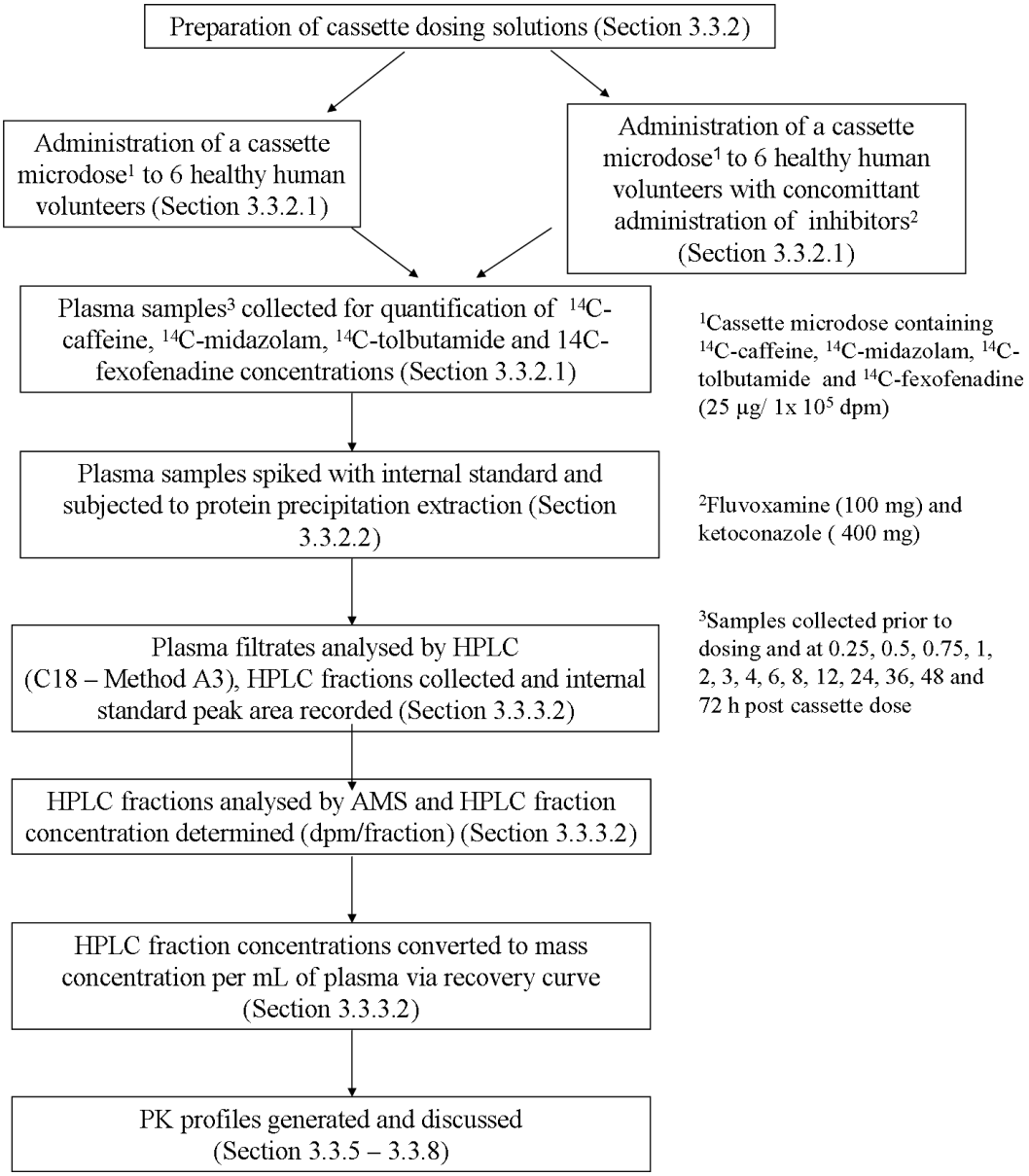

Figure 50: Schematic of cassette microdosing, sample collection and analysis of plasma samples by HPLC and AMS.

3.3 Results and discussion

3.3.1 Clinical study design and implementation

3.3.1.1 Selection of microdose compounds

Caffeine, tolbutamide, midazolam and fexofenadine were selected for microdose administration due to their well-characterised PK interactions with other drugs.

They are widely reported in the literature to be metabolised or cleared by CYP1A2, CYP2C9, CYP3A4 and P-gp, respectively [22, 36, 53, 152].

In addition, caffeine, midazolam and tolbutamide have been utilised as probes for CYP1A2, CYP3A4 and CYP2C9 in DDI studies (Section 1.7). All four compounds were available as ^{14}C-labelled compounds suitable for human administration. As all compounds are marketed drugs, there were no additional safety considerations as would be required on administration of a new drug, therefore streamlining ethical approval.

3.3.1.2 Selection of inhibitors

Ketoconazole and fluvoxamine were selected for their ability to inhibit specific P450 enzymes and transporters. Ketoconazole is a potent inhibitor of CYP3A4 and P-gp and a weak inhibitor of CYP2C9. It has been widely reported to inhibit the metabolism of midazolam, fexofenadine and tolbutamide [38, 74]. No clinically significant interactions with CYP1A2 have been reported [49]. Fluvoxamine is a potent inhibitor of CYP1A2 [48, 59] and a weak inhibitor of CYP3A4 and CYP2C9 [37] but has no reported effect on P-gp.

3.3.1.3 Dose administration design

The microdose designed for administration was an equal mixture of ^{14}C-caffeine, ^{14}C-midazolam, ^{14}C-tolbutamide and ^{14}C-fexofenadine, each dosed at 25 µg (1.11×10^5 dpm), therefore not exceeding the maximum microdose of 100 µg. A period of 14 days was introduced between microdose administrations to enable caffeine, midazolam, tolbutamide and fexofenadine to be fully eliminated from the body. A time-period of six times the half-life is typically applied to studies where multiple administrations are required. Caffeine, midazolam, tolbutamide and fexofenadine have typical $t_{1/2}$ of 4.9 h (250 mg dose) [42], 4.0 h (100 µg dose) [12], 7.7 h (125 mg dose) [149] and 14.4 h (60 mg dose) [150] respectively. Six fexofenadine half lives is less than 1 week, and therefore 2 weeks between doses is deemed sufficient. The sampling of pre-dose plasma before each microdose administration also enables the suitability of this washout period to be tested.

Ketoconazole (400 mg) and fluvoxamine (100 mg) were co-administered once daily prior to and after the cassette microdose administration to a single group of volunteers. Ketoconazole and fluvoxamine are known collectively to inhibit at least one of the drug metabolism enzymes or transporters responsible for the elimination of microdose compounds and the aim of the study was to assess whether these effects could be detected, and not to attribute these effects to a particular compound. The study was designed to include the administration of the cassette microdose alone and with a combined dose of ketoconazole and fluvoxamine. Ketoconazole and fluvoxamine were dosed to achieve steady state conditions [41, 153, 154], which were maintained up until the last sampling time.

3.3.1.4 Implementation of clinical study

A clinical study was carried out at Simbec Research Limited, Merthyr Tydfil, South Wales, CF48 4DR. The study clinical protocol was prepared in collaboration between the author and the Project Manager at Simbec. The protocol, volunteer consent forms and subject information were approved by the South East Wales Local Research Ethics Committee (LREC) on 7th March 2007. The study was performed in accordance with; the Declaration of Helsinki (South Africa, 1996), the ABPI Guidelines for Medical Experiments in Non-Patient Human Volunteers – 1988, amended May 1990, the ICH Harmonised Tripartite Guideline for Good Clinical Practice and The Medicines for Human Use (Clinical Trials) Regulations 2004 (Statutory Instrument 2004 No. 1031) as amended by the Medicines for Human Use (Clinical Trials) Amended Regulations 2006 (Statutory Instrument 2006 No. 1928). In addition, Clinical Trials Authorisation (CTA) was obtained from the Medicines and Healthcare Products Regulatory Agency (MHRA) on 28 February 2007 in accordance with Part 3, Regulation 12 of the UK Statutory Instrument.

The clinic selected six healthy male volunteers to participate in the study, and all volunteers met the study inclusion and exclusion criteria. All were aged between 26 and 51 and were non-smokers with a body mass index of between 25 and 30 kg/m^2.

3.3.2 Dose solution preparation and determination of specific activity

Oral dose solution was prepared by the author and shipped to the clinic for administration. ^{14}C-caffeine, ^{14}C-midazolam, ^{14}C-tolbutamide and ^{14}C-fexofenadine (nominally 1.11 x 10^5 dpm per compound) and non-labelled forms of each compound (25 µg) were formulated in bottled spring water: ethanol 90:10 (v/v) (Section 7.12.1). The specific activity was determined as 4.44 dpm/ng for each analyte dosed (Section 7.12.1).

3.3.2.1 Cassette dose administration and sample collection

Each volunteer received two identical doses of the cassette microdose either alone or after repeat daily administration of fluvoxamine (100 mg) and ketoconazole (400 mg) according to the dosing schedule (Section 7.12.2; Figure 51).

Day	1	2	3	4-7	8	9	10	11	12	13	14	15	16	17
Microdose administration	x											x		
Plasma collection	x	x	x									x	x	x
Inhibitor administration					x	x	x	x	X	x	x	x	x	x

Figure 51: Dosing schedule of cassette microdose and inhibitors.

Blood samples were collected (Section 7.12.2) and a sample removed and shipped to Delphic Laboratories (Kent, UK) for determination of CYP1A2, CYP2C9 and CYP3A4 genotypes. Plasma samples were prepared (Section 7.12.2) and the samples shipped to the AMS facility where they were stored at -80 ºC prior to analysis.

3.3.2.2 Determination of ^{14}C-caffeine, midazolam, tolbutamide and fexofenadine concentrations in post-dose plasma

Pre-dose and post-dose plasma samples were assigned a random number (using the Microsoft Excel RAND function) and subjected to protein precipitation extraction (Section 7.7.1) in ascending numerical order. Plasma filtrates were

assigned a second random number and analysed by HPLC (Method A3; Section 7.8.1: Figure 52) in ascending numerical order.

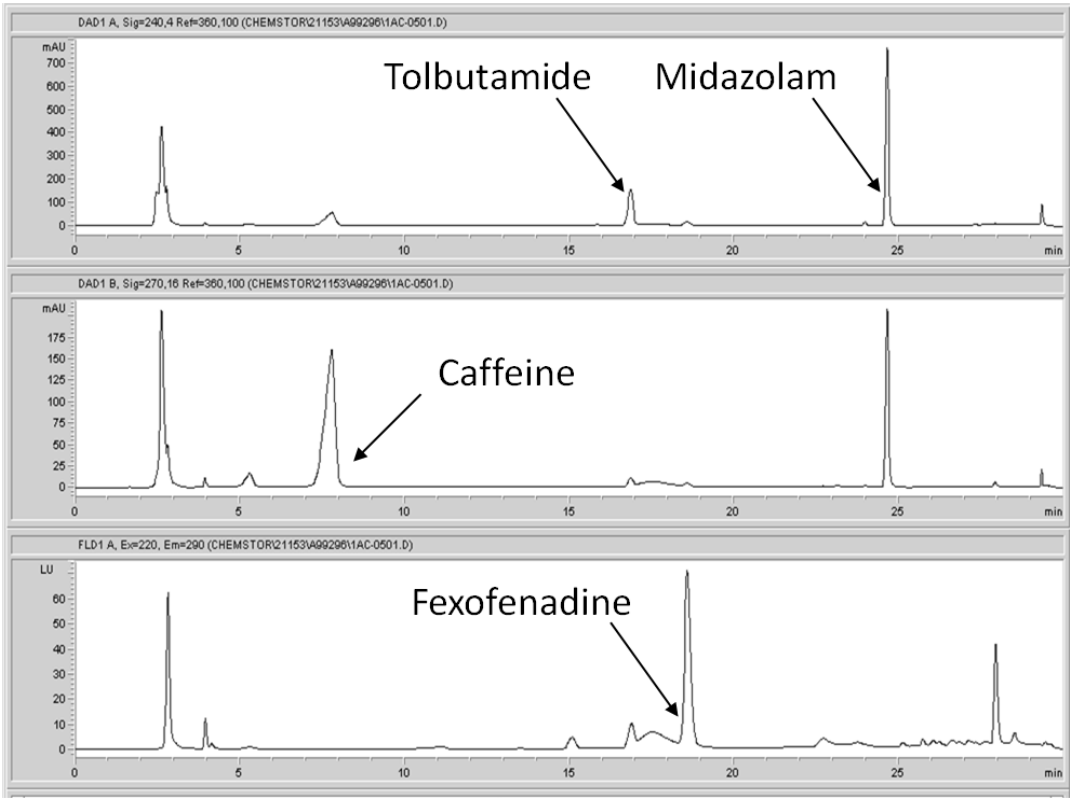

Figure 52: HPLC chromatogram of a plasma filtrate containing caffeine (270 nm), midazolam (240 nm), tolbutamide (240 nm) and fexofenadine at λ_{ex} 220 nm and λ_{em} 290 nm (Method A3).

Discrete fractions were collected over the retention times of caffeine, midazolam, tolbutamide and fexofenadine. HPLC fractions corresponding to caffeine, midazolam, tolbutamide and fexofenadine were analysed by AMS (Section 7.11). The ^{14}C:^{12}C ratio (pMC) determined for each fraction by AMS was converted to analyte concentrations (mass of analyte per mL of plasma) via the recovery curve method summarised previously (Section 2.3.6.2).

3.3.2.3 Limit of quantification

Analyte concentrations below the LOQ were excluded from PK calculations. The pMC value determined as the LOQ for the clinical plasma sample batch (3.833; Section 7.11.4.2) can be converted to a mass concentration, though this

depends on experimental variables such as fraction volumes and HPLC peak areas causing the LOQ to vary from sample to sample. Samples with concentrations below the LOQ in pMC are stated as such throughout the reporting of the data (Section 3.3.5 – 3.3.8).

3.3.3 Determination of total ^{14}C-concentrations in pre-dose plasma

Pre-dose plasma samples which were taken prior to the ^{14}C-doses were analysed by AMS (Section 7.11) to determine whether or not levels of ^{14}C were significantly higher on day 15 than on day 1 (Table 23), due to incomplete elimination of the cassette microdose administered on day 1. These were the only samples analysed for total ^{14}C-concentration. Plasma samples are often analysed for total ^{14}C-concentration in order to compare total drug related ^{14}C-material with parent and metabolite concentrations. As the dose administered in this study was a mixture of four compounds, total ^{14}C-concentration concentrations were not determined.

Table 23: Analysis of pre-dose plasma samples for determination of background ^{14}C levels.

Subject number	Day 1 pre-dose ^{14}C (pMC)	Day 15 pre-dose ^{14}C (pMC)
1	98.29	108.99
2	112.35	110.28
3	106.20	115.87
4	99.86	112.57
5	118.22	139.84
6	106.37	109.37
Mean	106.88	116.15
SD	7.51	11.88
% CV	7.03	10.23

The background percent modern carbon (pMC) concentration for biological samples is 110 pMC [123] (Section 1.10.3.1). There is no significant difference between the data obtained on day 1 and day 15 ($p<0.05$) indicating that the period between doses was sufficient to allow clearance of the first microdose.

3.3.4 Subject genotyping

Genotyping data (Table 24) were obtained only for consideration in analysis of plasma concentration data.

Table 24: Genotyping summary CYP3A4, CYP1A2 and CYP2C9.

Subject Number	CYP3A4 Genotype	CYP1A2 Genotype	CYP2C9 Genotype
1	CYP3A4*1	*1F/*1F	*1/*1
2	CYP3A4*1	*1F/*1F	*1/*1
3	CYP3A4*1	*1F/*1F	*1/*3
4	CYP3A4*1	*1F/*1F	*1/*2
5	CYP3A4*1	*1F/*1C	*1/*1
6	CYP3A4*1	*1F/*1F	*1/*1
% Frequency homozygous wild type subject:	100.00	0.00	66.67
% Frequency subject with one mutation:	0.00	0.00	33.33
% Frequency subject with two mutations:	0.00	100.00	0.00

No polymorphisms were observed in CYP3A4, with all subjects found to have the wild type CYP3A4*1 genotype. Five of the six subjects were genotyped as CYP1A2*1F/*1F, which is the wild type and is associated with high activity. The final subject (5) was found to carry CYP1A2 *1F/*1C, which is associated with diminished activity. Two subjects (3 and 4) carried a CYP2C9 mutation, CYP2C9 *1/*2 and *1/*3. Both polymorphisms are associated with a decrease in enzyme activity.

3.3.5 Caffeine microdosing data

Caffeine concentrations in post-dose plasma samples were above the limit of quantification (>LOQ) of 3.833 pMC for all subjects (*n*=6) to 12 h. The levels for several, but not all, subjects were >LOQ at 18 h (subjects 1, 2, 3 and 5) and 24 h (subjects 2 and 5) after administration of the microdose (Figure 53). Caffeine concentrations in samples analysed at 36 h, 48 h and 72 h were below the LOQ. After administration of the second microdose, during the period of administration of ketoconazole and fluvoxamine, plasma concentrations were >LOQ for all subjects (*n*=6) to 72 h (Figure 54). Individual subject data and

mean data are summarised in Appendix 2. PK data are summarised in Appendix 8. Inter-subject variability of calculated PK parameters was moderate with CVs of approximately 35% and 40% after administration of the first microdose and the second microdose, resectively.

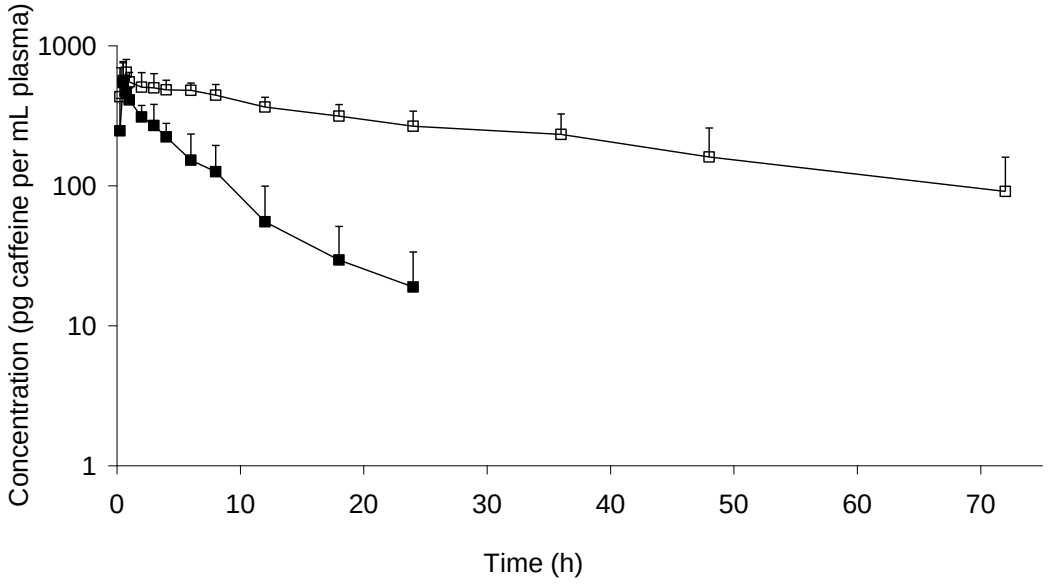

Figure 53: Semilog plot of mean caffeine plasma concentration data, before (closed squares, *n*=6 to 12 h, *n*=4 to 18 h and *n*=2 to 24 h) and after (open squares, *n*=6 to 72 h) daily repeat dosing of fluvoxamine and ketoconazole. Error bars represent one standard deviation.

3.3.5.1 Caffeine microdosing data vs. literature data

PK data obtained after administration of a microdose of caffeine are in close agreement with previously published data for doses of 100 mg [42] and a 250 mg [59] (Table 25).

Table 25: Plasma pharmacokinetic data obtained after administration of a caffeine microdose (25 µg) vs. literature data obtained after therapeutic doses.

Dose	Number of subjects	$t_{1/2}$ (h)	t_{max} (h)	C_{max} (ng/mL)		AUC_{0-t} (h.ng/mL)		Source
				A	B	A	B	
25 µg	6	4.14	0.58	0.612	24.48	2.62	104.8	Present study
100 mg	30	ND	0.5	2390	23.90	21300	213.0	[42]
250 mg	7	4.9	1.14	5810	23.24	46300	185.2	[59]

A-calculated from dose as administered B-dose normalised to 1 mg

When microdose and literature data are dose normalised, all PK parameters compare favourably. The normalised C_{max} values are very close, with data obtained after a microdose being within 3% and 5% of the C_{max} obtained after a 100 mg and 250 mg oral dose respectively. AUC_{0-t} data obtained after the microdose administration agree within a factor of 2.0 and 1.8 with those obtained for 100 mg and 250 mg doses respectively. The data represent the first reported for caffeine, suggesting dose-linear PK from a microdose (25 µg) to a dose 10000-fold higher (250 mg).

3.3.5.2 Effect of inhibitor administration on the pharmacokinetics of caffeine

Following repeat administration of ketoconazole and fluvoxamine, the PKs of caffeine show statistically significant ($p<0.01$) increases in AUC_{0-t} (× 6.7) and $t_{1/2}$ (× 6.3) from the baseline measurements (Table 26).

Table 26: Plasma pharmacokinetic data obtained after administration of a caffeine microdose (25 µg) and after administration of a caffeine microdose (25 µg) concomitantly with an inhibitor dose (*n*=6, mean, SD in parentheses).

PK parameter	25 µg dose	25 µg + inhibitor dose	Student's t-test p value	Increase factor on inhibitor administration
C_{max} (pg/mL)	612 (155)	732 (87.7)	0.162	1.2
$t_{1/2}$ (h)	4.15 (1.12)	26.2 (12.8)	0.008	6.3
AUC_{0-t} (h.pg/mL)	2620 (1060)	17600 (4800)	0.000	6.7
$AUC_{0-\infty}$ (h.pg/mL)	2670 (1050)	21900 (8900)	0.002	8.2
t_{max} (h)	0.583 (0.258)	0.875 (0.607)	0.328	1.5

These data are consistent with results obtained in a previous study, where caffeine (250 mg) was administered before and after daily repeat daily dosing of fluvoxamine (100 mg per day for 4 days). On co-administration of fluvoxamine, $t_{1/2}$ and AUC_{0-t} increased by factors of 11.4 and 13.7, respectively (Table 27). Metabolite concentrations were also examined in the previous study, with the AUC_{0-24h} of paraxanthine decreasing by a factor of 3 on co-administration of fluvoxamine [59].

Table 27: Plasma pharmacokinetic data obtained after administration of a caffeine microdose plus inhibitors vs. literature data obtained after administration of a therapeutic dose.

Dose	Increase factor for caffeine concentration on co-administration of fluvoxamine (and ketoconazole for 25 µg dose)				
	$t_{1/2\ (h)}$	t_{max} (h)	C_{max} (ng/mL)	AUC_{0-t} (h.ng/mL)	Source
25 µg[1]	6.3	1.5	1.2	6.7	Present study
250 mg[2]	11.4	4.0	1.4	13.7	[59]

[1] administered after repeat daily (8 day) dose of fluvoxamine (100 mg)
[2] administered after repeat daily (4 day) dose of fluvoxamine (100 mg)

A similar study in which caffeine (200 mg) was administered before and after daily administration of fluvoxamine saw general agreement, with the $t_{1/2}$ increasing approximately $\times$ 6.3 from 5 to 31 h. The *N*-3 demethylation of caffeine to paraxanthine decreased five-fold, showing that fluvoxamine inhibits the CYP1A2 biotransformation of caffeine [155]. The same inhibition is observed in the current study, where a significant prolongation of $t_{1/2}$ and increase in AUC of caffeine are observed, consistent with reduced clearance of caffeine due to inhibition of CYP1A2. There is no evidence in the literature to suggest that ketoconazole has a significant inhibitory effect on caffeine metabolism. Hence, it is likely that the administration of fluvoxamine was responsible for the changes in caffeine PK. The subjects enrolled in this study were genotyped for CYP1A2 polymorphisms and found to include two polymorphisms (Table 28).

Table 28: CYP1A2 genotyping of subjects 1-6.

Subject	CYP1A2*1C	CYP1A2*1F	CYP1A2 Genotype
1	2 mutations	2 mutations	*1F/*1F
2	2 mutations	2 mutations	*1F/*1F
3	2 mutations	2 mutations	*1F/*1F
4	2 mutations	2 mutations	*1F/*1F
5	2 mutations	1 mutation	*1F/*1C
6	2 mutations	2 mutations	*1F/*1F

Subjects 1 – 4 and 6 are carriers of the CYP1A2*1F variant which results in increased metabolism of caffeine. Subject 5 is a carrier of the CYP1A2*1C variant. Individuals, who carry one or more 1C alleles, metabolise caffeine more slowly. This polymorphism appears to be reflected in the data obtained in the current study (Table 29; subject 5 data highlighted in bold text).

Table 29: Plasma pharmacokinetic data obtained after administration of a microdose (25 µg) of caffeine – all subjects.

Subject Number	$t_{1/2}$ (h)	t_{max} (h)	C_{max} (pg/mL)	AUC_{0-t} (h.pg/mL)	$AUC_{0-\infty}$ (h.pg/mL)
1	3.58	1.00	529	2550	2590
2	3.94	0.75	476	2940	2880
3	3.85	0.50	825	2120	2210
4	4.15	0.25	491	1700	1830
5	**6.31**	**0.50**	**791**	**4560**	**4640**
6	3.07	0.50	562	1850	1890

By comparison with the mean data for the remaining five subjects, the data obtained from subject 5 shows increases in $t_{1/2}$ (× 1.7) and in AUC (× 2.0 for AUC_{0-t} and $AUC_{0-\infty}$ respectively). AUC and $t_{1/2}$ data were examined and each PK parameter was analysed for outliers using Dixon's Q-test. The $t_{1/2}$ and AUC_{0-t} for subject 5 were both determined to be outliers ($Q_{95\%}$). The sample size here is small (*n*=6) and inter-subject variability must be treated with caution, however, this does open up the possibility of the use of microdosing in detecting individual

subject polymorphisms. Enrolling larger numbers of subjects may allow this application of microdosing to be further explored.

3.3.6 Midazolam microdosing data

Midazolam concentrations in post-dose plasma samples were above the limit of quantification (>LOQ) of 3.833 pMC for all subjects (*n*=6) to 4 h. The levels for several subjects were >LOQ to 8 h (subjects 1 and 5) and 12 h (subject 5) after administration of the microdose (Figure 54). Midazolam concentrations in samples analysed at 12 h to 72 h were below the LOQ. After administration of the second microdose, during the period of administration of ketoconazole and fluvoxamine, plasma concentrations were >LOQ for all subjects (*n*=6) to 36 h (Figure 54). Several subjects were >LOQ at 48 h (subjects 1 to 5) and 72 h (subject 1, 4 and 5). Individual subject data and mean data are summarised in Appendix 3. PK data are summarised in Appendix 9.

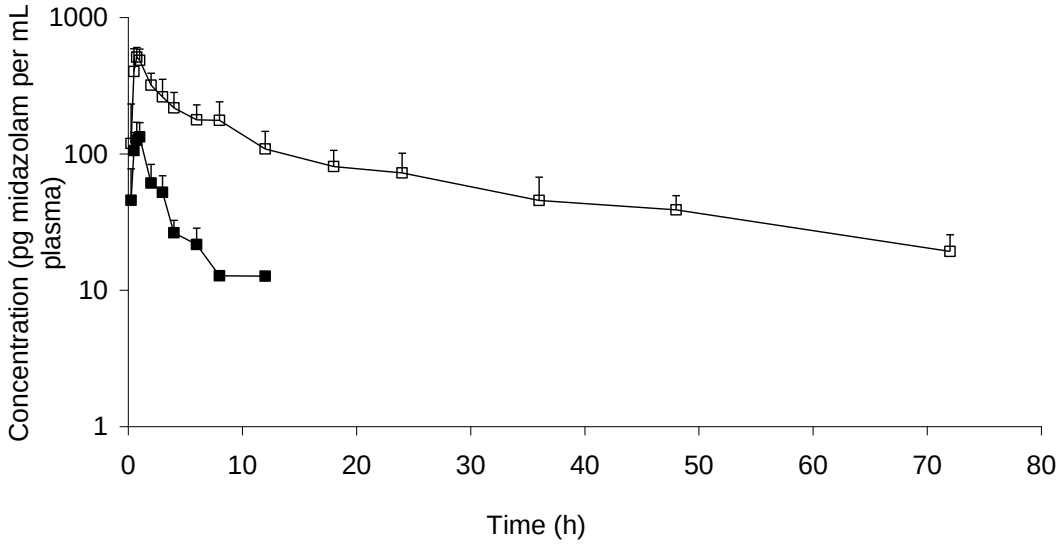

Figure 54: Semilog plot of midazolam mean plasma concentration, before (closed squares, *n*=6 to 4 h, *n*=2 to 8 h and *n*=1 to 12 h) and after (open squares, *n*=6 to 36 h, *n*=5 to 48 h and *n*=3 to 72 h) daily repeat dosing of fluvoxamine and ketoconazole. Error bars represent one standard deviation.

Two data points were excluded from calculations (microdose only, subject 3, 0.25 h, and microdose plus inhibitors, subject 2, 8 h) as these samples failed to meet the AMS acceptance criteria (Section 7.11.4). Inter-subject variability of calculated PK parameters was moderate with CVs of approximately 29% and 27% after administration of the first microdose and the second microdose, respectively.

3.3.6.1 Midazolam microdosing data vs. literature data

Midazolam microdose PK data obtained show concordance with data obtained after administration of a 7.5 mg and a 0.5 mg dose [12, 151]. $C_{max,}$ $AUC_{0-\infty}$ and $t_{1/2}$ agree with those previously reported for a 7.5 mg dose within a factor of 1.3, 1.5 and 1.2 respectively, and within a factor of 2.0, 2.0 and 1.7 for a 0.5 mg dose (Table 30).

Table 30: Plasma pharmacokinetic data obtained after administration of a midazolam microdose (25 µg) vs. literature data obtained after a microdose and therapeutic doses.

Dose	Number of subjects	$t_{1/2}$ (h)	t_{max} (h)	C_{max} (ng/mL)		AUC_{0-t} (h.ng/mL)		$AUC_{0-\infty}$ (h.ng/mL)		Source
				A	B	A	B	A	B	
25 µg	6	4.00	0.75	0.151	6.04	0.390	15.6	0.444	17.8	N/A
100 µg	6	3.95	0.56	0.37	3.70	0.89	8.90	1.02	10.2	[12]
0.5 mg	10	2.7	0.75	1.49	2.98	4.35	8.70	4.38	8.76	[151]
7.5 mg	6	3.31	0.63	34.0	4.53	81.8	10.91	87.0	11.6	[12]

A-calculated from dose as administered B-dose normalised to 1 mg

The midazolam data obtained after cassette microdosing compare favourably with microdose data obtained from a previous study [12]. $AUC_{0-\infty,}$ C_{max} and $t_{1/2}$ obtained after administration of a 25 µg dose agree within a factor of 1.7, 1.6 and 1.0, with data obtained for a 100 µg dose. These data demonstrate PK linearity over a 300-fold range.

3.3.6.2 Effect of inhibitor administration on the pharmacokinetics of midazolam

Following repeat administration of ketoconazole and fluvoxamine the PK of midazolam show a statistically significant ($p<0.01$) increases in $AUC_{0-\infty}$ (x 11.7), C_{max} (x 3.6) and $t_{1/2}$ (x 4.6) The t_{max} is unchanged (Table 31).

Table 31: Plasma pharmacokinetic data obtained after administration of a midazolam microdose (25 µg) and after administration of a midazolam microdose (25 µg) concomitantly with an inhibitor dose (*n*=6, mean, SD in parentheses).

PK parameter	25 µg dose	25 µg + inhibitor dose	Student's t-test p value	Increase factor on inhibitor administration
C_{max} (pg/mL)	151 (37.6)	549 (83.0)	0.000	3.6
$t_{1/2}$ (h)	4.00 (1.83)	18.2 (4.55)	0.000	4.6
AUC_{0-t} (h.pg/mL)	390 (83.3)	5210 (1660)	0.001	13.4
$AUC_{0-\infty}$ (h.pg/mL)	444 (101)	5200 (1900)	0.002	11.7
t_{max} (h)	0.750 (0.224)	0.708 (0.188)	0.741	0.9

These results are consistent with results obtained in a previous study [156] where co-administration of ketoconazole (200 mg daily for 3 days) and single dose of midazolam (6 mg) resulted in a increase in $AUC_{0-\infty}$ (x 13.6) and C_{max} (x 4.2) compared with midazolam administration only (Table 32).

Table 32: Plasma pharmacokinetic data obtained after administration of a midazolam microdose plus inhibitor vs. literature data obtained after administration of a therapeutic dose.

Dose	Increase factor for midazolam concentration on co-administration of repeat daily doses of ketoconazole					
	$t_{1/2}$ (h)	t_{max} (h)	C_{max} (ng/mL)	AUC_{0-t} (h.ng/mL)	$AUC_{0-\infty}$ (h.ng/mL)	Source
25 µg[1]	4.6	0.9	3.7	13.4	11.7	N/A
75 µg[2]	1.6	1	3.74	ND	6.47	[157]
6 mg[3]	ND	1	4.24	ND	13.6	[156]

[1] 400 mg for 8 days, [2] 200 mg for 2 days, [3] 200 mg for 3 days.

In a second study, midazolam was administered at reduced dose of 75 µg, both before and after twice daily doses of ketoconazole [157]. The C_{max} and $AUC_{0-\infty}$

saw statistically significant ($p>0.05$) approximate x 3.7-fold and x 7-fold increases, respectively. The magnitude of the increase in C_{max} and AUC on co-administration of ketoconazole and fluvoxamine appears to be equivalent irrespective of the midazolam dose administered. The increase in C_{max} may be explained by the inhibition of CYP3A, which reduces first pass metabolism. The increased $t_{1/2}$ is consistent with the reduction in clearance due to inhibition of CYP3A enzymes [158] by ketoconazole and fluvoxamine. While there is evidence to suggest that fluvoxamine does also inhibit the metabolism of midazolam [159, 160], the magnitude of the inhibition is much reduced compared to that caused by ketoconazole. A recent study examined the co-administration of midazolam with fluoxetine, fluvoxamine, nefazodone, and ketoconazole [159]. Ketoconazole co-administration resulted in an increase in midazolam AUC of 771.9%, compared with a 66.1% increase in AUC with fluvoxamine.

3.3.6.3 CYP3A4 polymorphisms affecting the metabolism of midazolam

All subjects were genotyped for CYP3A4 polymorphisms, and all subjects returned the CYP3A4 *1/*1 genotype associated with normal enzyme activity.

3.3.7 Tolbutamide microdosing data

Tolbutamide concentrations in post-dose plasma samples were >LOQ of 3.833 pMC for all subjects (*n*=6) to 36 h. The levels for several, but not all, subjects were >LOQ at 48 h (subjects 1 to 5) and 72 h (subjects 3 and 4) after administration of the microdose (Figure 55). After administration of the second microdose, during the period of administration of ketoconazole and fluvoxamine, plasma concentrations were >LOQ for all subjects (*n*=6) to 72 h (Figure 55). In addition, one pre-dose sample (subject 5) was >LOQ. Individual subject data and mean data are summarised in Appendix 4. PK data are summarised in Appendix 10.

One datum point was excluded from calculations (microdose following oral administration of ketoconazole and fluvoxamine, subject 1, 24 h) as this sample failed to meet the AMS acceptance criteria (Section 7.11.4). Inter-subject

variability of calculated PK parameters was moderate with CVs of approximately 37% and 54% after administration of the first microdose and the second microdose, respectively.

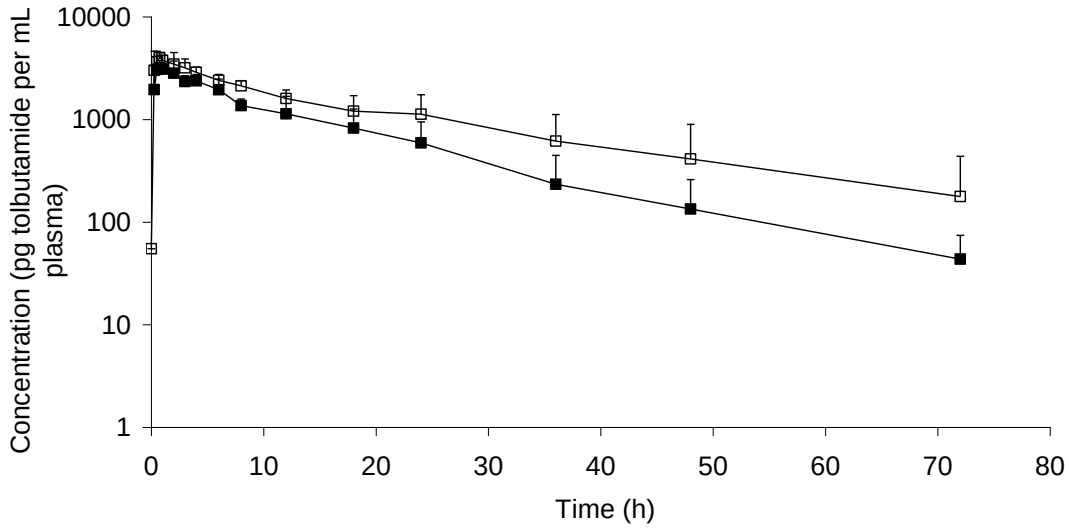

Figure 55: Semilog plot of tolbutamide mean plasma concentration, before (closed squares, *n*=6 to 36 h, *n*=5 to 48 h and *n*=2 to 72 h) and after (open squares, *n*=6 to 72 h) daily repeat dosing of fluvoxamine and ketoconazole. Error bars represent one standard deviation.

3.3.7.1 CYP2C9 polymorphisms affecting the metabolism of tolbutamide

After completion of the study, all subjects were genotyped for CYP2C9 (Table 33). Subjects 1, 2, 5 and 6 were genotyped as wild-type CYP2C9 (*1/*1), with no mutations found. Subject 3 was genotyped as CYP2C9 (*1/*3) and subject 4 was genotyped as CYP2C9 (*1/*2).

Table 33: CYP2C9 genotyping of subjects 1-6.

Subject number	CYP2C9*2	CYP2C9*3	CYP2C9 Genotype
1	No mutation	No mutation	*1/*1
2	No mutation	No mutation	*1/*1
3	**No mutation**	**One mutation**	***1/*3**
4	**One mutation**	**No mutation**	***1/*2**
5	No mutation	No mutation	*1/*1
6	No mutation	No mutation	*1/*1

The mutations result in reduced CYP2C9 activity [145, 161], with the CYP2C9 (*1/*3) polymorphism expected to be the more significant, hence the plasma concentrations of tolbutamide in these subjects would be expected to be elevated above the levels observed in the remaining four subjects. A study carried out by Kircheiner et al. determined that oral clearance of tolbutamide in CYP2C9 (*1/*2) and CYP2C9 (*1/*3) genotyped volunteers was reduced by approximately 12% and 51% respectively, compared with CYP2C9 (*1/*1) [62]. Mean data for subject 3 and 4 and the normal CYP2C9 (*1/*1) metabolisers indicate that two populations are evident (Figure 56).

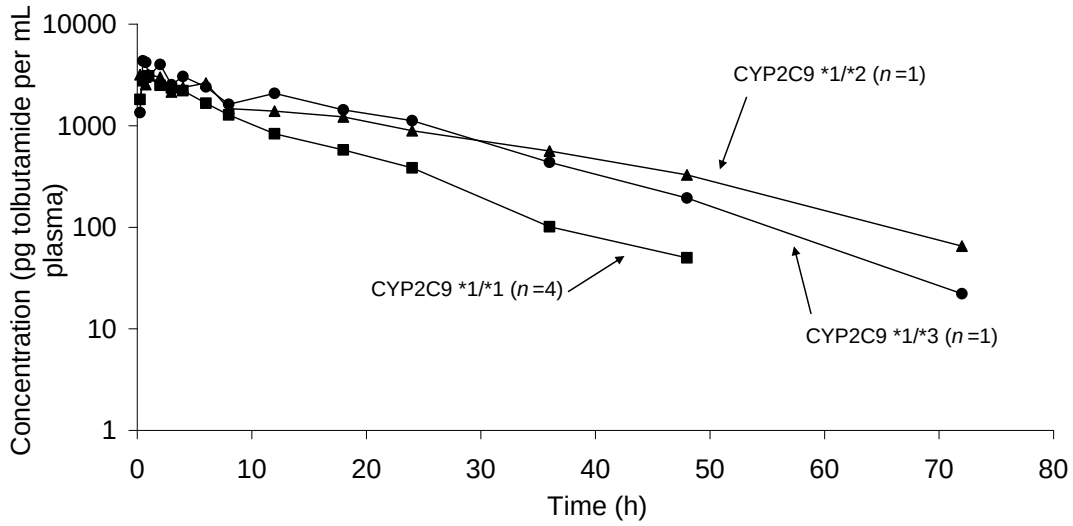

Figure 56: Concentration-time curves of ^{14}C-tolbutamide in venous plasma after administration of a microdose, CYP2C9 (*1/*1) genotyped subjects, *n*=4 (squares), CYP2C9 (*1/*2) genotyped subject 4, *n*=1 (triangles) and CYP2C9 (*1/*3) genotyped subject 3, *n*=1 (circles).

The $AUC_{0\text{-}t}$ for subject 3 is approximately two-fold higher than the mean $AUC_{0\text{-}t}$ for CYP2C9 (*1/*1) genotyped subjects (63.1 h.ng/mL *cf* a mean of 31.6 h.ng/mL). This has been observed previously *in vivo* [145] due to slower metabolic elimination of tolbutamide. The difference between the $AUC_{0\text{-}\infty}$ for subject 4, and the mean of CYP2C9 (*1/*1) genotyped subjects is of a similar magnitude (x 1.8). Dixon's Q-test was applied to the AUC data, and both subject 3 and subject 4 were found to be outliers ($Q_{90\%}$). Similarly, when co-administered with ketoconazole and fluvoxamine, subjects 3 and 4 show approximate increases in $AUC_{0\text{-}t}$ of 1.8 and 2.3-fold compared with the four CYP2C9 (*1/*1) genotyped subjects (Figure 57).

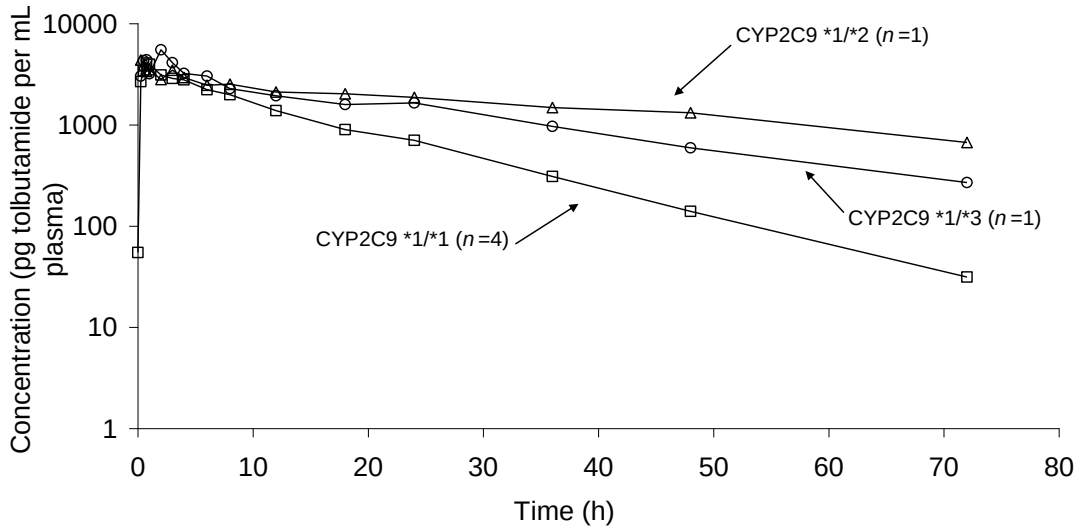

Figure 57: Concentration-time curves of ^{14}C-tolbutamide in venous plasma after microdose plus daily repeat dosing of fluvoxamine and ketoconazole, CYP2C9 (*1/*1) genotyped subjects, *n*=4 (squares), CYP2C9 (*1/*2) genotyped subject 4, *n*=1 (triangles) and CYP2C9 (*1/*3) genotyped subject 3, *n*=1 (circles).

When applying the Dixon's Q-test to the data, AUC_{0-t} values for subject 3 and subject 4 are outliers in comparison to mean AUC_{0-t} data for subjects 1, 2, 5 and 6 (to 99% confidence). While these data seem to indicate some significance, and are supported by literature data, they must be treated with caution, due to the small sample size. The data indicate that differences in CYP2C9 genotypes may be phenotyped using tolbutamide after administration of a microdose and therefore microdosing may have a potential application in phenotyping studies.

Due to these differences in genotype and subsequent phenotypic properties observed, data obtained after administration of the microdose and inhibitors are examined with and without inclusion of subjects 3 and 4.

3.3.7.2 Tolbutamide microdosing data vs. literature data

The PK data obtained after microdosing of tolbutamide show concordance with previously published data for a 125 mg dose [149]. The mean $t_{1/2}$ for subjects 1, 2, 5 and 6 is almost identical (8.13 h, *cf* 7.7 h for the 125 mg dose). The overall mean (*n*=6) is also close at 7.22 h. When normalised to the 125 mg dose, C_{max} (*n*=6) was within 14% of the reported C_{max} after an oral 125 mg dose. The $AUC_{0-\infty}$ for all subjects (*n*=6) was within 17% of the reported value for the 125 mg dose. Exclusion of subjects 3 and 4 from this mean value resulted in a slightly closer agreement of 11% (Table 34).

Table 34: Plasma pharmacokinetic data obtained after administration of a tolbutamide microdose (25 µg) vs. literature data obtained after therapeutic doses.

Dose	Number of subjects	$t_{1/2}$ (h)	t_{max} (h)	C_{max} (ng/mL)		AUC_{0-t} (h.ng/mL)		$AUC_{0-\infty}$ (h.ng/mL)		Source
				A	B	A	B	A	B	
25 µg	6 (all)	8.13	0.875	3.72	149	41.3	1650	41.8	1670	Present study
25 µg	4[1]	7.22	0.938	3.70	148	31.6	1264	32.1	1280	
25 µg	1[2]	8.51	0.500	4.34	173.6	63.1	2524	63.4	2536	
25 µg	1[3]	11.4	1.00	3.18	127.2	58.2	2358	59.3	2384	
125 mg	10	7.7	ND	16300	130.4	ND	ND	179000	1432	[149]

[1]subjects 1, 2, 5 & 6, [2]subject 3, [3]subject 4

Thus, the data show dose linearity over a 500-fold range. This degree of dose linearity has been demonstrated previously in the rat, where a microdose was compared with doses up to 1000 times higher [99]. Notably this is the first time PK dose linearity has been demonstrated for tolbutamide in humans.

Tolbutamide microdose data obtained for all subjects on co-administration of fluvoxamine and ketoconazole show a statistically significant ($p<0.01$) 1.2-fold increase in C_{max}, while AUC_{0-t} and $AUC_{0-\infty}$ show a 1.7-fold ($p<0.01$) and 1.8-fold ($p<0.05$) increase (Table 35).

Table 35: Plasma pharmacokinetic data obtained after administration of a tolbutamide microdose (25 µg) and after administration of a tolbutamide microdose (25 µg) concomitantly with an inhibitor dose (*n*=6, mean, SD in parentheses).

PK parameter	25 µg dose	25 µg + inhibitor dose	Student's t-test p value	Increase factor on inhibitor administration
C_{max} (ng/mL)	3.72 (0.429)	4.51 (0.516)	0.004	1.2
$t_{1/2}$ (h)	8.13 (2.05)	16.5 (10.7)	0.0717	2.0
AUC_{0-t} (h.ng/mL)	41.3 (15.8)	68.7 (29.2)	0.008	1.7
$AUC_{0-\infty}$ (h.ng/mL)	41.8 (16.0)	76.4 (42.5)	0.036	1.8
t_{max} (h)	0.875 (0.627)	0.708 (0.660)	0.712	0.8

[1]ketoconazole (2 x 200 mg) and fluvoxamine (1x100 mg) administered daily for 10 days

Exclusion of the two subjects determined to have reduced CYP2C9 activity does appear to alter the outcome of the statistical analysis (Table 36). In particular, the $t_{1/2}$ is now demonstrated to be significantly altered ($p<0.01$) by the co-administration of fluvoxamine and ketoconazole. On inclusion of these polymorphic subject data, the increase in $t_{1/2}$ is deemed statistically insignificant. Overall, the magnitude of the changes in PK parameters is similar on inclusion and exclusion of the polymorphic subject data.

Table 36: Plasma pharmacokinetic data obtained after administration of a tolbutamide microdose (25 µg) and after administration of a tolbutamide microdose (25 µg) concomitantly with an inhibitor dose (*n*=6, subjects 3 and 4 excluded).

PK parameter	25 µg dose	25 µg + inhibitor dose	Student's t-test p value	Increase factor on inhibitor administration
C_{max} (pg/mL)	3.70 (0.284)	4.29 (0.193)	0.025	1.2
$t_{1/2}$ (h)	7.22 (1.51)	10.6 (1.72)	0.003	1.5
AUC_{0-t} (h.ng/mL)	31.6 (6.27)	50.9 (6.31)	0.000	1.6
$AUC_{0-\infty}$ (h.ng/mL)	32.1 (6.51)	51.4 (6.62)	0.000	1.6
t_{max} (h)	0.938 (0.774)	0.500 (0.204)	0.367	0.5

[1]ketoconazole (2 x 200 mg) and fluvoxamine (1x100 mg) administered daily for 10 days

The data obtained in this study are consistent with data obtained in an *in vitro* study where ketoconazole was demonstrated to inhibit tolbutamide hydroxylation in liver microsomes by way of a 1.8-fold increase in $t_{1/2}$ [38]. *In vivo*, on co-administration with fluvoxamine, a reduction in the formation of

hydroxytolbutamide was observed, signifying a decrease in the clearance of tolbutamide [37]. This reduction in hydroxylation leads to an increase in the tolbutamide AUC, as was observed in this microdosing study (Table 37).

Table 37: Plasma pharmacokinetic data obtained after administration of a tolbutamide microdose plus inhibitors vs. literature data obtained after administration of a therapeutic dose.

Inhibitor	Dose	No of subjects	Fold increase observed in tolbutamide concentration on co-administration of fluvoxamine and ketoconazole				
			$t_{1/2}$ (h)	t_{max} (h)	C_{max} (ng/mL)	AUC_{0-t} (h.ng/mL	$AUC_{0-\infty}$ (h.ng/mL)
Fluvoxamine/ketoconazole[1]	25 µg	4[5]	2.0	0.8	1.2	1.7	1.8
Fluvoxamine/ketoconazole[1]	25 µg	1[6]	2.3	4.0	1.3	1.5	1.6
Fluvoxamine/ketoconazole[1]	25 µg	1[7]	3.2	0.3	1.4	2.0	2.6
Fluvoxamine [37]	500 mg	7	1.3	ND	ND	ND	ND
Ketoconazole [38]	150 mg[4]	7	3.3	ND	ND	1.8	ND

[1]ketoconazole (2 x 200 mg) and fluvoxamine (1 x 100 mg) administered daily for 10 days, [2]fluvoxamine (150 mg) administered daily for 5 days, [3]ketoconazole (200 mg) administered daily for 10 days, [4]daily for 5 days, [5]subjects 1, 2, 5 & 6, [6]subject 3, [7]subject 4

Although there is evidence that both ketoconazole and fluvoxamine inhibit the clearance of tolbutamide, both have an apparently weaker effect on CYP2C9 than on CYP3A4, CYP1A2 and P-gp. AUC_{0-t} for tolbutamide (normal metabolisers only) increased by a factor of 1.7 between doses, however the increases observed in the AUC_{0-t} for midazolam; x 13.4 (Section 3.3.6.2), caffeine; x 6.7 (Section 3.3.5.2) and fexofenadine; x 3.2 (Section 3.3.8.2) are much higher, indicating a greater effect of the inhibitors. Given the co-administration of fluvoxamine and ketoconazole, it is not possible to determine which has the greater inhibitory effect on tolbutamide metabolism as both inhibitors were co-administered.

3.3.8 Fexofenadine microdosing data

Fexofenadine concentrations in post-dose plasma samples were >LOQ of 3.833 pMC for all subjects (*n*=6) from 0.5 h to 4 h. Concentrations at 0.25 h were >LOQ for subjects 4 and 6 only. The levels for several, but not all, subjects were >LOQ to 8 h (subjects 1, 2, 3, 5 and 6) and 12 h (subjects 1 and 3) after administration of the microdose (Figure 58). Fexofenadine concentrations in

samples analysed at 18 h to 72 h were below the LOQ. After administration of the second microdose, during the period of administration of ketoconazole and fluvoxamine, plasma concentrations were >LOQ for all subjects (*n*=6) to 12 h, except for the 0.5 h sample for subject 6 (Figure 58). Several subjects, but not all, were >LOQ at 18 h (subjects 1, 3, 5 and 6), 24 h (subjects 1, 3 and 6) and 48 h (subject 3). All data points were included in calculations with the exception of four 12 h samples (microdose only, subjects 2 and 5, and microdose following oral administration of ketoconazole and fluvoxamine, subjects 2 and 3), which failed to meet the AMS acceptance criteria (Section 7.11.4). Individual subject data and mean data are summarised in Appendix 5. PK data are summarised in Appendix 11. Inter-subject variability of calculated PK parameters was moderate with CVs of approximately 38% and 40% after administration of the first microdose and the second microdose, respectively.

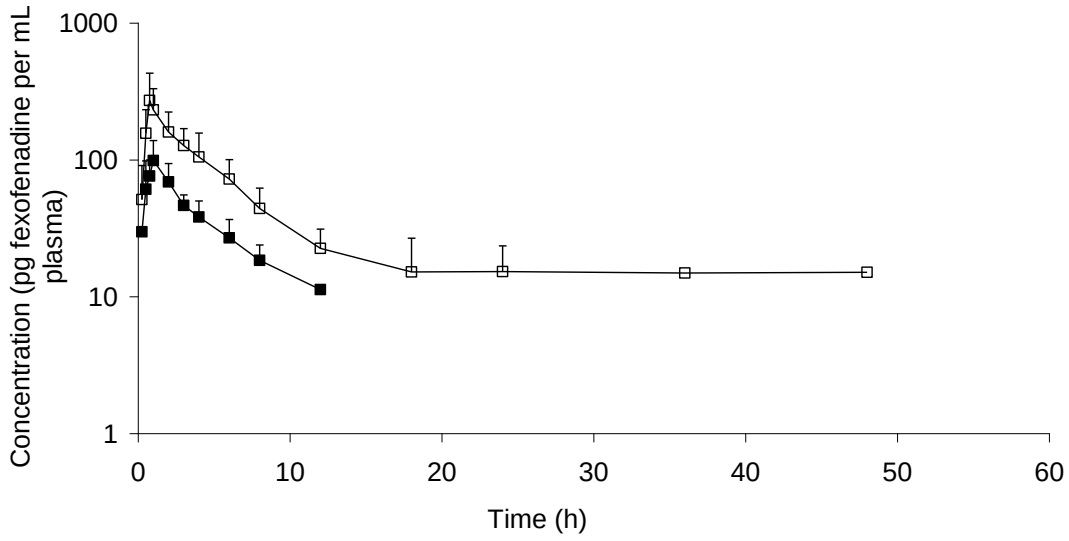

Figure 58: Semilog plot of fexofenadine mean plasma concentration, before (closed squares, *n*=6 to 4 h, *n*=5 to 8 h and *n*=2 to 12 h) and after (open squares, *n*=6 to 12 h, *n*=4 to 18 h, *n*=3 to 24 h and *n*=1 to 48 h) daily repeat dosing of fluvoxamine and ketoconazole. Error bars represent one standard deviation.

3.3.8.1 Fexofenadine microdosing data vs. literature data

PK data obtained for fexofenadine after microdosing show concordance with that previously reported for doses of 60 mg dose [150] and 120 mg [23] when normalised to a 1 mg dose (Table 38). C_{max} data obtained after a 25 µg dose are within 12% and 56% and $AUC_{0-\infty}$ data are within 22% and 8% of those previously obtained at a 60 and 120 mg dose respectively.

Table 38: Plasma pharmacokinetic data obtained after administration of a fexofenadine microdose (25 µg) vs. literature data obtained after therapeutic doses.

Dose	Number of subjects	$t_{1/2}$ (h)	t_{max} (h)	C_{max} (ng/mL)		AUC_{0-t} (h.ng/mL)		$AUC_{0-\infty}$ (h.ng/mL)		Source
				A	B	A	B	A	B	
25 µg	6	5.75	1.00	0.105	4.22	0.444	17.8	0.497	19.9	N/A
100 µg	6	16	1.2	0.310	3.10	2.51	25.1	2.77	27.7	[23]
60 mg	24	14.4	1.31	286	4.80	ND	ND	1520	25.4	[150]
120 mg	6	12	2.7	318	2.7	2130	17.7	2210	18.4	[23]

A-calculated from dose as administered B-dose normalised to 1 mg

The results obtained from this microdose administration of fexofenadine also show close agreement with oral microdose data obtained in a previous study [23], where the values obtained for C_{max} and $AUC_{0-\infty}$ were within 36% and 28% of previously reported microdose data. Thus, the data are consistent with fexofenadine demonstrating PK linearity over a 240-fold range. The half-life obtained after administration of a microdose (25 µg) is not in such close agreement with the values obtained previously. A 2.8, 2.5 and 2.1-fold difference is seen compared with the data obtained from 100 µg, 60 mg and 120 mg doses. The half-life for fexofenadine varies widely within the literature depending on the length of the sample collection period [162] as this can affect the shape of the curve. The elimination phase is poly-exponential, hence the $t_{1/2}$ of fexofenadine may be determined during both the α- and β- elimination phases (Figure 59). It was not possible to determine a reliable β-$t_{1/2}$ for microdose only data, as the majority of the data points are present in the α-$t_{1/2.}$

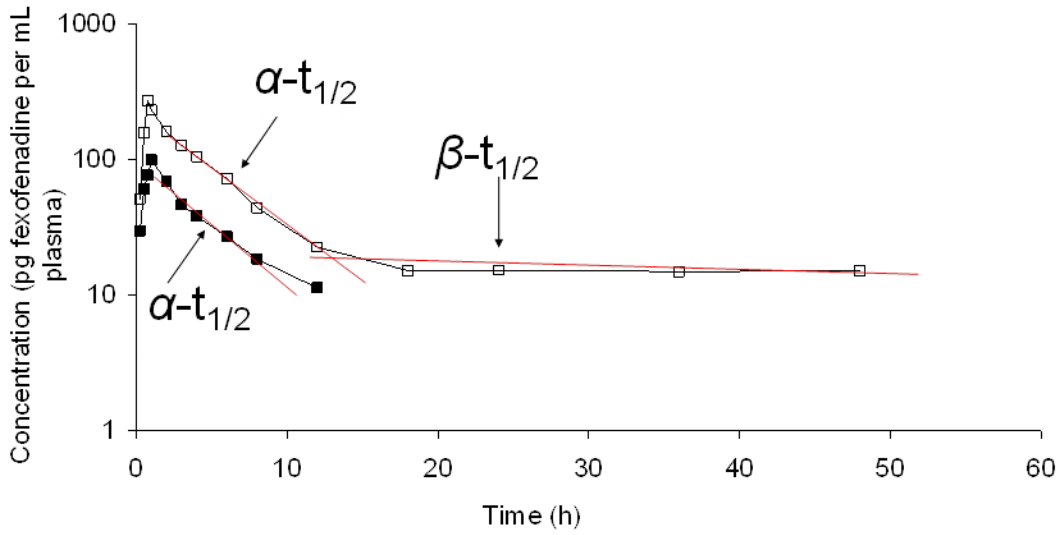

Figure 59: Semilog plot of fexofenadine plasma concentration before and after daily repeat dosing of fluvoxamine and ketoconazole with α-$t_{1/2}$ and β-$t_{1/2}$.

3.3.8.2 Effect of inhibitor administration on the pharmacokinetics of fexofenadine

The PK data for fexofenadine on co-administration of ketoconazole and fluvoxamine (Table 39), show statistically significant ($p<0.01$) increases in AUC_{0-t} and $AUC_{0-\infty}$ (x 3.2) and a statistically significant increase ($p<0.05$) in C_{max} (x 2.7).

Table 39: Plasma pharmacokinetic data obtained after administration of a fexofenadine microdose (25 µg) and after administration of a fexofenadine microdose (25 µg) concomitantly with an inhibitor dose (*n*=6, mean, SD in parentheses).

PK parameter	25 µg dose	25 µg + inhibitor[1] dose	Student's t-test p value	Increase factor on inhibitor administration
C_{max} (pg/mL)	105 (33.3)	285 (154)	0.022	2.7
$t_{1/2}$ (h)	5.75 (2.10)	13.8 (9.62)	0.067	2.4
AUC_{0-t} (h.pg/mL)	444 (152)	1430 (452)	0.000	3.2
$AUC_{0-\infty}$ (h.pg/mL)	497 (170)	1580 (455)	0.000	3.2
t_{max} (h)	1.00 (0.548)	0.875 (0.137)	0.581	0.9

[1]ketoconazole (2 x 200 mg) and fluvoxamine (1 x 100 mg) administered daily for 10 days

The increases in the three concentration-related parameters are consistent with the inhibition of the gut efflux transporter P-gp by ketoconazole, leading to an increase in absorption and hence an increase in C_{max} [163]. The resulting shape of the PK plasma concentration-time curve from C_{max} to 12 h is parallel to that of the untreated subjects, showing no evidence of inhibition of elimination mechanisms. These data are consistent with previous studies with ketoconazole and fexofenadine *in vitro* and *in vivo* (monkey) carried out to examine DDIs [74]. A study performed in human volunteers [163] found ketoconazole inhibition of P-gp decreased fexofenadine efflux, hence fexofenadine concentrations increased, leading to an increase in C_{max} of 135% and increase in AUC of 165%. A study was undertaken by Tannergren et al. [164] to confirm the involvement of P-gp in this DDI, specifically in the small intestine where P-gp is thought to be most prevalent. An intestinal Loc-I-Gut® perfusion technique was employed, allowing direct measurement of intestinal transport along with plasma concentration measurements. A jejunal segment of approximately 10 cm was isolated and was perfused with fexofenadine. This was repeated after 5 day repeat ketoconazole dosing and both perfusate leaving the jejunal segment and venous blood samples were collected. Examination of the data obtained during that study contradicted the hypothesis and it was found that the AUC of fexofenadine in plasma did not significantly increase on co-administration of ketoconazole. Furthermore, P_{eff}, the jejunal permeability and fractions absorbed also showed a negligible change in concentration after ketoconazole pre-treatment. A follow up study was undertaken where fexofenadine was administered with and without another P-gp inhibitor, verapamil. It was hypothesised that co-administration of fexofenadine and verapamil would result in an increase in fexofenadine plasma AUC and k_a. Also in the perfusate, P_{eff} would be expected to increase along with an increase in the fraction absorbed (f_{abs}) due to inhibition of P-gp activity by verapamil. While the hypothesis for plasma AUC was correct, with a significant increase in fexofenadine concentration being observed, there was still no significant difference in absorption [165].

The results obtained in these studies indicate that fexofenadine absorption mechanisms are not solely dependent on P-gp but may also depend on other

transporters such as the OATP family. Fexofenadine is a known substrate of OATP as well as P-gp [166]. P-gp and OATP are thought to work in opposite directions across enterocytes and inhibition of the two mechanisms may not result in significantly increased concentrations of metabolic targets (Figure 60).

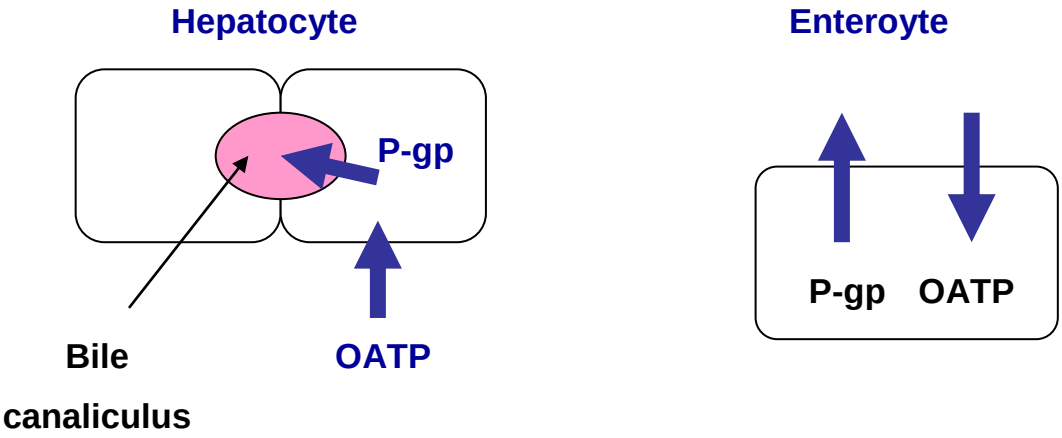

Figure 60: P-glycoprotein and OATP at hepatocytes and enterocytes [165].

By contrast, OATP and P-gp in the liver work in the same direction and if fexofenadine is highly hepatically extracted, inhibition of the liver uptake would result in increased plasma concentrations. The involvement of the liver in the uptake of fexofenadine was determined in a recent study by the first IV administration of fexofenadine, where 70% of the dose was hepatically cleared [23]. While the mechanisms are not yet fully understood, it appears that ketoconazole inhibits the efflux of P-gp, resulting in increased plasma concentrations, and that OATP may play a part in this inhibition.

3.4 Conclusions

Since the implementation of the very first microdosing study, there has been concern and much debate about the ability of microdose data to predict the PKs of a drug at the pharmacological dose. Over the last 10 years a growing number of compounds have been assessed for dose linearity between a microdose and a pharmacologic dose [10] (Section 1.8.1). In the current study, four compounds, caffeine, midazolam, tolbutamide and midazolam, were found to exhibit linearity from a microdose (25 µg) to higher doses reported in the literature. These

compounds were linear over a 10000, 300, 5000 and 4800-fold dose range for caffeine, midazolam, tolbutamide and fexofenadine respectively. Caffeine, midazolam, tolbutamide and fexofenadine are known to exhibit DDIs *in vivo* when co-administered with fluvoxamine and/or ketoconazole. Inhibitors were administered daily for eight days prior to the administration of the second cassette microdose, allowing ketoconazole and fluvoxamine levels to reach steady state [41, 153, 154]. These levels were maintained by continuation of this daily inhibitor dosing throughout the plasma sample collection period. All PK microdose data obtained after administration of fluvoxamine and ketoconazole show significant differences to the PK data obtained for the microdose only. In particular the AUC for all compounds was significantly increased ($p>0.05$).

The results obtained are in close agreement with literature data obtained during similar studies, the majority of which were obtained after administration of pharmacologic doses. While the present data show concordance, they have been obtained from relatively small numbers of volunteers, with only six participants in the cassette microdose study, and consequently the results are unlikely to reflect population variations. A considerable improvement to this study would be to obtain data from the same subjects after administration of a microdose and a pharmacologic dose, with and without inhibitors, which would allow direct comparison of data. Data obtained in this study were generated after a single microdose of each compound administered alone and with inhibitors. The majority of drugs are prescribed to patients as a course of treatment, not as a single dose. This study does not allow the effects of inhibitors once the compound itself has reached steady state to be examined and therefore is a limitation of this work.

In the current study, the inhibitors were co-administered, as the aim was to investigate the ability of a microdose to detect a DDI, not to attribute this to a particular inhibitor. Accordingly, the quantitative contribution and individual function of each inhibitor therefore could not be assessed. For example, CYP2C9 is known to be inhibited by both fluvoxamine and ketoconazole; the current study design does not allow differentiation between the two inhibitors and their individual effects on tolbutamide.

There has been some debate in the use of cassette doses, particularly in the context of DDI studies and the possibility that the different components in the cassette might interact with each other [65, 84]. Microdosing is not expected to produce pharmacological effects and is advantageous in cassette probe dosing, as interactions between compounds are very unlikely to occur. Data obtained in the current study support this theory as all PK data obtained on cassette microdosing were linear with pharmacologic doses, with no evidence of interactions between compounds within the cassette. There is negligible body burden, both from the respect of the radioactive dose administered, and the very low drug concentrations, which mean pharmacological effects are dramatically reduced resulting in no side effects. In addition, as the compounds are ^{14}C-labelled background substrate will not affect the data.

The maximum dose administered in a microdose study is 100 μg. Where multiple compounds are administered, the dose is shared. In this study, the dose was shared equally between all compounds and caffeine, midazolam, tolbutamide and fexofenadine concentrations in this study were quantifiable by AMS during the two dosing periods. For all four compounds, there were samples in which the levels were below the LOQ. The time-points to which each drug was quantifiable in plasma are summarised below (Table 40).

Table 40: Plasma samples analysed by HPLC-AMS with concentrations below the LOQ.

Dose	Caffeine	Midazolam	Tolbutamide	Fexofenadine
Microdose only	12 h (6 subjects) 18 h (4 subjects) 24 h (2 subjects)	4 h (6 subjects) 8 h (2 subjects) 18 h (1 subject)	36 h (6 subjects) 48 h (5 subjects) 72 h (2 subjects)	4 h (6 subjects) 8 h (5 subjects) 12 h (2 subjects)
Microdose plus inhibitors	72 h (6 subjects)	36 h (6 subjects) 48 h (5 subjects) 72 h (3 subjects)	72 h (6 subjects)	12 h (6 subjects) 18 h (4 subjects) 24 h (subjects) 48 h (1 subject)

With some simple steps, the quantifiable limit may have been reduced; however, plasma volumes are often a limiting factor. When implementing a cassette microdose study the number of compounds sharing the dose must be carefully considered to ensure that sensitivity is adequate. Generally, the greater the number of compounds sharing the dose, the higher the assay LOQ will be.

The LOQ in a microdosing study is dependent upon the specific radioactivity of the compound dosed. As shown in this study, the LOQ for a typical microdose equivalent to 25 μg, 1.11 x 10^5 dpm, is approximately 9 – 10 pg/mL. Reducing the mass dose, for example by administration of neat radiolabel at 2.22 x 10^6 dpm which requires the same regulatory approval as a conventional microdose study, would dramatically reduce the LOQ. Assuming a specific radioactivity of approximately 1 μg, 2.22 x 10^6 dpm, an LOQ of 0.01 pg/mL could be achieved, an approximate 1000-fold reduction on the current study, without additional optimisation of the current methods.

The concentrations measured in this study may also be detectable using an alternative method such as LC-MS. A microdosing study was recently performed in which midazolam was administered at 75 μg [157]. All analyses were carried out using LC-MS and the reported LOQ was 10 pg/mL, which is in the same order of magnitude as the LOQ obtained in this study. In addition, mass discrimination by LC-MS offers a clear advantage over the lengthy validations required for acceptance of data obtained by HPLC and AMS analysis in this study.

Each compound in the current study was quantified by AMS, which does not provide structural information, only an isotope ratio. It was therefore essential that each compound was chromatographically separated and resolved prior to AMS analysis. The efficacy of a method for separation of caffeine, midazolam, tolbutamide and fexofenadine from each other and from major metabolites was demonstrated using a 2D-HPLC method. The development of the HPLC method for the current study was straightforward as all compounds administered were established compounds with known and commercially available metabolites. It would be more difficult to develop such a method for a cassette microdose containing several NCEs if there was limited knowledge of their metabolism. Resolution can be assessed using a 2D-HPLC method as was performed in this study and if compounds were found to be unresolved, further method development would be required. As HPLC-AMS analysis is a lengthy offline process with at least 1 week between isolating an HPLC fraction and determining its isotope ratio by AMS, further method development could prove lengthy.

These problems are specific to the analysis of samples by HPLC-AMS after microdosing. An alternative technique such as LC-MS, which has the advantage of mass discrimination as well as analyte quantification may be preferable for some studies, though the response required may be inadequate without significant optimization of the analytical methods. Should sufficient limits of detection be achieved, the use of LC-MS would pose a significant advantage over HPLC-AMS in studies involving cassette microdosing.

Caffeine is a well established substrate for use as a DDI probe for CYP1A2 and it has been incorporated into several cocktails validated for investigation of CYP1A2 activity in human volunteers [42, 167]. Caffeine PKs obtained in the current study were significantly altered on co-administration of fluvoxamine and ketoconazole, thus demonstrating that DDIs may be detected after administration within a cassette microdose. The administration of a radiolabelled caffeine microdose has a significant advantage in cassette DDI studies over the administration of a non-labelled pharmacologic dose, allowing differentiation between the caffeine dosed and residual levels present in the body. Volunteers participating in studies involving the administration of non-labelled caffeine are often required to abstain from caffeine intake, e.g. tea, coffee and coca-cola prior to the start of the study. Even so, plasma samples are still found to contain residual caffeine levels [59], which are often difficult to correlate with caffeine consumption levels [168]. As the measurements made in this study were of ^{14}C-labelled material, there is very little possibility of background caffeine levels in the body having a significant effect on the data. The introduction of ^{14}C-labelled caffeine may present a significant benefit over current methods. It should also be noted that during CYP1A2 DDI studies, phenotypic caffeine to paraxanthine ratios are assessed and are most widely used as a benchmark due to the close correlation of this ratio with the systemic clearance of caffeine [84]. While the focus of this research was to determine the ability of a caffeine microdose to detect DDI effects when co-administered with fluvoxamine, the approach could readily be extended to assess caffeine metabolite ratios.

In conclusion, the data obtained demonstrate the concept of using a microdose to detect differences in PK parameters arising from inhibitory DDIs. The approach

has potential applications in phase 0 studies, in aiding the detection of DDIs early in the drug development process, as well as presenting potential improvements to standard assays currently employed in drug development.

CHAPTER 4

Development of HPLC and AMS methods for quantification of *R*- and *S*-verapamil in plasma

4.1 Introduction

A clinical study was carried out (Chapter 5), whereby a microdose of ^{14}C-labelled verapamil was intravenously administered to seven healthy human volunteers. The microdose was administered alone in period 1, and with a therapeutic oral dose in period 2. The main objective of the study was to quantify *R*- and *S*-verapamil and to evaluate PK parameters after microdose administration. A secondary objective was to compare the PK data obtained for each enantiomer in each dosing period. Due to the very low doses administered in the microdose, AMS detection was chosen for quantification of *R*- and *S*-verapamil in the plasma samples collected during the study. As verapamil was dosed as a racemic mixture, separation of the enantiomers was required, and therefore chiral chromatography was required.

As analytes cannot be identified by mass discrimination during AMS analysis (Section 1.10.1) *R*- and *S*-verapamil must be completely chromatographically resolved from each other and from potential co-eluting compounds prior to analysis. In this case, racemic verapamil was first resolved using an established HPLC method with a C18 stationary phase (Section 4.3.5). Isolated verapamil was then separated into its two enantiomers by chiral HPLC chromatography (Section 4.3.2) prior to AMS measurement. In addition to the HPLC method development and assessment of suitability, a method for the quantification of each enantiomer was developed (Section 4.3.7).

4.1.1 Verapamil

Verapamil is a calcium channel blocker and is used in the treatment of supraventricular arrhythmias, coronary heart disease and arterial hypertension [169]. *R*-verapamil is metabolised through *N*-demethylation, *O*-demethylation and *N*-dealkylation, processes mediated by CYP [170] (Figure 61).

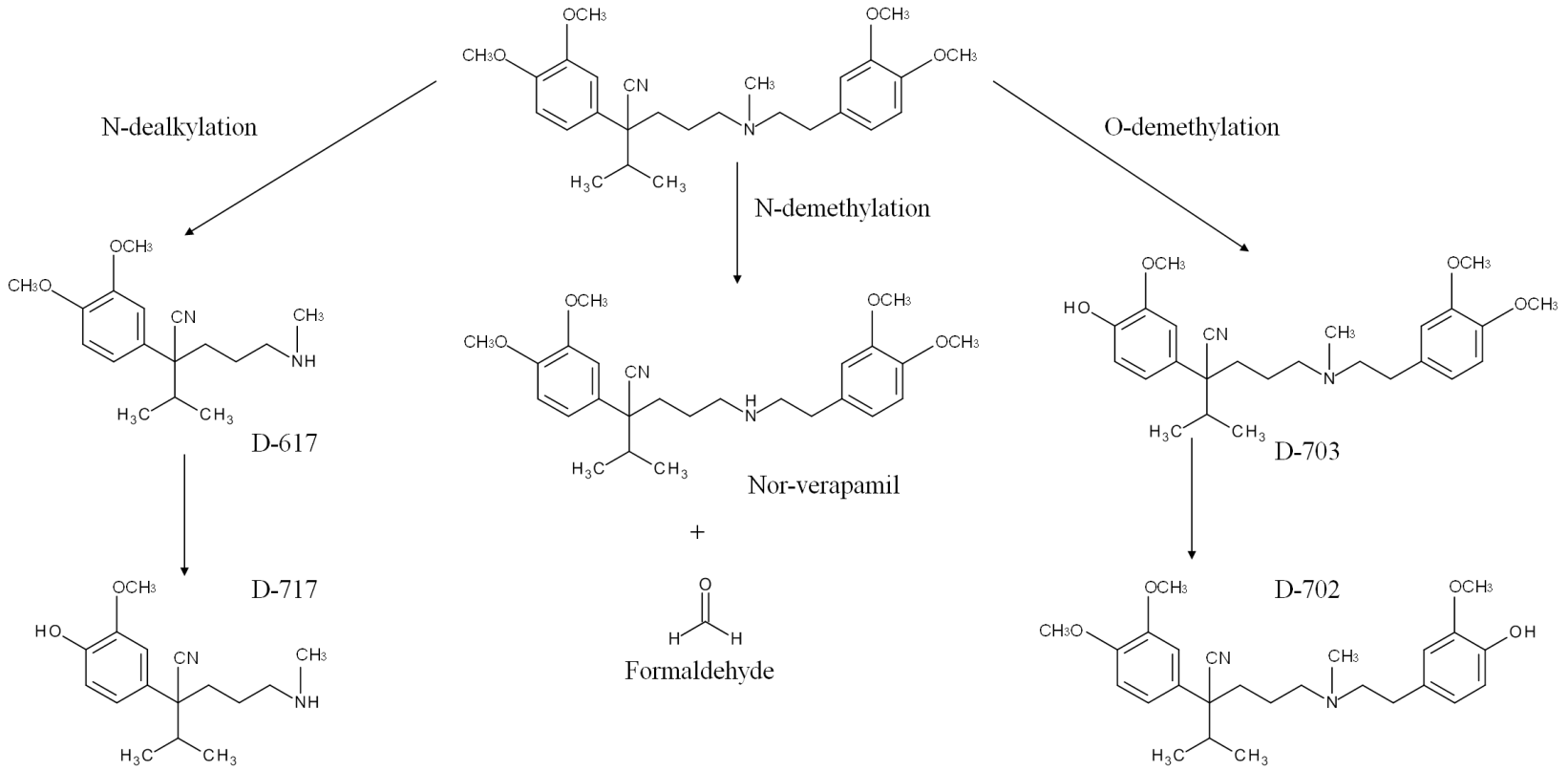

Figure 61: Main routes of verapamil metabolism.

Verapamil is administered as a racemic mixture and the enantiomers are shown in Figure 62, designated *R* and *S* according to the Cahn Ingold Prelog (CIP) rules. The CIP rules assign priorities to the groups attached to the chiral centres of optical isomers. Priorities are first assigned based on the atomic number of each directly attached group. Priority 1 is given to the atom with the highest atomic number, and 4 to the lowest. In cases where the two atoms have the same priority, the atoms attached directly to those atoms are next considered. After all groups have been assigned priorities, the molecule is visualised in 3D with the group of lowest priority to the back. Where the priority order flows in a clockwise rotation, the molecule is designated *R*. Where the priority order is anti-clockwise, the molecule is designated *S*.

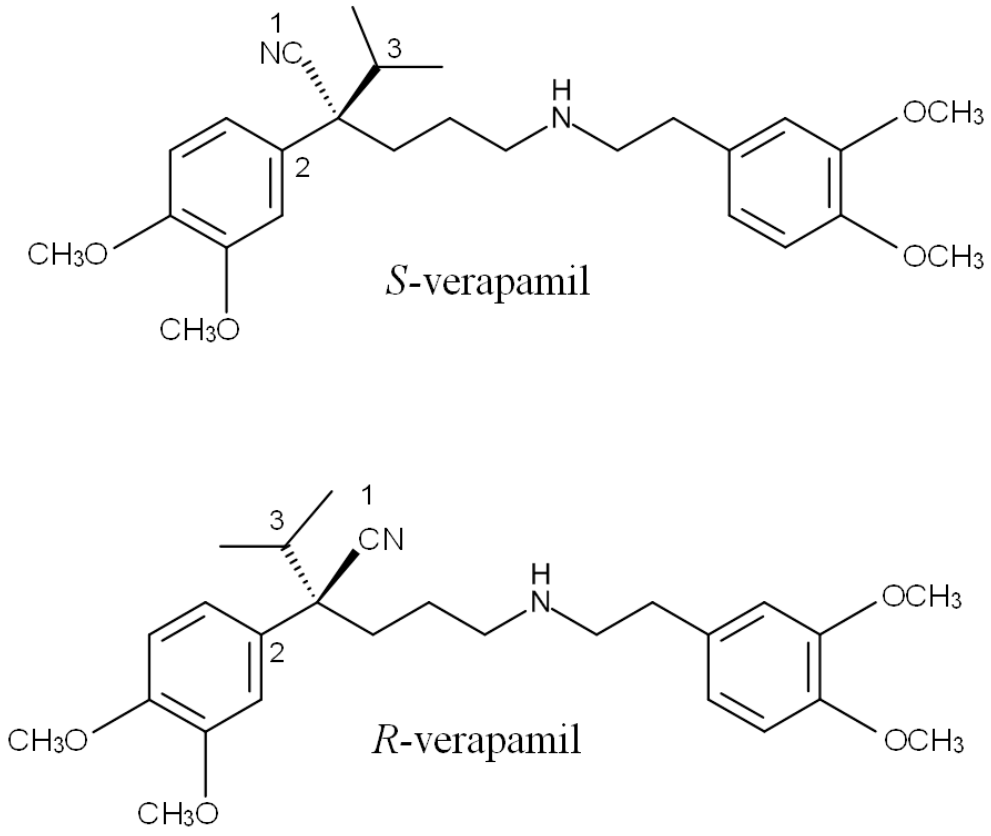

Figure 62: Structures of *S*- and *R*-verapamil showing assignment of groups attached to the chiral centre according to Cahn Ingold Prelog priority rules.

4.1.1.1 Chiral discrimination in HPLC chromatography

Several methods can be used to resolve enantiomers. The first is to react the chiral molecule with a chiral derivatising agent, yielding two diastereoisomers which can be separated by conventional HPLC [171]. An alternative is to add an enantiomerically pure compound to the HPLC mobile phase as a chiral mobile phase additive (CMPA). HPLC is then used to separate the diastereomic complexes that form between the analyte and the CMPA [171]. A third and more commonly used method is the use of a chiral stationary phase (CSP). The CSP interacts with the enantiomers to form short-lived diastereomic complexes. One complex will have a slightly stronger binding strength with the CSP, resulting in separation of the enantiomers. The ability of the analyte to form a transient diastereomic complex is dictated by hydrogen-bonding, π-π interactions, dipole stacking, inclusion complexing and steric bulk [171].

There are four main types of CSP; cyclodextrin, Pirkle, protein and carbohydrate, all of which may be used in reverse phase chromatography. Each of these CSPs has a slightly different chiral recognition mechanism. Cyclodextrin CSPs interact with the analyte by hydrogen bonding and inclusion complexation. These interactions are driven by the ability of the analyte to fit into the cyclodextrin cavity [171]. Pirkle CSPs operate based on the three-point rule, which states that for chiral recognition to occur there must be three simultaneous points of interaction between the analyte and the CSP with at least one of these interactions being stereochemically dependent [171]. Pirkle columns preferentially bind one enantiomer to the CSP through a combination of π-π bonding, hydrogen bonding, steric interactions and dipole stacking. The chiral recognition mechanisms of protein and carbohydrate columns are not as well elucidated as Pirkle and cyclodextrin columns, however they are applicable to a wider range of compounds [171]. Carbohydrate CSPs do not require a specific combination of functional groups to chirally separate enantiomers. Inclusion complexation and attractive interactions are thought to play a major role in the separation of enantiomers using a carbohydrate CSP [171].

4.2 Aims

The primary aims of the work presented in this chapter were (Figure 63):

- to develop a method for the extraction of verapamil from plasma, prior to analysis by HPLC;

- to develop an HPLC method for the C18-chiral separation of *R*- and *S*-verapamil;

- to assess the compatibility of the plasma extraction method and HPLC method;

- to verify the chromatographic separation of ^{14}C-*R*- and *S*-verapamil from ^{14}C-drug related material and to demonstrate the applicability of the method to samples of human plasma;

- to develop a quantification method for *R*- and *S*-verapamil in samples of human plasma;

- to determine the specific radioactivity of the dosing solutions for conversion of AMS data (pMC) to mass concentrations of *R*- and *S*-verapamil per mL of plasma.

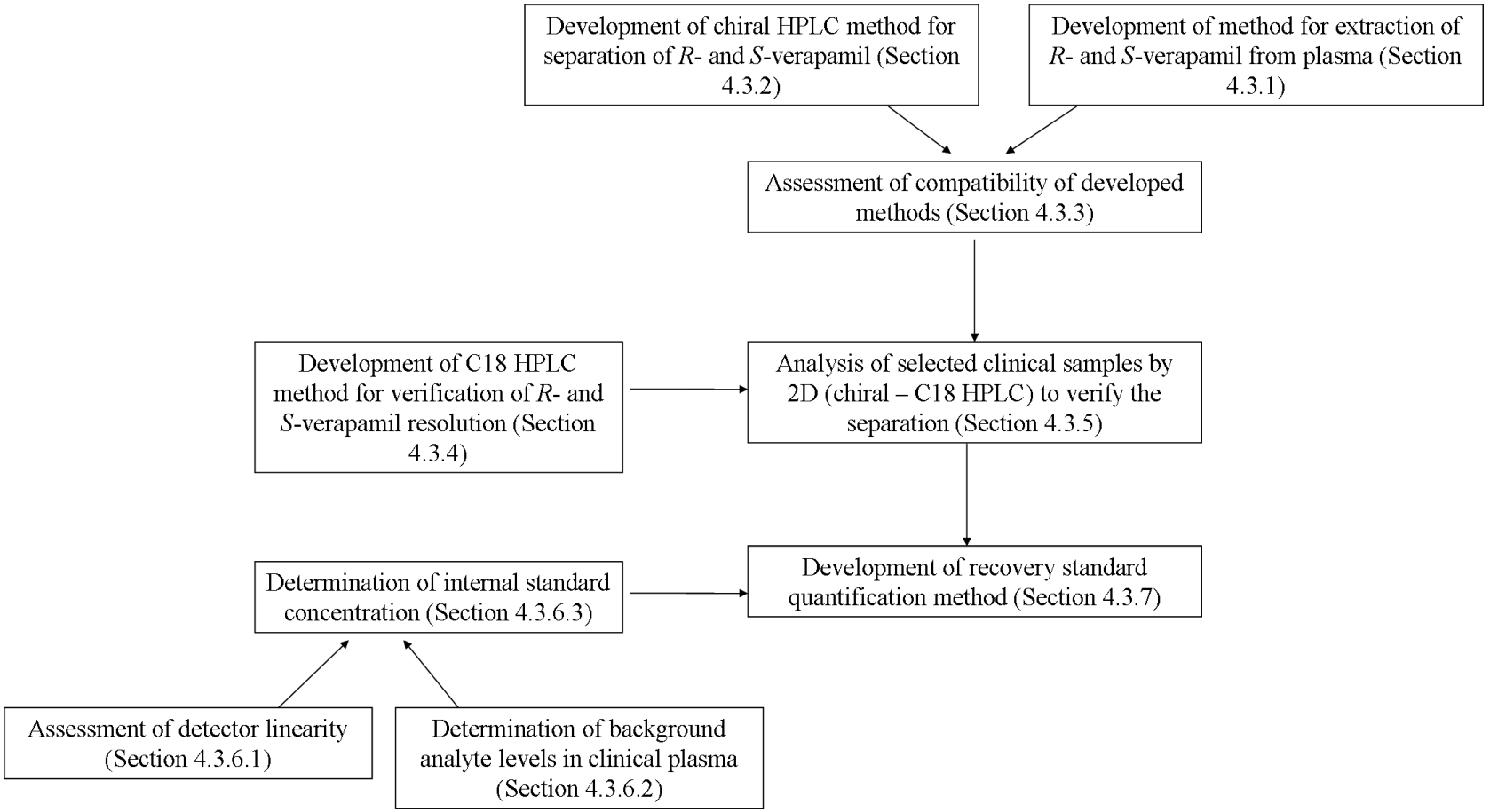

Figure 63: Schematic of method development and verification of methods for quantification of *R*- and *S*-verapamil.

4.3 Results and discussion

4.3.1 Development of methods for pre-treatment of plasma

The protein precipitation extraction method chosen for development in Chapter 2 (Section 2.3.2.1) was selected for the preparation of verapamil samples. Complex methods including the use of solid phase extraction have been reported for verapamil assays [169, 170]. These methods specifically apply to the separation and quantification of verapamil and metabolites. The method development reported here focuses only on the removal of verapamil from plasma, as metabolites did not require quantification by HPLC-AMS. The simplicity of an extraction method is important in HPLC-AMS analysis, as there are a significant number of manual steps. The method employed in Section 2.3.1 was assessed for suitability with verapamil. Methanol and acetonitrile were chosen as solvents for initial extraction experiments. The purpose of the method development was to evaluate:

- the overall recovery from plasma vs. recovery after introduction of a volume reduction step;
- the difference in recovery of analyte when using acetonitrile and methanol.

Plasma samples spiked with ^{14}C-verapamil were prepared and subjected to protein precipitation extraction (Section 7.5.2) as follows:

- Method 1 – acetonitrile;
- Method 2 – acetonitrile, followed by reduction to dryness under N_2 and reconstitution in the initial mobile phase composition (Section 4.3.2);
- Method 3 – methanol;
- Method 4 – methanol, followed by reduction to dryness under N_2 and reconstitution in the initial mobile phase composition (Section 4.3.2).

Mean extraction efficiencies were calculated for each analyte (Equation 14, Section 2.3.2.1). Mean recovery of verapamil from plasma was >76% (Table 41) for all methods.

Table 41: Verapamil extraction efficiency data for Methods 1 – 4.

Extraction solvent	Mean extraction efficiency of neat plasma filtrate (%)	Mean extraction efficiency of reduced and reconstituted plasma filtrate (%)
Acetonitrile	86.3 (1.85)	81.8 (1.99)
Methanol	76.9 (1.92)[1]	71.4 (3.22)

[1]based on 2 replicates only, 3rd replicate discarded as sample only partially extracted, value in parentheses = % difference from mean value

Better recoveries were observed with acetonitrile than with methanol. The introduction of solvent reduction followed by reconstitution of the dried plasma filtrate in mobile phase (200 μL) resulted in a further loss of approximately 5% (Table 41). Despite this loss, Method 2 was chosen for further development of the HPLC-AMS assay as it provides a larger proportion of the analyte for HPLC analysis when analysing the same volume of sample by HPLC. The recoveries represent those of racemic verapamil. It was not possible to ascertain the individual extraction efficiencies of *R*- and *S*-verapamil using this method as individual ^{14}C-labelled *R*- and *S*-verapamil standards were not available. Hence, it was assumed that ^{14}C-labelled *R*- and *S*-verapamil were extracted with the same efficiency. Given that the recovery of each individual sample was to be determined via a recovery curve quantification method, this assumption would not affect the final plasma concentration data.

4.3.2 Development of a chiral HPLC method for separation of *R*- and *S*-verapamil (Method C1)

A HPLC method was obtained for a Phenomenex Lux Cellulose-1 column (Phenomonex, Personal Communication). The column consists of a polysaccharide based chiral stationary phase, cellulose tris (3,5-dimethylphenylcarbamate) (Figure 64).

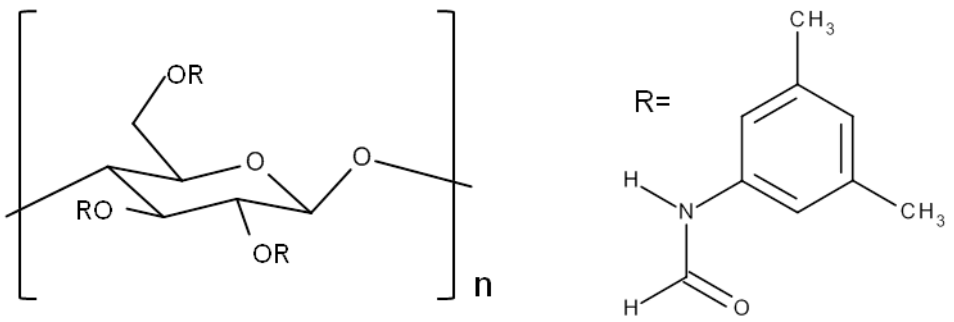

Figure 64: Lux Cellulose-1 stationary phase [172].

Although polysaccharide stationary phases are readily available, the retention process has not been elucidated [171]. Unlike columns such as Pirkle columns, which operate based on the three point rule, polysaccharide stationary phases are applicable to a wider range of analytes as they do not require specific combinations of functional groups [171]. Polysaccharide stationary phases are most often operated in normal phase conditions. There is recent limited experience with reverse phase solvents. The mobile phases used in the chiral verapamil HPLC method are acetonitrile and potassium hexafluorophosphate (KPF_6). KPF_6 is a chaotropic salt, which forms an ion pair with positively charged basic analytes, resulting in a neutral ion pair and therefore increasing separation [173].

Racemic verapamil, *R*-verapamil and *S*-verapamil (1 mg/mL; Section 7.2.4) were analysed (5 µL) by HPLC and the column (40°C) eluted with 50 mM KPF_6: acetonitrile at 1 mL/min. Elution was achieved with a gradient from 60:40 (v/v) to 40:60 (v/v) over 25 min followed by a column flush and re-equilibration (Method C1; Section 7.8.2). The method translated well with baseline resolution being achieved for *R*- and *S*-verapamil. Analysis of each separate enantiomer (*R*-verapamil and *S*-verapamil reference standards) with fluorescence detection showed *R*-verapamil to elute at 13.9 min, followed by *S*-verapamil at 15.3 min (Figure 65).

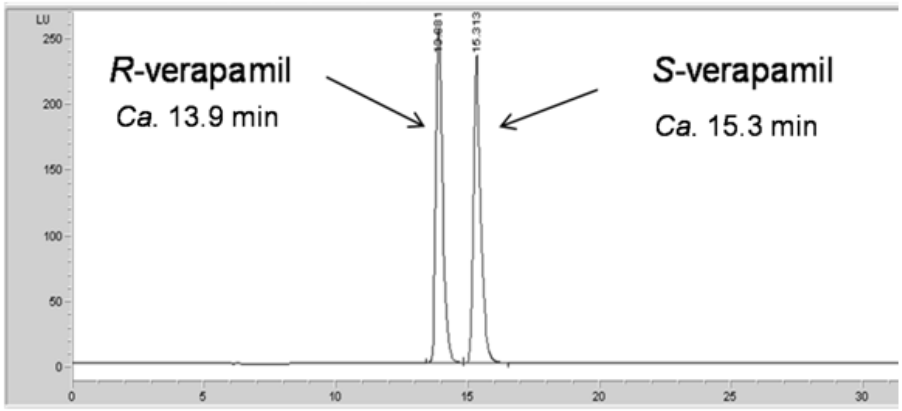

Figure 65: HPLC chromatogram of verapamil at λ_{ex} 276 nm and λ_{em} 290 nm (Method C1).

4.3.2.1 Assessment of method repeatability and carryover

Repeatability was evaluated by multiple injections of the verapamil reference standard (1 mg/mL; 5 x 1 µL), with a blank injection after injection 5 for evaluation of carryover. Further analyses were performed on a second day to assess the inter-day repeatability of the HPLC method. Replicate injections (*n*=5) on day 1 resulted in mean retention times of 13.4 and 14.9 min for *R*- and *S*-verapamil (Table 42). The precision at each retention time was good (CV<2%).

Table 42: Day 1 repeatability data for *R*-and *S*-verapamil (HPLC Method C1).

Injection number	*R*-verapamil retention time (min)	*S*-verapamil retention time (min)	*R*-verapamil peak area (LU)	*S*-verapamil peak area (LU)
1	13.0	14.5	1007	1008
2	13.5	15.0	1020	1020
3	13.5	15.1	1018	1017
4	13.5	15.0	1016	1018
5	13.5	15.0	1015	1014
Mean	13.4	14.9	1015	1015
% CV	1.68	1.60	0.46	0.45

Blank injections gave no detector response at the retention times corresponding to *R*- and *S*-verapamil, indicating that there was no carryover. The mean retention times obtained on day 2 were identical to those obtained on day 1

(Table 43). The precision at each retention time on day 2 was very good (CV<0.5%).

Table 43: Day 2 repeatability data for *R*-and *S*-verapamil (HPLC Method C1).

Injection number	*R*-verapamil retention time (min)	*S*-verapamil retention time (min)	*R*-verapamil peak area (LU)	*S*-verapamil peak area (LU)
1	13.5	15.0	1017	1016
2	13.5	15.0	1020	1019
3	13.4	14.9	1015	1014
4	13.4	14.9	1018	1018
5	13.4	14.8	1019	1020
Mean	13.4	14.9	1018	1017
% CV	0.32	0.49	0.19	0.25

4.3.3 Compatibility of the protein precipitation extraction and HPLC method C1

Protein precipitation extraction Method 2 was assessed for its compatibility with chiral HPLC Method C1. Specifically, human clinical plasma filtrates were assessed for the presence of components eluting at the retention times of *R*- and *S*-verapamil.

4.3.3.1 Assessment of detector interference from plasma filtrate

Pre-dose plasma samples were pooled across all subjects and subjected to protein precipitation extraction and HPLC analysis (Method C1; Section 7.6.4). Pooled samples were used to retain the plasma and in addition, to capture subject specific interferences that may be present. Subject 2 did not complete the microdose only part of the study and so plasma was not available. The absence of detector response at the retention times of *R*- and *S*-verapamil indicated no appreciable interference.

4.3.3.2 Assessment of fraction alignment and isotopic fractionation

Post-dose human plasma samples were pooled across all subjects, spiked with non-labelled verapamil to allow *R*- and *S*- verapamil to be identified in the UV

chromatogram, and subjected to protein precipitation extraction. Plasma filtrate was analysed by chiral HPLC Method C1 (Section 7.6.5). Discrete fractions were collected at 12 s intervals across the elution times of *R*- and *S*-verapamil (11.0 to 12.6 min). Aliquots of each fraction were analysed by AMS and the pMC values determined.

Table 44: Verification of *R*-and *S*-verapamil peak purity.

Fraction start / end time (min)	Fluorescence response	pMC	Fraction number	pMC per enantiomer
11.0 / 11.2	*R*-verapamil	12.89	20	1845.48
11.2 / 11.4	*R*-verapamil	1612.40	21	
11.4 / 11.6	*R*-verapamil	220.19	22	
11.8 / 11.8	N/A	<LOQ	23	
11.8 / 12.0	*S*-verapamil	<LOQ	24	1829.48
12.0 / 12.2	*S*-verapamil	626.92	25	
12.2 / 12.4	*S*-verapamil	1159.48	26	
12.4 / 12.6	*S*-verapamil	43.38	27	

From the fluorescence response, seven fractions were identified to correspond to either *R*- or *S*-verapamil. Six of these fractions contained quantifiable levels of ^{14}C as measured by AMS (Table 44). For *S*-verapamil, the ^{14}C was contained within fractions 25 to 27. Fraction 24 was identified from the fluorescence response as containing unlabelled *S*-verapamil, though this was a very small amount eluting at the start of the analyte peak. The corresponding fraction was below the AMS LOQ (Section 7.11.4.1). The fraction that separated the two enantiomers was also below the LOQ, showing their resolution. In addition to confirming that ^{14}C-*R*- and *S*-verapamil were aligned with the peaks identified by the fluorescence detector, this experiment also determined the ratio of *R*- and *S*-verapamil at 50.2:49.8 *R:S*.

4.3.4 Development of a HPLC method for demonstration of separation of *R*- and *S*-verapamil (Method D1)

To ensure complete resolution of ^{14}C-*R*- and *S*-verapamil from ^{14}C-containing components in the clinical plasma samples, an orthogonal element was built into the separation. A C18 method for the resolution of verapamil from its metabolites was obtained (Phenomenex, personal communication). The Waters Xterra MS C18 column (Method D1; Section 7.8.2) was eluted with 20 mM potassium phosphate: acetonitrile:water 22:35 v/v with a gradient decreasing from 90:10 v/v to 43:57 v/v over 5 min. These conditions were maintained for 7 min after which the ratio was decreased to 20:80 v/v over 1.5 min, then to 10:90 over 1.5 min. The elution gradient was followed by a column flush and re-generation (Section 7.8.2). The retention time of verapamil was 11.2 min (Figure 66).

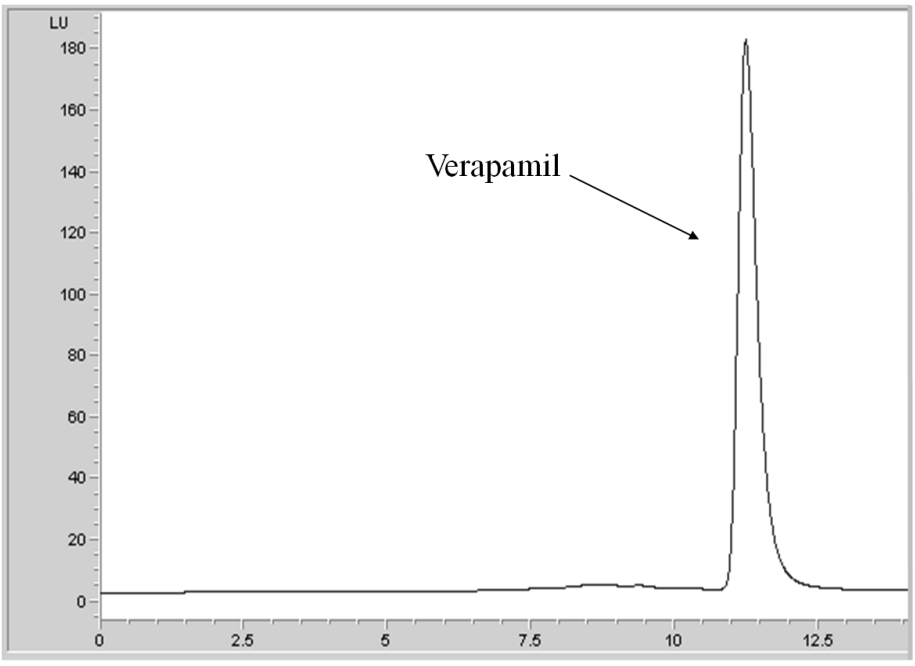

Figure 66: HPLC chromatogram of verapamil at λ_{ex} 276 nm and λ_{em} 290 nm (Method D1).

4.3.4.1 Assessment of method repeatability

The repeatability of the C18 HPLC Method D1 was evaluated by analysis of replicate injections (3 x 1 µL) of verapamil (1 mg/mL; Section 7.2.4) followed immediately by a blank injection after the third replicate for evaluation of

carryover. Replicate injections (*n*=3) resulted in mean retention times of 11.2 min for day 1 and 11.3 min for day 2 (Table 45). The precision on each occasion was good (CV<0.78%). Blank injections gave no appreciable detector response at the retention time corresponding to verapamil, indicating that there was no detectable carryover.

Table 45: Intra-day and inter-day repeatability data for verapamil (HPLC Method D1).

Injection Number	Day 1 verapamil retention time (min)	Day 2 verapamil retention time (min)
1	11.3	11.3
2	11.2	11.4
3	11.1	11.2
Mean	11.2	11.3
% CV	0.78	0.56

4.3.5 Verification of the chromatographic separation of *R*- and *S*-verapamil

Prior to its application in the clinical study the combination of the two chromatographic methods (chiral and C18 stationary phases) was evaluated to ensure that the *R*- and *S*-verapamil obtained was chromatographically resolved from other ^{14}C-containing components present in clinical samples of human plasma (Section 5.3.1). Four plasma pools were created at time-points chosen to represent a range of times across which metabolites may be formed.

- microdose only – 5 and 12 h post administration;
- microdose and therapeutic dose – 1 and 24 h post administration.

Plasma filtrates were prepared and analysed by chiral HPLC (Method C1; Section 7.8.2). Discrete fractions were collected across the retention times for *R*- and *S*-verapamil, reduced to dryness under N_2 and reconstituted in initial mobile phase composition. An aliquot of each reconstituted eluate was analysed by HPLC using C18 Method D1. Fractions of 15 s duration collected over the second dimension separation for *R*- and *S*-verapamil were analysed by AMS and

the concentration (dpm) of each fraction determined and plotted vs. the fraction collection time (Section 7.6.6; Figure 67 and Figure 68). *R*- and *S*-verapamil concentrations of the 12 h and 24 h plasma samples and *S*-verapamil concentrations of the 5 h plasma samples were below the AMS LOQ (Section 7.11.4.1).

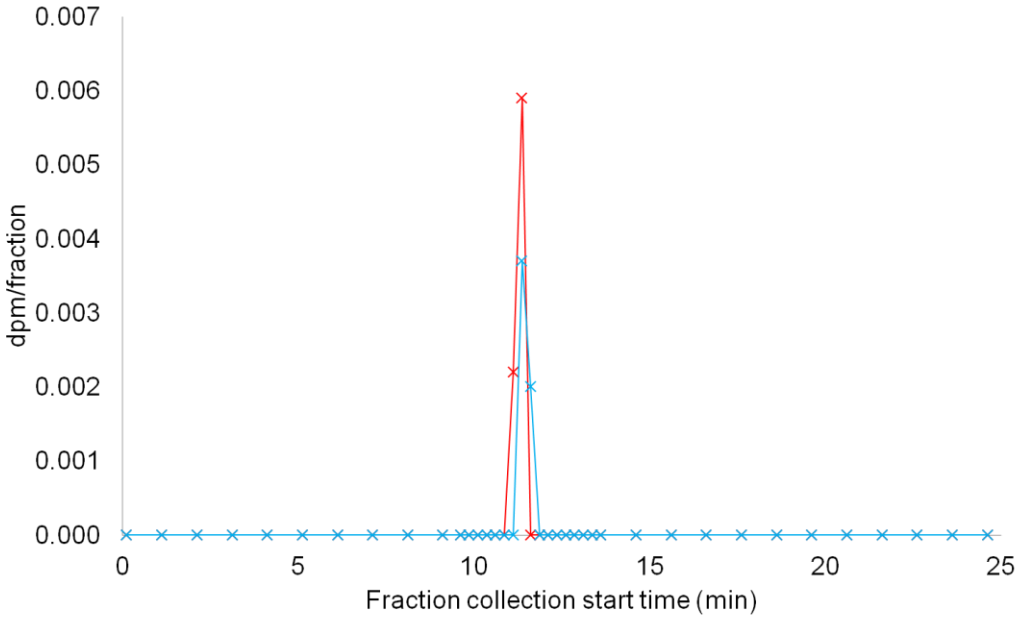

Figure 67: Reconstructed *R*-verapamil radio-chromatogram, legend: blue line = 1 h, red line = 5 h.

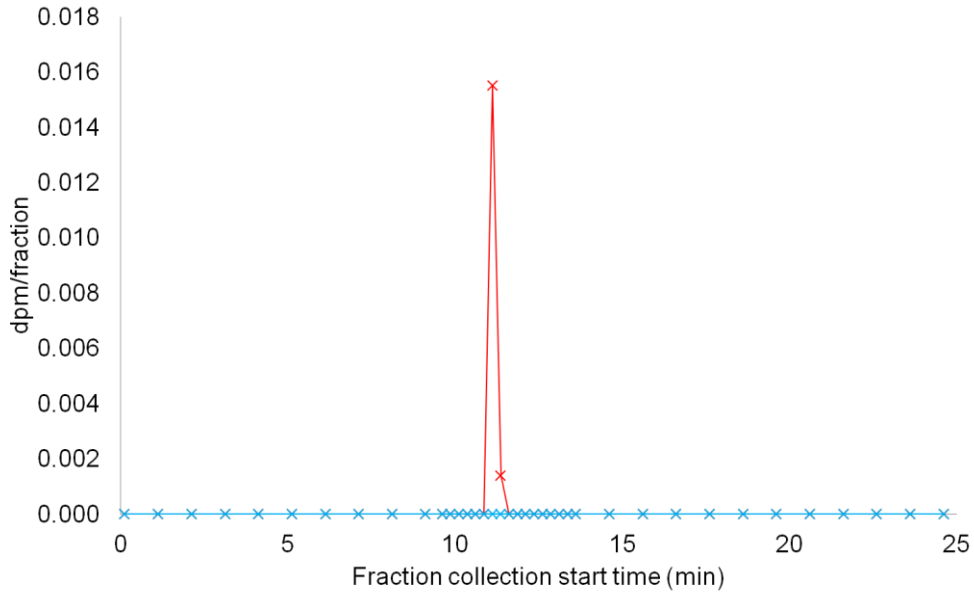

Figure 68: Reconstructed *S*-verapamil radiochromatogram legend: blue line = 1 h, red line = 5 h.

All of the detectable ^{14}C recovered from *R*- and *S*-verapamil fractions collected using the chiral HPLC method was contained exclusively in the fractions corresponding to the retention time of verapamil on C18 analysis. The absence of ^{14}C in the eluate collected over the remainder of the chromatogram verified that the HPLC fractions corresponding to the *R*- and *S*-verapamil peaks obtained during chiral HPLC separation contained only the ^{14}C-analyte. Of the plasma samples analysed at the four time points only the 1 h (*R*- and *S*-verapamil) and 5 h (*R*-verapamil) fractions were above the LOQ. Thus, employing the method in the quantification of *R*- and *S*-verapamil, would limit the data obtained, due to the amounts of ^{14}C being close to the LOQ. Increasing the injection volume for the chiral separation from 50 to 100 µL would double the amount of radioactivity in the aliquot collected for AMS and this was applied in the analysis of clinical plasma samples (Chapter 5).

4.3.6 Determination of the internal standard concentration

The amount of internal standard (non-labelled verapamil) for HPLC analysis must be above the LOQ of the fluorescence detector, without exceeding the linear range (Section 1.10.7.2). In addition, inherent levels of non-labelled analyte must be negligible with respect to the amount of internal standard added. Due to the administration of the microdose (50 µg) with the therapeutic dose (80 mg) in period 2, non-labelled *R*- and *S*-verapamil concentrations are expected to be much higher than those in period 1, where *R*- and *S*-verapamil concentrations result from the microdose (50 µg) alone.

4.3.6.1 Assessment of detector response linearity

Verapamil solutions were prepared over the range 3.13 – 2500 ng for each of *R*- and *S*-verapamil (Section 7.2.4) and fluorescence response for chiral HPLC Method C1 (5 µL; Section 7.8.2) assessed with triplicate injections at each concentration. The amount of analyte vs. detector response gave R^2 of > 0.999 for both analytes over the range 3.125 ng to 500 ng (Figure 69 and Figure 70). *R*- and *S*-verapamil showed a non-linear fluorescence response between 500 ng and 2500 ng (data not shown).

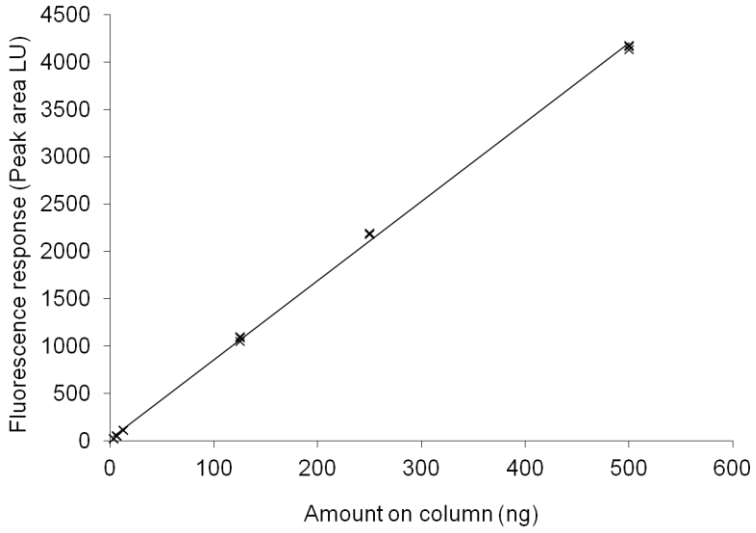

Figure 69: Assessment of detector response for *R*-verapamil (R^2=0.999).

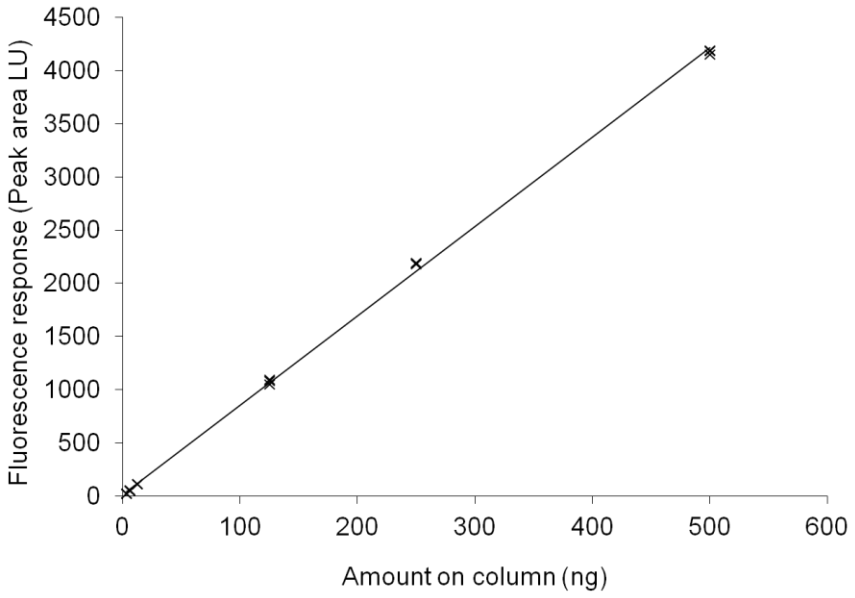

Figure 70: Assessment of detector response for *S*-verapamil (R^2=0.999).

4.3.6.2 Determination of non-labelled verapamil in clinical plasma

Based on published data, the expected C_{max} of verapamil after administration of the 80 mg dose is 29.1 – 97.5 ng/mL [174]. The protein precipitation extraction and HPLC methods developed above (Sections 4.3.1, 4.3.2 and 4.3.4) assume the following:

- plasma volume taken for extraction – 200 µL;
- plasma filtrate reduced and reconstituted – 200 µL;
- reconstituted plasma filtrate analysed by C18 HPLC – 100 µL;
- HPLC fraction reduced to complete dryness under N_2 and reconstituted in chiral mobile phase and the entire volume taken for chiral HPLC analysis – 100 µL.

Application of the dilutions noted above results in the equivalent of $1/10^{th}$ of the analyte that is present in 1 mL of plasma being available for chiral HPLC analysis. Hence, assuming a C_{max} of 97.5 ng/mL, which is the maximum quoted

value, 9.75 ng of verapamil or 4.88 ng of each enantiomer is expected to be present in every HPLC fraction, giving a fluorescence response of approximately 40 LU (determined from the linearity data).

4.3.6.3 Calculation of internal standard amount

Addition of internal standard to plasma, such that 500 ng is present in the reconstituted plasma filtrate taken for chiral HPLC analysis (100 µL), results in a fluorescence response of approximately 2200 LU per enantiomer (from Figure 69 and 70).

The maximum estimated amount of ^{12}C inherent to the samples collected in period 2 is 40 LU, representing 1.8% of internal standard peak response (2200 LU) assuming 100 % process recovery.

Thus the amount of IS required for chiral HPLC analysis was determined as 500 ng, significantly above inherent ^{12}C, while remaining in the linear range of the fluorescence detector.

4.3.7 Development of a method for quantification of ^{14}C-*R*- and *S*-verapamil in plasma by HPLC-AMS

A quantification method to complement the extraction and separation methods was developed (Figure 71) by modifying the recovery curve quantification method described previously (Section 1.10.6).

4.3.7.1 Confirmation of analyte purity

The radiochemical purity value for verapamil provided by the supplier was 99.6% (Section 7.2.3). Non-labelled verapamil was purchased at 98.9% chemical purity (Section 7.2.2) and assessed for ^{14}C contamination by AMS (Section 7.11) prior to development of the assay. One replicate failed to meet the AMS acceptance criteria (Section 7.11.3). The remaining four replicates returned pMC values below the LOQ of the AMS instrument (Section 7.11.4.1; Table 46).

Table 46: Non-labelled verapamil analysis by AMS for determination of background ^{14}C.

Replicate	pMC
1	1.16
2	Failed AMS acceptance criteria (Section 7.11.3)
3	1.14
4	0.97
5	1.03

4.3.7.2 Preparation of the recovery curve

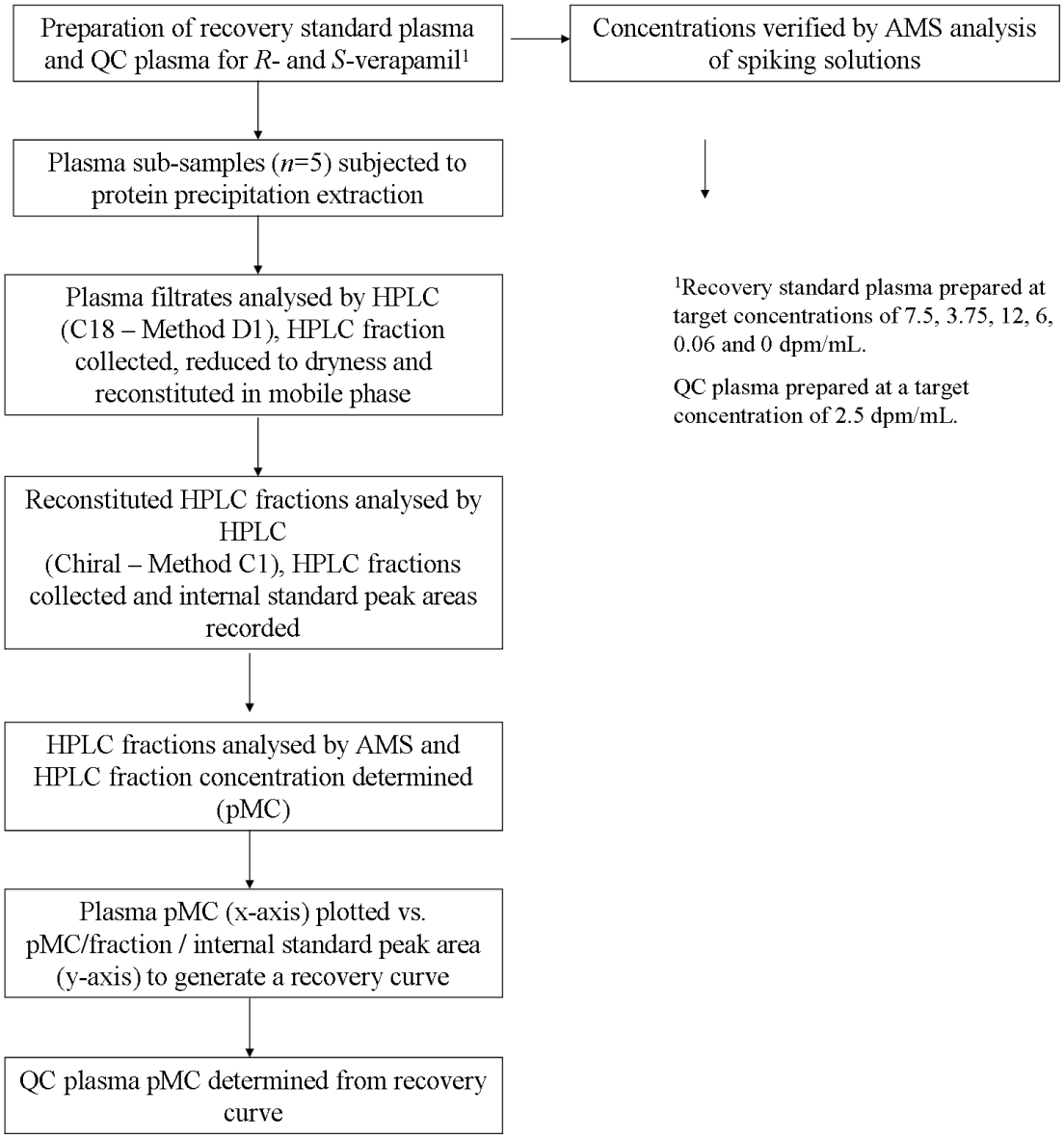

Figure 71: Schematic of sample preparation and analysis for preparation of a recovery curve and QC samples.

^{14}C-verapamil recovery standards and QC plasma samples were prepared (Section 7.4.2). Solutions used in the generation of recovery standard and QC plasma were analysed by AMS (*n*=5; Section 7.11). Spiking solutions with concentrations >20 dpm/mL were diluted prior to AMS analysis. Spiking solution concentration data and solvent volumes were used to calculate the concentration of each recovery standard and QC plasma sample (Table 47). The

precision of the replicates was good (CV<15%). Two values were excluded from calculations as they failed to meet the AMS acceptance criteria (Section 7.11.3).

Table 47: Spiking solution AMS data and calculation of ^{14}C-verapamil concentrations.

Sample ID	Target spiking solution / plasma concentration (dpm/mL)	Spiking solution ^{14}C-verapamil concentration (dpm/mL)[1]	Calculated plasma ^{14}C-verapamil concentration (dpm/mL)[2]	Mean plasma ^{14}C-verapamil concentration (dpm/mL)[3]
Recovery Standard 1	120 / 7.5	132.0	8.25	7.51 / 3.76
		116.2	7.26	
		108.6 (7.8)	6.79	
		117.1	7.32	
		127.2	7.95	
Recovery Standard 2	60 / 3.75	49.71	3.11	3.27 / 1.64
		50.21	3.14	
		47.39 (11.1)	2.96	
		62.30	3.89	
		52.33	3.27	
Recovery Standard 3	12 / 0.75	9.790	0.612	0.763 / 0.382
		12.14	0.759	
		13.12 (14.3)	0.820	
		LCU	LCU	
		13.77	0.861	
Recovery Standard 4	6 / 0.375	5.925	0.370	0.387 / 0.194
		6.436	0.402	
		5.949 (6.1)	0.372	
		6.748	0.422	
		5.918	0.370	
Recovery Standard 5	0.6 / 0.0375	0.6924	0.0433	0.0403/ 0.0201
		0.6159	0.0385	
		0.6065 (11.7)	0.0379	
		0.7467	0.0467	
		0.5587	0.0349	
Recovery Standard 6	0.06 / 0.00375	0.06130	0.00383	0.00426 /
		0.06160	0.00385	
		0.06620 (10.8)	0.00414	
		0.07690	0.00481	
		0.07480	0.00468	
QC	40 / 2.5	47.73	2.98	2.80 / 1.40
		LCU	LCU	
		45.09 (6.9)	2.82	
		45.88	2.87	
		40.48	2.53	

[1]precision (% CV), [2] ^{14}C-verapamil (15 µL) added to plasma (225 µL), [3]verapamil concentration / enantiomer concentration

Recovery standard (*n*=5) and QC plasma (*n*=8) were subjected to protein precipitation extraction (Section 7.7.2), followed by C18 HPLC analysis (Method D1; 100 µL; Section 7.8.2). Replicate 1 recovery standards were analysed first from the zero sample through to the sample of the highest concentration. Replicates 2 to 5 were analysed in sequence order in the same way. QC samples

were interspersed among the recovery standards. The fraction corresponding to verapamil was collected and reduced to complete dryness under N_2. Residues were reconstituted in the mobile phase initial composition (100 µL) and analysed by chiral HPLC (Section 7.8.2) with collection of discrete fractions over the retention times of *R*– and *S*-verapamil. HPLC fractions corresponding to *R*- and *S*-verapamil were collected (approximately 550 µL) and aliquots taken for analysis by AMS (Section 7.11).

HPLC data were reviewed throughout the analysis to ensure that chromatographic resolution of *R*- and *S*-verapamil was maintained. A minimum resolution (R_s) of 2.15 was calculated for QC samples interspersed throughout the recovery curve standards. The retention times of *R*- and *S*-verapamil varied by less than 0.5 min (Table 48).

Table 48: QC resolution data for *R*- and *S*-verapamil.

Replicate	*R*-verapamil retention time (min)	*S*-verapamil retention time (min)	R_s
1	12.0	13.6	2.14
2	12.0	13.7	2.17
3	12.2	13.8	2.15
4	12.5	14.1	2.01
5	12.2	13.8	2.19
6	12.1	13.7	2.11
7	12.1	13.7	2.21
8	12.0	13.7	2.21
Mean	12.1	13.8	2.15
% CV	1.39	1.09	2.97

4.3.7.3 Processing of AMS data to generate recovery curve

A detector-based trigger activated by the fluorescence response was used to generate HPLC fractions. As every analysis differs slightly due to differences in analytical recovery of the internal standard, the fraction volume may also vary slightly between samples. The pMC value obtained on analysis of a HPLC fraction will vary depending on the sample volume. The recovery curve quantification method described in Section 1.10.6 was modified to allow adjustments to be made to pMC values to account for these variations.

The concentration of a ^{14}C-*R*- and *S*-verapamil HPLC fraction assuming 100% analyte recovery was calculated (Equation 18).

$$F_c = \left(\frac{K_p}{S_F} \right) \qquad \textbf{Equation 18}$$

Where:

F_c = fraction concentration (dpm)
K_p = plasma concentration (dpm/mL)
S_F = sample processing factor

Where S_F accounts for plasma, HPLC fractions and plasma filtrate volumes (Equation 19).

$$SF = \left(\frac{F_v}{F_A} \right) x \left(\frac{E_v}{E_i} \right) x \left(\frac{1}{P_E} \right) \qquad \textbf{Equation 19}$$

Where:

F_V = total fraction volume (mL)
F_A = fraction volume taken for AMS (mL)
E_V = plasma filtrate volume (mL)
E_I = plasma filtrate volume analysed by HPLC (mL)
P_E = plasma volume extracted (mL)

The HPLC fraction concentration (dpm) was then converted back to pMC (Equation 20) and plotted on the *x*-axis.

$$pMC\ per\ fraction\ (100\%\ recovery) = \frac{\left(\frac{dpm/fraction}{0.01356}\right)}{\varphi} x\ 100 \qquad \textbf{Equation 20}$$

The HPLC fraction isotope ratio (pMC) / IS detector response was plotted on the *y*-axis. The slope of the curve (m) and intercept on the *y*-axis (c) were determined and these values used to correct for losses in recovery on analysis of QC samples using Equation 21. Note this equation gives the pMC of the entire fraction after correction for the procedural loss of analyte.

$$K\ (pMC\ per\ \ fraction) = \left(\frac{R_{AX} - c}{mU}\right) \qquad \textbf{Equation 21}$$

Where R_{AX} is the pMC of the entire fraction, and may be converted to a concentration of dpm/fraction via equation 22.

$$K\ (dpm/fraction) = \left(\frac{K\ (pMC\ \ per\ \ fraction)}{100}\right) x\ 1.63\ x\ 0.01356 \qquad \textbf{Equation 22}$$

Converting the concentration from dpm/fraction to dpm/mL is carried out using Equation 23.

$$K\ (dpm/mL) = \frac{E_v}{E_i}\ \ x\ \ \frac{1}{P_E} \qquad \textbf{Equation 23}$$

The recovery curve *x*-axis was created as described above and a worked example is given below for clarity.

The sample processing factor (S_F; equation 19) for *R*-verapamil, recovery standard 1 (3.76 dpm/mL), replicate 1 was 19.67, where the total fraction volume was 590 µL and 300 µL was taken for AMS analysis.

$$S_F = \frac{0.590}{0.300}\ \ x\ \ \frac{0.2}{0.1}\ \ x\ \ \frac{1}{0.2}$$

Assuming 100% recovery, this sample processing factor was applied to the plasma concentration determined for recovery standard 1 (3.76 dpm/mL) to give the fraction concentration (F_c – dpm/fraction).

$$F_c = \frac{3.76}{19.67}$$

The radioactivity fraction concentration (0.191 dpm) was converted to pMC using equation 21.

$$pMC\ per\ fraction\ (100\%\ recovery) = \frac{0.191}{(0.01356)}\ /\ 1.63\ \ x\,100$$

This calculation results in 864 pMC, which represents the isotope ratio for a HPLC fraction of volume 590 µL for recovery standard 1, and values calculated in this way form the *x*-axis of the recovery curve.

4.3.7.4 Recovery curves and assessment of precision

The AMS response for HPLC fractions from plasma at target concentrations of 0.00375 dpm/mL were below the AMS LOQ (Section 7.11.4.3) and were not included in the recovery curve. All remaining points were included.

Linear regression for the recovery curve for *R*-verapamil gave a slope (m) of 0.000504 (Figure 72).

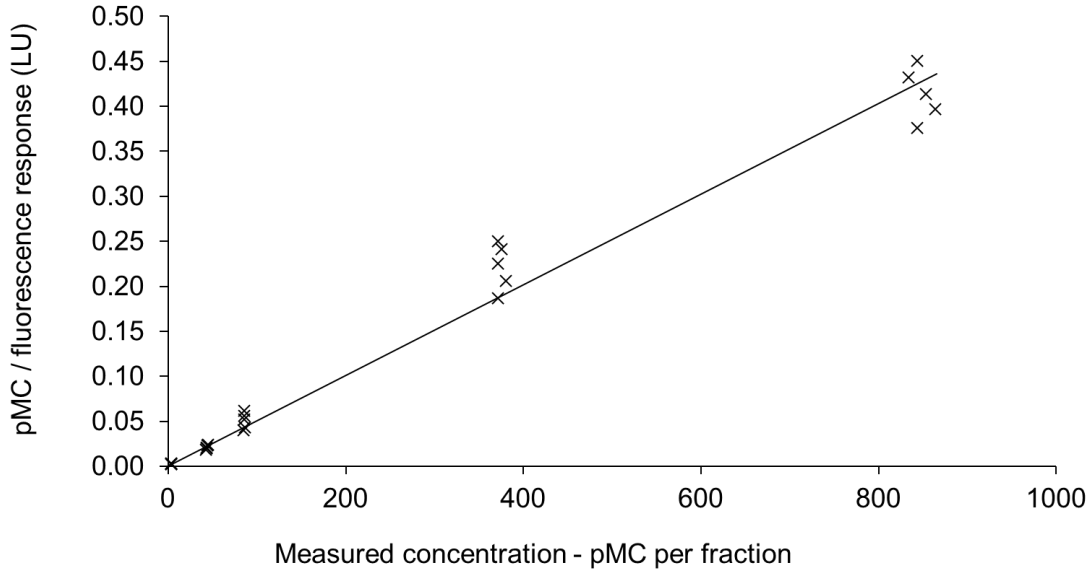

Figure 72: *R*-verapamil recovery curve.

The recovery curve for *S*-verapamil gave a slope (m) of 0.000463 (Figure 73).

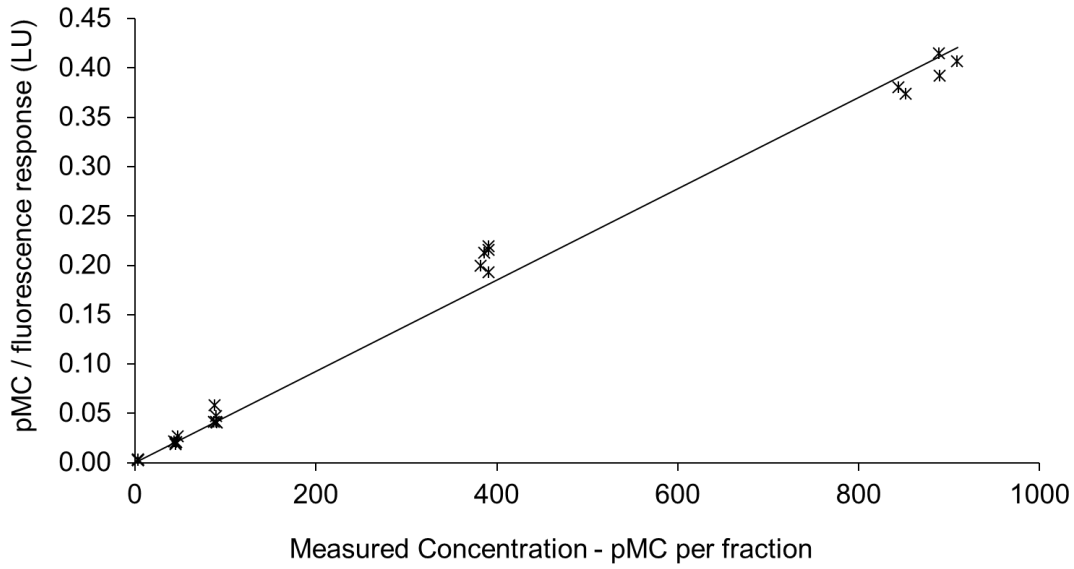

Figure 73: *S*-verapamil recovery curve.

The pMC of each QC was determined (Table 49). All measured QC concentrations (individual and mean values) were within ±20% of the actual concentrations. The precision of the method was 12.7% for *R*-verapamil and 2.32% for *S*-verapamil. The data were scrutinised to determine a cause of the slightly wider variation for *R*-verapamil compared to *S*-verapamil. Although pMC data obtained on AMS analysis were slightly more variable, there was no obvious cause for this. Despite this variation, the data still met acceptance criteria for accuracy and precision.

Table 49: QC accuracy and precision data for *R*- and *S*-verapamil (*n*=8).

Replicate	***R*-verapamil plasma concentration (pMC)**	***S*-verapamil plasma concentration (pMC)**
1	708	674
2	707	645
3	548	657
4	743	651
5	661	651
6	615	680
7	559	645
8	539	635
Mean plasma concentration (pMC)	635	655
Actual plasma concentration (pMC)	633	633
Mean accuracy (%)	99.7	103
Mean precision (% CV)	12.7	2.32

4.3.8 Suitability of the developed methods

A document including recommended procedures for carrying out a HPLC-AMS assay is now available [124]. In a similar way to the critique of the method developed in Chapter 2, the 2D chiral HPLC-AMS assay described here was assessed for suitability with respect to these recommendations, focusing specifically on; 1) the selectivity and chromatographic resolution of the analyte, 2) carryover, 3) recovery and 4) accuracy and precision. The importance of each of these factors is discussed in detail in Chapter 2.

4.3.8.1 Selectivity

Subjects chosen for this study had not participated in a ^{14}C study in the year prior to commencing the present study, therefore the presence of background levels of ^{14}C was minimised. The presence of unknown ^{14}C-metabolites was evaluated in pooled clinical plasma samples at 1, 5, 12 and 24 h. The results demonstrated that the HPLC fraction corresponding to each analyte determined for the internal standard, contained ^{14}C-analyte only, verifying the method for use. The published HPLC-AMS guidance document suggests taking samples from the elimination phase at 1 – 2 times the half-life for such an investigation [124]. Approximate half lives of *R*- and *S*-verapamil of 4.07 and 5.01 h are quoted in the literature for a 5 mg dose [174]. Due to levels being below the LOQ at 12 h, data were not available. Ideally, this experiment would have been repeated prior to commencing with the study. Data obtained at 1 h and 5 h (for *R*-verapamil only) showed that the enantiomers were well resolved. In addition, although limited data were obtained prior to analysis of the clinical human plasma samples, all samples were eventually analysed using the two-dimensional method, which minimises the risk of co-elution.

4.3.8.2 Carryover

Carryover of non-labelled material was assessed by HPLC in blank injections made following replicate injections of reference standards. The absence of significant fluorescence detector response at the retention time of the analyte demonstrated negligible carryover. ^{14}C carryover may also be determined from blank plasma analysed immediately after the analysis of the plasma samples containing relatively high concentrations of ^{14}C, i.e. in QC or recovery standards. In retrospect, this should have been included in method development, and is a criticism of the method. The inclusion of a blank plasma sample analysed immediately after recovery standard 1, would have confirmed that there was no carryover. The data obtained show very low pMC values for samples at 0 dpm/mL (pMC<1) indicating that the residual level of ^{14}C in the system is at a minimum. Accordingly an assumption is made that carryover between samples is also minimal.

4.3.8.3 Recovery

Recovery in a HPLC-AMS assay relates both to the mass and the radioactivity of the sample [124]. It is only the isotope ratio that is measured during AMS analysis and the majority of ^{12}C measured is isotopic diluent, not ^{12}C inherent to the sample. It is recommended that the material used in the preparation of recovery standards and QCs contains the same ^{14}C and mass ratio, i.e. has the same specific radioactivity, as the material administered to volunteers in the clinical study. This eliminates mass concentration dependent effects during sample processing, particularly during the addition of ^{14}C material to plasma, and the subsequent extraction of the analyte [124].

Spiking solutions for preparation of recovery standards and QC plasma were prepared by dilution of the solution of radiolabelled material at the specific activity provided by the supplier. An ethanol solution of non-labelled verapamil was added at a constant amount throughout the preparation of the recovery standards and QC plasma to act as both a diluent and internal standard (Section 1.10.6). This material was at a significantly higher level than that inherent to the sample. Thus, the specific radioactivity was lower than that dosed in the clinical

study. Although the radioactivity concentrations were representative of those measured in clinical samples, the mass concentrations were not, preventing direct translation of AMS measurement to mass concentrations. Given that the specific radioactivity was not equivalent to that dosed in the clinical study, only comparisons at the pMC or dpm level could be made. Although this makes the explanation of the data slightly more complex, it does not change the outcome of the study.

4.3.8.4 Accuracy and precision of the assay

Recommended guidelines for accuracy and precision of HPLC-AMS assays, state that measured QC values should be within 20% of the true concentrations and the error should not exceed 20%. All QC data are within 20% of the true concentration and the precision of the *R*- and *S*-verapamil assay was 12.8% and 2.3% respectively. As discussed in Chapter 2 the most recently published recommended guidelines state that QCs should ideally be prepared at three concentrations encompassing the range of plasma concentrations anticipated in the clinical study (in mass/mL) [124].

The guidelines also recommend that true plasma concentrations be determined by AMS. In the work reported here, true concentrations were determined by analysis of spiking solutions used in the preparation of the spiked samples. These solutions were diluted where radioactive concentrations exceeded the AMS upper limit of detection. This method introduces the potential for error due to the additional dilution step. While the recommendation is for direct AMS analysis of plasma, this is only possible for samples with concentrations sufficiently above the AMS background. Plasma samples have a natural background carbon level that is much higher than that of HPLC mobile phase, for example (110 pMC vs. 0 pMC). Plasma concentrations generating a pMC<110 must be estimated, either on dilution steps, or by direct analysis of spiking solutions.

As in Chapter 2, a potential improvement to this method, which also introduces an independent measurement of plasma concentrations, is to determine plasma

concentrations by LSC analysis. Determination of stock solution concentrations for a statistically accurate count time (typically at least 2%2σ) and accounting for dilutions in the calculation of plasma concentrations eliminates the introduction of sample manipulation. The recommendations made in Chapter 2 for further development of a quantification method also apply here.

The data were processed such that results from analysis of clinical plasma could be converted directly from pMC to mass concentrations per mL of plasma, without the need to determine the radioactivity concentrations per fraction (dpm) as an intermediate step. Instead of constructing a recovery curve where the concentrations in HPLC fractions (in dpm/fraction) were plotted vs. plasma concentration (dpm/mL) as described in Chapter 2, the axes in this case represent pMC. All analytical variables remained constant throughout the analysis, with the only variable being the volume of HPLC fractions. As fractions were collected using a peak-based mode, triggered by the fluorescence response, the volume varied slightly between analyses. Accordingly, the pMC value was determined for the aliquot taken and then corrected to account for the entire fraction.

4.3.9 Development of an alternative quantification method using a recovery constant

Although the plasma samples used to generate the recovery curve encompass a range of ^{14}C-concentrations, this is not essential, as AMS is known to be linear. Thus, an alternative single point calibration method is described here. A recovery constant was determined for each concentration (n=5) measured for the recovery curve using Equation 24 [129].

$$m = \left(\frac{F_r}{U} \right) \qquad \textbf{Equation 24}$$

The fraction recovered (F_r) and UV response were used to determine a value for *m*, the recovery constant. The fraction recovered is a value for the overall recovery of the analyte, expressed as a value of <1. The calculated values for m range from 0.000465 – 0.000591 LU/s for *R*-verapamil and 0.000445 – 0.000571 LU/s for *S*-verapamil. Processing QC data for *R*- and *S*-verapamil using each recovery constant gave similar results to those obtained when using the recovery curve method (Table 50 and Table 51).

Table 50: *R*-verapamil QC data calculated using m values determined from recovery constants (RC) and recovery curve (RS).

	RC1	RC2	RC3	RC4	RC5	RS
Accuracy (%)	115	95.3	103	121*	102	112
	115	95.1	103	121*	102	112
	89.3	73.7*	79.5*	93.6	79.2*	86.6
	121*	100	108	127*	107	117
	108	88.9	96.0	113	95.5	104
	100	82.6	89.2	105	88.8	97.2
	91.0	75.1*	81.1	95.4	80.7	88.3
	87.9	72.6*	78.4*	92.2	78.0*	85.2
Mean accuracy (%)	103	85.4	92.3	109	91.7	100

* >±20% of actual concentration

Table 51: *S*-verapamil QC data calculated using m values determined from recovery constants (RC) and recovery curve (RS).

	RC1	RC2	RC3	RC4	RC5	RS
Accuracy (%)	110	92.1	97.2	110	86.1	106
	105	88.2	93.0	106	82.4	102
	107	89.8	94.7	108	83.9	104
	106	89.0	93.9	107	83.1	103
	106	88.9	93.8	107	83.1	103
	111	93.0	98.0	111	86.8	107
	105	88.2	93.1	106	82.4	102
	103	86.8	91.6	104	81.1	100
Mean accuracy (%)	107	89.5	94.4	107	83.6	103

* >±20% of actual concentration

Mean QC data for *S*-verapamil were accurate within ±20% of the target concentration, though 10 of 60 individual calculated recovery values for *R*-verapamil were outside this range. Although the precision for *R*-verapamil QCs was previously calculated to be higher than for *S*-verapamil (12.8% CV compared to 2.3% CV), all individual values were within ±20%. Applying individually calculated RC values results in at least one sample on each occasion failing to meet an accuracy of ±20%. The handling of the data in this way gave no significant change in the outcome of the QC data for *S*-verapamil, but *R*-verapamil data points were affected. This highlights greater variability in the *R*-verapamil method compared to *S*-verapamil. On examination of the data, it is apparent that the variability stems from variability in pMC data obtained on analysis of HPLC fractions as all peak area data are similar. The recovery curve method used in subsequent calculations results in all individual data points falling within ±20%, and hence is an acceptable method for quantification. The manipulation of the data to determine recovery constants does present a possible improvement, though it would require further investigation of the variability of the data.

4.3.10 Dose solution preparation and analysis

Dosing solution was prepared at the Medical University of Vienna. Dosing solution comprised ^{11}C-*R*-verapamil, ^{14}C-verapamil and non-labelled verapamil (Section 5.3.1.2).

4.3.10.1 Dosing solution analysis and determination of specific activity

In order to determine the specific activity of the dosing solution, the amount of non-labelled verapamil must be accurately calculated. This was complicated by the addition of ^{11}C-*R*-verapamil, which results in a disruption to the natural 50:50 ratio of *R*- and *S*- verapamil present. This ratio was determined by HPLC-UV and used along with the calculated amounts present as a result of ^{14}C-labelled and non-labelled verapamil to determine the mass of each enantiomer. The mass and measured ^{14}C-concentrations were used to determine the specific activity of each enantiomer in every dosing solution.

4.3.10.2 Determination of ^{14}C-verapamil concentration in dosing solution by LSC

The concentration of all dosing solutions was determined by duplicate analysis of weighed aliquots of dosing solution by LSC (Section 7.9, Equation 25). Mean duplicate data had a precision of less than 4% (Table 52).

$$Dosing\ \ solution\ concentrat\ ion\ (dpm) = \frac{dpm/g\ \ of\ \ dosing\ \ solution\ (g)}{weight\ \ of\ \ dosing\ \ solution\ (g)} \quad \textbf{Equation 25}$$

Table 52: Determination of ^{14}C-verapamil concentration in dosing solution.

Dosing solution	Dose solution weight (mg)	Concentration (dpm/mass taken)	Concentration (dpm/g)	Mean concentration (dpm/g)[1]
P1, Sub 1	25.9	1359.95	52507.7	54462.1(3.59)
	24.6	1387.85	56416.5	
P2, Sub 1	25.6	1742.59	68069.8	69323.3 (1.81)
	25.3	1785.59	70576.7	
P2, Sub 2	25.8	1160.16	44967.5	44298.8 (1.51)
	26.1	1138.75	43630.1	
P1, Sub 3	25.7	797.98	31050.0	31750.7 (2.21)
	25.8	837.25	32451.4	
P2, Sub 3	25.2	1282.24	50882.4	50577.3 (0.60)
	25.2	1266.86	50272.1	
P1, Sub 4	25.8	1946.55	75447.8	76605.3 (1.51)
	25.6	1990.73	77762.8	
P2, Sub 4	26.2	1352.41	51618.8	52880.0 (2.39)
	25.1	1358.95	54141.2	
P1, Sub 5	25.5	1452.58	56963.8	57446.9 (0.84)
	25.6	1483.00	57929.9	
P2, Sub 5	25.6	1743.16	68092.3	69249.3 (1.67)
	24.4	1717.91	70406.2	
P1, Sub 6	25.2	949.22	37667.6	37596.7 (0.19)
	24.7	926.88	37525.7	
P2, Sub 6	25.1	1079.00	42987.9	42341.7 (1.53)
	25.8	1075.74	41695.4	
P1, Sub 7	25.6	1172.04	45782.9	46127.0 (0.75)
	25.6	1189.66	46471.0	
P2, Sub 7	25.7	1126.36	43827.3	45136.3 (2.90)
	24.7	1147.20	46445.2	

[1]value in parentheses = % difference from the mean value, P = period, Sub = subject

4.3.10.3 Determination of amount of *R*- and *S*-verapamil present as a result of non-labelled and ^{14}C-verapamil addition

The specific radioactivity of the ^{14}C-material was certified (Section 7.2.3) as 0.94 GBq/mmol, which is equivalent to 1.146 x 10^5 dpm/µg. The weight of the dosing solution provided by the clinic was used along with LSC data to determine the amount of non-labelled *R*- and *S*-verapamil present in each dosing solution as a direct result of ^{14}C-verapamil addition (Equation 26; Table 53).

$$M_{14}(\mu g) = \left(\frac{dosing\ \ solution\ concentrat\ ion\ (dpm)}{specific\ activity\ \ of\ \ neat\ radiolabel\ led\ \ material\ (dpm/\mu g)\ x2} \right)$$

Equation 26

The non-labelled verapamil mass was 50 µg (25 µg per enantiomer). The amount of non-labelled *S*-verapamil (M_{14S}) was calculated using Equation 27.

$$M_{14s} = M_{14} + 25$$ **Equation 27**

Table 53: Determination of non-labelled verapamil present in ^{14}C-verapamil.

Dosing solution	Mean dpm/g of dosing solution	Weight of product solution (g)	dpm/dose preparation	Mass of non-labelled verapamil added (µg)	Mass of each enantiomer (µg) M_{14}	Mass of *S*-verapamil (µg) M_{14S}
P1, Sub 1	54462.1	4.8050	261690	2.28	1.14	26.1
P2, Sub 1	69323.3	3.2212	223300	1.95	0.98	26.0
P2, Sub 2	44298.8	6.8329	302690	2.64	1.32	26.3
P1, Sub 3	31750.7	8.1773	259640	2.27	1.34	26.3
P2, Sub 3	50577.3	5.2438	265220	2.31	1.56	26.6
P1, Sub 4	76605.3	3.2066	245640	2.14	1.07	26.1
P2, Sub 4	52880.0	4.5880	242610	2.12	1.06	26.1
P1, Sub 5	57446.9	4.9803	286100	2.50	1.25	26.3
P2, Sub 5	69249.3	3.6064	249740	2.18	1.09	26.1
P1, Sub 6	37596.7	6.6034	248270	2.17	1.09	26.1
P2, Sub 6	42341.7	4.1296	174850	1.53	0.77	25.8
P1, Sub 7	46127.0	5.5782	257310	2.25	1.13	26.1
P2, Sub 7	45136.3	6.0301	272180	2.37	1.19	26.2

P1, microdose only, P2, microdose plus therapeutic dose, Sub = subject

4.3.10.4 Measurement of *R*- and *S*-verapamil ratio in dosing solution by HPLC-UV

Each dosing solution was analysed by the chiral HPLC (50 µL, weight recorded; Section 7.8.2) and the peak areas recorded. UV detection was used, as fluorescence detection was not available with the instrument (Shimadzu; Section 7.8.2) used for the analysis of dosing solution. The method was transferred and repeatability confirmed prior to proceeding with analysis of dosing solutions. All solutions were analysed in the same way. Several samples were analysed in duplicate to assess variability between analyses. The ratio of non-labelled *R*- and *S*-verapamil present was determined (Table 54).

Table 54: Determination of *R*- and *S*-verapamil ratio in dosing solution.

Dosing solution	*R*-verapamil peak area (mAU)	*S*-verapamil peak area (mAU)	*R* %	*S* %
P1, Sub 1	445487	379064	54.0	46.0
P2, Sub 1	328346	249447	56.8	43.2
P2, Sub 2	420491	261570	61.7	38.4
P1, Sub 3	229400	187812	55.0	45.0
P2, Sub 3	406497	313401	56.5	43.5
P1, Sub 4	149263	59877	71.4	28.6
P2, Sub 4	302185	230631	56.7	43.3
P1, Sub 5	368048	298114	55.3	44.8
P2, Sub 5	633296	387366	62.1	38.0
P1, Sub 6	573815	448424	56.1	43.9
P2, Sub 6	441580	351409	55.7	44.3
P1, Sub 7	360255	262759	57.8	42.2
P2, Sub 7	156429	101784	60.6	39.4

P1, period 1 microdose only, P2, period 2 microdose plus therapeutic dose, Sub = subject

Due to the small volume of dosing solution available, it was not possible to analyse all samples in duplicate, and therefore a selection of samples with sufficient sample remaining were analysed to determine the accuracy of the data (Table 55). Duplicate analysis of dosing solutions administered to subjects 1, 3 and 4 (period 1) and subject 3 (period 2) were analysed a second time and the percentage difference from the original result was determined to be less than 0.45% (Table 55).

Table 55: Confirmation of *R*-and *S*-verapamil ratio in selected samples of dosing solutions.

Dosing solution	*R*-verapamil peak area (LU)	*S*-verapamil peak area (LU)	*R* %	% difference from original ratio	*S* %	% difference from original ratio
P1, Sub 1	445487	379064	54.0	-0.09	46.0	0.11
	310241	264505	54.0		46.0	
P1, Sub 3	229400	187812	55.0	0.2	45.0	-0.24
	160418	130764	55.1		44.9	
P2, Sub 3	406497	313401	56.5	-0.25	43.5	0.32
	133358	103372	56.3		43.7	
P1, Sub 4	149263	59877	71.4	-0.18	28.6	0.45
	174801	70551	71.2		28.8	

P = period, Sub = subject

Original data for all solutions were, therefore, used in the calculation of the amount of *R*-verapamil present in dosing solutions (Table 56).

$$M_{14R} = \frac{M_{14s}}{Ratio\ of\ \ S\text{ - }verapamil}\ x\ Ratio\ of\ \ R\text{ - }verapamil \qquad \textbf{Equation 28}$$

Table 56: Determination of total mass of *R*- and *S*-verapamil present in dosing solution.

Dosing solution	*R* %	*S* %	Total *S*-verapamil mass (µg)	Total *R*-verapamil mass (µg)
P1, Sub 1	54.0	46.0	26.1	30.7
P2, Sub 1	56.8	43.2	26.0	34.2
P2, Sub 2	61.7	38.4	26.3	42.3
P1, Sub 3	55.0	45.0	26.1	31.9
P2, Sub 3	56.5	43.5	26.2	34.0
P1, Sub 4	71.4	28.6	26.1	65.1
P2, Sub 4	56.7	43.3	26.1	34.2
P1, Sub 5	55.3	44.8	26.3	32.5
P2, Sub 5	62.1	38.0	26.1	42.7
P1, Sub 6	56.1	43.9	26.1	33.4
P2, Sub 6	55.7	44.3	25.8	32.4
P1, Sub 7	57.8	42.2	26.1	35.8
P2, Sub 7	60.6	39.4	26.2	40.3

The specific radioactivity (dpm / µg) was determined for *R*- and *S*-verapamil (Equations 29 and 30).

$$Specific\ \ activity\,(R\text{ - }verapamil) = \frac{dosing\ \ \ solution\ \ concentrat\,ion\ /2}{M_{14R}} \qquad \textbf{Equation 29}$$

$$Specific\ \ activity\,(S\text{ - }verapamil) = \frac{dosing\ \ \ solution\ \ concentrat\,ion\ /2}{M_{14S}} \qquad \textbf{Equation 30}$$

Using the ratio of *R*- and *S*-verapamil present, the amount of non-labelled verapamil (50 µg) added to the dosing solution and the non-labelled verapamil resulting from addition of ^{14}C-verapamil, the amount of *R*- and *S*-verapamil (µg) was calculated (Table 57). The specific activities of *R*- and *S*-verapamil were calculated (Table 56).

Table 57: Determination of specific radioactivity of *R*- and *S*-verapamil in dosing solution.

Dosing solution	Total amount of *R*-verapamil (µg)	Total amount of *S*-verapamil (µg)	Amount of ^{14}C verapamil per enantiomer (dpm)	*R*-verapamil specific radioactivity (dpm/pg)	*S*-verapamil specific radioactivity (dpm/pg)
P1, Sub 1	30.7	26.1	261690	4.26	5.01
P2, Sub 1	34.2	26.0	223300	3.27	4.29
P2, Sub 2	42.3	26.3	302690	3.58	5.76
P1, Sub 3	31.9	26.1	259640	4.07	4.97
P2, Sub 3	34.0	26.2	265220	3.90	5.06
P1, Sub 4	65.1	26.1	245640	1.80	4.71
P2, Sub 4	34.2	26.1	242610	3.55	4.65
P1, Sub 5	32.5	26.3	286100	4.40	5.44
P2, Sub 5	42.7	26.1	249740	2.92	4.78
P1, Sub 6	33.4	26.1	248270	3.72	4.76
P2, Sub 6	32.4	25.8	174850	2.70	3.39
P1, Sub 7	35.8	26.1	257310	3.59	4.93
P2, Sub 7	40.3	26.2	272180	3.38	5.19

4.4 Conclusions

This chapter details a method for the quantification of *R*- and *S*-verapamil in plasma involving two-dimensional chiral HPLC-AMS analysis. Despite involving a complex multi-step process, accuracy and precision fall within the recommended guidelines pertaining to HPLC-AMS assay for accuracy and precision (±20%). It should also be noted that standard bioanalytical guidelines require accuracy and precision to be within ±15%. These acceptance criteria were intentionally widened due to the nature of a HPLC-AMS assay, specifically the number of off-line steps required. In this particular case, the data meet both the HPLC-AMS recommended guidelines and the standard bioanalytical guidelines, the overall precision being <12.8%. All QC plasma samples also had accuracies of <15% of the target concentration, with the exception of 1 replicate (*R*-verapamil, replicate 4) which was +20% from the target concentration.

CHAPTER 5

Combination of accelerator mass spectrometry and positron emission tomography in the determination of *R*- and *S*-verapamil pharmacokinetics after administration of a microdose

5.1 Introduction

A typical microdosing study (Section 1.8) provides information on the distribution of a drug within the central blood compartment, but it does not provide information on the distribution of a drug within the rest of the body unless biopsy samples are taken. In many cases, these may not be easily taken from healthy human volunteers. Positron emission tomography (PET) is an imaging technique, which is used to monitor drug distribution in tissue and PK after the administration of a drug containing a positron-emitting radionuclide, either as a direct label or as a ligand. Typical positron-emitting isotopes used in PET are ^{11}C, ^{13}N, ^{15}O and ^{11}F [175, 176]. These short-lived isotopes are unstable proton-rich or neutron-deficient isotopes, which achieve stability through the emission of a positron (β+). The isotope used in this study, ^{11}C, decays according to the following reaction (Equation 31) where β+ is the positron and ν is the neutrino:

$$^{11}C \rightarrow {}^{11}B + \beta^{+} + \nu + energy(97keV) \qquad \textbf{Equation 31}$$

After emission, the positron collides with electrons in the surrounding tissue, losing energy until it annihilates with an electron, typically within 1 to 2 mm of the labelled atom (Figure 74).

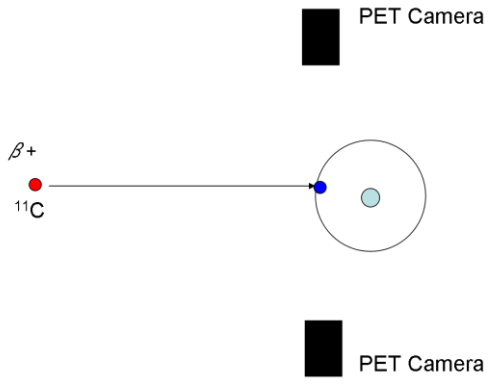

Figure 74: ^{11}C emission and collision with an electron.

The annihilation of the positron with the electron produces two gamma rays, called annihilation photons. These annihilation photons, each with 511 kEV of

energy are scattered perpendicular to the electron and are detected by the PET cameras which produce an image (Figure 75).

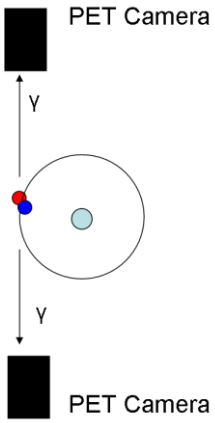

Figure 75: Production of gamma rays and detection by PET camera.

Positron emitting radionuclides have relatively short half-lives. ^{11}C has a half life of 20.4 min, while ^{18}F and ^{15}O have half lives of 109.8 min and 2.0 min, respectively [175]. The experimental design of PET studies is limited by the short radioactive half-lives. The ^{11}C-labelled material must be prepared (normally in a cyclotron) in close proximity to the PET scanner to enable administration before significant radioactive decay has occurred. In addition, dosing must be IV as there is insufficient time to measure absorption after extra-vascular routes of administration. The doses administered are normally at a high specific radioactivity, where each molecule of the drug administered contains one ^{11}C isotope. Due to the administration of this low mass, high radioactive dose, these studies are classed as microdose studies.

While PET is advantageous in that it provides distribution data, the short half-lives mean that the determination of PK data is only possible over short periods of time which is often impractical for studies requiring extended PK information. Combining the use of AMS and PET as complementary analytical techniques enables drug distribution and PK data to be obtained simultaneously in the same subjects, thus maximising the outcome of the study without significant extra resource.

A study was proposed, whereby a dual-labelled ^{14}C and ^{11}C microdose of verapamil was administered to human volunteers. The aim of the study was to simultaneously determine PK in plasma, by AMS analysis, and in the brain, by PET analysis in the same subjects. As verapamil is racemic, determination of the plasma PK of each individual enantiomer was proposed. The study was a collaboration between the author and Claudia Wagner, a PhD student registered at the Medical University of Vienna. The author was responsible for obtaining and interpreting AMS data only and these data are the focus of this chapter. The PET methodology and data reported in this chapter were the work of Claudia Wagner and are presented for data comparison purposes.

5.2 Aims

The primary aims of the work presented in this chapter were (Figure 76):

- to determine plasma PKs of *R*- and *S*-verapamil using 2 dimensional RP-chiral chromatography;

- to determine differences in PK parameters for *R*- and *S*-verapamil and to compare these observations with literature data;

- to assess the linearity of PK data obtained after an intravenous microdose compared with that obtained after concomitant intravenous microdose and oral therapeutic dose;

- to compare AMS data with brain imaging and PK data obtained after PET analysis.

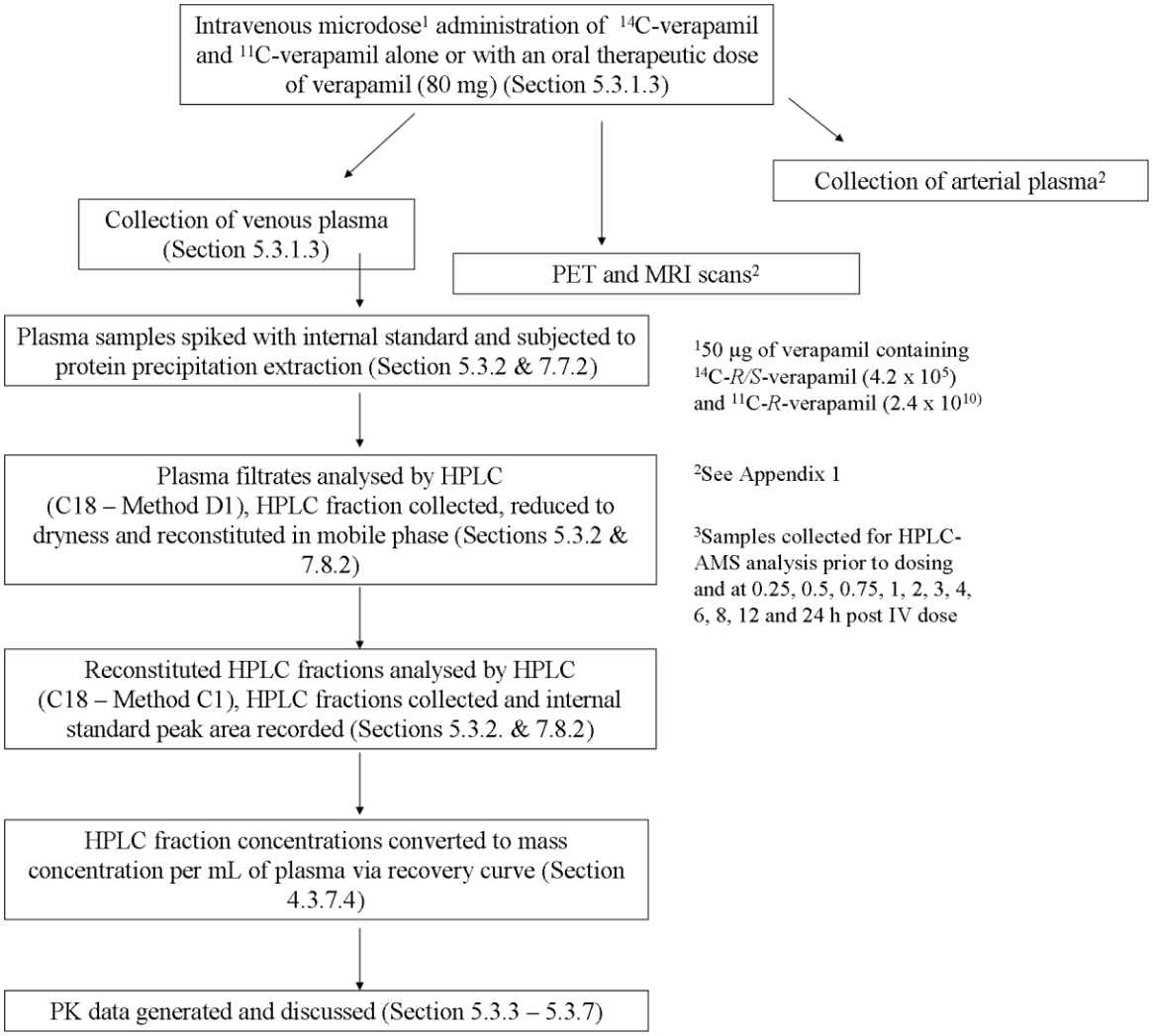

Figure 76: Schematic of verapamil dosing, sample collection and analysis of plasma samples by HPLC and AMS.

5.3 Results and discussion

5.3.1 Clinical study

5.3.1.1 Choice of test compound

Verapamil was chosen as the test compound, as it has been studied extensively in PET studies and the chemistry of ^{11}C-labelling is also well established [170, 177, 178] It is a calcium channel blocker with a well established safety profile [169]. Verapamil is a racemic drug, with both enantiomers being substrates for P-gp. The P-gp-driven transport of verapamil across the blood brain barrier (BBB) has been the focus of several PET studies [73, 179, 180]. The clearance and hepatic

metabolism of *S*-verapamil in humans have been shown to be higher than for *R*-verapamil, resulting in higher *R*-verapamil concentrations. In addition, levels of protein binding are increased for *S*-verapamil, therefore suggesting that tissue uptake may also differ [170, 174]. As PET analysis cannot differentiate between the two enantiomers, the *R*-verapamil has been developed for the study of the kinetic modelling of PET data [169, 178, 180]. *R*-verapamil is metabolised through *N*-demethylation, *O*-demethylation and *N*-dealkylation, processes mediated by CYP. *N*-demethylation forms the polar metabolites, norverapamil and ^{11}C-formaldehyde, which account for approximately 70% of the total plasma radioactivity after 1 h in initial studies in rats [170]. The metabolites formed by *N*-dealkylation and *O*-demethylation have similar lipophilic properties to *R*-verapamil and were found to cross the BBB readily. As with verapamil, they are rapidly transported back out of the brain by P-gp. Although the *N*-demethylation metabolites may also pass through the BBB they have no affinity for P-gp, resulting in significant amounts being present in the brain (approximately 50%) 1 hour after administration [170, 178].

Further studies in human volunteers showed a difference in the metabolism of *R*-verapamil to that observed in the rat. Metabolism occurred mainly by the *N*-dealkylation route and to a lesser degree, *N*-demethylation. *O*-demethylation metabolites were not found in the brain in humans. The *N*-demethylation fraction accounted for approximately 20% of the blood radioactivity, compared to 70% in rats. This lower blood concentration was suggested to be related to much lower concentrations of polar metabolites in the brain [178].

While PET cannot differentiate between the verapamil enantiomers, they can each be determined during AMS microdosing studies as analytes can be separated by HPLC prior to AMS analysis. The dose selected for the current study was a mixture of ^{11}C-*R*-verapamil and ^{14}C-verapamil. Separation of the enantiomers prior to AMS analysis would allow determination of differences in PK to be determined. The majority of PK studies only report data for racemic verapamil with only a few having investigated the PK parameters of the individual enantiomers [174, 181]. This is the first reported microdose study, where PK parameters are determined following microdose administration.

5.3.1.2 Clinical study design and implementation

The clinical study was performed at the Medical University of Vienna, Austria in 2008. A clinical protocol was prepared and approved by the ethics committee of the Medical University of Vienna, and the Vienna General hospital. The study was performed in accordance with the Declaration of Helsinki (1964, revised 2000), the International Conference of Harmonisation (ICH) guidelines, good clinical practice (GCP) guidelines and the Austrian drug law (Arzneimittelgesetz). Seven healthy male volunteers gave written consent for their involvement in the study and met required inclusion and exclusion criteria.

The study was a crossover design, consisting of a dual labelled ^{11}C-*R*-verapamil and ^{14}C-verapamil microdose (period 1) and the same intravenous microdose co-administered with an oral therapeutic verapamil dose (period 2) separated by a 14 day washout period. Period 2 was introduced to enable investigation of the linearity of *R*- and *S*-verapamil PK following a microdose and a therapeutic dose in the same subjects.

5.3.1.3 Dose administration and sample collection

Dose solutions were prepared at the Department of Nuclear Medicine (University of Vienna, Section 7.12.3) and transported to the PET camera. Each volunteer received two identical intravenous doses of the microdose, the first administered alone (period 1) and the second administered 2 h following an oral therapeutic dose of verapamil at the estimated t_{max} of the oral dose (period 2) (Section 7.12.4).

Blood samples were collected at regular intervals to 24 h (Section 7.12.4) and throughout the first 60 min each volunteer was subjected to PET imaging (Section 7.12.4). Plasma samples were prepared (Section 7.12.4) and the samples shipped to the AMS facility where they were stored at -80 ºC prior to analysis.

Six volunteers completed both study periods whilst one subject (2) completed period 2 only. Subjects 1, 3, 6 and 7 completed period 1 first and subjects 4 and 5 completed period 2 first.

5.3.2 Determination of ^{14}C-*R*- and *S*-verapamil concentrations in plasma

Plasma samples were split into two batches consisting of period 1 and period 2 samples (Section 7.12.4) and each batch of samples was randomised. QC samples were prepared (Section 7.4.2) and replicates (*n*=8) interspersed throughout each batch of clinical plasma samples. Plasma filtrates were prepared (Section 7.7.2) and aliquots (100 µL) were analysed by C18 HPLC (Method D1; Figure 77; Section 7.8.2) and fractions corresponding to ^{14}C-verapamil, identified by the verapamil internal standard were collected and reduced to complete dryness under N_2.

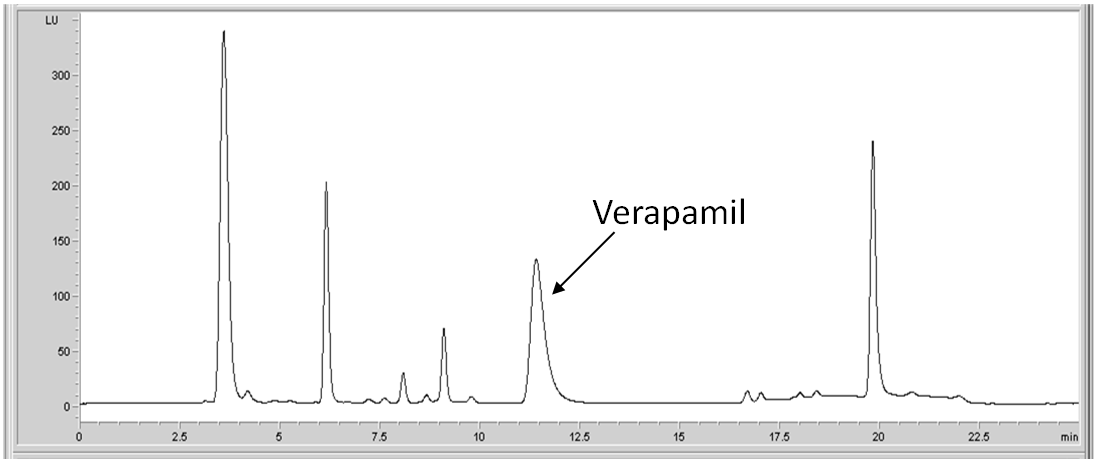

Figure 77: Example chromatogram, analysis of plasma filtrate containing verapamil at λ_{ex} 276 nm and λ_{em} 290 nm (Method D1)..

The residue was reconstituted in mobile phase at starting conditions (Method C1; Section 7.8.2; 100 µL). The entire reconstituted HPLC fraction was analysed by chiral HPLC (Method C1; Figure 78; Section 7.8.2) and fractions corresponding to *R*- and *S*-verapamil collected.

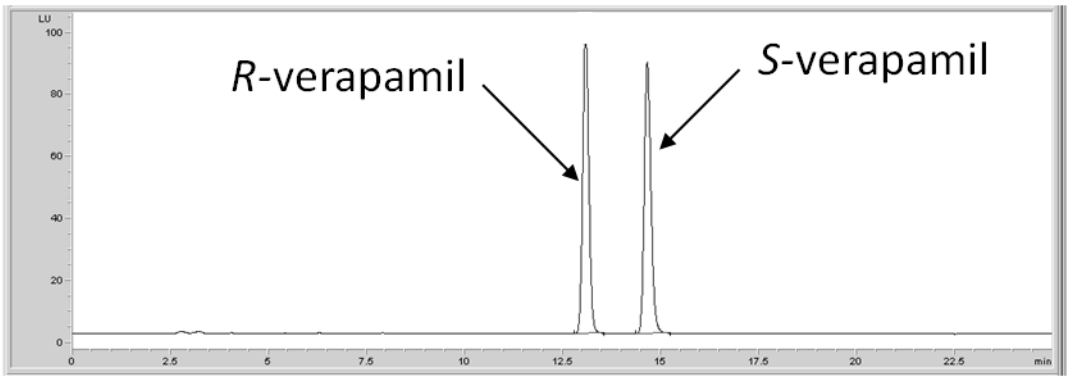

Figure 78: Example chromatogram, analysis of reconstituted HPLC fraction containing verapamil at λ_{ex} 276 nm and λ_{em} 290 nm (Method C1).

Fractions were analysed by AMS (Section 7.11), pMC data corrected to account for fraction volumes (QCs) and converted to mass concentrations of *R*- and *S*-verapamil (clinical plasma samples) via the recovery curve (Section 4.3.7.4).

5.3.3 *R*- and *S*-verapamil data obtained after administration of a microdose of verapamil

5.3.3.1 Period 1 batch suitability

Analyte retention times showed a slight drift of approximately 0.3 min; however, peak resolution was ≥2.0 (Table 58).

Table 58: Period 1 QC resolution data for *R*- and *S*-verapamil.

Replicate	*R*-verapamil retention time (min)	*S*-verapamil retention time (min)	R_s
1	12.8	14.4	2.0
2	12.4	14.1	2.1
3	12.5	14.1	2.1
4	12.7	14.3	2.0
5	12.9	14.5	2.0
6	13.0	14.6	2.1
7	13.2	14.7	2.1
8	13.2	14.7	2.2
Mean	12.8	14.4	2.1
% CV	2.3	1.7	3.6

QC plasma data showed mean accuracy of 11% for *R*-verapamil and less than 1% for *S*-verapamil with acceptable precision (CV<19%). Four individual QC concentrations were between ±20% and ±25%, with a fifth, replicate 3 (*R*-verapamil), seeing a % difference of -27%. The HPLC fraction for this sample had a pMC value that was slightly lower than the remaining samples within the data set. The AMS data were examined and there was no indication of the root cause of this unexpectedly low result (Table 59).

Table 59: Period 1 QC plasma concentration data for *R*- and *S*-verapamil.

Replicate	*R*-verapamil plasma concentration (pMC)	*S*-verapamil plasma concentration (pMC)
1	532	657
2	536	482*
3	464*	561
4	502*	550
5	528	697
6	675	711
7	776*	787*
8	517	638
Mean plasma concentration (pMC)	566	635
Actual plasma concentration (pMC)	633	633
Mean accuracy (%)	89.5	100
Mean precision (% CV)	18.4	15.7

*< ±20% of isotope ratio for plasma

Mean data for accuracy and precision were within the acceptance criteria stated in the recommended guidelines for accuracy (±20%) and precision (≤20% CV) [124] and based on these criteria the clinical plasma sample batch is deemed acceptable for use.

5.3.3.2 Period 1 *R*- and *S*-verapamil plasma concentration data

Plasma concentrations were mostly above the limit of quantification (>LOQ) of 1.611 pMC (*R*-verapamil) and 1.696 pMC (*S*-verapamil) for all subjects (*n*=6) to 24 h (Figure 79). Exceptions to this were the final (24 h) samples for *S*-verapamil (subjects 3 and 4) and *R*-verapamil (subject 4). Individual subject data

and mean data are summarised in Appendices 6 and 7. PK data are summarised in Appendices 12 and 13.

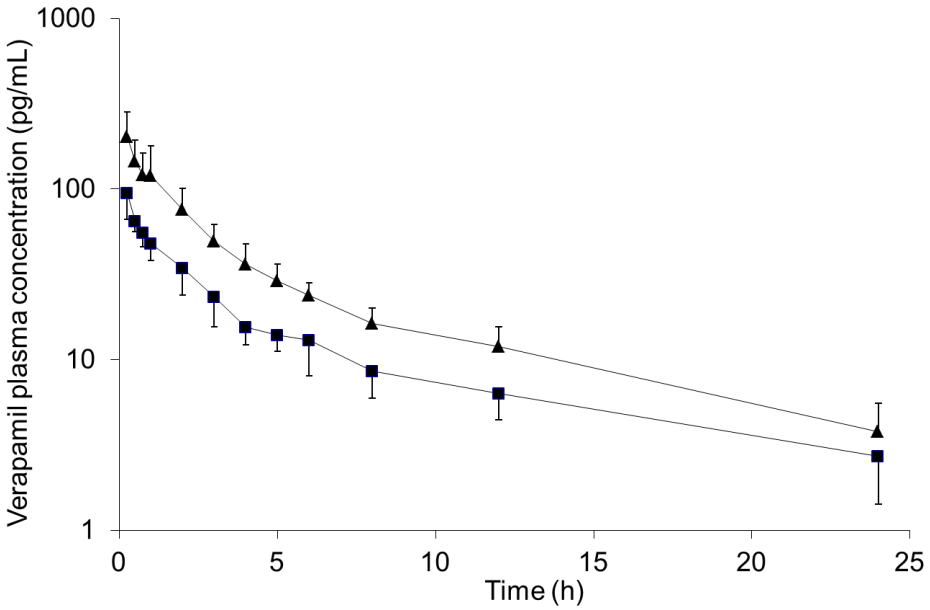

Figure 79: Semilog plot of mean *R*-verapamil (triangles, *n*=6 to 12 h, *n*=5 to 24 h) and *S*-verapamil (squares, *n*=6 to 12 h, *n*=6 to 24 h) plasma concentration data after administration of an intravenous microdose (nominally 50 µg) of ^{14}C-verapamil (*n*=6). Error bars represent one standard deviation.

The *S*-verapamil concentration for subject 1 at 6 h was unusually high within the data set at 38.6 pg/mL plasma. This is a higher concentration than obtained for the previous three time points (3 h, 36.8 pg/mL; 4 h, 17.5 pg/mL and 5 h, 17.2 pg/mL). The mean half-life increases slightly on inclusion of this point in PK calculations (from 7.44 h to 7.57 h) and the V increases from 893 L to 905 L. The percentage difference when including and excluding this data point is small at less than 2%. This value is excluded from the PK data summarised in Table 60. There was no significant difference between the mean half-lives (6.89 h and 7.44 h) observed for *R*- and *S*-verapamil. All other parameters (Table 60) were significantly lower for *S*-verapamil than for *R*-verapamil ($AUC_{0\text{-}t}$, $AUC_{0\text{-}\infty}$, CL and V_{ss} ($p<0.01$); C_{max} and V ($p<0.05$). Inter-subject variability observed in PK parameters was moderate with CVs of approximately 24% and 28% for *R*-verapamil and *S*-verapamil, respectively.

Table 60: Period 1 *R*- and *S*-verapamil microdosing pharmacokinetic summary data (*n*=6, mean, SD in parentheses).

PK parameter	*R*-verapamil	*S*-verapamil	Students t-test p value
$t_{1/2}$ (h)	6.89 (1.97)	7.44 (2.19)	0.336
C_{max} (pg/mL)	206 (77.9)	94.4 (28.0)	0.012
AUC_{0-t} (h.pg/mL)	607 (126)	291 (81.2)	0.005
$AUC_{0-\infty}$ (h.pg/mL)	649 (147)	329 (88.3)	0.005
CL (L/h)	58.2 (12.0)	84.6 (23.6)	0.004
V (L)	556 (78.0)	893 (306)	0.029
V_{ss} (L)	374 (76.8)	622 (144)	0.005

5.3.4 *R*- and *S*-verapamil data obtained after administration of a microdose of verapamil concomitantly with a therapeutic dose

5.3.4.1 Period 2 batch suitability

During the analysis of period 2 samples, the retention times drifted by approximately 2.7 min (Table 61). Although the mean peak resolution was 1.3, individual values for resolution varied. The column was regenerated once during these analyses (after analysis of replicate 6) because of the decreased resolution. Further column degradation was apparent towards the end of the analyses. HPLC fractions were collected based on a fluorescence detector trigger. Although the decrease in resolution is not ideal, the HPLC fractions were separated by a minimum of 0.28 min, ensuring that each peak contained pure *R*- or *S*-verapamil only.

Table 61: Period 2 QC resolution data for *R*- and *S*-verapamil.

Replicate	*R*-verapamil retention time (min)	*S*-verapamil retention time (min)	R_s
1	13.6	15.2	1.9
2	13.7	15.3	1.6
3	13.8	15.3	1.6
4	13.6	15.2	1.6
5	16.7	17.7	1.0
6	16.9	18.0	0.9
7	16.0	17.2	1.5
8	16.8	18.9	0.9
Mean	15.1	16.6	1.3
% CV	10.5	9.1	27.8

To investigate the decrease in resolution further and to confirm that this was appropriate for the measurement, the mean (±SD) of peak areas for period 1 and period 2 analysis were summarised and determined (Table 62).

Table 62: Comparison of period 1 and period 2 mean pharmacokinetic data for *R*- and *S*-verapamil.

Period	Enantiomer	Mean peak area (LU)[1]
1	*R*-verapamil	1540 (220)
2	*S*-verapamil	1440 (184)
1	*R*-verapamil	1490 (258)
2	*S*-verapamil	1421 (192)

[1] SD in parentheses

Although a slight decrease in peak area for *R*-verapamil was observed for batch 2 compared to batch 1, it was also mirrored for *S*-verapamil. This suggests that the overall analyte recovery for batch 2 was slightly lower than for batch 1 and the data were therefore accepted.

QC plasma data showed mean accuracy within 5% and good precision (CV > 15%) for *R*- and *S*-verapamil (Table 63).

Table 63: Period 2 QC plasma concentration data for *R*- and *S*-verapamil.

Replicate	*R*-verapamil plasma concentration (dpm/mL)	*S*-verapamil plasma concentration (dpm/mL)
1	446*	649
2	592	621
3	602	592
4	605	723
5	695	794*
6	715	828*
7	714	706
8	714	757
Mean plasma concentration (pMC)	635	709
Actual plasma concentration (pMC)	633	633
Mean accuracy	100	112
Mean precision (% CV)	14.8	11.8

*< ±20% of isotope ratio for plasma

Three samples had recoveries that showed greater variability than ±20%. *R*-verapamil replicate one had a slightly elevated peak area, but lower pMC value than the remainder of the samples, resulting in an overall recovery of 70%. In addition, the accuracy of replicate six was 122%. There was no indication of unusual variation in either the peak area, or pMC value for this sample. In addition, mean values for accuracy and precision were within ±20% and 20% CV. Clinical plasma batch data were deemed acceptable for use.

5.3.4.2 Period 2 *R*- and *S*-verapamil plasma concentration data

Plasma concentrations were above the limit of quantification (>LOQ) of 1.611 pMC (*R*-verapamil) and 1.696 pMC (*S*-verapamil) for all subjects (n=7) to 24 h (Figure 80), with the exception of the final (24 h) sample for *S*-verapamil (subject 6). In addition, concentration data were not obtained for several samples, due to the data failing to meet the AMS acceptance criteria (Section 7.11.3). These samples were *R*-verapamil, subject 5 collected at 12 h, subject 6 collected at 1 h and subject 7 collected at 3 h. For *S*-verapamil, the 0.75 h sample for subject 2 was excluded. Individual subject data and mean data are summarised in Appendices 6 and 7. PK data are summarised in Appendices 12 and 13.

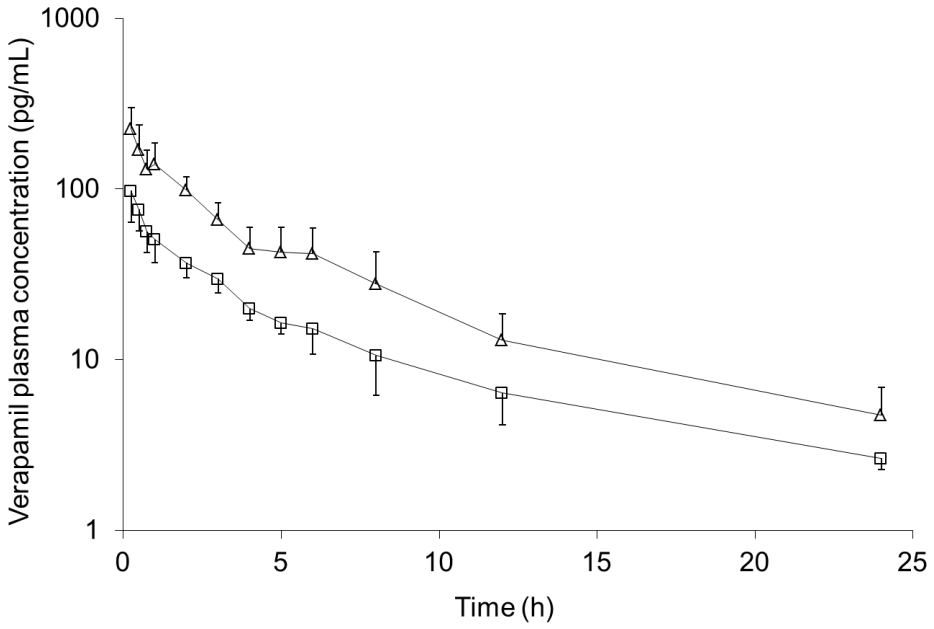

Figure 80: Semilog plot of mean *R*-verapamil (triangles, *n*=6) and *S*-verapamil (squares, *n*=6 to 12 h, *n*=5 to 24 h) plasma concentration data, after administration of an oral therapeutic dose (80 mg) of verapamil, followed by an intravenous microdose (nominally 50 µg) of ^{14}C-verapamil (*n*=6). Error bars represent one standard deviation.

All PK parameters are significantly lower ($p<0.01$) values for *S*-verapamil when compared to *R*-verapamil, with the exception of $t_{1/2}$ (Table 64) Inter-subject variability observed in PK parameters was moderate with CVs of approximately 27% and 23% for *R*-verapamil and *S*-verapamil respectively. Subject 2 was excluded from mean PK assessments, as this subject did not complete both study periods. These data are shown in Appendices 7, 12 and 13.

Table 64: Period 2 *R*- and *S*-verapamil microdosing pharmacokinetic summary data (*n*=6, mean, SD in parentheses)

PK parameter	*R*-verapamil	*S*-verapamil	Students t-test p value
$t_{1/2}$ (h)	6.27(1.30)	7.72 (1.59)	0.075
C_{max} (pg/mL)	240 (83.1)	105 (34.2)	0.003
AUC_{0-t} (h.pg/mL)	793 (276)	321 (65.3)	0.004
$AUC_{0-\infty}$ (h.pg/mL)	831 (288)	354 (54.4)	0.005
CL (L/h)	46.7 (11.4)	75.3 (12.0)	0.000
V (L)	420 (122)	851 (276)	0.003
V_{ss} (L)	285 (73.0)	584 (196)	0.003

5.3.5 Comparison of period 1 and 2 data and assessment of dose linearity

The PK data for period 2 show a general trend towards a slightly higher C_{max}, $AUC_{0\text{-}24h}$ and $AUC_{0\text{-}\infty}$ and lower CL, and V_{ss} than those obtained for period 1 (Figure 81 and Figure 82).

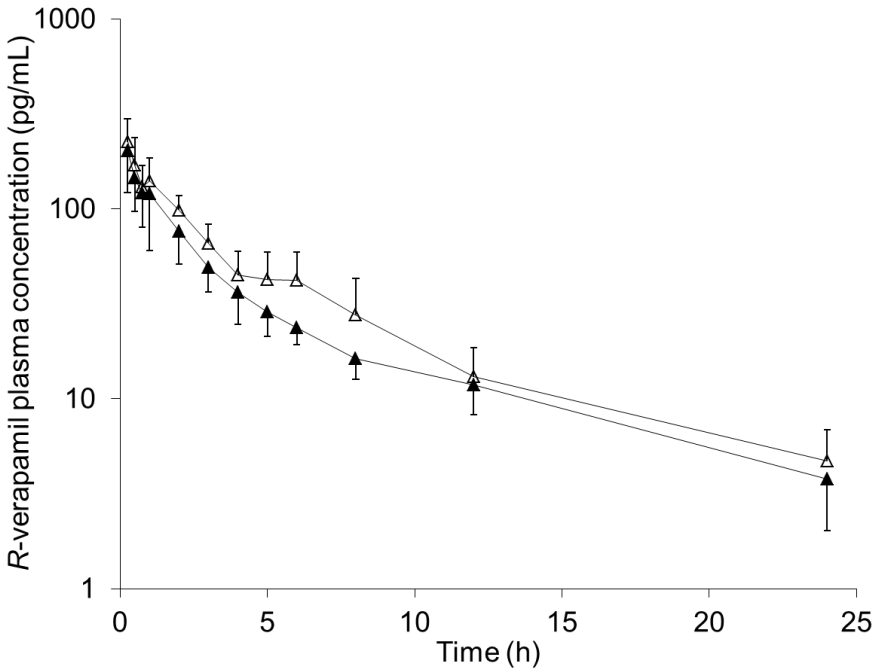

Figure 81: Semilog plot of mean *R*-verapamil plasma concentration data, after administration of an intravenous microdose (nominally 50µg) of ^{14}C-verapamil (filled triangles, *n*=6) and after administration of an oral therapeutic dose (80 mg) of verapamil followed by an intravenous microdose (nominally 50µg) of ^{14}C-verapamil (open triangles, *n*=7). Error bars represent one standard deviation.

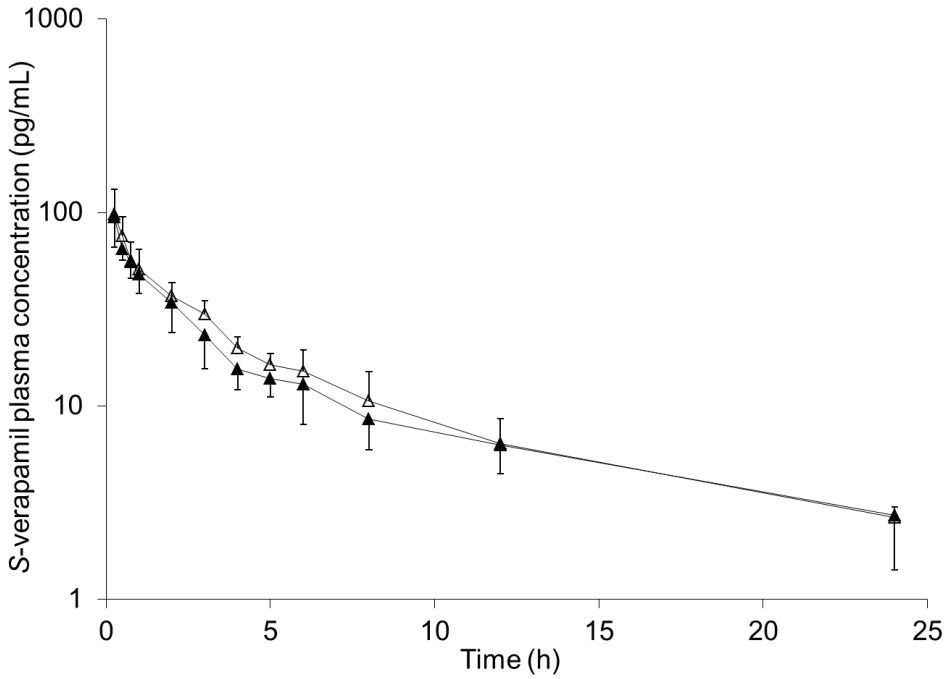

Figure 82: Semilog plot of mean *S*-verapamil plasma concentration data, after administration of an intravenous microdose (nominally 50µg) of ^{14}C-verapamil (filled triangles, *n*=6) and after administration of an oral therapeutic dose (80 mg) of verapamil followed by an intravenous microdose (nominally 50µg) of ^{14}C-verapamil (open triangles, *n*=7). Error bars represent one standard deviation.

The increase is not statistically significant except for V for *R*-verapamil (Table 65), which decreases from 556 L for period 1 to 420 L during period 2 ($p<0.05$).

Table 65: Comparison of period 1 and period 2 mean pharmacokinetic data for *R*- and *S*-verapamil.

PK parameter	*R*-verapamil % difference between P1 & P2	Students t-test p value	*S*-verapamil % difference between P1 & P2	Students t-test p value
$t_{1/2}$ (h)	-9.94	0.533	3.65	0.804
C_{max} (pg/mL)	14.4	0.474	10.3	0.564
AUC_{0-t} (h.pg/mL)	23.4	0.165	9.28	0.500
$AUC_{0-\infty}$ (h.pg/mL)	21.8	0.200	7.07	0.568
CL (L/h)	-24.5	0.120	-12.3	0.411
V (L)	-32.4	0.044	-4.89	0.809
V_{ss} (L)	-31.4	0.066	-6.60	0.706

The statistical difference is likely to be an anomalous result, as V is related to CL and $t_{1/2}$ by Equation 32. Since there is no significant difference between $t_{1/2}$ and CL then according to Equation 32, there should not be a significant difference in V due to the relation of V to the $t_{1/2}$ and CL.

$$t_{1/2} = V_d / CL \times 0.693 \qquad \textbf{Equation 32}$$

There is no significant difference between the *R*-verapamil $t_{1/2}$ and CL determined in period 1 and period 2. The individual PK data (Appendix 12) do not appear to contain outliers that could contribute to this anomaly. V shows higher precision in period 1 (14%) compared with period 2 (29%). Although this parameter shows a statistical difference at the 95% confidence level, this is not statistically different at 99% confidence. The statistical difference between the two parameters, therefore, should be treated with caution.

A previous study showed that dose dependent kinetics were observed after oral administration of verapamil. Verapamil was found to show non-linear PKs over the range 100 µg (microdose) to 80 mg, with AUCs being 1.19, 1.83 and 2.30 times higher after a 3, 16 and 80 mg oral dose compared with the microdose [93]. This non-linearity was hypothesised by the authors to be due to saturation of intestinal CYP3A4 and MDR1 (Section 1.8.1). The same magnitude of difference in AUC was not observed in the present study after administration of a 50 µg microdose and a 50 µg microdose concomitantly administered with an 80 mg oral dose. Differences in AUC of 1.4 and 1.1-fold were observed for *R*- and *S*-verapamil respectively between the two doses. These data do not show the same non-linearity, which supports the findings made in previous studies, where dose non-linear PK tend to be observed after extra-vascular routes of administration but not observed on oral administration (Section 1.8.1).

5.3.6 Comparison of *R*- and *S*-verapamil pharmacokinetics with previous studies

All PK parameters obtained for *R*-verapamil compared with *S*-verapamil (period 1) were statistically significant different with the exception of $t_{1/2.}$ These differences were also reflected for period 2 samples. The difference in the

metabolism of *R*- and *S*-verapamil is well documented [174, 182] and was quantified in a previous study after administration of a 5 mg IV dose [174].

Table 66: Comparison of *R*-verapamil pharmacokinetic data obtained after administration of a microdose and a microdose concomitantly with an oral therapeutic dose of *R/S*-verapamil, with literature data obtained after a 5 mg intravenous dose.

Nominal dose	Number of subjects	$t_{1/2}$ (h)	CL (L/h)	V (L)	V_{ss} (mL)	Source
50 µg	6	6.89	58.2	556	374	Present study
50 µg (80 mg)	6	6.27	46.7	420	285	Present study
5 mg[1]	5	4.07	45.1	266	200	[174]
Factor difference, 50 µg to 5 mg	5	1.7	1.3	1.4	1.9	[174]
Factor difference, 50 µg (80 mg) to 5 mg	5	1.6	1.0	1.6	1.4	[174]

[1]data were converted from reported units to those equivalent to measurements made in this study

All PK data obtained in the present study agree with previously published data [174] within a factor of 2 (Table 66 and Table 67), with the data for *S*-verapamil showing slightly closer correlation (Table 67). Verapamil, particularly the *S*-enantiomer undergoes extensive first pass metabolism. The preferential clearance observed for *S*-verapamil observed in both the current study and in previously reported data has been investigated *in vitro*. I*n vitro* studies showed that the enantiomers were found to be primarily converted to different metabolites, at different rates with CYP3A4, CYP3A5 and CYP2C8 [183]. CYP3A4 resulted in the formation of norverapamil when *S*-verapamil was the substrate and D-617 when *R*-verapamil was the substrate, with similar K_m values being obtained for both processes. The K_m value for CYP3A4 metabolism to D-620 (a metabolite of norverapamil) was four-fold higher for *R*-verapamil than for *S*-verapamil. CYP3A5 resulted in the equal metabolism of *R*– and *S*-verapamil to norverapamil, whereas D620 formation was two-fold higher for *S*-verapamil than for *R*-verapamil. CYP2C8 also resulted in the formation of norverpamil as the major metabolite on administration of *R*- and *S*-verapamil [183]. Elevated K_m values were observed for formation of D617 and PR-22 (a metabolite of norverapamil) from *S*-verapamil than from the racemic mixture. These data support the preferential clearance of *S*-verapamil by CYP enzymes [183].

Verapamil is also a substrate for P-gp [177]. A previous study demonstrated that the uptake of verapamil into mouse brain by P-gp was found to be equal for both enantiomers. The same study also confirmed *in vitro*, that there was no difference in the P-gp transport of *R*- and *S*-verapamil [177]. These findings indicate that the difference in the metabolism of *R*- and *S*-verapamil is due to CYP enzymes, primarily the CYP3A enzymes and not due to P-gp uptake.

Table 67: Comparison of *S*-verapamil pharmacokinetic data obtained after administration of a microdose and a microdose concomitantly with an oral therapeutic dose of *R/S*-verapamil, with literature data obtained after a 5 mg intravenous dose.

Nominal dose	Number of subjects	$t_{1/2}$ (h)	CL (L/h)	V (L)	V_{ss} (mL)	Source
50 µg	6	7.44	84.6	894	622	Present study
50 µg (80 mg)	6	7.72	75.3	851	584	Present study
5 mg	5	5.01	82.2	577	470	[174]
Factor difference, 50 µg to 5 mg	5	1.5	1.0	1.5	1.3	[174]
Factor difference, 50 µg (80 mg) to 5 mg	5	1.6	1.1	1.5	1.2	[174]

[1]data were converted from reported units to those equivalent to measurements made in this study

The findings reported here corroborate the pronounced differences in CL, V and V_{ss} observed in studies after administration of an IV 5 mg dose and show that these differences can be detected after administration of a microdose.

5.3.7 Comparison of *R*- and *S*-verapamil AMS data with PET data

The PK data obtained after administration of ^{14}C-verapamil were compared with the data obtained after PET analysis in the same subjects. Total ^{11}C-*R*-verapamil radioactivity concentrations measured in the brain by PET analysis and in arterial plasma using a gamma counter [184] were plotted vs. the sampling time (Figure 83 and Figure 84) and show no significant differences in the resulting AUCs.

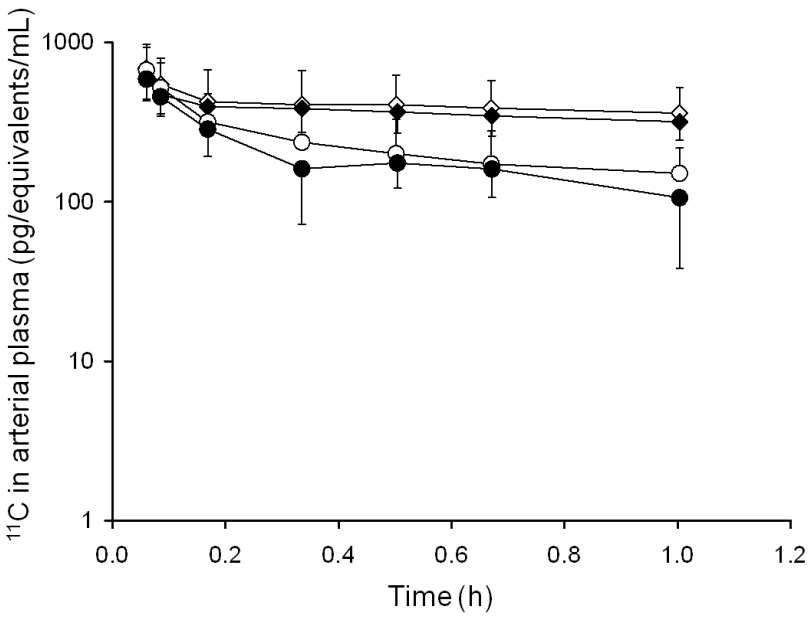

Figure 83: Semilog plot of mean total ^{11}C-radioactivity (squares) and ^{11}C-*R*-verapamil (circles) in arterial plasma. Period 1 = open symbols, period 2 = filled symbols.

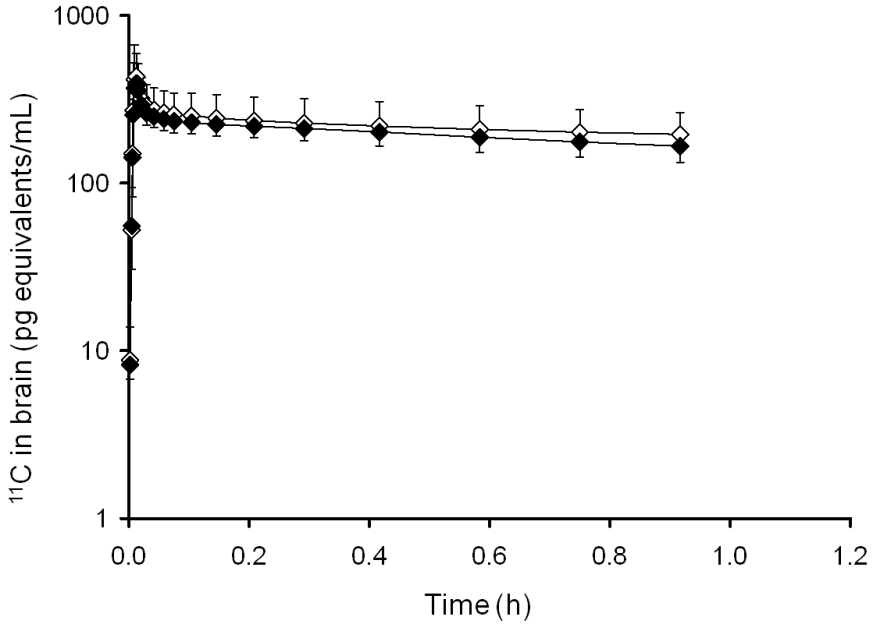

Figure 84: Semilog plot of total ^{11}C-radioactivity in whole brain grey matter. Period 1 = open symbols, period 2 = filled symbols.

^{11}C-*R*-verapamil concentrations measured in arterial plasma by solid phase extraction followed by HPLC [184] and plotted vs. collection time (Figure 84) show no significant differences between administration of doses in period 1 and period 2, suggesting no dose dependent effects. It should be noted that *R*-verapamil metabolism was slightly (but not significantly) lower for period 2, with the fraction of polar radiometabolites being reduced. This correlates with the decrease in CL between period 1 and period 2 previously observed after analysis of ^{14}C-*R*-verapamil.

Although the degree of non-linearity is not statistically significant, this cannot be ignored. This could be investigated further by carrying out an additional study whereby IV doses of verapamil are administered to volunteers at doses greater than 80 mg. The data obtained for ^{14}C-*R*-verapamil in the present study were more variable in period 2 than in period 1. Thus enrolling a larger number of subjects may also be advantageous in such a study.

5.4 Conclusions

This study presents the first report of the quantification of *R*- and *S*-verapamil by C18-chiral HPLC-AMS after administration of an IV microdose. Despite the complex methodology, consisting of off-line 2 dimensional C18 and chiral HPLC chromatography and the use of a bespoke quantification method, QC data analysed alongside clinical plasma samples showed mean accuracy and precision of <19%. This variability, while slightly higher than that required for conventional bioanalytical studies (<15%) [185] agrees with recently published guidelines for bioanalytical studies using AMS analysis [124]. It should be noted, that these guidelines assume a single chromatographic method and additionally do not specifically apply to chiral methods, further highlighting the robust nature of the assay.

In agreement with previous studies, significant differences were observed in CL, V and V_{ss} for *R*- and *S*-verapamil, with *S*-verapamil showing higher clearance and volume of distribution. These data support the use of a microdose in predicting the individual PK parameters of enantiomers after administration of a

racemic mixture. PK parameters for each enantiomer were compared across dosing periods and slight increases were observed in C_{max}, $AUC_{0\text{-}24h}$, $AUC_{0\text{-}\infty}$ values and decreases in CL, V and V_{ss} for period 2 compared with period 1. With the exception of V for *R*-verapamil, none of these differences was found to be statistically significant. Due to the small sample size it is not possible to determine whether the data set exhibits slight non-linearity as was predicted for verapamil at an 80 mg dose level [186]. As only V shows a statistically significant difference ($p<0.05$) but CL, V_{ss} and $t_{1/2}$ do not these data alone must be treated with caution. This trend is supported by decreased metabolism of ^{11}C-*R*-verapamil for period 2 than for period 1, and cannot be ignored. Further analysis would be necessary with larger numbers of subjects and the administration of a wider range of doses to ascertain whether this difference is due to an underlying dose dependent mechanism or whether these effects are true anomalies within the data set.

PET imaging data provided the measurement of total ^{11}C-*R*-verapamil concentrations in whole brain grey matter. PET does not distinguish between unchanged drug and metabolites, however analysis of arterial plasma showed that 60 min after IV dosing, total plasma radioactivity was the sum of (*R*)-^{11}C-verapamil (42±8%), lipophilic *N*-dealkylation products (31±8%), and polar radiometabolites (28±9%) [184]. Administration of an oral and IV ^{14}C-microdose in the same subjects at a microdose, 10 mg, 80 mg, 160 mg and 240 mg would open up the possibility of examining dose dependent effects. In addition to this isolation and enantiomeric separation of each of the metabolites would enable differences in metabolism to be observed between the *R*- and *S*-metabolites, and to determine dose dependent effects on their production. Inclusion of the oral dose would allow direct correlation between the two doses in the same subjects. A previous study employed LC-MS as the analytical technique after administration of a 100 µg microdose [186]. The LOQ obtained was 1 pg/mL for verapamil compared with 1.5 pg/mL for *R*-verapamil and *S*-verapamil in the present study. Employing chiral LC-MS would be an obvious choice for these analyses.

The reported HPLC-AMS method resulted in the 24 h sample for several subjects being below the LOQ. The following modifications would allow the LOQ to be reduced: 1) increasing the plasma volume taken for extraction, 2) reducing the reconstitution volume to concentrate the plasma filtrate; 3) taking the entire sample for HPLC analysis and 4) taking the entire fraction for analysis by AMS. In the present study the volumes for points 1) – 4) listed above were 200 µL, 200 µL, 100 µL and approximately half of the resulting fraction. Altering the amount of plasma taken for extraction to 400 µL, reconstituting the sample in 100 µL and taking this entire volume for HPLC analysis, and then analysing the entire HPLC fraction would result in the concentration of analyte taken for AMS being eight times greater, an LOQ of 0.2 pg/mL. This LOQ may be more appropriate for the quantification of metabolites of *R*- and *S*-verapamil and the quantification method should be carefully considered.

The data reported in this chapter show the value of combining PET and AMS after administration of a dual-labelled microdose. Obtaining imaging data (Appendix 1) allows the distribution of the drug to be studied, while PK data are obtained simultaneously. This could prove to be very useful in situations where outlier subject data are obtained. For example, if a subject showed particularly unusual PET data, for example increased levels of drug concentration in the brain compared with other subjects, the corresponding plasma PK data may provide additional insight into the possible cause.

PET cannot provide extensive data due to the short ^{11}C-half life. Adding a ^{14}C-tracer to an already existing PET study could provide this valuable information, without significant additional resource. The current study was complicated somewhat by the complex methodology required for separating and analyzing individual enantiomers and method development would be much reduced for a simpler compound. Despite the complexities detailed here it has been demonstrated that enantiomeric mixtures may be analysed by HPLC-AMS, and the accuracy and precision of such data fall within recommended guidelines.

CHAPTER 6

Overall conclusions and further work

6.1 Overall summary and conclusions

This thesis describes the development of two applications of microdosing for characterising human PKs prior to phase 1 clinical trials. Separation and quantification techniques were developed for HPLC and AMS analysis of trace levels of drug compounds. Application of these methods in the development of a NCE has the potential to reduce resource requirements.

The first application was developed to explore the use of cassette microdosing in clinical trials and the ability of the cassette microdose approach to detect drug-drug interactions. Although cassette dosing is a valuable tool in drug candidate selection, it is not routinely utilised in phase 0 studies. In the current study, a 2D C18-phenyl HPLC method was employed and separation was verified prior to clinical plasma sample analysis. Due to the low doses administered, AMS was chosen as the quantification method. Each analyte was quantified via a recovery constant method. Mean accuracy for all analytes was within 13% of the measured plasma concentration with good precision (CV<20%), meeting recommended acceptance criteria for HPLC-AMS assays [124].

In the current study, method development was simplified as information regarding the PK profiles and expected plasma metabolites of each analyte was available. With NCEs, information regarding metabolism and PK is often limited and although cassette microdosing has its value, the unavailability of a suitable analytical technique may limit its use. Administration of several NCEs within a cassette microdose would allow PK data to be obtained for multiple compounds within a single clinical trial. A recent publication by a separate research group corroborates this use of cassette microdosing [117].

The PK data obtained after administration of a cassette microdose was shown to be quantitatively consistent with previously reported data for therapeutic doses. The study represents the first report of microdose PK data for caffeine and tolbutamide. Although the data were obtained from a relatively small number of subjects, microdosing was able to detect differences in PK parameters potentially attributable to CYP polymorphisms. The application of microdosing would be

particularly useful for detecting CYP2C9 polymorphisms, which vary widely across populations.

PK parameters for each analyte determined after cassette microdose administration were significantly altered on co-administration of inhibitors. The magnitude of DDIs in humans is often difficult to predict prior to clinical studies. The microdose DDI approach allows early identification of interactions involving CYP or P-gp. The use of a microdose is not sufficient to cause enzyme saturation or show dose dependent effects and as a result, DDIs detected after a microdose may appear more pronounced than with therapeutic doses of an NCE. The observation of a DDI may be sufficient to enable a decision to be made as to whether to continue or abandon the development of the NCE.

The ability to determine PKs of enantiomers after administration of a racemic drug was explored. In the same way as in the cassette microdose study, complete resolution of *R*- and *S*-verapamil was achieved using a 2D-HPLC method. Each analyte was quantified via a recovery constant which was derived from a recovery curve method. Mean accuracy for both analytes was within 12% of the measured plasma concentration with good precision (CV<18%), meeting published recommended acceptance criteria for HPLC-AMS assays. The method differed slightly from that developed for cassette microdosing in that each clinical plasma sample was subjected to two-dimensional chromatography, not just those samples selected for verification of analyte purity. This method is particularly applicable where the quantification of the target analyte is hindered by the presence of a co-eluting metabolite.

In agreement with previous studies, significant differences in several PK parameters were observed for *R*- and *S*-verapamil. *S*-verapamil showed higher clearance and a larger volume of distribution when compared to *R*-verapamil. Significant differences were not observed for either enantiomer after microdose only vs. microdose concomitantly with a therapeutic dose. This is the first report of the separation and quantification of enantiomers by HPLC-AMS after administration of a racemic microdose, which supports the applicability of the method in the study of enantiomeric mixtures in the early phases of drug

development. *S*-verapamil is the pharmacologically active enantiomer and, although verapamil is administered in its racemic form, identification of enantiomeric PK differences may be advantageous in optimizing the development of racemic NCEs.

PK data obtained in the brain and arterial plasma for ^{11}C-*R*-verapamil were consistent with the data simultaneously obtained for ^{14}C-*R*-verapamil, confirming the benefit of combining AMS and PET. Combination of AMS and PET microdosing in a single clinical study allows long-term PK data to be obtained along with tissue distribution data in the same subjects. Addition of a ^{14}C-labelled microdose to an existing PET study allows valuable information to be obtained without significant additional resource.

6.2 Future work and applications

Administration of a number of drugs within a cassette allows PKs to be obtained for all compounds in the same subjects after a single dose. In addition to developing a method capable of completely resolving each analyte prior to AMS analysis, an additional challenge in a study of this type is the development of an analytical technique capable of quantification of each NCE, as the maximum permitted dose of 100 µg is shared between the components of the cassette. Although LC-MS/MS has been shown to be capable of quantifying analyte concentrations after microdose administration (typically 100 µg doses), quantification becomes more challenging as the dose decreases. Estimations of the analyte LOQ may be made prior to commencing with a microdosing study, although are not always possible, due to limited NCE metabolism information. AMS, therefore, may be a more suitable technique in cases where a separation technique capable of resolving all analytes is also readily available or developed with minimal resource.

The addition of a DDI study to an existing microdose NCE study could provide valuable data. A simple study design would involve the administration of the NCE alone and with therapeutic doses of CYP or transporter inhibitors. This approach was reported by a separate research group in 2011 and further supports

the application of microdosing in detecting DDIs [116]. Another useful development would be to replace the inhibitors with inducers, with a study design similar to the inhibitor assessment reported in this thesis. If this concept was proven an efficient way of identifying induction effects, this may be added to the inhibitor study described above.

Microdosing may be useful in obtaining PK data from humans in the disease state, for example subjects who are hepatically or renally impaired. Because of ethical constraints, it is difficult to assess the magnitude that such impairments have on the metabolism and PKs of drugs, as the normal dose levels required may be harmful. Administering a microdose to patients and to healthy volunteers (where baseline data are required) and comparing the PKs obtained would be a valuable application of the technology. In addition, the examination of DDIs and the differences in the magnitude of such interactions may be explored using a study design similar to that reported in the thesis, without causing harm to the volunteer. This approach would also be useful in the study of DDIs in the elderly, who are particularly vulnerable to DDIs and are often prescribed multiple drugs that are taken concomitantly.

The addition of a ^{14}C-labelled microdose to a PET study has a wide range of applications, particularly in the determination of PK together with the location of a drug within the body. This approach would be of particular interest in cancer studies with a tumour being the target tissue. The study would involve the concomitant administration of an IV dose of the drug labeled with both a positron emitter and a ^{14}C label and an oral therapeutic dose. This approach would allow absolute bioavailability data to be obtained together with information regarding the IV PK of the drugs and the amount of drug reaching the target tissue. An area of recent research in cancer treatment is the co-administration of cancer therapies with P-gp inhibitors to reduce the efflux of the drug from the tissue. Administration of the dose described above with and without a P-gp inhibitor would enable the effectiveness of co-administration to be assessed and would provide an insight into the effect of the P-gp inhibitor on the plasma PKs.

An investigation that could be carried out to extend the current study would involve the quantification of the individual metabolites of *R*- and *S*-verapamil in plasma. Although the differences in the PKs of *R*- and *S*-verapamil are well documented, the mechanisms underlying the differences are not as well defined. Quantification of the major *N*-demethylation, *O*-demethylation and *N*-dealkylation metabolites of *R*- and *S*-verapamil would provide information regarding the major routes of metabolism. A further study could then be conducted to examine the metabolite concentrations for a microdose compared to therapeutic doses, particularly in the expected range where dose dependent effects may be observed. Differences in metabolite concentrations could then be used to determine the metabolic pathways(s) affected by enzyme or transporter saturation after administration of increasing doses of verapamil.

The applications of microdosing presented here have the potential to identify at the earliest stage of drug development NCEs with poor PK profiles, or those that pose significant risk due to DDIs. Studying the distribution of a drug along with its plasma PK after microdose administration, provides valuable data which cannot currently be easily obtained during phase 0 studies with any other approach. Obtaining such data prior to a phase 1 clinical trial allows resources to be used most effectively, increasing the efficiency of a drug development program.

CHAPTER 7

Materials and methods

7.1 Chemicals

7.1.1 Reagents used in preparation of reference material, protein precipitation and HPLC analysis

HPLC grade water, acetonitrile, methanol and formic acid were purchased from Fisher Scientific (Leicestershire, UK). Ethanol, ammonium acetate (≥98%), potassium hexafluorophosphate (>99.5%), and monobasic potassium phosphate (≥98%) were purchased from Sigma Aldrich Company Ltd (Dorset, UK).

7.1.2 Reagents used in LSC analysis

Gold Star liquid scintillant was obtained from Meridian Biotechnologies Ltd, South Yorkshire, UK.

7.1.3 Reagents used in the graphitisation process

Liquid paraffin was purchased from Lloyds Pharmacy (Coventry, UK). Copper (II) oxide wire, cobalt powder (100 mesh, 99.9%), zinc powder (100 mesh, 99.9%), titanium (II) hydride (325 mesh, 98%) and aluminium powder were purchased from Sigma Aldrich Company Ltd (Dorset, UK). Synthetic graphite (200 – 325 mesh, 99.99%) was purchased from Alfa Aesar (Lancashire, UK). Australian National University (ANU) sugar was purchased from Quaternary Dating Research Centre, Australian National University (Canberra, Australia).

7.2 Reference material

7.2.1 Control plasma

Control non-filtered plasma (K_2EDTA) was obtained from BioReclamation (New York, USA).

7.2.2 Non-labelled reference material

Caffeine, paraxanthine, theobromine, theophylline, fexofenadine, tolbutamide, 4-hydroxytolbutamide, carboxytolbutamide, 1'-hydroxymidazolam, 4-hydroxymidazolam, fexofenadine, *R/S*-verapamil, *R*-verapamil and *S*-

verapamil were obtained from Sigma-Aldrich Company Ltd. (Dorset, UK). Midazolam HCl was obtained from Toronto Research Chemicals (Ontario, Canada). All reference material was obtained at >98% purity.

7.2.3 ^{14}C-labelled reference material

^{14}C-caffeine (1,3,7-trimethyl-[^{14}C]-1*H*-purine-2,6(3*H*,7*H*)-dione) and ^{14}C-tolbutamide (3-butyl-1-(4-methylphenyl)-[^{14}C]-sulfonyl-urea) were supplied by American Radiolabelled Chemicals Inc. (Cardiff, UK) with specific activities of 1.93 GBq/mmol and 2.04 GBq/mmol and radiopurities of >96% and >99%, respectively.^{14}C-fexofenadine(2-[4-[1-hydroxy-4-[4-(hydroxy-diphenyl-[^{14}C]-ethyl)-1-piperidyl]butyl]phenyl]-2-methyl-propanoic acid), with a specific activity of 1.86 Gbq/mmol, was a gift from Sanofi-Aventis (Germany), and was re-purified by Biodynamics (Northamptonshire, UK) to a radiopurity of 98.9%. ^{14}C-midazolam (4H-imidazo(1,5-a)-[^{14}C]-(1,4)benzodiazepine,8-chloro-6-(2-fluorophenyl)-1-ethyl) was supplied by F. Hoffman La Roche (Basel, Switzerland) with a specific activity of 1.9 GBq/mmol and radiopurity of >98%. ^{14}C-verapamil (2-(3,4-dimethoxyphenyl)-5-{2-(3,4-dimethyoxyphenyl)ethyl-[^{14}C]-methylamino]-propan-2-ylpentanenitrile) was supplied by Biodynamics Research (Northamptonshire, UK) with a specific activity of 0.94 GBq/mmol and a radiopurity of >98%.

7.2.4 Preparation of reference standard solutions

All reference material was dispensed using an AT200 analytical balance (Mettler Toledo, Leicestershire, UK). Solvent addition was performed using calibrated pipettes (Rainin LTS, Mettler Toledo, Leicestershire, UK). All verapamil reference material was prepared in ethanol and the remainder prepared in acetonitrile, except where otherwise stated. Solutions for determination of detector linearity were prepared at 200 – 1000 µg/mL (caffeine and tolbutamide), 400 – 2000 µg/mL (midazolam and fexofenadine) and 3.13 – 1000 µg/mL for verapamil. All other reference standard solutions were prepared at 1 mg/mL except where otherwise stated.

7.3 Preparation of internal standard solutions

7.3.1 Preparation of caffeine, midazolam, tolbutamide and fexofenadine internal standard solution

Non-labelled caffeine, midazolam, tolbutamide and fexofenadine (1.5 mg; Section 7.2.2) were dispensed into a 1 mL volumetric flask using an AT200 analytical balance (Mettler Toledo, Leicestershire, UK). Acetonitrile was added to the mark and the solution was vortex-mixed. Where larger volumes of internal standard solution were required, the weights and volumes were scaled accordingly.

7.3.2 Preparation of verapamil internal standard solution

Non-labelled verapamil (783 µg; Section 7.2.2) was dispensed into a 10 mL volumetric flask using an AT200 analytical balance (Mettler Toledo, Leicestershire, UK). Ethanol was added to the mark and the solution was vortex-mixed. Where larger volumes of internal standard solution were required, the weights and volumes were scaled appropriately.

7.4 Preparation of recovery standard and QC plasma

7.4.1 Preparation of caffeine, midazolam, tolbutamide and fexofenadine recovery standard and QC plasma

Stock solutions of ^{14}C-caffeine, ^{14}C-midazolam, ^{14}C-tolbutamide and ^{14}C-fexofenadine (Section 7.2.3) were diluted to a concentration of 2.5 x 10^5 dpm/mL in acetonitrile. Each ^{14}C-stock solution was serially diluted (Table 68) to generate recovery standard and QC spiking solutions.

Table 68: Preparation of recovery standard and QC spiking solutions.

Sample ID	^{14}C solution taken	^{14}C concentration (dpm/mL)	Volume of ^{14}C-stock solution	Volume of acetonitrile (µL)	Final ^{14}C concentration (dpm/mL)
Recovery standard 1	Diluted ^{14}C-stock solution	250000	20	4980	1000
Recovery standard 2	Recovery standard 1	1000	2000	2000	500
Recovery standard 3	Recovery standard 2	500	1000	1000	250
Recovery standard 4	Recovery standard 3	250	1000	1000	125
QC	Recovery standard 4	125	320	1680	20
Zero	N/A	0	0	2000	0

Spiking solutions and QC stock solutions (150 µL) were added to control human plasma (2850 µL; Section 7.2.1) to generate recovery standards at target concentrations of approximately 50, 25, 12.5 and 6.25 dpm/mL, and QC plasma at a concentration of approximately 1 dpm/mL.

7.4.2 Preparation of verapamil recovery standard and QC plasma

^{14}C-verapamil stock solution (10 µL; Section 7.2.3) was diluted with internal standard solution (Section 7.3.2) to a concentration of 3125 dpm/mL and 78.3 µg/mL. The ^{14}C-stock solution was serially diluted (Table 69) with non-labelled verapamil (78.3 µg/mL) to generate recovery standard and QC spiking solutions.

Table 69: Preparation of recovery standard and QC spiking solutions.

Sample ID	^{14}C solution taken	^{14}C concentration (dpm/mL)	Volume of ^{14}C-stock solution (µL)	Volume of non-labelled standard in acetonitrile (µL)	Final ^{14}C concentration (dpm/mL)
Recovery standard 1	Diluted ^{14}C-stock solution	3125	100	2500	120
Recovery standard 2	Recovery standard 1	120	1000	1000	60
Recovery standard 3	Recovery standard 2	60	400	1600	12
Recovery standard 4	Recovery standard 3	12	1000	1000	6
Recovery standard 5	Recovery standard 4	6	10	990	0.06
QC	Recovery standard 1	40	500	1000	40
Zero (LOQ)	N/A	0	0	2000	0

Spiking solutions and QC stock solutions (150 µL) were added to control human plasma (2250 µL; Section 7.2.1) to generate recovery standards at target concentrations of approximately 7.5, 3.75, 0.78, 0.0375 and 0.00375 dpm/mL and QC plasma at a concentration of approximately 2.5 dpm/mL. The final mass concentration of each plasma sample was 4.9 µg/mL.

7.5 Methods for determination of extraction efficiency

All protein precipitation extractions were performed using a Sirocco protein precipitation extraction (PPE) plate (Waters, Hertfordshire, UK).

7.5.1 Protein precipitation extraction method development for caffeine, midazolam, tolbutamide and fexofenadine from plasma (Method 1, 2a, 2b and 3)

Stock solutions of ^{14}C-caffeine, ^{14}C-midazolam, ^{14}C-tolbutamide and ^{14}C-fexofenadine (Section 7.2.3) were spiked into plasma (Section 7.2.1; Table 70).

Table 70: Preparation of spiked plasma

Analyte	Concentration of stock solution (dpm/mL)	Volume of stock solution (µL)	Volume of plasma (µL)
Caffeine	2.30×10^6	10	2295
Midazolam	2.48×10^6	10	2475
Tolbutamide	1.81×10^6	10	1805
Fexofenadine	2.88×10^6	10	2880

Accurate plasma concentrations of ^{14}C-caffeine, ^{14}C-midazolam, ^{14}C-tolbutamide and ^{14}C-fexofenadine were determined by direct analysis of each sample (2 x 100 µL) by LSC (Section 7.9). Protein precipitation solvent and plasma (*n*=2) were added to wells of the PPE plate (Table 71). The plate was agitated (15 min) and placed under vacuum until the filtrate was collected (approximately 20 min). Plasma filtrates were analysed by LSC (entire filtrate volume, Section 7.9).

Table 71: Sample volumes for protein precipitation extraction Method 1, Method 2a, Method 2b and Method 3.

Method	Volume of plasma extracted (µL)	Extraction solvent /volume (µL)	Reduction and reconstitution assessed?
1	200	Acetonitrile / 600	Y
2a	100	Acetonitrile / 200	N
2b	100	Acetonitrile / 300	N
3	100	Methanol / 200	N

Additional samples (*n*=2) were subjected to PPE for Method 1 only. The resulting filtrates were reduced to complete dryness under N_2 and reconstituted in acetonitrile (200 µL). Reconstituted plasma filtrates were analysed by LSC (entire filtrate volume; Section 7.9).

7.5.2 Protein precipitation extraction method development for verapamil

A stock solution of ^{14}C-verapamil (1×10^5 dpm/mL) was prepared in ethanol and spiked (200 µL) into plasma (3800 µL; Section 7.2.1). The plasma concentration was confirmed by direct analysis of each sample (2 x 200 µL) by LSC (Section

7.9). Protein precipitation solvent (600 µL) and plasma (200 µL; *n*=3) were added to wells of a PPE plate (Waters, Hertfordshire, UK; Table 72).

Table 72: Sample volumes for verapamil protein precipitation.

Method	Extraction solvent /volume (µL)	Reduction and reconstitution assessed?
1	Acetonitrile	N
2	Acetonitrile	Y
3	Methanol	N
4	Methanol	Y

The plate was agitated (15 min) and placed under vacuum until the filtrate was collected (approximately 20 min). Where an additional reduction and reconstitution step was required, filtrates were reduced to complete dryness under a stream of N_2 gas and the dried filtrate reconstituted in 50 mM potassium hexafluorophosphate: acetonitrile 60:40 v/v (200 µL). Each filtrate (entire volume) was analysed by LSC (Section 7.9).

7.6 Preparation and analysis of plasma filtrates for assessment of HPLC method compatibility

7.6.1 Preparation and analysis of plasma filtrate containing caffeine, midazolam, tolbutamide and fexofenadine for HPLC Method A3 assessment

Equal volumes of pre-dose human plasma from all subjects (Section 7.12.2) were combined to create a single pooled plasma sample. Non-labelled caffeine reference standard (20 µL; 1 mg/mL; Section 7.2.4) was added to pooled pre-dose plasma (980 µL). Three further spiked plasma samples were prepared in the same way, each containing midazolam, tolbutamide or fexofenadine.

Plasma (100 µL) was added to the wells of a PPE plate containing acetonitrile (200 µL; Method 2a) or methanol (200 µL; Method 3). The plate was agitated (15 min) and placed under vacuum until the filtrate was collected (approximately

20 min). Aliquots of each filtrate (100 µL) were analysed by HPLC under Method A2 conditions (Section 7.8.1).

7.6.2 Preparation and analysis of plasma filtrate for HPLC Method A3 assessment

Equal volumes of pre-dose human plasma from all subjects (Section 7.12.2) were combined to create a single pooled plasma sample. Plasma (100 µL) was added to methanol in the wells of a PPE plate. The plate was agitated (15 min) and placed under vacuum until the filtrate was collected (approximately 20 min). Aliquots of each filtrate (100 µL) were analysed by HPLC under Method A2 conditions (Section 7.8.1).

7.6.3 Preparation and analysis of plasma filtrate for verification of caffeine, midazolam, tolbutamide and fexofenadine separation in clinical plasma

Clinical plasma (100 µL; Section 7.12.4) was pooled across all subjects at the following time-points to yield eight pooled plasma samples:

- 1, 6, 12 and 24 h post administration, dosing period 1;
- 1,6,12 and 24 h post administration, dosing period 2.

Caffeine, midazolam, tolbutamide and fexofenadine were dispensed (6 mg of each) into a single vial and acetonitrile (1 mL) added. The solution (10 µL) was added to aliquots of each of the prepared pooled plasma samples (190 µL). Plasma (100 µL) was added to the wells of a PPE plate containing methanol (200 µL). The plate was agitated (15 min) and placed under vacuum until the filtrate was collected (approximately 20 min). Aliquots of each filtrate (100 µL) were analysed by HPLC under Method A3 conditions (Section 7.8.1). Fractions were collected across the retention times of caffeine, midazolam, tolbutamide and fexofenadine. HPLC fractions were reduced to approximately 100 µL under N_2 and analysed by HPLC with phenyl stationary phase using Method B1 to Method B4 (Section 7.8.1). HPLC fractions at the retention times of caffeine, midazolam, tolbutamide and fexofenadine were collected and analysed by AMS

(Section 7.11). HPLC fraction concentrations were calculated via Equation 16 (Section 2.3.6.2).

7.6.4 Assessment of compatibility of protein precipitation extraction method with HPLC method C1

Clinical pre-dose human plasma samples (Section 7.12.4) collected from all subjects were combined (100 µL) as follows:

- plasma obtained from microdose only (period 1) – subjects 1, 3, 4, 5, 6 and 7;

- plasma obtained from microdose plus therapeutic dose (period 2) – subjects 1 – 7

Pooled pre-dose plasma (200 µL) was added to wells of a PPE plate containing acetonitrile (600 µL). The plate was agitated (15 min) and placed under vacuum until the filtrate was collected (approximately 20 min). Filtrates were reduced to complete dryness under N_2 and dried filtrates were reconstituted in 50 mM potassium hexafluorophosphate: acetonitrile 60:40 v/v (200 µL). Aliquots of each filtrate (50 µL) were analysed by HPLC under Method C1 conditions (Section 7.8.2).

7.6.5 Preparation and analysis of samples for assessment of verapamil fraction alignment and isotopic fractionation

Equal volumes (100 µL) of human plasma collected from all subjects at 0.5 h (Section 7.12.4) were combined (period 1 only). Pooled plasma (240 µL) was spiked with non-labelled verapamil in ethanol (1 mg/mL; 10 µL; Section 7.2.4). Pooled spiked plasma (200 µL) was added to wells of a PPE extraction plate containing acetonitrile (600 µL). The plate was agitated (15 min) and placed under vacuum until the filtrate was collected (approximately 20 min). Filtrates were reduced to complete dryness under N_2 and dried filtrates were reconstituted in 50 mM potassium hexafluorophosphate: acetonitrile 60:40 v/v (200 µL). Aliquots of each filtrate (50 µL) were analysed by HPLC under Method C1 conditions (Section 7.8.2).

7.6.6 Preparation and analysis of plasma filtrates for verification of the chromatographic separation of *R*- and *S*-verapamil

Equal volumes (100 µL) of human plasma collected from all subjects at 1, 5, 12 and 24 h (Section 7.12.4) were combined to create four plasma pools.

- microdose only – 5 and 12 h post administration;
- microdose and therapeutic dose – 1 and 24 h post administration.

Each plasma sample (300 µL) was spiked with non-labelled verapamil (20 µL; 1 mg/mL; Section 7.2.4). Pooled spiked plasma (200 µL) was added to wells of a PPE plate containing acetonitrile (600 µL). The plate was agitated (15 min) and placed under vacuum until the filtrate was collected (approximately 20 min). Filtrates were reduced to complete dryness under N_2 and dried filtrates were reconstituted in 50 mM potassium hexafluorophosphate: acetonitrile 60:40 v/v (200 µL). Aliquots of each filtrate (50 µL) were analysed by HPLC under Method C1 conditions (Section 7.8.2). Discrete fractions of approximately 0.5 min were collected across the retention times for *R*- and *S*-verapamil. HPLC fractions were reduced to dryness under N_2 and reconstituted in initial mobile phase composition (100 µL; Method D1; Section 7.8.2). An aliquot (95 µL) of each reconstituted eluate was analysed by HPLC using C18 Method D1 (Section 7.8.2).

Fractions of 15 s duration collected over the second dimension separation for *R*- and *S*-verapamil were analysed by AMS and the concentration (dpm/fraction) determined via Equation 14 (Section 2.3.6.2).

7.7 Preparation of plasma filtrates from clinical, recovery standard and QC plasma

7.7.1 Preparation of plasma filtrates from clinical, recovery standard and QC plasma containing caffeine, midazolam, tolbutamide and fexofenadine

Plasma (190 µL) was spiked with internal standard (10 µL; Section 7.3.1). Methanol (200 µL) and spiked plasma (100 µL) were added to wells of a PPE

plate. The plate was agitated (15 min) and placed under vacuum until all the filtrate was collected (approximately 20 min).

7.7.2 Preparation of plasma filtrates from clinical, recovery standard and QC plasma containing verapamil

Clinical plasma (225 µL) was spiked with verapamil internal standard (Section 7.3.2). Acetonitrile (600 µL) and spiked clinical plasma (200 µL), recovery standard and QC plasma were added to wells of a PPE plate (Waters, Hertfordshire, UK). The plate was agitated (15 min) and placed under vacuum until all the filtrate was collected (approximately 20 min). The filtrate was reduced to complete dryness under N_2 followed by reconstitution in 50 mM potassium hexafluorophosphate: acetonitrile 60:40 v/v (200 µL).

7.8 HPLC methods

All HPLC analysis was carried out using an Agilent 1200 series HPLC system fitted with a 96-well plate fraction collector (Agilent Technologies, Berkshire, UK) with the exception of the analysis of cassette dosing solutions which was performed using a Shimadzu LC10 (Shimadzu, Buckinghamshire, UK).

7.8.1 HPLC methods for separation of caffeine, midazolam, tolbutamide and fexofenadine

Reference standards (5-10 µL), plasma filtrates (50-100 µL) and reconstituted HPLC fractions (95-100 µL) were analysed under the following chromatographic conditions.

Table 73: HPLC Conditions for separation of caffeine, midazolam, tolbutamide and fexofenadine (Method A1).

Column	XTerra MS C18, 5 µm, 4.6 x 250 mm (Waters, Hertfordshire, UK)	
Column temperature	40°C	
Flow rate	1 mL/min	
UV detection	240 nm (midazolam, tolbutamide), 270 nm (caffeine),	
Fl detection	220 nm (ex) and 290 nm (em)	
Time (min)	0.1 M ammonium acetate (%)	Acetonitrile (%)
0 – 20	50	50

Table 74: HPLC Conditions for separation of caffeine, midazolam, tolbutamide and fexofenadine (Method A2).

Column	XTerra MS C18, 5 µm, 4.6 x 250 mm (Waters, Hertfordshire, UK)	
Column temperature	40°C	
Flow rate	1 mL/min	
UV detection	240 nm (midazolam, tolbutamide), 270 nm (caffeine),	
Fl detection	220 nm (ex) and 290 nm (em)	
Time (min)	0.1 M ammonium acetate (%)	Acetonitrile (%)
0	90	10
15	50	50

Table 75: HPLC Conditions for separation of caffeine, midazolam, tolbutamide and fexofenadine (Method A3).

Column	XTerra MS C18, 5 µm, 4.6 x 250 mm (Waters, Hertfordshire, UK)	
Column temperature	40°C	
Flow rate	1 mL/min	
UV detection	240 nm (midazolam, tolbutamide), 270 nm (caffeine),	
Fl detection	220 nm (ex) and 290 nm (em)	
Time (min)	0.1 M ammonium acetate (%)	Acetonitrile (%)
0	90	10
7	81	19
8	80	20
9	79	21
11	66	34
14	62	38
20	50	50
22	10	90

Table 76: HPLC Conditions for resolution of caffeine (Method B1).

Column	Synergi Polar RP, 4 µm, 4.6 x 250 mm (Phenomenex, Cheshire, UK)	
Column temperature	40°C	
Flow rate	1 mL/min	
UV detection	270 nm	
Time (min)	Water (%)	Methanol (%)
0	90	10
3	50	50
5	10	90
8	10	90

Table 77: HPLC Conditions for resolution of midazolam (Method B2).

Column	Synergi Polar RP, 4 µm, 4.6 x 250 mm (Phenomenex, Cheshire, UK)	
Column temperature	40°C	
Flow rate	1 mL/min	
UV detection	240 nm	
Time (min)	10 mM potassium phosphate (%)	Acetonitrile (%)
0	90	10
3	50	50
10	0	100
11	0	100

Table 78: HPLC Conditions for resolution of tolbutamide (Method B3).

Column	Gemini C6 phenyl, 3 µm, 4.6 x 150 mm (Phenomenex, Cheshire, UK)	
Column temperature	40°C	
Flow rate	1 mL/min	
UV detection	240 nm	
Time (min)	0.1% formic acid (%)	Methanol (%)
0	70	30
25	10	90

Table 79: HPLC Conditions for resolution of fexofenadine (Method B4).

Column	Gemini C6 phenyl, 3 µm, 4.6 x 150 mm (Phenomenex, Cheshire, UK)	
Column temperature	40°C	
Flow rate	1 mL/min	
Fl detection	220 nm (ex) and 290 nm (em)	
Time (min)	Water (%)	Acetonitrile (%)
0	90	10
10	10	90

7.8.2 HPLC methods for separation of *R*- and *S*-verapamil

Table 80: HPLC Conditions for separation of *R*- and *S*-verapamil (Method C1).

Column	Lux Cellulose-1, 3 µm, 250 x 4.6 mm (Phenomenex, Cheshire, UK)	
Column temperature	25°C	
Flow rate	1 mL/min	
UV detection	220 nm	
Fl detection	276 nm (ex) and 310 nm (em)	
Time (min)	50 mM potassium hexafluorophosphate (%)	Acetonitrile (%)
0	60	40
25	40	60
30	10	90
32	10	90

NB: Shimadzu LC10 was used for the analysis of dosing solution, Agilent 1200 used for all other analysis

Table 81: HPLC Conditions for isolation of verapamil (Method D1).

Column	XTerra MS C18, 5 µm, 4.6 x 250 mm (Waters, Hertfordshire, UK)	
Column temperature	25°C	
Flow rate	1 mL/min	
Fl detection	276 nm (ex) and 310 nm (em)	
Time (min)	20 mM potassium phosphate (aq.) (%)	Acetonitrile: Methanol 22:35 v/v (%)
0.0	90	10
5.0	43	57
12.0	43	57
13.5	20	80
15.0	10	90
18.0	10	90

7.9 LSC analysis

Sample aliquots were added directly to Gold Star liquid scintillant in a liquid scintillation vial. A blank sample was prepared, comprising liquid scintillant only and used for background subtraction. The vials were capped, gently shaken and dark adapted for at least 1 h in a Tricarb 2770 TR liquid scintillation counter (Perkin Elmer, Cambridgeshire, UK) before counting to 2%2σ [187]. The

number of counts per min (cpm) for each sample aliquot was converted to dpm using Equation 33.

$$dpm = (cpm\,(sample) - cpm\,(blank)) \times \left(\frac{100}{count\ efficiency\,(\%)} \right) \qquad \textbf{Equation 33}$$

7.10 Spectrophotometric analysis of caffeine, midazolam and tolbutamide

A Shimadzu 1600 UV-visible spectrophotometer (Shimadzu, Buckinghamshire, UK) was used to determine the λ_{max} prior to HPLC analysis. A system performance check was performed and the baseline set to zero. Samples were analysed in spectrum mode from 180 nm to 350 nm and the λ_{max} recorded.

7.11 AMS analysis

7.11.1 Preparation of samples for AMS analysis

Sample aliquots were added to quartz sample tubes containing copper (II) oxide (40 ± 10 mg) and liquid paraffin (containing 1.7 ± 0.17 mg carbon) and the aliquot volumes recorded. Plasma samples were analysed with copper (II) oxide only. Aliquot volumes are summarised in Table 82.

Table 82: Sample volumes taken for analysis by AMS

Sample type	Aliquot volume (µL)
Plasma	60
^{12}C-reference standards (1 mg/mL solution)	200
^{14}C-caffeine, midazolam, tolbutamide & fexofenadine spiking	50
^{14}C-verapamil spiking solutions	50
HPLC fractions (containing ^{14}C caffeine)	375 (250)
HPLC fractions (containing ^{14}C fexofenadine)	375 (250)
HPLC fractions (containing ^{14}C midazolam)	250 (150)
HPLC fractions (containing ^{14}C tolbutamide)	250 (150)
HPLC fractions (containing ^{14}C *R*-and S- verapamil)	500 (300)

*values in parentheses are volumes used in repeat analysis

The following process controls were dispensed:

- Copper (II) oxide and liquid paraffin (*n*=7), used to determine pMC of isotopic dilutor for background subtraction;

- Copper (II) oxide and ANU sugar (*n*=6), used for data acceptance;

- Copper (II) oxide and graphite (*n*=4), used to show ^{14}C contamination had not occurred during sample processing;

The maximum number of samples processed with each batch of controls was 110. Glass tubes were placed in a rotary evaporator (Savant environmental speedvac, Thermo Fisher, Leicestershire, UK) and reduced to complete dryness. Dried samples were subjected to graphitisation as described in brief in Section 1.10.2 and according to Garner et al. [188]. The borosilicate glass tube containing the graphite formed during the process was removed and carefully tipped into an aluminium cathode and compressed to form a tablet. The samples and controls were placed into a 134-position AMS sample wheel for analysis. In addition to the process controls, the wheel also contained a solid aluminium cathode (National Electrostatics Corp, Middleton, WI, USA) and two pre-prepared synthetic graphite samples (machine blank) and a graphite sample (POCO Graphite Inc, Decatur, TX, USA) containing depleted levels of ^{14}C which was used for instrument tuning. In addition, pre-prepared graphitised ANU sugar (*n*=3) was also added for normalisation.

7.11.2 AMS analysis of graphite samples

The sample wheel was placed into the multi-cathode negative ion source (MC-SNICS, NEC, WI, USA) [188] of the NEC 15SDH pelletron accelerator mass spectrometer (National Electrostatics Corp, Middleton, WI, USA). The burn time for each sample was set to 600 cycles, with 1000 cycles (100.7 s) for each analysis.

7.11.3 AMS sample acceptance criteria

Analyses were considered acceptable for sample and controls where the current was ≥ 1 μAmp, $^{13}C/^{12}C$ ratio was <1.1 ± 15% and at least three measurements were made on each cathode. Where a sample exceeded the maximum number of counts, three full measurements were not made and the data were rejected. A minimum of four ANU sugar, five liquid paraffin and two process graphite cathodes were required to meet the following acceptance criteria:

1. Process graphite – pMC≤8
2. ANU sugar – pMC =150.61± 15%
3. Liquid paraffin – pMC≤8

In addition machine and process control were required to meet the following acceptance criteria:

1. Synthetic graphite – pMC≤3
2. ANU sugar – pMC = 150.61±15%

Where the minimum number of standards and controls failed to meet the acceptance criteria, the data for the entire wheel were rejected and the samples were reprocessed.

7.11.4 Limit of quantification

7.11.4.1 Limit of quantification for method development

The LOQ for each sample batch was calculated by a statistical method as detailed by Young et al. [189]. The isotopic ratio of the isotopic dilutor (liquid paraffin, *n*=7) analysed with each batch of samples (≤110) was determined. The LOQ was determined as the mean liquid paraffin + 5xSD.

7.11.4.2 Limit of quantification for caffeine, midazolam, tolbutamide and fexofenadine in clinical plasma

The LOQ was determined from all liquid paraffin samples analysed throughout the 28 sample batches containing recovery curve, QC and clinical plasma HPLC fractions. The LOQ was determined using the statistical method stated above (Section 7.11.4.1) as 3.833 pMC.

7.11.4.3 Limit of quantification for verapamil in clinical plasma

The LOQ was determined from control plasma (n=5) which was processed with the recovery curve, QC and clinical plasma samples. The LOQ was determined using the statistical method stated above (Section 7.11.4.1) as 1.611 pMC (*R*-verapamil) and 1.696 pMC (*S*-verapamil).

7.12 Clinical study design and sample collection

7.12.1 Preparation of cassette dosing solutions

^{14}C-caffeine, ^{14}C-fexofenadine, ^{14}C-tolbutamide and ^{14}C-midazolam (Section 7.2.3) were prepared in ethanol and the concentration of each solution determined by LSC (Section 7.9). Caffeine, midazolam, tolbutamide and fexofenadine (Section 7.2.2) were prepared in ethanol (1 mg/mL) and added (625 µL) to a volumetric flask. In addition, aliquots of ^{14}C-labelled caffeine, midazolam, tolbutamide, and fexofenadine were added (Table 83). Evian bottled mineral water (450 mL) was added and the flask filled to the mark with ethanol. The final solution was mixed well and sub-aliquoted (18 x 24 mL) and shipped to the clinic for dosing. Dosing solutions were stored at 4°C for 24 days throughout the clinical study and routinely analysed to ensure sample integrity was maintained prior to dosing.

Table 83: Caffeine, tolbutamide, midazolam and fexofenadine dose solution analysis and determination of specific radioactivity.

Analyte	^{14}C-concentration (dpm/mL)	Volume taken (µL)	Amount of non-labelled analyte added (µg)	Specific activity (dpm/µg)
Caffeine	4.59×10^6	604	625	4440
Tolbutamide	4.80×10^6	578	625	4440
Midazolam	3.59×10^6	773	625	4440
Fexofenadine	5.64×10^6	492	625	4440

7.12.2 Cassette dose administration and sample collection

Two hours after breakfast on day 1, a venous pre-dose plasma sample was collected from each of the six volunteers followed by administration of the first cassette microdose, which was taken with 100 mL water. Venous plasma samples were collected at 0.25, 0.5, 0.75, 1, 2, 3, 4, 6, 8, 12, 24, 36, 48 and 72 h after administration. After four days without treatment (days 4-7), fluvoxamine (100 mg tablet) and ketoconazole (2 x 200 mg tablets) were administered orally on day 8 after breakfast with 200 mL water. This administration continued daily to day 17. Two hours after breakfast on day 15, a venous pre-dose plasma sample was collected from each of the six volunteers. Volunteers were administered a second cassette microdose (identical to day 1 administration). Venous plasma samples were collected at 0.25, 0.5, 0.75, 1, 2, 3, 4, 6, 8, 12, 24, 36, 48 and 72 h after cassette microdose administration. Blood samples were collected into pre-chilled vials containing EDTA and the tube inverted several times to ensure mixing. Plasma samples were prepared by centrifugation at 1500 g, for 10 min at 4°C.

7.12.3 Preparation of verapamil dosing solution

An aliquot (20 µL) of non-labelled verapamil solution containing a mass of 50 µg of racemic verapamil (Section 7.2.2.1) was added to a sterile vial containing ^{14}C-verapamil (approximately 4.2×10^5 dpm in 200 µL of ethanol; Section 7.2.3). An aliquot (6 mL) of *R*-^{11}C-verapamil (approximately 2.4×10^{10} dpm) was added to the same vial. *R*-^{11}C-verapamil was prepared in a cyclotron at the

Medical University of Vienna according to the method summarised by Abrahim et al. [169]. The sample was vortex-mixed and filtered (Millex-GS 0.22 µm) into a sterile (10 mL) vial. The solution was diluted to 10 mL with sterile physiological saline solution and transported to the PET camera for dosing.

7.12.4 Verapamil dose administration and sample collection

On study day 1, each subject first ingested 500 mL of tap water. A venous catheter was placed in one arm for drug infusion, and a radial artery catheter was placed in the same arm for arterial blood sampling. A second venous catheter was place in the other arm for parallel venous blood sampling. The radioactivity of the syringe containing the dosing solution was recorded using a well counter and once the ^{11}C activity decreased to <450 MBq (2.7×10^{10} dpm) the dose was administered intravenously over 30 s into the first subject (approximately 2 h after administration of the non-labelled *R*-S verapamil). The ^{11}C activity remaining in the syringes was recorded along with the dose administration end time. This was repeated for the remaining six volunteers. Blood was sampled over a 24 h period and PET analysis performed over the first hour. The PET images were acquired using an Advance PET scanner (General Electrics Medical Systems, WI, USA) run in 3D mode (Appendix 1).

The process was repeated on study day 2 with the addition of an oral therapeutic dose of racemic verapamil (80 mg, Isoptin tablets, Abbott, Vienna), followed 2 h later by a second intravenous dose of labelled drug. Blood sampling and PET analysis was carried out as on study day 1. Venous blood samples were collected for AMS analysis after administration of the microdose only at pre-dose, 0.25, 0.5, 0.75, 1, 2, 3, 4, 6, 8, 12 and 24 h. Venous blood samples were collected at 15, 30, 60 and 120 min after oral administration, plus 0.25, 0.5, 0.75, 1, 2, 3, 4, 6, 8, 12 and 24 h after IV microdose administration. Blood samples were collected into pre-chilled vials and the tube inverted several times to ensure mixing. Plasma was obtained by centrifugation of blood samples at 3000 g, for 10 min at room temperature.

7.13 Pharmacokinetic data analysis

Pharmacokinetic calculations were performed using WinNonLin software, version 4.1 (Pharsight, Mountain View, CA, USA).

7.13.1 Determination of pharmacokinetics of caffeine, midazolam, tolbutamide and fexofenadine

The data input consisted of plasma drug concentrations (pg/mL), plasma sampling times (h) and the administered dose (25 μg). Output consisted of C_{max}, t_{max}, $t_{1/2}$, AUC_{0-t} and $AUC_{0-\infty}$. AUCs were determined using a linear trapezoidal method.

7.13.2 Determination of pharmacokinetics of *R*- and *S*-verapamil

The data input consisted of plasma drug concentrations (pg/mL), plasma sampling times (h) and the administered dose (Section 4.3.11.3). Output consisted of C_{max}, t_{max}, $t_{1/2}$, CL, V, V_{ss}, AUC_{0-t} and $AUC_{0-\infty}$. AUCs were determined using a linear trapezoidal method.

7.14 Statistical data analysis

7.14.1 Statistical analysis of caffeine, midazolam, tolbutamide and fexofenadine data

Statistical analyses were performed in Microsoft Excel. PK data obtained from all subjects after each microdose administration (day 1 and day 15) were assessed for significant differences using a Student's two-tailed t-test. Outliers were determined using Dixon's Q-test.

7.14.2 Statistical analysis of *R*- and *S*-verapamil data

Statistical analyses were performed in Microsoft Excel. PK data obtained from subjects 1, 3, 4, 5, 6 and 7 for each enantiomer after microdose administration (period 1 and period 2) were assessed for significant differences using a Student's two-tailed t-test. Data for each enantiomer measured within the two periods were compared in the same way.

Appendices

Appendix 1. PET analysis

The PET data reported in the following section were produced in their entirety by the Medical University of Vienna. Comparisons of these data with AMS data reported in this thesis are a result of a joint collaboration with Claudia Wagner and Oliver Langer at the University of Vienna.

A1.1 PET and MRI analysis

Imaging was performed with the volunteer positioned supine on the imaging bed of the PET camera, the head in a restraining device to prevent movement during imaging. PET images were acquired with an Advance PET Scanner, which was run in 3D mode with a transversal field of view of 55 cm, axial field of view of 15cm and axial slice thickness of 4.25 mm. A transmission scan was performed prior to radiotracer injection to correct for tissue attenuation of photons. The scan lasted 5 min using 400 MBq ^{68}Ge. After intravenous microdose administration, PET imaging commenced using the following frame sequence: 1 x 15 s, 3 x 5 s, 3 x 10 s, 2 x 30 s, 3 x 60 s, 2 x 150 s, 2 x 300 s and 4 x 600 s. A T1 weighted MRI scan of each subject was recorded 1 month prior to PET scanning and whole brain grey matter region of interested was defined using Hammersmith n30r83 3D maximum probability atlas of the human brain [190]. MRI and PET data were processed as detailed by Langer et al. [180]. Radioactivity concentrations (measured as kBq/g tissue) were converted into pg equivalents per mL using the specific radioactivity of the dose administered. The mass of *R*-verapamil present in the dosing solution was determined in Section 4.3.10. The ^{11}C-concentration was determined by LSC analysis immediately prior to dosing.

A1.2 Blood and metabolite analysis

Arterial blood and plasma concentrations were measured with a Packard Cobra II autogamma counter (Packard Instrument Company, Meridian, CT, USA). The instrument was calibrated with the PET camera.

^{11}C-*R*-verapamil radiometabolite concentrations were quantified via an SPE-HPLC method. The polar metabolites were determined by SPE and lipophilic metabolite concentrations were determined by HPLC.

The arterial input function of ^{11}C-verapamil was corrected to account for polar radio-metabolites.

A1.3 Pharmacokinetic modelling

Standard 1-tissue 2-rate constant (1T2K) or 2-tissue 4-rate (2T4K) compartment models were fitted to concentration-time curves for ^{11}C in whole brain grey matter. Rate constants of radioactivity exchange were estimated (K_1, k_2, k_3 and k_4), along with volume of distribution (V_T).

A1.4 Statistical analysis

Statistical analysis was carried out using STATISTICA software (Release 6.1, StatSoft, Inc, Tulsa, OK, USA). Rate constants (K1, k2, k3, and k4) were compared using the Wilcoxon matched pairs test.

A1.5 PET imaging data

Transaxial PET summation images and MRI images were co-registered in order to determine the area of drug uptake in the brain.

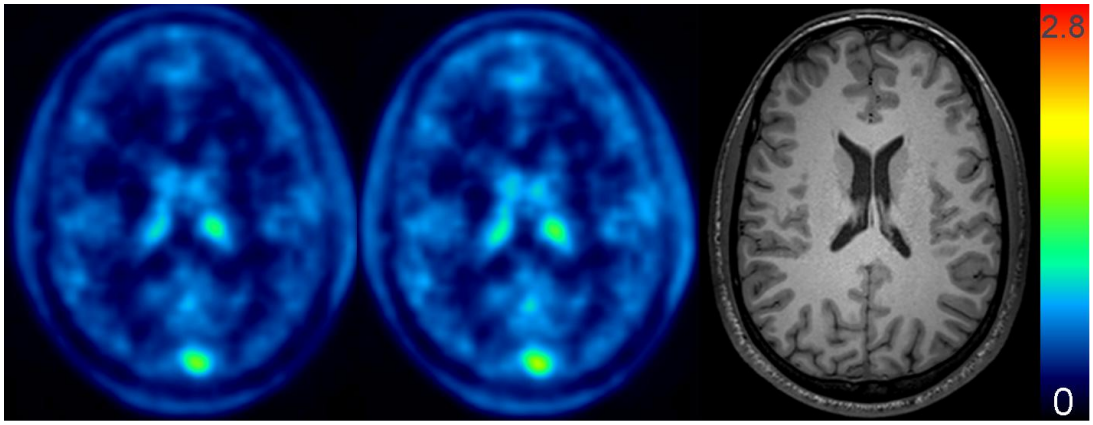

Figure A1.1. PET image of subject 1 brain after period 1 and period 2 microdose administration (left and centre) and MRI scan taken 1 month prior to PET analysis (right)

The activity concentration was normalised to injected dose per subject body weight, and expressed as the standardized uptake value (SUV). Figure A1.1 is a representation of the PET and MRI scans from subject 1 where the radiation scale was set from zero to 2.8 SUV. The PET scan to the left was taken after period 1 dosing and the scan in the middle was taken after period 2 dosing. The MRI scan on the right of the figure shows a transaxial T1-weighted MRI of the same subject. A 2-tissue 4-rate constant model provided the best fit for the PET data and parameter estimates for the exchange of activity between plasma and brain returned from the 2t4k model were calculated.

Table A1.1: Parameters obtained for 2-tissue-4-rate constant (2t4k) compartment model.

Parameter	**[1]Period 1**	**[1]Period 2**
K1 (mL/mL/min)	0.030±0.003 (10)	0.031±0.005 (9)
k2 (min^{-1})	0.099±0.006 (49)	0.095±0.008 (40)
k3 (min^{-1})	0.100±0.001 (90)	0.101±0.000 (96)
k4 (min^{-1})	0.092±0.029 (26)	0.159±0.063 (42)
V_d (mL/mL)	0.66±0.12 (4)	0.56±0.11 (2)
V_T (Logan) (mL/mL)	0.66±0.11 (2)	0.57±0.11 (1)

[1] mean ± SD (%CV)

K_1 and k_2 describe the transport of activity from plasma to and from the first tissue compartment (by P-gp). k_3 and k_4 characterise the exchange of activity between the first and second tissue compartments. There were no significant differences in model outcome parameters between the 2 doses with the exception of k_4 which was higher for dose 2 ($p>0.05$). The volume of distribution (V_d) is not the same as the volume of distribution determined in standard PK analysis. For this specific model V_d is considered an estimate of the brain tissue-plasma partition coefficient at equilibrium. An independent estimate of V_d was determined by application of Logan graphical analysis to PET and arterial plasma data (using MATLAB) to determine V_T. The Logan derived V_T was in good agreement with compartmental derived V_d values.

Appendix 2. Caffeine plasma concentration data

Table A2.1: Caffeine plasma concentration data after oral administration of microdose.

Time (h)	Plasma concentration (pg/mL)								
	Subject 1	Subject 2	Subject 3	Subject 4	Subject 5	Subject 6	Mean	SD	% CV
0	<LOQ	<LOQ	<LOQ	<LOQ	<LOQ	<LOQ	N/A	N/A	N/A
0.25	55.4	183	144	491	171	436	247	175	70.8
0.5	258	425	825	414	791	562	546	225	41.2
0.75	410	476	560	258	690	366	460	152	33.0
1	529	458	431	279	433	331	410	90.4	22.0
2	385	392	286	232	291	275	310	64.2	20.7
3	162	347	204	241	459	203	269	112	41.7
4	273	213	198	163	307	186	223	55.2	24.7
6	128	206	101	76.6	293	108	152	82.0	53.9
8	139	142	90	67.5	248	68.7	126	68.2	54.2
12	58.0	70.7	33.5	12.9	134	22.0	55.2	44.3	80.3
18	19.8	19.5	16.6	<LOQ	62.0	<LOQ	29.5	21.7	73.7
24	<LOQ	8.52	<LOQ	<LOQ	29.3	<LOQ	18.9	14.7	77.7
36	<LOQ	<LOQ	<LOQ	<LOQ	<LOQ	<LOQ	N/A	N/A	N/A
48	<LOQ	<LOQ	<LOQ	<LOQ	<LOQ	<LOQ	N/A	N/A	N/A
72	<LOQ	<LOQ	<LOQ	<LOQ	<LOQ	<LOQ	N/A	N/A	N/A

<LOQ, below limit of quantification (pMC = 3.833)

Table A2.2: Caffeine plasma concentration data after oral administration of microdose & inhibitors.

Time (h)	Plasma concentration (pg/mL)								
	Subject 1	Subject 2	Subject 3	Subject 4	Subject 5	Subject 6	Mean	SD	% CV
0	<LOQ	<LOQ	<LOQ	<LOQ	<LOQ	<LOQ	N/A	N/A	N/A
0.25	143	647	454	708	560	82.4	247	175	70.8
0.5	593	523	720	751	580	212	546	225	41.2
0.75	593	498	688	504	709	894	460	152	33.0
1	669	595	492	445	638	479	410	90.4	22.0
2	406	549	735	420	562	365	310	64.2	20.7
3	472	613	704	419	435	361	269	112	41.7
4	641	445	465	444	500	409	223	55.2	24.7
6	529	452	570	402	489	441	152	82.0	53.9
8	395	365	408	467	421	604	126	68.2	54.2
12	314	402	294	346	468	366	55.2	44.3	80.3
18	254	258	305	302	434	333	29.5	21.7	73.7
24	142	322	268	243	363	259	18.9	14.7	77.7
36	136	191	183	221	400	267	N/A	N/A	N/A
48	56.8	110	110	156	337	193	N/A	N/A	N/A
72	14.8	52.2	48.4	86.3	198	147	N/A	N/A	N/A

<LOQ, below limit of quantification (pMC = 3.833)

Appendix 3. Midazolam plasma concentration data

Table A3.1: Midazolam plasma concentration data after oral administration of microdose.

Time (h)	Plasma concentration (pg/mL)								
	Subject 1	Subject 2	Subject 3	Subject 4	Subject 5	Subject 6	Mean	SD	% CV
0	<LOQ	<LOQ	<LOQ	<LOQ	<LOQ	<LOQ	N/A	N/A	N/A
0.25	<LOQ	17.1	ND	85.9	23.1	56.8	45.7	32.0	69.9
0.5	65.6	60.8	107	112	131	158	106	37.5	35.5
0.75	99.7	109	122	93.4	214	116	126	44.5	35.4
1	167	130	96.9	87.6	177	142	133	36.2	27.1
2	106	59.5	52.1	50.3	55.1	43.0	61.0	22.7	37.2
3	39.6	39.2	37.5	51.7	68.4	76.9	52.2	16.8	32.2
4	33.5	23.9	28.8	22.0	32.3	17.6	26.4	6.23	23.6
6	16.8	<LOQ	<LOQ	<LOQ	26.5	<LOQ	21.7	6.86	31.7
8	13.2	<LOQ	<LOQ	<LOQ	12.3	<LOQ	12.8	0.636	4.99
12	<LOQ	<LOQ	<LOQ	<LOQ	12.7	<LOQ	12.7	N/A	N/A
18	<LOQ	<LOQ	<LOQ	<LOQ	<LOQ	<LOQ	N/A	N/A	N/A
24	<LOQ	<LOQ	<LOQ	<LOQ	<LOQ	<LOQ	N/A	N/A	N/A
36	<LOQ	<LOQ	<LOQ	<LOQ	<LOQ	<LOQ	N/A	N/A	N/A
48	<LOQ	<LOQ	<LOQ	<LOQ	<LOQ	<LOQ	N/A	N/A	N/A
72	<LOQ	<LOQ	<LOQ	<LOQ	<LOQ	<LOQ	N/A	N/A	N/A

<LOQ, below limit of quantification (pMC = 3.833)

Table A3.2: Midazolam plasma concentration data after oral administration of microdose & inhibitor administration.

Time (h)	Plasma concentration (pg/mL)								
	Subject 1	Subject 2	Subject 3	Subject 4	Subject 5	Subject 6	Mean	SD	% CV
0	<LOQ	<LOQ	<LOQ	<LOQ	<LOQ	<LOQ	N/A	N/A	N/A
0.25	30.3	319	69.0	80.9	185	31.6	119	113	94.7
0.5	321	541	424	535	529	62.5	402	187	46.6
0.75	598	428	535	467	630	416	512	89.6	17.5
1	516	485	406	446	667	396	486	99.8	20.5
2	287	291	458	296	321	263	319	70.4	22.1
3	255	198	390	354	203	169	262	90.7	34.7
4	228	147	251	220	313	143	217	64.6	29.8
6	206	121	230	189	213	107	178	51.2	28.8
8	301	149	164	168	164	111	176	64.7	36.7
12	116	92.9	87.1	115	175	65.7	109	37.6	34.6
18	83.5	60.7	94.6	96.8	108	40.8	80.7	25.3	31.3
24	86.8	63.4	67.9	76.3	114	27.0	72.6	28.7	39.5
36	67.8	39.7	30.1	47.7	72.3	15.7	45.6	21.8	47.9
48	38.3	40.7	28.7	31.1	55.5	<LOQ	38.9	10.5	27.1
72	16.6	<LOQ	<LOQ	14.8	26.4	<LOQ	19.3	6.24	32.4

LOQ, below limit of quantification (pMC = 3.833)

Appendix 4. Tolbutamide plasma concentration data

Table A4.1: Tolbutamide plasma concentration data after oral administration of microdose.

Time (h)	Plasma concentration (pg/mL)								
	Subject 1	Subject 2	Subject 3	Subject 4	Subject 5	Subject 6	Mean	SD	% CV
0	<LOQ	<LOQ	<LOQ	<LOQ	<LOQ	<LOQ	N/A	N/A	N/A
0.25	556	1270	1342	3170	1360	4060	1960	1350	68.7
0.5	1850	1770	4340	3080	3650	3780	3080	1060	34.5
0.75	3060	2890	4210	2540	3460	2590	3130	629	20.1
1	3720	2420	3080	3180	3280	2910	3100	429	13.9
2	3010	3370	4000	3000	1770	1820	2830	879	31.1
3	2620	2050	2530	2150	2740	1980	2350	324	13.8
4	2210	2510	3050	2380	2020	2100	2380	375	15.8
6	1300	2100	2410	2620	1800	1450	1950	525	27.0
8	1300	1560	1620	1470	1170	1080	1370	218	15.9
12	755	972	2080	1390	1085	520	1130	549	48.5
18	512	805	1430	1220	738	251	826	438	53.0
24	438	437	1120	891	534	127	591	357	60.3
36	90.4	151	435	563	140	22.1	234	214	91.8
48	32.2	59.0	194	328	58.4	<LOQ	134	125	93.4
72	<LOQ	<LOQ	22.1	65.2	<LOQ	<LOQ	43.7	30.5	69.8

<LOQ, below limit of quantification (pMC = 3.833)

Table A4.2: Tolbutamide plasma concentration data after oral administration of microdose & inhibitors.

Time (h)	Plasma concentration (pg/mL)								
	Subject 1	Subject 2	Subject 3	Subject 4	Subject 5	Subject 6	Mean	SD	% CV
0	<LOQ	<LOQ	<LOQ	<LOQ	54.9	<LOQ	54.9	N/A	N/A
0.25	1890	3830	3040	4380	4530	439	3020	1595	52.9
0.5	4130	4130	4300	3920	3730	1710	3650	972	26.6
0.75	4080	3560	4400	3380	4350	4350	4020	444	11.1
1	3810	3950	3200	3510	4510	3620	3770	446	11.9
2	2830	3410	5510	2810	3300	2920	3460	1030	29.8
3	3060	3680	4110	3470	2200	2560	3180	715	22.5
4	3210	2610	3220	2940	3010	2320	2890	355	12.3
6	2320	2080	3040	2470	2400	2110	2400	349	14.5
8	1870	1970	2280	2530	1880	2220	2130	263	12.4
12	1340	1280	1940	2110	1480	1440	1600	342	21.4
18	944	1000	1590	2030	975	683	1200	503	41.8
24	ND	768	1650	1870	933	409	1130	614	54.5
36	277	391	966	1485	353	218	615	504	82.0
48	97.6	168	593	1320	232	62.6	412	484	118
72	19.5	43.3	269	671	51.0	12.1	178	260	146

<LOQ, below limit of quantification (pMC = 3.833), ND- data failed AMS acceptance criteria (Section 7.11.3)

Appendix 5. Fexofenadine plasma concentration data

Table A5.1: Fexofenadine plasma concentration data after oral administration of microdose.

Time (h)	Plasma concentration (pg/mL)								
	Subject 1	Subject 2	Subject 3	Subject 4	Subject 5	Subject 6	Mean	SD	% CV
0	<LOQ	<LOQ	<LOQ	<LOQ	<LOQ	<LOQ	N/A	N/A	N/A
0.25	<LOQ	<LOQ	<LOQ	29.2	<LOQ	30.5	29.9	0.92	3.08
0.5	29.5	18.4	77.2	61.0	57.8	123	61.2	37.2	60.9
0.75	83.6	42.6	87.5	52.2	86.6	105	76.3	23.8	31.2
1	125	59.5	133	39.5	126	111	99.0	39.5	39.9
2	94.7	64.4	101	36.9	49.1	68.5	69.1	25.0	36.2
3	36.9	33.3	54.3	54.2	50.8	49.4	46.5	9.09	19.6
4	46.9	30.9	51.5	20.9	46.5	32.7	38.2	11.9	31.0
6	19.7	16.8	35.8	<LOQ	38.6	23.7	26.9	9.75	36.2
8	17.1	12.7	17.6	<LOQ	27.4	17.5	18.5	5.40	29.2
12	11.0	ND	11.6	<LOQ	ND	<LOQ	11.3	0.42	3.8
18	<LOQ	<LOQ	<LOQ	<LOQ	<LOQ	<LOQ	N/A	N/A	N/A
24	<LOQ	<LOQ	<LOQ	<LOQ	<LOQ	<LOQ	N/A	N/A	N/A
36	<LOQ	<LOQ	<LOQ	<LOQ	<LOQ	<LOQ	N/A	N/A	N/A
48	<LOQ	<LOQ	<LOQ	<LOQ	<LOQ	<LOQ	N/A	N/A	N/A
72	<LOQ	<LOQ	<LOQ	<LOQ	<LOQ	<LOQ	N/A	N/A	N/A

<LOQ, below limit of quantification (pMC = 3.833), ND- data failed AMS acceptance criteria (Section 7.11.3)

Table A5.2: Fexofenadine plasma concentration data after oral administration of microdose & inhibitors.

Time (h)	Plasma concentration (pg/mL)								
	Subject 1	Subject 2	Subject 3	Subject 4	Subject 5	Subject 6	Mean	SD	% CV
0	<LOQ	<LOQ	<LOQ	<LOQ	<LOQ	<LOQ	N/A	N/A	N/A
0.25	8.45	102	21.9	18.2	81.0	76.8	51.4	39.7	77.3
0.5	104	157	179	74.4	270	<LOQ	157	75.6	48.2
0.75	496	185	194	96.4	442	217	272	159	58.6
1	224	193	210	96.1	398	271	232	99.6	42.9
2	148	122	177	60.9	234	218	160	64.1	40.1
3	127	104	156	58.1	176	143	127	41.9	32.9
4	129	64.2	88.2	49.7	194	105	105	52.0	49.5
6	66.1	45.4	81.7	38.4	110	93.7	72.6	27.9	38.4
8	41.3	35.4	34.4	22.5	63.4	68.4	44.2	17.9	40.5
12	18.8	ND	ND	14.4	34.5	22.5	22.6	8.63	38.3
18	7.39	<LOQ	32.3	<LOQ	11.8	9.23	15.2	11.6	76.1
24	10.7	<LOQ	24.8	<LOQ	<LOQ	10.4	15.3	8.23	53.8
36	<LOQ	<LOQ	14.9	<LOQ	<LOQ	<LOQ	14.9	N/A	N/A
48	<LOQ	<LOQ	15.1	<LOQ	<LOQ	<LOQ	15.1	N/A	N/A
72	<LOQ	<LOQ	<LOQ	<LOQ	<LOQ	<LOQ	N/A	N/A	N/A

<LOQ, below limit of quantification (pMC = 3.833), ND- data failed AMS acceptance criteria (Section 7.11.3)

Appendix 6. *R*-verapamil plasma concentration data

Table A6.1: *R*-verapamil plasma concentration data after IV administration of microdose.

Time (h)	Plasma concentration (pg/mL)								
	Subject 1	Subject 3	Subject 4	Subject 5	Subject 6	Subject 7	Mean	SD	% CV
0	137	148	324	184	282	139	202	80.9	40.0
0.25	158	127	235	124	132	95.9	145	48.2	33.2
0.5	144	84.7	184	95.5	137	80.2	121	41.0	33.9
0.75	81.8	88.4	233	112	133	71.9	120	59.6	49.7
1	70.6	60.3	109	104	60.2	51.0	75.9	24.6	32.4
2	52.6	46.6	69.8	48.4	47.6	30.3	49.2	12.7	25.8
3	28.9	31.1	58.4	39.0	32.0	27.8	36.2	11.6	31.9
4	33.3	25.2	40.4	21.2	30.4	22.0	28.8	7.41	25.8
6	31.4	22.6	25.4	19.3	23.2	20.1	23.7	4.38	18.5
8	13.4	15.0	22.5	16.6	18.0	12.4	16.3	3.65	22.4
12	7.95	9.54	11.8	9.34	16.4	16.2	11.9	3.65	30.7
24	2.69	3.16	<LOQ	3.16	6.93	2.97	3.78	1.77	46.8

<LOQ, below limit of quantification (pMC = 1.611)

Table A6.2: *R*-verapamil plasma concentration data after IV administration of microdose plus oral therapeutic dose.

Time (h)	Plasma concentration (pg/mL)									
	Subject 1	Subject 2	Subject 3	Subject 4	Subject 5	Subject 6	Subject 7	Mean	SD	% CV
0	256	227	106	311	199	174	303	225	73.0	32.4
0.25	171	181	80.7	202	293	135	124	170	67.8	40.0
0.5	118	166	83.8	142	190	91.3	119	130	38.6	29.7
0.75	150	169	53.6	183	152	ND	131	140	45.8	32.8
1	80.2	103	81.6	104	134	101	85.8	98.5	18.7	19.0
2	64.7	65.3	50.3	87.0	84.0	45.0	ND	66.1	17.1	25.8
3	38.8	62.0	33.9	35.8	70.2	32.7	40.0	44.8	15.0	33.5
4	31.4	48.9	30.0	44.6	76.9	32.8	33.4	42.6	16.8	39.4
6	16.9	62.3	38.7	24.2	53.1	38.6	59.4	41.9	17.4	41.4
8	17.2	38.0	13.3	18.7	52.9	15.5	37.9	27.6	15.2	55.1
12	6.97	21.4	9.89	12.5	ND	9.56	17.8	13.0	5.51	42.3
24	2.67	8.01	2.56	5.62	7.02	3.81	3.32	4.72	2.18	46.3

ND, data failed AMS acceptance criteria (Section 7.11.3)

Appendix 7. *S*-verapamil plasma concentration data

Table A7.1: *S*-verapamil plasma concentration data after IV administration of microdose.

Time (h)	Plasma concentration (pg/mL)								
	Subject 1	Subject 3	Subject 4	Subject 5	Subject 6	Subject 7	Mean	SD	% CV
0	86.7	94.6	81.0	95.3	146	62.7	94.4	28.0	29.6
0.25	70.9	70.5	52.3	67.7	70.9	56.3	64.8	8.29	12.8
0.5	63.7	50.3	43.6	67.7	59.5	47.4	55.4	9.66	17.4
0.75	49.4	44.8	40.1	55.1	63.0	35.7	48.0	10.0	20.9
1	47.7	29.8	24.2	45.8	33.5	24.5	34.3	10.3	30.1
2	36.0	27.8	13.9	19.2	21.4	21.3	23.3	7.67	33.0
3	17.2	20.4	13.4	16.8	13.8	11.2	15.5	3.30	21.3
4	16.9	14.7	9.47	12.8	16.3	13.1	13.9	2.72	19.6
6	37.8	17.7	5.68	17.0	13.6	10.8	13.0	4.92	38.0
8	11.5	7.70	4.65	11.2	9.45	7.03	8.59	2.64	30.7
12	6.96	6.86	3.36	5.21	8.82	6.60	6.30	1.85	29.3
24	2.33	<LOQ	<LOQ	2.22	4.61	1.70	2.72	1.29	47.6

<LOQ, below limit of quantification (pMC = 1.696)

Table A7.2: *S*-verapamil plasma concentration data after IV administration of microdose plus oral therapeutic dose.

Time (h)	Plasma concentration (pg/mL)									
	Subject 1	Subject 2	Subject 3	Subject 4	Subject 5	Subject 6	Subject 7	Mean	SD	% CV
0	105	78.7	58.3	164	75.9	92.5	109	97.6	34.1	35.0
0.25	68.7	76.6	41.4	92.5	102	78.3	71.5	75.9	19.3	25.4
0.5	70.5	ND	37.8	71.1	55.5	42.9	60.3	56.4	13.9	24.6
0.75	58.2	60.6	30.4	68.6	56.6	41.0	39.7	50.7	13.8	27.1
1	37.4	33.0	28.2	46.0	45.6	33.7	34.2	36.9	6.67	18.1
2	28.9	30.8	26.4	37.1	26.0	23.5	36.1	29.8	5.17	17.3
3	22.6	20.4	24.3	18.2	19.9	18.1	15.6	19.9	2.93	14.7
4	16.0	19.0	12.3	17.2	18.8	15.8	15.6	16.4	2.28	13.9
6	11.3	16.4	12.7	10.5	23.3	15.0	16.7	15.1	4.34	28.7
8	9.85	11.6	5.46	8.01	15.2	6.61	17.4	10.6	4.43	41.9
12	4.54	8.08	4.81	4.38	9.05	4.74	8.99	6.4	2.21	34.7
24	2.23	3.17	2.96	2.52	2.70	<LOQ	2.30	2.6	0.370	14.0

<LOQ, below limit of quantification (pMC = 1.696)
ND-data failed AMS acceptance criteria (Section 7.11.3)

Appendix 8. Caffeine pharmacokinetic data

Table A8.1: Caffeine pharmacokinetic data after administration of microdose & microdose plus inhibitors.

	Subject Number	$t_{1/2}$ (h)	t_{max} (h)	C_{max} (ng/mL)	AUC_{0-t} (h.ng/mL)	$AUC_{0-\infty}$ (h.ng/mL)
Microdose only	1	3.58	1.00	0.529	2.55	2.59
	2	3.94	0.75	0.476	2.94	2.88
	3	3.85	0.50	0.825	2.12	2.21
	4	4.15	0.25	0.491	1.70	1.83
	5	6.31	0.50	0.791	4.56	4.64
	6	3.07	0.50	0.562	1.85	1.89
	Mean	4.15	0.583	0.612	2.62	2.67
	Median	3.90	0.500	0.546	2.34	2.40
	SD	1.12	0.258	0.155	1.05	1.04
	% CV	27	44	25	40	39
	Subject Number	**$t_{1/2}$ (h)**	**t_{max} (h)**	**C_{max} (ng/mL)**	**AUC_{0-t} (h.ng/mL)**	**$AUC_{0-\infty}$ (h.ng/mL)**
Microdose plus inhibitors	1	11.4	1.00	0.669	12.00	12.10
	2	18.3	0.25	0.647	15.90	17.30
	3	19.2	2.00	0.720	15.70	17.00
	4	26.7	0.50	0.751	16.60	19.90
	5	34.9	0.75	0.709	26.20	36.10
	6	46.5	0.75	0.894	19.10	28.90
	Mean	26.2	0.875	0.73	17.6	21.9
	Median	23.0	0.750	0.71	16.3	18.6
	SD	12.8	0.607	0.0877	4.80	8.90
	% CV	49	69	12	27	41
Ratio		6.3	1.5	1.2	6.7	8.2
T-Test result		0.0081	0.3284	0.1621	0.0003	0.0024
Statistical difference observed?		Y	N	N	Y	Y

Appendix 9. Midazolam pharmacokinetic data

Table A9.1: Midazolam pharmacokinetic data after administration of microdose & microdose plus inhibitors.

	Subject Number	**$t_{1/2}$ (h)**	**t_{max} (h)**	**C_{max} (ng/mL)**	**AUC_{0-t} (h.ng/mL)**	**$AUC_{0-\infty}$ (h.ng/mL)**
Microdose only	1	6.35	1.00	167	480	553
	2	5.79	1.00	130	392	490
	3	1.47	0.75	122	272	290
	4	4.00	0.50	112	358	400
	5	2.77	0.75	214	489	538
	6	3.63	0.50	158	347	390
	Mean	4.00	0.750	151	390	444
	Median	3.82	0.750	144	375	445
	SD	1.83	0.224	38	83	101
	% CV	46	30	25	21	23
	Subject Number	**$t_{1/2}$ (h)**	**t_{max} (h)**	**C_{max} (pg/mL)**	**AUC_{0-t} (h.pg/mL)**	**$AUC_{0-\infty}$ (h.pg/mL)**
Microdose plus inhibitors	1	18.0	0.75	598	6300	3730
	2	19.5	0.50	541	4740	5040
	3	13.7	0.75	535	4820	5380
	4	21.4	0.50	535	5540	6000
	5	23.3	1.00	667	7370	8250
	6	13.3	0.75	416	2470	2770
	Mean	18.2	0.7	549	5210	5200
	Median	18.8	0.8	538	5180	5210
	SD	4.06	0.19	83.0	1660	1900
	% CV	22	27	15	32	37
Ratio		4.5	0.9	3.6	13.4	11.7
T-Test result		0.0003	0.7412	0.0000	0.0007	0.0016
Statistical difference observed?		Y	N	Y	Y	Y

Appendix 10. Tolbutamide pharmacokinetic data

Table A10.1: Tolbutamide pharmacokinetic data after administration of microdose & microdose plus inhibitors.

	Subject Number	$t_{1/2}$ (h)	t_{max} (h)	C_{max} (ng/mL)	AUC_{0-t} (h.ng/mL)	$AUC_{0-\infty}$ (h.ng/mL)
Microdose only	1	7.32	1.00	3.72	31.2	31.5
	2	8.31	2.00	3.37	36.8	37.5
	3	8.51	0.50	4.34	63.1	63.4
	4	11.40	1.00	3.18	58.2	59.3
	5	8.20	0.50	3.65	35.5	36.2
	6	5.06	0.25	4.06	22.9	23.1
	Mean	8.13	0.875	3.720	41.3	41.8
	Median	8.26	0.750	3.685	36.2	36.9
	SD	2.05	0.627	0.429	15.8	16.0
	% CV	25	72	12	38	38
	Subject Number	**$t_{1/2}$ (h)**	**t_{max} (h)**	**C_{max} (ng/mL)**	**AUC_{0-t} (h.ng/mL)**	**$AUC_{0-\infty}$ (h.ng/mL)**
Microdose plus inhibitors	1	9.63	0.50	4.13	50.0	50.3
	2	11.7	0.50	4.13	54.0	54.7
	3	19.7	2.00	5.51	91.8	99.5
	4	36.8	0.25	4.38	117	153
	5	12.3	0.25	4.53	57.1	58.0
	6	8.65	0.75	4.35	42.5	42.7
	Mean	16.5	0.7083	4.51	68.7	76.4
	Median	12.0	0.500	4.37	55.6	56.4
	SD	10.7	0.660	0.516	29.2	42.5
	% CV	65	93	11	42	56
Ratio		2.0	0.8	1.2	1.7	1.8
T-Test result		0.0716	0.7121	0.0038	0.0082	0.0363
Statistical difference observed?		Y	N	N	Y	Y

Appendix 11. Fexofenadine pharmacokinetic data

Table A11.1: Fexofenadine pharmacokinetic data after administration of microdose & microdose plus inhibitors.

	Subject Number	$t_{1/2}$ (h)	t_{max} (h)	C_{max} (pg/mL)	AUC_{0-t} (h.pg/mL)	$AUC_{0-\infty}$ (h.pg/mL)
Microdose only	1	8.69	1.00	125	519	578
	2	3.33	2.00	64.4	245	306
	3	6.98	1.00	133	568	634
	4	4.72	0.50	61.0	274	282
	5	6.95	1.00	126	603	686
	6	3.85	0.50	123	455	493
	Mean	5.75	1.000	105	444	497
	Median	5.84	1.000	124	487	536
	SD	2.10	0.548	33	152	170
	% CV	37	55	32	34	34
	Subject Number	**$t_{1/2}$ (h)**	**t_{max} (h)**	**C_{max} (pg/mL)**	**AUC_{0-t} (h.pg/mL)**	**$AUC_{0-\infty}$ (h.pg/mL)**
Microdose plus inhibitors	1	25.0	0.75	496	1400	1590
	2	9.00	1.00	193	1080	1190
	3	25.5	1.00	210	2070	2300
	4	14.4	0.75	96	864	1080
	5	4.29	0.75	442	1830	1880
	6	4.51	1.00	271	1350	1420
	Mean	13.8	0.875	285	1430	1580
	Median	11.7	0.875	241	1380	1500
	SD	9.62	0.137	154	452	455
	% CV	70	16	54	32	29
Ratio		2.4	0.9	2.7	3.2	3.2
T-Test result		0.0670	0.5805	0.0222	0.0007	0.0004
Statistical difference observed?		Y	N	N	Y	Y

Appendix 12. *R*-verapamil pharmacokinetic data

Table A12.1. *R*-verapamil pharmacokinetic data after administration of IV microdose.

Subject Number	$t_{1/2}$ (h)	C_{max} (pg/mL)	AUC_{0-t} (h.pg/mL)	$AUC_{0-\infty}$ (h.pg/mL)	CL (L/h)	V (L)	V_{ss} (L)	Missing Data Point
1	5.50	158	530	551	55.7	434	314	
3	6.43	148	504	533	58.9	555	394	
4	5.23	324	794	833	73.7	556	324	24 h
5	6.84	184	590	621	52.3	516	311	
6	10.7	282	728	835	40.0	620	390	
7	6.63	139	495	523	68.4	655	511	
Mean	6.89	206	607	649	58.2	556	374	
SD	1.97	77.9	126	147	12.0	78.0	76.8	
%CV	28.7	37.9	20.7	22.7	20.6	14.0	20.5	
Geomean	6.69	195	597	636	57.1	551	368	

Table A12.2. *R*-verapamil pharmacokinetic data after administration of IV microdose plus oral therapeutic dose.

Subject Number	$t_{1/2}$ (h)	C_{max} (pg/mL)	AUC_{0-t} (h.pg/mL)	$AUC_{0-\infty}$ (h.pg/mL)	CL (L/h)	V (L)	V_{ss} (L)	Missing Data Point
1	6.48	256	642	667	51.3	480	252	
*2	6.71	227	991	1070	39.6	383	310	
3	5.20	106	507	526	64.7	485	400	
4	7.24	311	836	894	38.2	400	245	
5	5.89	293	1270	1330	32.2	273	217	12 h
6	8.14	174	602	646	50.1	589	351	1 h
7	4.64	303	898	920	43.8	293	243	3 h
Mean	6.27	240	793	831	46.7	420	285	
SD	1.30	83.1	276	288	11.4	122	73.0	
%CV	20.7	34.5	34.9	34.7	24.4	29.1	25.7	
Geomean	6.15	225	756	793	45.6	405	278	

*excluded from mean

Appendix 13. *S*-verapamil pharmacokinetic data

Table A13.1. *S*-verapamil pharmacokinetic data after administration of IV microdose plus oral therapeutic dose.

Subject Number	$t_{1/2}$ (h)	C_{max} (pg/mL)	AUC_{0-t} (h.pg/mL)	$AUC_{0-\infty}$ (h.pg/mL)	CL (L/h)	V (L)	V_{ss} (L)
1	5.99	86.7	378	398	65.5	567	443
3	5.34	94.6	254	307	85.1	657	528
4	8.00	81.0	175	214	122	1409	794
5	6.74	95.3	318	339	77.5	754	528
6	11.5	146	378	454	57.4	951	669
7	7.08	62.7	243	260	100	1020	771
Mean	7.44	94.4	291	329	84.6	893	622
SD	2.19	28.0	81.2	88.3	23.6	306	144
%CV	29.40	29.6	27.9	26.9	27.9	34.2	23.1
Geomean	7.21	91.3	281	319	81.9	853	608

Table A13.2. *S*-verapamil pharmacokinetic data after administration of IV microdose plus oral therapeutic dose.

Subject Number	$t_{1/2}$ (h)	C_{max} (pg/mL)	AUC_{0-t} (h.pg/mL)	$AUC_{0-\infty}$ (h.pg/mL)	CL (L/h)	V (L)	V_{ss} (L)	Missing Data Point
1	7.02	105	319	341	76.5	775	507	
*2	8.63	78.7	350	390	67.5	840	605	0.75 h
3	9.68	58.3	247	288	91.0	1270	959	
4	9.17	164	370	403	64.8	856	442	
5	6.52	102	383	408	64.0	601	484	
6	8.34	92.5	236	293	88.2	1060	637	24 h
7	5.61	109	370	389	67.4	546	473	
Mean	7.72	105	321	354	75.3	851	584	
SD	1.59	34.2	65.3	54.4	12.0	276	196	
%CV	20.6	32.5	20.4	15.4	15.9	32.0	33.6	
Geomean	7.58	101	315	350	74.5	815	561	

*excluded from mean

Glossary

λ	wavelength
ACN	acetonitrile
AMS	accelerator mass spectrometry
ANU	Australian national university
AUC_{0-t}	Area under the concentration time curve from time zero to time t
BBB	blood brain barrier
Bq	becquerel
C_{max}	time to maximum concentration
CL	clearance
cpm	counts per minute
CTA	clinical trials application
CV	coefficient of variation
CYP	cytochrome P450
Da	Dalton
DDI	drug-drug interaction
dpm	disintegrations per minute
Fl	fluorescence
GI	gastrointestinal
h	hour
HPLC	high performance liquid chromatography
HIV	human immune deficiency virus
IV	intravenous
L_{mass}	mass specific activity
LOQ	limit of quantification
LP	liquid paraffin
LSC	liquid scintillation counter
LU	luminescence units
MeOH	methanol
min	minute
NCE	new chemical entity
OATP	organic anion transporter protein

PD	pharmacodynamic
PET	positron emission tomography
PI	protease inhibitor
PK	pharmacokinetic
PD	pharmacodynamic
pMC	percent modern carbon
PXR	pregnane X receptor
Rs	resolution
RP	reverse phase
SD	standard deviation
$t_{1/2}$	the elimination half-life
t_{max}	the time at which the drug reaches maximum concentration
UV	ultraviolet
V	volume of distribution
V_d	brain tissue-plasma partition coefficient at equilibrium
V_{ss}	volume of distribution at steady state
V_T	brain tissue-plasma partition coefficient at equilibrium (Logan derived)

References

1. Mahajan, R. and K. Gupta, *Food and drug administration's critical path initiative and innovations in drug development paradigm: Challenges, progress, and controversies.* J Pharm Bioallied Sci, 2010. **2**: 307-13.
2. Lappin, G., *Radiotracers and drug registration*, in *Radiotracers in drug development*, G. Lappin and S. Temple, Editors. 2006, Taylor & Francis: Boca Raton. p. 1-15.
3. Collier, R., *Drug development cost estimates hard to swallow.* Cmaj, 2009. **180**: 279-80.
4. Hosea, N.A., W.T. Collard, S. Cole, T.S. Maurer, R.X. Fang, H. Jones, S.M. Kakar, Y. Nakai, B.J. Smith, R. Webster, and K. Beaumont, *Prediction of human pharmacokinetics from preclinical information: comparative accuracy of quantitative prediction approaches.* J Clin Pharmacol, 2009. **49**: 513-33.
5. Beaumont, K. and D.A. Smith, *Does human pharmacokinetic prediction add significant value to compound selection in drug discovery research?* Curr Opin Drug Discov Devel, 2009. **12**: 61-71.
6. Lappin, G. and R.C. Garner, *Big physics, small doses: the use of AMS and PET in human microdosing of development drugs.* Nat Rev Drug Discov, 2003. **2**: 233-40.
7. Langley, G. and S. Farnaud, *Opinion: Microdosing: safer clinical trials and fewer animal tests.* Bioanalysis, 2010. **2**: 393-5.
8. Seymour, M., *The best model for humans is human -- how to accelerate early drug development safely.* Altern Lab Anim, 2009. **37 Suppl 1**: 61-5.
9. (CHMP), C.f.m.p.f.h.u., *Position Paper on Non-clinical Safety Studies to Support Clinical Trials with a Single Microdose.* , EMEA, Editor. 2004.
10. Lappin, G. and C. Garner, *The utility of microdosing over the past 5 years.* Expert Opin Drug Metab Toxicol, 2008. **4**: 1499-1506.
11. Lappin, G., Y. Shishikura, R. Jochemsen, R.J. Weaver, C. Gesson, J. Brian Houston, B. Oosterhuis, O.J. Bjerrum, G. Grynkiewicz, J. Alder, M. Rowland, and C. Garner, *Comparative pharmacokinetics between a microdose and therapeutic dose for clarithromycin, sumatriptan, propafenone, paracetamol (acetaminophen), and phenobarbital in human volunteers.* Eur J Pharm Sci, 2011. **43**: 141-150.
12. Lappin, G., W. Kuhnz, R. Jochemsen, J. Kneer, A. Chaudhary, B. Oosterhuis, W.J. Drijfhout, M. Rowland, and R.C. Garner, *Use of microdosing to predict pharmacokinetics at the therapeutic dose: Experience with 5 drugs.* Clin Pharmacol Ther, 2006. **80**: 203-215.
13. Harrison, A., I. Gardner, T. Hay, M. Dickins, K. Beaumont, A. Phipps, L. Purkins, G. Allan, R. Christian, J. Duckworth, I. Gurrell, S. Kempshall, M. Savage, M. Seymour, M. Simpson, L. Taylor, and P. Turnpenny, *Case studies addressing human pharmacokinetic uncertainty using a combination of pharmacokinetic simulation and alternative first in human paradigms.* Xenobiotica, 2012. **42**: 57-74.
14. Madan, A., Z. O'Brien, J. Wen, C. O'Brien, R.H. Farber, G. Beaton, P. Crowe, B. Oosterhuis, R.C. Garner, G. Lappin, and H.P. Bozigian, *A pharmacokinetic evaluation of five H1 antagonists after an oral and*

intravenous microdose to human subjects. Br J Clin Pharmacol, 2008. **67**: 288-298.
15. Lappin, G., *Microdosing: current and the future.* Bioanalysis, 2010. **2**: 509-17.
16. Ings, R., *Microdosing: a valuable tool for accelerating drug development and the role of bioanalytical methods in meeting the challenge.* Bioanalysis, 2009. **1**: 1293-1305.
17. Lappin, G. and R.C. Garner, *A review of human phase 0 and microdosing clinical trials following the US food and drug administration exploratory investigational new drug studies guidance.* In J Pharm Med, 2006. **30**: 159-165.
18. MHRA. *Sitaxentan (Thelin): worldwide withdrawal from the market due to hepatotoxicity*. 2011 [cited 2012 29 September 2012]; Available from: http://www.mhra.gov.uk/Safetyinformation/DrugSafetyUpdate/CON105752.
19. Lappin, G., *The study of drug metabolism using radiotracers*, in *Radiotracers in drug development*, G. Lappin and S. Temple, Editors. 2006, Taylor & Francis: Boca Raton. p. 41-118.
20. Kwon, Y., *Metabolism*, in *Handbook of essential pharmacokinetics, pharmacodynamics and drug metabolism for industrial scientists*. 2001, Springer-Verlag: New York. p. 121-168.
21. Coleman, M.D., *Drug biotransformational systems - origin and aims*, in *Human drug metabolism*. 2005, Wiley: Chichester. p. 13-22.
22. Cvetkovic, M., B. Leake, M.F. Fromm, G.R. Wilkinson, and R.B. Kim, *OATP and P-glycoprotein transporters mediate the cellular uptake and excretion of fexofenadine*. Drug Metab Dispos, 1999. **27**: 866-71.
23. Lappin, G., Y. Shishikura, R. Jochemsen, R.J. Weaver, C. Gesson, B. Houston, B. Oosterhuis, O.J. Bjerrum, M. Rowland, and C. Garner, *Pharmacokinetics of fexofenadine: Evaluation of a microdose and assessment of absolute oral bioavailability.* . Eur J Pharm Sci, 2010. **40**: 125–131.
24. Coleman, M.D., *How oxidative systems metabolise substrates*, in *Human drug metabolism*. 2005, Wiley: Chichester. p. 23-56.
25. Nelson, D. *Cytochrome P450*. 2006 [cited 5 December 2006]; Available from: http://drnelson.utmem.edu/CytochromeP450.html.
26. Clarke, S.E., Jones, B.C., *Human cytochromes P450 and their role in mechanism-based drug-drug interactions*, in *Drug-drug interactions*, M. Dekker, Editor. 2002, Rodrigues, A.D.: New York. p. 55-88.
27. Spina, E., F. Pisani, and E. Perucca, *Clinically significant pharmacokinetic drug interactions with carbamazepine. An update.* Clin Pharmacokinet, 1996. **31**: 198-214.
28. Barone, G.W., B.J. Gurley, B.L. Ketel, M.L. Lightfoot, and S.R. Abul-Ezz, *Drug interaction between St. John's wort and cyclosporine.* Ann Pharmacother, 2000. **34**: 1013-6.
29. Oda, Y., K. Mizutani, I. Hase, T. Nakamoto, N. Hamaoka, and A. Asada, *Fentanyl inhibits metabolism of midazolam: competitive inhibition of CYP3A4 in vitro.* Br J Anaesth, 1999. **82**: 900-3.
30. Tompkins, L.M. and A.D. Wallace, *Mechanisms of cytochrome P450 induction.* J Biochem Mol Toxicol, 2007. **21**: 176-81.

31. Wang, Z., J.C. Gorski, M.A. Hamman, S.M. Huang, L.J. Lesko, and S.D. Hall, *The effects of St John's wort (Hypericum perforatum) on human cytochrome P450 activity.* Clin Pharmacol Ther, 2001. **70**: 317-26.
32. Yuan, R., S. Madani, X.X. Wei, K. Reynolds, and S.M. Huang, *Evaluation of cytochrome P450 probe substrates commonly used by the pharmaceutical industry to study in vitro drug interactions.* Drug Metab Dispos, 2002. **30**: 1311-9.
33. Huang, S.M. and L.J. Lesko, *Drug-drug, drug-dietary supplement, and drug-citrus fruit and other food interactions: what have we learned?* J Clin Pharmacol, 2004. **44**: 559-69.
34. Dilger, K., U. Hofmann, and U. Klotz, *Enzyme induction in the elderly: effect of rifampin on the pharmacokinetics and pharmacodynamics of propafenone.* Clin Pharmacol Ther, 2000. **67**: 512-20.
35. Coleman, M.D., *Cytochrome P450 inhibition*, in *Human drug metabolism*. 2005, Wiley: Chichester. p. 75-99.
36. Miners, J.O. and D.J. Birkett, *Cytochrome P4502C9: an enzyme of major importance in human drug metabolism.* Br J Clin Pharmacol, 1998. **45**: 525-38.
37. Madsen, H., T.P. Enggaard, L.L. Hansen, N.A. Klitgaard, and K. Brosen, *Fluvoxamine inhibits the CYP2C9 catalyzed biotransformation of tolbutamide.* Clin Pharmacol Ther, 2001. **69**: 41-7.
38. Krishnaiah, Y.S., S. Satyanarayana, and D. Visweswaram, *Interaction between tolbutamide and ketoconazole in healthy subjects.* Br J Clin Pharmacol, 1994. **37**: 205-7.
39. Wang, L.S., B. Zhu, A.M. El-Aty, G. Zhou, Z. Li, J. Wu, G.L. Chen, J. Liu, Z.R. Tang, W. An, Q. Li, D. Wang, and H.H. Zhou, *The influence of St John's wort on CYP2C19 activity with respect to genotype.* J Clin Pharmacol, 2004. **44**: 577-81.
40. Jeppesen, U., L.F. Gram, K. Vistisen, S. Loft, H.E. Poulsen, and K. Brosen, *Dose-dependent inhibition of CYP1A2, CYP2C19 and CYP2D6 by citalopram, fluoxetine, fluvoxamine and paroxetine.* Eur J Clin Pharmacol, 1996. **51**: 73-8.
41. Christensen, M., G. Tybring, K. Mihara, N. Yasui-Furokori, J.A. Carrillo, S.I. Ramos, K. Andersson, M.L. Dahl, and L. Bertilsson, *Low daily 10-mg and 20-mg doses of fluvoxamine inhibit the metabolism of both caffeine (cytochrome P4501A2) and omeprazole (cytochrome P4502C19).* Clin Pharmacol Ther, 2002. **71**: 141-52.
42. Turpault, S., W. Brian, R. Van Horn, A. Santoni, F. Poitiers, Y. Donazzolo, and X. Boulenc, *Pharmacokinetic assessment of a five-probe cocktail for CYPs 1A2, 2C9, 2C19, 2D6 and 3A.* Br J Clin Pharmacol, 2009. **68**: 928-35.
43. Hellum, B.H., Z. Hu, and O.G. Nilsen, *Trade herbal products and induction of CYP2C19 and CYP2E1 in cultured human hepatocytes.* Basic Clin Pharmacol Toxicol, 2009. **105**: 58-63.
44. Rizzo, N., E. Hispard, S. Dolbeault, S. Dally, R. Leverge, and C. Girre, *Impact of long-term ethanol consumption on CYP1A2 activity.* Clin Pharmacol Ther, 1997. **62**: 505-9.
45. Pratt-Hyatt, M., H.L. Lin, and P.F. Hollenberg, *Mechanism-based inactivation of human CYP2E1 by diethyldithocarbamate.* Drug Metab Dispos. **38**: 2286-92.

46. Ono, S., T. Hatanaka, H. Hotta, M. Tsutsui, T. Satoh, and F.J. Gonzalez, *Chlorzoxazone is metabolized by human CYP1A2 as well as by human CYP2E1.* Pharmacogenetics, 1995. **5**: 143-50.
47. Manyike, P.T., E.D. Kharasch, T.F. Kalhorn, and J.T. Slattery, *Contribution of CYP2E1 and CYP3A to acetaminophen reactive metabolite formation.* Clin Pharmacol Ther, 2000. **67**: 275-82.
48. Brosen, K., E. Skjelbo, B.B. Rasmussen, H.E. Poulsen, and S. Loft, *Fluvoxamine is a potent inhibitor of cytochrome P4501A2.* Biochem Pharmacol, 1993. **45**: 1211-4.
49. Venkatakrishnan, K., L.L. von Moltke, and D.J. Greenblatt, *Effects of the antifungal agents on oxidative drug metabolism: clinical relevance.* Clin Pharmacokinet, 2000. **38**: 111-80.
50. Boxenbaum, H., *Cytochrome P450 3A4 in vivo ketoconazole competitive inhibition: determination of Ki and dangers associated with high clearance drugs in general.* J Pharm Pharm Sci, 1999. **2**: 47-52.
51. Meyer, U.A. and U.M. Zanger, *Molecular mechanisms of genetic polymorphisms of drug metabolism.* Annu Rev Pharmacol Toxicol, 1997. **37**: 269-96.
52. Goldstein, J.A., *Clinical relevance of genetic polymorphisms in the human CYP2C subfamily.* Br J Clin Pharmacol, 2001. **52**: 349-55.
53. Brosen, K., *Drug interactions and the cytochrome P450 system. The role of cytochrome P450 1A2.* Clin Pharmacokinet, 1995. **29 Suppl 1**: 20-5.
54. Faber, M.S., A. Jetter, and U. Fuhr, *Assessment of CYP1A2 activity in clinical practice: why, how, and when?* Basic Clin Pharmacol Toxicol, 2005. **97**: 125-34.
55. Hakooz, N. and I. Hamdan, *Effects of dietary broccoli on human in vivo caffeine metabolism: a pilot study on a group of Jordanian volunteers.* Curr Drug Metab, 2007. **8**: 9-15.
56. Fontana, R.J., K.S. Lown, M.F. Paine, L. Fortlage, R.M. Santella, J.S. Felton, M.G. Knize, A. Greenberg, and P.B. Watkins, *Effects of a chargrilled meat diet on expression of CYP3A, CYP1A, and P-glycoprotein levels in healthy volunteers.* Gastroenterology, 1999. **117**: 89-98.
57. Haslemo, T., P.H. Eikeseth, L. Tanum, E. Molden, and H. Refsum, *The effect of variable cigarette consumption on the interaction with clozapine and olanzapine.* Eur J Clin Pharmacol, 2006. **62**: 1049-53.
58. Kunze, K.L. and W.F. Trager, *Isoform-selective mechanism-based inhibition of human cytochrome P450 1A2 by furafylline.* Chem Res Toxicol, 1993. **6**: 649-56.
59. Culm-Merdek, K.E., L.L. von Moltke, J.S. Harmatz, and D.J. Greenblatt, *Fluvoxamine impairs single-dose caffeine clearance without altering caffeine pharmacodynamics.* Br J Clin Pharmacol, 2005. **60**: 486-93.
60. Wang, B., J. Wang, S.Q. Huang, H.H. Su, and S.F. Zhou, *Genetic polymorphism of the human cytochrome P450 2C9 gene and its clinical significance.* Curr Drug Metab, 2009. **10**: 781-834.
61. Belic, A., M. Temesvari, K. Kohalmy, R. Vrzal, Z. Dvorak, D. Rozman, and K. Monostory, *Investigation of the CYP2C9 induction profile in human hepatocytes by combining experimental and modelling approaches.* Curr Drug Metab, 2009. **10**: 1066-74.

62. Kirchheiner, J., S. Bauer, I. Meineke, W. Rohde, V. Prang, C. Meisel, I. Roots, and J. Brockmoller, *Impact of CYP2C9 and CYP2C19 polymorphisms on tolbutamide kinetics and the insulin and glucose response in healthy volunteers.* Pharmacogenetics, 2002. **12**: 101-9.
63. Galetin, A., K. Ito, D. Hallifax, and J.B. Houston, *CYP3A4 substrate selection and substitution in the prediction of potential drug-drug interactions.* J Pharmacol Exp Ther, 2005. **314**: 180-90.
64. Zhou, S., E. Chan, L.Y. Lim, U.A. Boelsterli, S.C. Li, J. Wang, Q. Zhang, M. Huang, and A. Xu, *Therapeutic drugs that behave as mechanism-based inhibitors of cytochrome P450 3A4.* Curr Drug Metab, 2004. **5**: 415-42.
65. Blakey, G.E., J.A. Lockton, J. Perrett, P. Norwood, M. Russell, Z. Aherne, and J. Plume, *Pharmacokinetic and pharmacodynamic assessment of a five-probe metabolic cocktail for CYPs 1A2, 3A4, 2C9, 2D6 and 2E1.* Br J Clin Pharmacol, 2004. **57**: 162-9.
66. Kim, M.J., H. Kim, I.J. Cha, J.S. Park, J.H. Shon, K.H. Liu, and J.G. Shin, *High-throughput screening of inhibitory potential of nine cytochrome P450 enzymes in vitro using liquid chromatography/tandem mass spectrometry.* Rapid Commun Mass Spectrom, 2005. **19**: 2651-8.
67. Fuhr, U., A. Jetter, and J. Kirchheiner, *Appropriate phenotyping procedures for drug metabolizing enzymes and transporters in humans and their simultaneous use in the "cocktail" approach.* Clin Pharmacol Ther, 2007. **81**: 270-83.
68. von Moltke, L.L., D.J. Greenblatt, S.X. Duan, J.S. Harmatz, and R.I. Shader, *In vitro prediction of the terfenadine-ketoconazole pharmacokinetic interaction.* J Clin Pharmacol, 1994. **34**: 1222-7.
69. Troutman, M., G. Luo, B.M. Knight, D.R. Thakker, and L.S. Gan, *The role of P-glycoprotein in drug disposition: Significance to drug development*, in *Drug-drug interactions*, A.D. Rodrigues, Editor. 2008, Marcel Dekker: New York. p. 295-358.
70. Kusuhara, H. and Y. Suguyama, *Drug-drug interactions involving the membrane transport process*, in *Drug-drug interactions*, A.D. Rodrigues, Editor. 2002, Marcel Dekker: New York. p. 123-188.
71. Linardi, R.L. and C.C. Natalini, *Multi-drug resistance (MDR1) gene and P-glycoprotein influence on pharmacokinetic and pharmacodynamic of therapeutic drugs.* Ciencia Rural, 2006. **36**: 336-341.
72. Sharom, F.J., *ABC multidrug transporters: structure, function and role in chemoresistance.* Pharmacogenomics, 2008. **9**: 105-27.
73. Toornvliet, R., B.N. van Berckel, G. Luurtsema, M. Lubberink, A.A. Geldof, T.M. Bosch, R. Oerlemans, A.A. Lammertsma, and E.J. Franssen, *Effect of age on functional P-glycoprotein in the blood-brain barrier measured by use of (R)-[(11)C]verapamil and positron emission tomography.* Clin Pharmacol Ther, 2006. **79**: 540-8.
74. Ogasawara, A., T. Kume, and E. Kazama, *Effect of oral ketoconazole on intestinal first-pass effect of midazolam and fexofenadine in cynomolgus monkeys.* Drug Metab Dispos, 2007. **35**: 410-8.
75. Hennessy, M., D. Kelleher, J.P. Spiers, M. Barry, P. Kavanagh, D. Back, F. Mulcahy, and J. Feely, *St Johns wort increases expression of P-glycoprotein: implications for drug interactions.* Br J Clin Pharmacol, 2002. **53**: 75-82.

76. Dresser, G.K., J.D. Spence, and D.G. Bailey, *Pharmacokinetic-pharmacodynamic consequences and clinical relevance of cytochrome P450 3A4 inhibition.* Clin Pharmacokinet, 2000. **38**: 41-57.
77. Nahin, R.L., M. Pecha, D.B. Welmerink, K. Sink, S.T. DeKosky, and A.L. Fitzpatrick, *Concomitant use of prescription drugs and dietary supplements in ambulatory elderly people.* J Am Geriatr Soc, 2009. **57**: 1197-205.
78. FDA. *Preventable adverse drug reactions: A focus on drug interactions*. 2002 [cited 2012 27 September 2012]; Available from: http://www.fda.gov/cder/drug/drugReactions/default.htm.
79. Honig, P.K., D.C. Wortham, K. Zamani, D.P. Conner, J.C. Mullin, and L.R. Cantilena, *Terfenadine-ketoconazole interaction. Pharmacokinetic and electrocardiographic consequences.* Jama, 1993. **269**: 1513-8.
80. Handley, D.A., A. Magnetti, and A.J. Higgins, *Therapeutic advantages of third generation antihistamines.* Expert Opin Investig Drugs, 1998. **7**: 1045-54.
81. Flexner, C., *Dual protease inhibitor therapy in HIV-infected patients: pharmacologic rationale and clinical benefits.* Annu Rev Pharmacol Toxicol, 2000. **40**: 649-74.
82. Zhou, H., Z. Tong, and J.F. McLeod, *"Cocktail" approaches and strategies in drug development: valuable tool or flawed science?* J Clin Pharmacol, 2004. **44**: 120-34.
83. He, K., M. Qian, H. Wong, S.A. Bai, B. He, B. Brogdon, J.E. Grace, B. Xin, J. Wu, S.X. Ren, H. Zeng, Y. Deng, D.M. Graden, T.V. Olah, S.E. Unger, J.M. Luettgen, R.M. Knabb, D.J. Pinto, P.Y. Lam, J. Duan, R.R. Wexler, C.P. Decicco, D.D. Christ, and S.J. Grossman, *N-in-1 dosing pharmacokinetics in drug discovery: Experience, theoretical and practical considerations.* J Pharm Sci, 2007. **7**: 2568-80.
84. Christensen, M., K. Andersson, P. Dalen, R.A. Mirghani, G.J. Muirhead, A. Nordmark, G. Tybring, A. Wahlberg, U. Yasar, and L. Bertilsson, *The Karolinska cocktail for phenotyping of five human cytochrome P450 enzymes.* Clin Pharmacol Ther, 2003. **73**: 517-28.
85. Frye, R.F., G.R. Matzke, A. Adedoyin, J.A. Porter, and R.A. Branch, *Validation of the five-drug "Pittsburgh cocktail" approach for assessment of selective regulation of drug-metabolizing enzymes.* Clin Pharmacol Ther, 1997. **62**: 365-76.
86. Yamane, N., T. Takami, Z. Tozuka, Y. Sugiyama, A. Yamazaki, and Y. Kumagai, *Microdose clinical trial: quantitative determination of nicardipine and prediction of metabolites in human plasma.* Drug Metab Pharmacokinet, 2009. **24**: 389-403.
87. Yamazaki, A., Y. Kumagai, N. Yamane, Z. Tozuka, Y. Sugiyama, T. Fujita, S. Yokota, and M. Maeda, *Microdose study of a P-glycoprotein substrate, fexofenadine, using a non-radioisotope-labelled drug and LC/MS/MS.* J Clin Pharm Ther, 2010. **35**: 169-75.
88. Yamane, N., Z. Tozuka, Y. Sugiyama, T. Tanimoto, A. Yamazaki, and Y. Kumagai, *Microdose clinical trial: quantitative determination of fexofenadine in human plasma using liquid chromatography/electrospray ionization tandem mass spectrometry.* J Chromatogr B Analyt Technol Biomed Life Sci, 2007. **858**: 118-28.

89. Vuong, L.T., J.L. Ruckle, A.B. Blood, M.J. Reid, R.D. Wasnich, H.A. Synal, and S.R. Dueker, *Use of accelerator mass spectrometry to measure the pharmacokinetics and peripheral blood mononuclear cell concentrations of zidovudine.* J Pharm Sci, 2007. **97**: 2833-43.
90. Zhou, X.J., R.C. Garner, S. Nicholson, C.J. Kissling, and D. Mayers, *Microdose pharmacokinetics of IDX899 and IDX989, candidate HIV-1 non-nucleoside reverse transcriptase inhibitors, following oral and intravenous administration in healthy male subjects.* J Clin Pharmacol, 2009. **49**: 1408-16.
91. Mahajan, R., A. Parvez, and K. Gupta, *Microdosing vs. therapeutic dosing for evaluation of pharmacokinetic data: A comparative study.* J Young Pharmacists, 2009. **1**: 290-294.
92. Tozuka, Z., H. Kusuhara, K. Nozawa, Y. Hamabe, I. Ikushima, T. Ikeda, and Y. Sugiyama, *Microdose study of 14C-acetaminophen with accelerator mass spectrometry to examine pharmacokinetics of parent drug and metabolites in healthy subjects.* Clin Pharmacol Ther, 2010. **88**: 824-30.
93. Maeda, K., J. Takano, Y. Ikeda, T. Fujita, Y. Oyama, K. Nozawa, Y. Kumagai, and Y. Sugiyama, *Nonlinear pharmacokinetics of oral quinidine and verapamil in healthy subjects: a clinical microdosing study.* Clin Pharmacol Ther. **90**: 263-70.
94. Maeda, K., Y. Ikeda, T. Fujita, K. Yoshida, Y. Azuma, Y. Haruyama, N. Yamane, Y. Kumagai, and Y. Sugiyama, *Identification of the rate-determining process in the hepatic clearance of atorvastatin in a clinical cassette microdosing study.* Clin Pharmacol Ther. **90**: 575-81.
95. Ieiri, I., Y. Doi, K. Maeda, T. Sasaki, M. Kimura, T. Hirota, T. Chiyoda, M. Miyagawa, S. Irie, K. Iwasaki, and Y. Sugiyama, *Microdosing clinical study: Pharmacokinetic, pharmacogenomic (SLCO2B1), and interaction (grapefruit juice) profiles of celiprolol following the oral microdose and therapeutic dose.* J Clin Pharmacol, 2011. **52**: 1078-89.
96. Ieiri, I., C. Nishimura, K. Maeda, T. Sasaki, M. Kimura, T. Chiyoda, T. Hirota, S. Irie, H. Shimizu, T. Noguchi, K. Yoshida, and Y. Sugiyama, *Pharmacokinetic and pharmacogenomic profiles of telmisartan after the oral microdose and therapeutic dose.* Pharmacogenet Genomics. **21**: 495-505.
97. Kusuhara, H., S. Ito, Y. Kumagai, M. Jiang, T. Shiroshita, Y. Moriyama, K. Inoue, H. Yuasa, and Y. Sugiyama, *Effects of a MATE protein inhibitor, pyrimethamine, on the renal elimination of metformin at oral microdose and at therapeutic dose in healthy subjects.* Clin Pharmacol Ther. **89**: 837-44.
98. Sandhu, P., J.S. Vogel, M.J. Rose, E.A. Ubick, J.E. Brunner, M.A. Wallace, J.K. Adelsberger, M.P. Baker, P.T. Henderson, P.G. Pearson, and T.A. Baillie, *Evaluation of microdosing strategies for studies in preclinical drug development: demonstration of linear pharmacokinetics in dogs of a nucleoside analog over a 50-fold dose range.* Drug Metab Dispos, 2004. **32**: 1254-9.
99. Balani, S.K., N.V. Nagaraja, M.G. Qian, A.O. Costa, J.S. Daniels, H. Yang, P.R. Shimoga, J.T. Wu, L.S. Gan, F.W. Lee, and G.T. Miwa, *Evaluation of microdosing to assess pharmacokinetic linearity in rats*

using liquid chromatography-tandem mass spectrometry. Drug Metab Dispos, 2006. **34**: 384-8.
100. Mclean, M.A., C.-Y. Tam, J, M.T. Baratta, C.L. Holliman, R. Ings, and G.R. Galluppi, *Accelerating Drug Development: Methodology to Support First-in-Man Pharmacokinetic Studies by the use of Drug Candidate Microdosing.* Drug Dev Res, 2007. **68**: 14-22.
101. Ni, J., H. Ouyang, M. Aiello, C. Seto, L. Borbridge, T. Sakuma, R. Ellis, D. Welty, and A. Acheampong, *Microdosing assessment to evaluate pharmacokinetics and drug metabolism in rats using liquid chromatography-tandem mass spectrometry.* Pharm Res, 2008. **25**: 1572-1582.
102. Nagilla, R. and K.W. Ward, *A comprehensive analysis of the role of correction factors in the allometric predictivity of clearance from rat, dog, and monkey to humans.* J Pharm Sci, 2004. **93**: 2522-34.
103. Sarapa, N., P.H. Hsyu, G. Lappin, and R.C. Garner, *The application of accelerator mass spectrometry to absolute bioavailability studies in humans: simultaneous administration of an intravenous microdose of 14C-nelfinavir mesylate solution and oral nelfinavir to healthy volunteers.* J Clin Pharmacol, 2005. **45**: 1198-205.
104. Gao, L., J. Li, C. Kasserra, Q. Song, A. Arjomand, D. Hesk, and S.K. Chowdhury, *Precision and accuracy in the quantitative analysis of biological samples by accelerator mass spectrometry: Application in microdose absolute bioavailability studies.* Anal Chem, 2011.
105. Smith, D.A., *The debate is over: accelerator MS provides the route to better drug-development paradigms/protocols.* Bioanalysis, 2011. **3**: 391-392.
106. Lappin, G., M. Seymour, G. Young, D. Higton, and H.M. Hill, *An AMS method to determine analyte recovery from pharmacokinetic studies with concomitant extravascular and intravenous administration.* Bioanalysis, 2011. **3**: 407-10.
107. Rowland, M., *Microdosing and the 3Rs*, in *National Centre for the Replacement, Refinement & Reduction of animals in Research*. 2006, NC3Rs: Manchester.
108. Amidon, G.L., H. Lennernas, V.P. Shah, and J.R. Crison, *A theoretical basis for a biopharmaceutic drug classification: the correlation of in vitro drug product dissolution and in vivo bioavailability.* Pharm Res, 1995. **12**: 413-20.
109. Wu, C.Y. and L.Z. Benet, *Predicting drug disposition via application of BCS: transport/absorption/ elimination interplay and development of a biopharmaceutics drug disposition classification system.* Pharm Res, 2005. **22**: 11-23.
110. Benet, L.Z., F. Broccatelli, and T.I. Oprea, *BDDCS applied to over 900 drugs.* Aaps J, 2011. **13**: 519-47.
111. FDA, *Guidance for industry: Safety testing of drug metabolites*, F.a.D.A.U.D.o.H.a.H. Services, Editor. 2008.
112. ICH, *ICH Topic M3: Note for guidance on non-clinical safety pharmacology studies for human pharmaceuticals*, ICH, Editor. 2009.
113. Maeda, K. and Y. Sugiyama, *Novel stratergies for microdose studies using non-radiolabeled compounds.* Adv Drug Deliv Rev, 2011. **63**: 532-538.

114. Ieiri, I., C. Nishimura, K. Maeda, T. Sasaki, M. Kimura, T. Chiyoda, T. Hirota, S. Irie, H. Shimizu, T. Noguchi, K. Yoshida, and Y. Sugiyama, *Pharmacokinetic and pharmacogenomic profiles of telmisartan after the oral microdose and therapeutic dose.* Pharmacogenet Genomics, 2011. **21**: 495-505.
115. Ieiri, I., S. Higuchi, and Y. Sugiyama, *Genetic polymorphisms of uptake (OATP1B1, 1B3) and efflux (MRP2, BCRP) transporters: implications for inter-individual differences in the pharmacokinetics and pharmacodynamics of statins and other clinically relevant drugs.* Expert Opin Drug Metab Toxicol, 2009. **5**: 703-29.
116. Kusuhara, H., S. Ito, Y. Kumagai, M. Jiang, T. Shiroshita, Y. Moriyama, K. Inoue, H. Yuasa, and Y. Sugiyama, *Effects of a MATE protein inhibitor, pyrimethamine, on the renal elimination of metformin at oral microdose and at therapeutic dose in healthy subjects.* Clin Pharmacol Ther, 2011. **89**: 837-44.
117. Maeda, K., Y. Ikeda, T. Fujita, K. Yoshida, Y. Azuma, Y. Haruyama, N. Yamane, Y. Kumagai, and Y. Sugiyama, *Identification of the rate-determining process in the hepatic clearance of atorvastatin in a clinical cassette microdosing study.* Clin Pharmacol Ther, 2011. **90**: 575-81.
118. Mazzu, A.L., K.C. Lasseter, E.C. Shamblen, V. Agarwal, J. Lettieri, and P. Sundaresen, *Itraconazole alters the pharmacokinetics of atorvastatin to a greater extent than either cerivastatin or pravastatin.* Clin Pharmacol Ther, 2000. **68**: 391-400.
119. Neuvonen, P.J., T. Kantola, and K.T. Kivisto, *Simvastatin but not pravastatin is very susceptible to interaction with the CYP3A4 inhibitor itraconazole.* Clin Pharmacol Ther, 1998. **63**: 332-41.
120. Lappin, G. and L. Stevens, *Biomedical accelerator mass spectrometry: recent applications in metabolism and pharmacokinetics.* Expert Opin Drug Metab Toxicol, 2008. **4**: 1021-33.
121. Garner, R.C., *Accelerator mass spectrometry in pharmaceutical research and development--a new ultrasensitive analytical method for isotope measurement.* Curr Drug Metab, 2000. **1**: 205-13.
122. Beumer, J.H., R.C. Garner, M.B. Cohen, S. Galbraith, G.F. Duncan, T. Griffin, J.H. Beijnen, and J.H. Schellens, *Human mass balance study of the novel anticancer agent ixabepilone using accelerator mass spectrometry.* Invest New Drugs, 2007. **25**: 327-334.
123. Lappin, G., *Biomedical accelerator mass spectrometry*, in *Radiotracers in drug development*, G. Lappin and S. Temple, Editors. 2006, Taylor & Francis: Boca Raton. p. 233-249.
124. Lappin, G., M. Seymour, G. Young, D. Higton, and H.M. Hill, *AMS method validation for quantitation in pharmacokinetic studies with concomitant extravascular and intravenous administration.* Bioanalysis, 2011. **3**: 393-405.
125. Vogel, J.S., *Rapid production of graphite without contamination for biomedical AMS.* Radiocarbon 1992. **34**: 344 - 350.
126. Thomas, A.T., T. Ognibene, P. Daley, K. Turteltaub, H. Radousky, and G. Bench, *Ultrahigh efficiency moving wire combustion interface for online coupling of high-performance liquid chromatography (HPLC).* Anal Chem, 2011. **83**: 9413-7.

127. FDA, *Guidance for industry investigators and reviewers. Bioanalytical method validation*, F.a.d.a.U.d.o.h.a.h. services, Editor. 2001.
128. Lappin, G., *Radioactivity and radiotracers* in *Radiotracers in drug development*, G. Lappin and S. Temple, Editors. 2006, Taylor & Francis: Boca Raton. p. 17-39.
129. Lappin, G., M. Simpson, Y. Shishikura, and C. Garner, *High-performance liquid chromatography accelerator mass spectrometry: Correcting for losses during analysis by internal standardization.* Anal Biochem, 2008. **378**: 93-95.
130. Snyder, L.R., Kirkland, J.J, and Glajch, J.L., *Sample preparation*, in *Practical HPLC method development*. 1997, John Wiley and Sons. p. 100-173.
131. Vogel, J. and A.H. Love, *Quantitating isotopic molecular labels with accelerator mass spectrometry*, in *Methods in Enzymology*, A.L. Burlingame, Editor. 2005, Academic Press: New York. p. 402-422.
132. Nehlig, A., *Are we dependent upon coffee and caffeine? A review on human and animal data.* Neurosci Biobehav Rev, 1999. **23**: 563-76.
133. Fredholm, B.B., K. Battig, J. Holmen, A. Nehlig, and E.E. Zvartau, *Actions of caffeine in the brain with special reference to factors that contribute to its widespread use.* Pharmacol Rev, 1999. **51**: 83-133.
134. Lelo, A., D.J. Birkett, R.A. Robson, and J.O. Miners, *Comparative pharmacokinetics of caffeine and its primary demethylated metabolites paraxanthine, theobromine and theophylline in man.* Br J Clin Pharmacol, 1986. **22**: 177-82.
135. Muchohi, S.N., S.A. Ward, L. Preston, C.R. Newton, G. Edwards, and G.O. Kokwaro, *Determination of midazolam and its major metabolite 1'-hydroxymidazolam by high-performance liquid chromatography-electrospray mass spectrometry in plasma from children.* J Chromatogr B Analyt Technol Biomed Life Sci, 2005. **821**: 1-7.
136. Xu, H., M. Murray, and A.J. McLachlan, *Influence of genetic polymorphisms on the pharmacokinetics and pharmaco-dynamics of sulfonylurea drugs.* Curr Drug Metab, 2009. **10**: 643-58.
137. Miura, M. and T. Uno, *Clinical pharmacokinetics of fexofenadine enantiomers.* Expert Opin Drug Metab Toxicol. **6**: 69-74.
138. Rowland, M. and T.N. Tozer, *Physiologic concepts and kinetics*, in *Clinical pharmacokinetics: Concepts and applications*, W.a.W. Lippincott, Editor. 1995, Lippincott, Williams and Wilkins: Philadelphia. p. 109-118.
139. Kwon, Y., *Absorption*, in *Handbook of essential pharmacokinetics, pharmacodynamics anddrug metabolism for industrial scientists*. 2001, Springer-Verlag: New York. p. 35-72.
140. Wishart, D.S., C. Knox, A.C. Guo, D. Cheng, S. Shrivastava, D. Tzur, B. Gautam, and M. Hassanali, *DrugBank: a knowledgebase for drugs, drug actions and drug targets.* Nucleic Acids Res, 2008. **36**: D901-6.
141. Society, A.C., *SciFinder*. 2013, CAS.
142. Moynihan, H.A. and A.M. Crean, *Drug partitioning across biological barriers*, in *The physiochemical basis of pharmaceuticals*. 2009, Oxforn University Press: Oxford. p. 212-253.

143. Hardman, J.G., L.E. Limbird, and A.G. Gilman, *Goodman and Gilman's Pharmacological Basis of Therapeutics*. 11 ed. 2004: McGraw Hill Medical Publishing.
144. Waters. *Sirocco protein precipitation plate*. 2013 [cited 2013 10 April 2013]; Available from: http://www.waters.com/waters/en_GB/Sirocco-Protein-Precipitation-Plate/nav.htm?cid=513160.
145. Jetter, A., M. Kinzig-Schippers, A. Skott, A. Lazar, D. Tomalik-Scharte, J. Kirchheiner, M. Walchner-Bonjean, U. Hering, V. Jakob, M. Rodamer, W. Jabrane, D. Kasel, J. Brockmoller, U. Fuhr, and F. Sorgel, *Cytochrome P450 2C9 phenotyping using low-dose tolbutamide.* Eur J Clin Pharmacol, 2004. **60**: 165-71.
146. Waters. *Xterra columns*. 2013 [cited 2013 10 April 2013]; Available from: http://www.waters.com/waters/en_GB/XTerra-Columns/nav.htm?cid=513769.
147. Uno, T., N. Yasui-Furukori, T. Takahata, K. Sugawara, and T. Tateishi, *Liquid chromatographic determination of fexofenadine in human plasma with fluorescence detection.* J Pharm Biomed Anal, 2004. **35**: 937-42.
148. Watson, D.G., *High pressure liquid chromatography*, in *Pharmaceutical analysis*, D.G. Watson, Editor. 2002, Churchill Livingstone: London. p. 237-276.
149. Uchida, S., H. Yamada, X.D. Li, S. Maruyama, Y. Ohmori, T. Oki, H. Watanabe, K. Umegaki, K. Ohashi, and S. Yamada, *Effects of Ginkgo biloba extract on pharmacokinetics and pharmacodynamics of tolbutamide and midazolam in healthy volunteers.* J Clin Pharmacol, 2006. **46**: 1290-8.
150. Robbins, D.K., M.A. Castles, D.J. Pack, V.O. Bhargava, and S.J. Weir, *Dose proportionality and comparison of single and multiple dose pharmacokinetics of fexofenadine (MDL 16455) and its enantiomers in healthy male volunteers.* Biopharm Drug Dispos, 1998. **19**: 455-63.
151. Lilja, J.J., J.T. Backman, and P.J. Neuvonen, *Effects of daily ingestion of cranberry juice on the pharmacokinetics of warfarin, tizanidine, and midazolam-probes of CYP2C9, CYP1A2, and CYP3A4.* Clin Pharmacol Ther, 2007. **81**: 833-9.
152. Eap, C.B., T. Buclin, E. Hustert, G. Bleiber, K.P. Golay, A.C. Aubert, P. Baumann, A. Telenti, and R. Kerb, *Pharmacokinetics of midazolam in CYP3A4- and CYP3A5-genotyped subjects.* Eur J Clin Pharmacol, 2004. **60**: 231-6.
153. Van Harten, J., *Overview of the pharmacokinetics of fluvoxamine.* Clin Pharmacokinet, 1995. **29 Suppl 1**: 1-9.
154. Jakate, A.S., P. Roy, A. Patel, W. Abramowitz, S. Persiani, J. Wangsa, and R. Kapil, *Effect of azole antifungals ketoconazole and fluconazole on the pharmacokinetics of dexloxiglumide.* Br J Clin Pharmacol, 2005. **60**: 498-507.
155. Jeppesen, U., S. Loft, H.E. Poulsen, and K. Brsen, *A fluvoxamine-caffeine interaction study.* Pharmacogenetics, 1996. **6**: 213-22.
156. Tsunoda, S.M., R.L. Velez, L.L. von Moltke, and D.J. Greenblatt, *Differentiation of intestinal and hepatic cytochrome P450 3A activity with use of midazolam as an in vivo probe: effect of ketoconazole.* Clin Pharmacol Ther, 1999. **66**: 461-71.

157. Eap, C.B., T. Buclin, G. Cucchia, D. Zullino, E. Hustert, G. Bleiber, K.P. Golay, A.C. Aubert, P. Baumann, A. Telenti, and R. Kerb, *Oral administration of a low dose of midazolam (75 microg) as an in vivo probe for CYP3A activity.* Eur J Clin Pharmacol, 2004. **60**: 237-46.
158. Patki, K.C., L.L. Von Moltke, and D.J. Greenblatt, *In vitro metabolism of midazolam, triazolam, nifedipine, and testosterone by human liver microsomes and recombinant cytochromes p450: role of cyp3a4 and cyp3a5.* Drug Metab Dispos, 2003. **31**: 938-44.
159. Lam, Y.W., C.L. Alfaro, L. Ereshefsky, and M. Miller, *Pharmacokinetic and pharmacodynamic interactions of oral midazolam with ketoconazole, fluoxetine, fluvoxamine, and nefazodone.* J Clin Pharmacol, 2003. **43**: 1274-82.
160. Kashuba, A.D., A.N. Nafziger, G.L. Kearns, J.S. Leeder, R. Gotschall, M.L. Rocci, Jr., R.W. Kulawy, D.J. Beck, and J.S. Bertino, Jr., *Effect of fluvoxamine therapy on the activities of CYP1A2, CYP2D6, and CYP3A as determined by phenotyping.* Clin Pharmacol Ther, 1998. **64**: 257-68.
161. Li, J., S.Y. Wen, R. Wang, K. Chen, Y. Fang, F. Pei, and S.Q. Wang, *[Influence of cytochrom P450 CYP2C9 polymorphism on the pharmacokinetics of tolbutamide metabolism using oligonucleotide genotyping microarray]*. Yao Xue Xue Bao, 2005. **40**: 695-9.
162. Chen, C., *Some pharmacokinetic aspects of the lipophilic terfenadine and zwitterionic fexofenadine in humans.* Drugs R D, 2007. **8**: 301-14.
163. Davit, B., K. Reynolds, R. Yuan, F. Ajayi, D. Conner, E. Fadiran, B. Gillespie, C. Sahajwalla, S.M. Huang, and L.J. Lesko, *FDA evaluations using in vitro metabolism to predict and interpret in vivo metabolic drug-drug interactions: impact on labeling.* J Clin Pharmacol, 1999. **39**: 899-910.
164. Tannergren, C., T. Knutson, L. Knutson, and H. Lennernas, *The effect of ketoconazole on the in vivo intestinal permeability of fexofenadine using a regional perfusion technique.* Br J Clin Pharmacol, 2003. **55**: 182-90.
165. Tannergren, C., N. Petri, L. Knutson, M. Hedeland, U. Bondesson, and H. Lennernas, *Multiple transport mechanisms involved in the intestinal absorption and first-pass extraction of fexofenadine.* Clin Pharmacol Ther, 2003. **74**: 423-36.
166. Shimizu, M., K. Fuse, K. Okudaira, R. Nishigaki, K. Maeda, H. Kusuhara, and Y. Sugiyama, *Contribution of OATP (organic anion-transporting polypeptide) family transporters to the hepatic uptake of fexofenadine in humans.* Drug Metab Dispos, 2005. **33**: 1477-81.
167. Sharma, A., S. Pilote, P.M. Belanger, M. Arsenault, and B.A. Hamelin, *A convenient five-drug cocktail for the assessment of major drug metabolizing enzymes: a pilot study.* Br J Clin Pharmacol, 2004. **58**: 288-97.
168. Kennedy, J.S., L.L. von Moltke, J.S. Harmatz, N. Engelhardt, and D.J. Greenblatt, *Validity of self-reports of caffeine use.* J Clin Pharmacol, 1991. **31**: 677-80.
169. Abrahim, A., G. Luurtsema, M. Bauer, R. Karch, M. Lubberink, E. Pataraia, C. Joukhadar, K. Kletter, A.A. Lammertsma, C. Baumgartner, M. Muller, and O. Langer, *Peripheral metabolism of (R)-[(11)C]verapamil in epilepsy patients.* Eur J Nucl Med Mol Imaging, 2008. **35**: 116-23.

170. Luurtsema, G., C.F. Molthoff, R.C. Schuit, A.D. Windhorst, A.A. Lammertsma, and E.J. Franssen, *Evaluation of (R)-[11C]verapamil as PET tracer of P-glycoprotein function in the blood-brain barrier: kinetics and metabolism in the rat.* Nucl Med Biol, 2005. **32**: 87-93.
171. Snyder, L.R., J.J. Kirkland, J.L. Glajch, J. Kern, and K. Kirkland, *Chiral separations*, in *Practical HPLC method development*, J.W.a. Sons, Editor. 1997, John Wiley and Sons. p. 537-615.
172. Phenomenex. *Polysaccharide chiral HPLC columns*. 2013 [cited 2013 10 April 2013]; Available from: http://www.phenomenex.com/Products/HPLCDetail/Lux/Cellulose-1.
173. Ates, H., D. Mangelings, and Y. Vander Heyden, *High throughput screening and method development strategies*, in *Chiral separation methods for pharmaceutical and biotechnological products*, S. Ahuja, Editor. 2010.
174. Eichelbaum, M., G. Mikus, and B. Vogelgesang, *Pharmacokinetics of (+)-, (-)- and (+/-)-verapamil after intravenous administration.* Br J Clin Pharmacol, 1984. **17**: 453-8.
175. Koetz, B.S. and P.M. Price, *Positron Emission Tomography*, in *Radiotracers in Drug Development*, G. Lappin and S. Temple, Editors. 2006, Taylor Francis: Boca Raton. p. 251-267.
176. Wagner, C.C., M. Muller, G. Lappin, and O. Langer, *Positron emission tomography for use in microdosing studies.* Curr Opin Drug Discov Devel, 2008. **11**: 104-10.
177. Luurtsema, G., C.F. Molthoff, A.D. Windhorst, J.W. Smit, H. Keizer, R. Boellaard, A.A. Lammertsma, and E.J. Franssen, *(R)- and (S)-[11C]verapamil as PET-tracers for measuring P-glycoprotein function: in vitro and in vivo evaluation.* Nucl Med Biol, 2003. **30**: 747-51.
178. Lubberink, M., G. Luurtsema, B.N. van Berckel, R. Boellaard, R. Toornvliet, A.D. Windhorst, E.J. Franssen, and A.A. Lammertsma, *Evaluation of tracer kinetic models for quantification of P-glycoprotein function using (R)-[11C]verapamil and PET.* J Cereb Blood Flow Metab, 2007. **27**: 424-33.
179. Franssen, E.J., G. Luurtsema, and A.A. Lammertsma, *Imaging P-glycoprotein at the human blood-brain barrier.* Clin Pharmacol Ther, 2006. **80**: 302-3; author reply 303-4.
180. Langer, O., M. Bauer, A. Hammers, R. Karch, E. Pataraia, M.J. Koepp, A. Abrahim, G. Luurtsema, M. Brunner, R. Sunder-Plassmann, F. Zimprich, C. Joukhadar, S. Gentzsch, R. Dudczak, K. Kletter, M. Muller, and C. Baumgartner, *Pharmacoresistance in epilepsy: a pilot PET study with the P-glycoprotein substrate R-[(11)C]verapamil.* Epilepsia, 2007. **48**: 1774-84.
181. Busse, D., S. Templin, G. Mikus, M. Schwab, U. Hofmann, M. Eichelbaum, and K.T. Kivisto, *Cardiovascular effects of (R)- and (S)-verapamil and racemic verapamil in humans: a placebo-controlled study.* Eur J Clin Pharmacol, 2006. **62**: 613-9.
182. Tannergren, C., H. Engman, L. Knutson, M. Hedeland, U. Bondesson, and H. Lennernas, *St John's wort decreases the bioavailability of R- and S-verapamil through induction of the first-pass metabolism.* Clin Pharmacol Ther, 2004. **75**: 298-309.

183. Tracy, T.S., K.R. Korzekwa, F.J. Gonzalez, and I.W. Wainer, *Cytochrome P450 isoforms involved in metabolism of the enantiomers of verapamil and norverapamil.* Br J Clin Pharmacol, 1999. **47**: 545-52.
184. Wagner, C.C., M. Simpson, M. Zeitlinger, M. Bauer, R. Karch, A. Abrahim, T. Feurstein, M. Schutz, K. Kletter, M. Muller, G. Lappin, and O. Langer, *A combined accelerator mass spectrometry-positron emission tomography human microdose study with 14C- and 11C-labelled verapamil.* Clin Pharmacokinet, 2010. **50**: 111-20.
185. (CHMP), C.f.m.p.f.h.u., *Guideline on Bioanalytial Method Validation*, in *EMEA./CHMP/EWP/192217/2009*, EMEA, Editor. 2011.
186. Maeda, K., J. Takano, Y. Ikeda, T. Fujita, Y. Oyama, K. Nozawa, Y. Kumagai, and Y. Sugiyama, *Nonlinear pharmacokinetics of oral quinidine and verapamil in healthy subjects: a clinical microdosing study.* Clin Pharmacol Ther, 2011. **90**: 263-70.
187. Temple, S., *Statistics in liquid scintillation counting*, in *Radiotracers in drug development*, G. Lappin and S. Temple, Editors. 2006, Taylor & Francis: Boca Raton. p. 183-191.
188. Garner, R.C., J. Barker, C. Flavell, J.V. Garner, M. Whattam, G.C. Young, N. Cussans, S. Jezequel, and D. Leong, *A validation study comparing accelerator MS and liquid scintillation counting for analysis of 14C-labelled drugs in plasma, urine and faecal extracts.* J Pharm Biomed Anal, 2000. **24**: 197-209.
189. Young, G., W. Ellis, J. Ayrton, E. Hussey, and B. Adamkiewicz, *Accelerator mass spectrometry (AMS): recent experience of its use in a clinical study and the potential future of the technique.* Xenobiotica, 2001. **31**: 619-32.
190. Hammers, A., R. Allom, M.J. Koepp, S.L. Free, R. Myers, L. Lemieux, T.N. Mitchell, D.J. Brooks, and J.S. Duncan, *Three-dimensional maximum probability atlas of the human brain, with particular reference to the temporal lobe.* Hum Brain Mapp, 2003. **19**: 224-47.